UNIVERSIDAD NACIONAL AUTÓNOMA DE MÉXICO

Maestría y Doctorado en Ciencias Bioquímicas

CARACTERIZACIÓN DE LA 7-METILGUANOSINA TRIFOSFATO (CAP) EN LOS EXTREMOS 5´ DE LOS TRANSCRITOS VIRALES EN EL CICLO REPLICATIVO DE ROTAVIRUS

TESIS

QUE PARA OPTAR POR EL GRADO DE:

Doctor en Ciencias

PRESENTA:
M. en C. JOAQUÍN MORENO CONTRERAS

TUTORA PRINCIPAL
Dra. SUSANA LÓPEZ CHARRETÓN
Instituto de Biotecnología, UNAM

MIEMBROS DEL COMITÉ TUTORAL
Dr. JOSÉ LUIS REYES TABOADA
Instituto de Biotecnología, UNAM
Dra. ROSA MARTHA EUGENIA YUCOPICIO MONROY
Universidad Autónoma de la Ciudad de México, UACM

Cuernavaca, Morelos. Enero, 2023

El presente trabajo se realizó en el departamento de Genética del Desarrollo y Fisiología Molecular del Instituto de Biotecnología de la Universidad Nacional Autónoma de México, bajo la dirección de la Dra. Susana López Charretón y contó con el apoyo de los donativos 1-S-15356 y 302965 del CONACyT y el Papiit DGAPA IV200420 de la UNAM. El alumno Joaquín Moreno Contreras contó con una beca otorgada por CONACyT #385106 y apoyo del "Programa de Apoyo a los estudios de Posgrado" (PAEP) para la asistencia a congresos y estancias.

Comité tutoral:

Dra. Susana López Charretón
Dra. Rosa Martha Eugenia Yucopicio Monroy
Dr. José Luis Reyes Taboada

Jurado de examen de grado:

Presidente Dr. Takuya Nishigaki Shimizu
Secretario Dra. Hilda María Lomeli Buyoli
Vocal Dr. Ramón Antonio González García Conde
Vocal Dra. Ana Lorena Escolano Gutierrez
Vocal Dr. Juan Ernesto Ludert León

Agradecimiento Técnico

El autor de la tesis agradece la asesoría y el excelente apoyo técnico proporcionado por el M en C. Marco Antonio Espinoza Torres y la Q.F.B. Rafaela María del Pilar Espinosa Organista.

A Eliseo Moreno Contreras y

Miguelina Contreras Moreno

ÍNDICE GENERAL

ÍNDICE DE FIGURAS

ÍNDICE DE TABLAS

Siglas, abreviaturas y acrónimos

DLP	Partícula de doble capa
dsRNA	RNA de cadena doble
EDTA	Ácido Etilendiaminotetraacético
ELISA	Ensayo por inmunoabsorción ligado a enzimas
GTasa	RNA Guanililtransferasa
hpi	Horas post infección
HBGA	Histo antígenos del grupo sanguíneo
hsc70	Proteína de choque térmico 70
IFN	Interferón
lncRNA	RNAs largos no codificantes
MOI	Multiplicidad de infección
mRNA	RNA mensajero
NSP	Proteína no estructural
MTasa	Guanina-N7-metiltransferasa
MDA5	del inglés Melanoma Differentiation-Associated protein 5
MEM	Medio mínimo esencial Eagle
OAS	Oligoadenilato sintetasa
ORF	Marco de lectura abierto
PDE	Fosfodiesterasa
PRRs	Receptores de reconocimiento de patrones
PBS	Amortiguador de fosfatos salino
RE	Retículo endoplasmático

RIG-1	del inglés Retinoic Acid Inducible 1
RdRp	RNA polimerasa dependiente de RNA
Rpm	Revoluciones por minuto
RRV	Rotavirus del mono *Rhesus*
SAM	S-adenosilmetionina
SINV	Virus Sindbis
SDS	Dodecil sulfato de sodio
SFB	Suero fetal bovino
siRNA	RNA pequeño de interferencia
snoRNAs	RNAs pequeños nucleolares
snRNAs	RNAs pequeños nucleares
+RNA	RNA de polaridad positiva
RT	Reversa transcriptasa
qPCR	PCR cuantitativa
TA	Temperatura ambiente
TLP	Partícula de triple capa
RTPasa	RNA 5´ trifosfatasa
UTR	Región no traducida
VP	Proteína viral
2´-O-MTasa	RNA 2´-O-ribosa metiltransferasa
2´-5-A	2´5-oligoadenilatos

RESUMEN

La adición del cap al extremo 5´ de los transcritos virales es uno de los mecanismos que permite a los virus sintetizar de manera eficiente sus proteínas y evadir la respuesta inmune del hospedero durante la infección. Los rotavirus codifican en el segmento 3 de su genoma a la proteína VP3, que tiene todos los dominios necesarios para adicionar un cap tipo 1 a los RNAs virales; además, también posee en el extremo carboxilo terminal la actividad de fosfodiesterasa (PDE) que le permite inhibir la activación de vía oligoadenilato sintetasa (OAS)-RNasa L. En este trabajo caracterizamos de manera cuantitativa la abundancia de los RNAs virales con y sin cap durante la infección de rotavirus; encontramos que no todo el dsRNA genómico presente en las partículas virales presenta cap. Por otra parte, mediante ensayos de transcripción *in vitro,* evaluamos la eficiencia de adición de cap de VP3 que resulto ser cercana al 50%. En contraste, cuando evaluamos la proporción de transcritos virales con y sin cap durante el ciclo replicativo de rotavirus encontramos una mayor proporción de RNAs sin cap a tiempos tempranos de la infección, y proporciones similares de RNAs con y sin cap a tiempos tardíos, sugiriendo que hay una regulación dinámica de la abundancia de estos RNAs durante el ciclo replicativo viral. Al silenciar la expresión de VP3 y caracterizar las partículas virales producidas en esta condición, de manera inesperada encontramos que presentaban una infectividad específica mayor, que no fue debido a la presencia de cap ya que detectamos proporciones similares de RNA con y sin cap en el RNA genómico; en contraste, los transcritos producidos por estas partículas en su mayoría no tenían cap. Por otra parte, al cuantificar la abundancia de cap en células en las que se co-silenció la expresión de VP3 y RNasa L, detectamos una mayor

cantidad de RNAs con cap a tiempos tardíos de la infección; sin embargo, las partículas virales producidas en esta condición contenían la misma proporción de RNAs con y sin cap (1:1). Nuestros resultados sugieren que durante el proceso de encapsidación del RNA viral hay un empaquetamiento selectivo ya que, aunque se encontraron diferentes proporciones de RNAs con y sin cap en las células infectadas, al final siempre se detectó una proporción similar (1:1) de RNAs con y sin cap en las partículas virales.

INTRODUCCIÓN

GENERALIDADES

Rotavirus

Durante los primeros años de vida en humanos y animales, las gastroenteritis no bacterianas son causadas por un pequeño número de agentes virales, entre los cuales el más importante es el rotavirus. La principal vía de transmisión de estos virus es la fecal-oral, aunque también se pueden transmitir mediante fomites contaminados. Se estima que cada año este virus es la causa de más de 258 millones de casos de diarrea y alrededor de 128,000 muertes de niños menores de 5 años en todo el mundo. La mayoría de las muertes ocurren en países en vías de desarrollo, aunque también se reportan muertes en países desarrollados, esto a pesar de que se cuenta con vacunas comerciales disponibles las cuales han demostrado ser seguras y efectivas contra las formas graves de la infección (1).

Los rotavirus pertenecen a la familia *Reoviridae*, son partículas con simetría icosaédrica, y carecen de una membrana lipídica. El genoma viral consiste de 11 segmentos RNA de doble cadena (dsRNA) con tamaños de entre 0.7 y 3.3 kb, que codifican por 6 proteínas estructurales: VP1-VP4, VP6 y VP7 (VP del inglés Viral Protein) y seis no estructurales: NSP1-NSP6 (NSP del inglés Non-Structural Protein). El virión maduro (Figura 1 A) tiene un diámetro aproximado de 70 a 100 nm; estructuralmente está formado por tres capas concéntricas de proteínas: 1) El “core” o núcleo viral, el cual encierra el genoma viral, está formado por las proteínas VP2 y pequeñas cantidades de VP1 (RNA polimerasa dependiente de RNA) y VP3 (guanilil-metil-transferasa). En conjunto estas tres proteínas forman el complejo

enzimático de transcripción. 2) La partícula de doble capa o DLP (del inglés “Double Layered Particle”), está formada por las proteínas que conforman el “core” más una capa de la proteína VP6. Las DLPs son transcripcionalmente activas tanto *in vivo*, como *in vitro.* 3) La partícula de tres capas o TLP (del inglés “Triple Layered Particle”), es la partícula madura e infecciosa de rotavirus que en su capa externa tiene a la glicoproteína VP7 a la cual se encuentran unidas las espículas formadas por la proteína VP4. La proteína VP4 tiene funciones durante la unión al receptor y la penetración a la célula huésped, por lo que es importante para la determinación del tropismo.

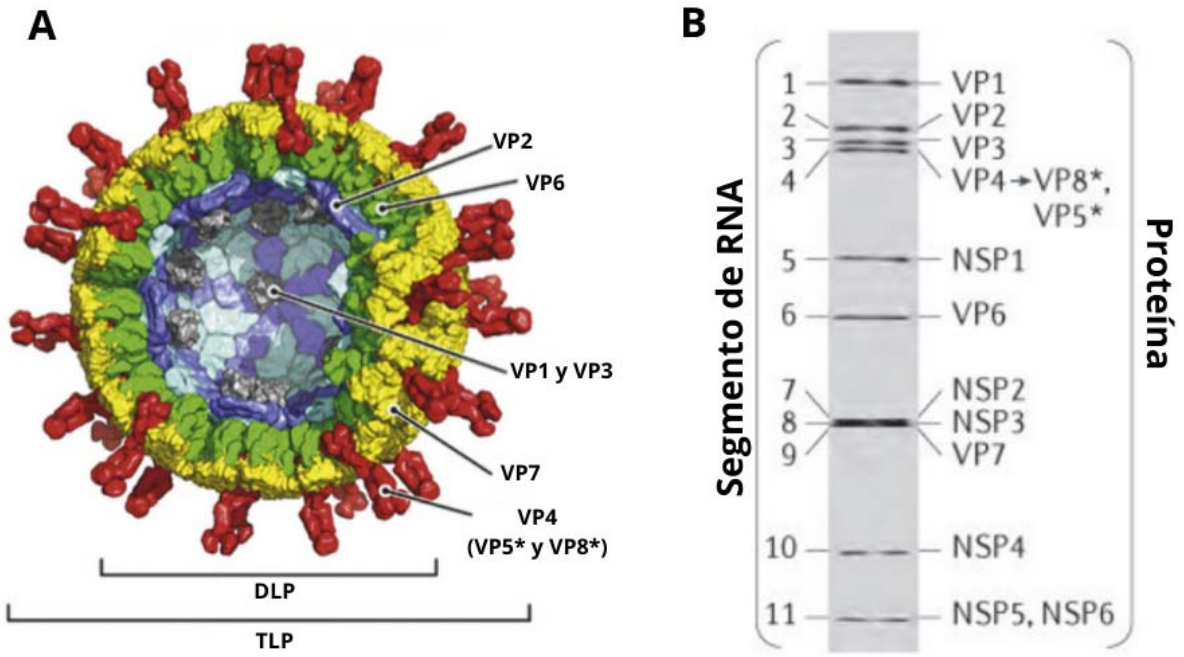

Figura 1. Estructura de rotavirus. A) La partícula viral está formada por un “core” o núcleo, formado por la proteína estructural VP2 (azul) y las enzimas VP1 y VP3 (gris) las cuales están unidas a los 11 segmentos que dsRNA que conforman el genoma viral. La capa intermedia está compuesta por la proteína VP6 (verde), y junto con el “core” forman la partícula de doble capa o DLP. Finalmente, unidas a VP6 se encuentran las proteínas de capa externa VP7 (amarillo) y VP4 (rojo) completando la partícula infecciosa de tres capas

o TLP. B) Patrón electroforético de los 11 segmentos de dsRNA del genoma de rotavirus. Se indican las proteínas para las que codifica cada segmento. Imágenes modificadas de (2) y (3).

Clasificación de rotavirus

Los rotavirus están clasificados inmunológicamente en 7 serogrupos primarios (A-G), de los cuales solamente los serogrupos A, B y C contienen virus que infectan a humanos y animales, mientras que los serogrupos D, E, F y G solo infectan animales. Los rotavirus del grupo A son los más estudiados e importantes epidemiológica y clínicamente ya que son los causantes más comunes de infecciones en humanos (4). Los rotavirus del grupo A están a su vez subdivididos en serotipos y genotipos, clasificación basada tanto inmunológicamente por su reactividad a anticuerpos (serotipos), como por la secuencia de los genes que codifican por las proteínas de capa externa VP4 y VP7 (genotipos). Hasta ahora, se han identificado 36 genotipos G (Glicoproteína) de VP7 y 51 genotipos P (proteína sensible a proteasa) de VP4, aunque globalmente los dominantes son los 6 genotipos G (G1, G2, G3, G4, G9 y G12) y los 3 genotipos P (P[4], P[6] y P[8]). Estudios epidemiológicos muestran que seis genotipos (G1P[8], G2P[4], G3P[8], G4P[8], G9P[8] y G12P[8]) representan más del 90% de las cepas de rotavirus A que están circulando globalmente (5)(6), de estos, el genotipo G1P[8] es el predominante en países desarrollados como Estados Unidos, Reino Unido y Australia, así como en varios países de América Latina (6).

Genoma viral

Como se mencionó anteriormente, el genoma de rotavirus está compuesto por 11 segmentos de RNA de doble cadena (dsRNA), que codifican por 12 proteínas, 6 proteínas estructurales (VP1, VP2, VP3, VP4, VP6, VP7) y 6 no estructurales (NSP1-NSP6) (Figura 1 B). Los RNAs de polaridad positiva (+RNAs) de rotavirus tienen una estructura cap en el extremo 5´, pero no se encuentran poliadenilados en el extremo 3´. Los extremos 5´ y 3´ no traducidos (UTRs del inglés un translated regions) de los 11 segmentos del genoma viral presentan variaciones en tamaño y secuencia; sin embargo, todos tienen una secuencia consenso de 4 nucleótidos en el extremo 3´ (5´-GACC-3´) la cual se encuentra conservada en los 11 genes virales, a esta, se une la proteína viral NSP3 a través de su dominio amino terminal (7)(8). Adicionalmente, en los extremos 3´ de los mRNAs de rotavirus se encuentra otra secuencia consenso (5´-UGUGACC-3´) que es reconocida por la proteína VP1, que tiene una actividad de RNA polimerasa dependiente de RNA (RdRp); esta interacción es importante para iniciar la síntesis del RNA intermediario de polaridad negativa (-RNA) que da lugar a los dsRNA, proceso conocido como replicación del RNA viral (9).

La mayoría de los segmentos que forman el genoma viral son monocistrónicos, conteniendo un solo marco de lectura abierto (OFR), a excepción del segmento 11 de algunas cepas de rotavirus, el cual contiene dos ORFs que codifican para las proteínas no estructurales NSP5 y NSP6. El +RNA viral tiene dos papeles: puede ser utilizado para dirigir la síntesis de proteínas, o como molde para la síntesis del dsRNA, que es empleado como el genoma de las nuevas partículas virales (10). El tener un genoma segmentado, le permite a los rotavirus generar cepas rearreglantes cuando una célula es co-infectada con dos cepas diferentes, lo

que les proporciona un elemento de diversidad, aunado a los cambios puntuales que se generan durante la replicación del genoma. Además de los conocidos sistemas de genética reversa basados en la generación de cepas rearreglantes, recientemente se ha desarrollado un sistema de genética reversa para rotavirus basado en plásmidos. Este sistema, a diferencia de los virus rearreglantes, permite recuperar virus infecciosos con cambios puntuales en el genoma, que pueden ser empleados para estudiar diversos aspectos del ciclo replicativo, la patogénesis causada por este virus, así como para facilitar el desarrollo de terapias y vacunas (11).

Ciclo replicativo

Los rotavirus presentan un tropismo celular especifico ya que infectan y se replican principalmente en los enterocitos maduros presentes en la región media y las puntas de las microvellosidades y en las células enteroendocrinas del intestino delgado, aunque también se ha descrito que pueden diseminarse extraintestinalmente, causando viremia, a través de la vía linfática (12). El conocimiento acerca del mecanismo de entrada y replicación se ha derivado principalmente de estudios *in vitro,* utilizando líneas celulares de origen renal o intestinal, que son permisivas para la replicación de este virus. Recientemente se ha implementado el uso de cultivos de enteroides intestinales humanos (13), que asemejan más la infección *in vivo*.

El proceso de entrada en rotavirus es complejo y se lleva a cabo mediante diversos pasos que inician con la interacción entre la partícula viral y su receptor presente en la membrana de la célula hospedera. Para que las partículas virales

sean infecciosas, la proteína de capa externa VP4 tiene que ser procesada por proteasas parecidas a tripsina en el lumen intestinal, este corte produce dos polipéptidos de menor peso molecular, llamados VP5 y VP8. La proteína VP8 media la interacción inicial del virus con sialoglicanos presentes en la superficie celular (acidos siálicos y gangliósidos GM1 y GD1a) y con antígenos del grupo sanguíneo (HBGAs), dependiendo de la cepa viral (14). Posteriormente, VP5 y la glicoproteína VP7 interaccionan con diferentes co-receptores presentes en la superficie de la célula. VP7 se une a las integrinas $\alpha v\beta 3$ y $\alpha \chi \beta 2$, mientras que VP5 se une a la integrina $\alpha 2\beta 1$ y también interacciona con la proteína de choque térmico 70 (hsc70) (15). No todas las cepas de rotavirus interaccionan con todos los receptores putativos, mientras que la interacción con integrinas es dependiente de la cepa. Sin embargo, se ha reportado que todas las cepas de rotavirus requieren de interaccionar con hsc70 para poder infectar a las células (16). No es claro si todas las interacciones mencionadas se llevan a cabo de manera secuencial o algunas de estas son alternativas. Recientemente se demostró que, para algunas cepas de rotavirus, las proteínas de uniones estrechas JAM-A, ocludina y ZO-1 también son importantes durante el proceso de entrada a la célula (17).

Posterior al paso de unión, los rotavirus son internalizados en células MA104 mediante endocitosis, empleando diferentes vías endocíticas dependiendo de la cepa de rotavirus (16). Las cepas de rotavirus animales (UK, YM, SA11-4S, nar3) o humanas (Wa, DS-1, WI-69) entran a la célula mediante endocitosis mediada por clatrina, mientras que la cepa de simio RRV ingresa a través de una vía independiente de clatrina y caveolina pero que depende de la presencia de dinamina

2, GTPasa Rho A, Cdc42, actina4 y colesterol (18)(14). Recientemente se reportó que la vía endocítica empleada, ya sea dependiente o independiente de clatrina, es determinada por la proteína VP4 (19). Independientemente de la vía de entrada, todas las cepas de rotavirus llegan inicialmente a los endosomas tempranos y egresan al citoplasma en diferentes etapas de maduración de los endosomas. Las cepas RRV y SA11-4 salen de los endosomas en maduración, mientras que otras cepas egresan en etapas maduración posteriores, en los endosomas tardíos.

El micro-ambiente de los endosomas, como el pH y las bajas concentraciones de Ca^{2+} entre otros factores, permiten que durante el proceso de internalización, el virión sufra cambios estructurales que le permiten perder las proteínas externas VP7 y VP4, generándose las DLPs que son liberadas en el citoplasma celular (14). En este compartimento las DLPs son activas transcripcionalmente e inician la síntesis de los 11 segmentos de +RNAs los cuales, como se ha mencionado, tienen cap en el extremo 5´, pero no están poliadenilados. Estos +RNAs son utilizados para la síntesis de proteínas virales y como moldes para la producción de dsRNA. Una vez que se ha sintetizado una masa crítica de proteínas virales, se forman estructuras electrodensas que reciben el nombre de viroplasmas, que comienzan a detectarse a partir de las 3-4 hpi (20) y contienen principalmente proteínas virales (NSP2, NSP4, NSP5, VP1, VP2, VP3, VP6) y RNA viral.

Recientemente se caracterizó la organización espacial de las proteínas virales que forman a los viroplasmas. Mediante microscopia de alta resolución se determinó que la proteína no estructural NSP5 se localiza en el centro de los viroplasmas y está rodeada de las proteínas NSP2 y NSP4, seguida por una zona en la que se encuentran VP1, VP2, VP6, la proteína VP4 forma un anillo alrededor

de esta estructura y finalmente se localiza una capa de VP7 (21). Dentro de los viroplasmas se lleva a cabo la segunda ronda de transcripción y replicación del genoma viral y se inicia el ensamble de las partículas subvirales. El proceso de empacado del genoma es iniciado por las proteínas VP1 y VP3 las cuales se unen respectivamente a los extremos 3´ y 5´ de los segmentos del RNA viral. Posteriormente, la proteína VP2 en forma de decámeros se asocia a VP1 y VP3 iniciando de la síntesis del dsRNA; finalmente se ensambla la proteína de capa intermedia VP6 generando las DLPs (22), que inician un segundo ciclo de transcripción, amplificando la cantidad de mRNAs virales.

En la última etapa de la morfogénesis, las DLPs geman hacia membranas autofagosómicas provenientes del retículo endoplasmático, en un proceso mediado por la proteína NSP4. Durante este paso adquieren una membrana transitoria de lípidos y se asocia la proteína VP7; una vez en el retículo endoplásmico, la membrana lipídica es eliminada por un mecanismo poco caracterizado y finalmente se ensambla la proteína de capa externa VP4, generando la partícula viral madura (TLP). Los nuevos viriones pueden ser liberados por lisis celular, aunque también se ha descrito un proceso de salida no lítico, dependiendo de la línea celular (Figura 2) (23)(24).

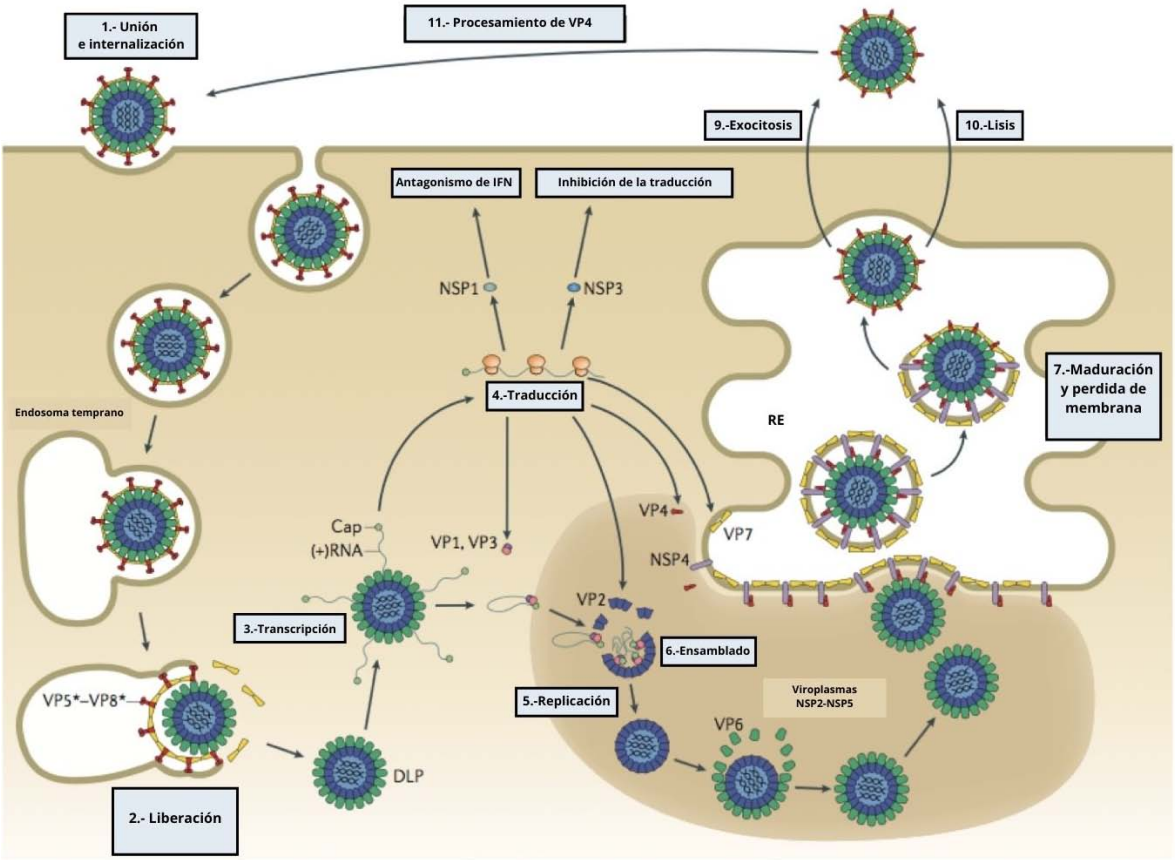

Figura 2. Ciclo replicativo de rotavirus. El primer paso es la unión del virión a la célula hospedera. El virión ingresa a la célula mediante endocitosis, donde las proteínas de capa externa VP4 y VP7 son eliminadas. Posteriormente, la partícula de doble capa (DLP) es liberada en el citoplasma, donde lleva se lleva a cabo la transcripción del genoma viral para generar el +RNA, que sirve como molde para la síntesis de proteínas virales y como templado para generar dsRNA. La traducción de las proteínas virales se lleva a cabo en el citoplasma celular. El ensamblado de las DLPs se lleva a cabo en los viroplasmas; para que la DLP madure tiene que gemar hacia el retículo endoplasmático, durante este paso la DLP adquiere una membrana transitoria de lípidos la cual es eliminada. El proceso de maduración termina con la incorporación de VP4 y VP7. Finalmente, el virión sale mediante lisis celular o exocitosis. Modificada de (25).

El CAP EN LOS mRNAS CELULARES

Los RNAs mensajeros (mRNAs) eucarióticos maduros contienen varias características: la parte central de la secuencia de un mRNA es el fragmento que codifica por una proteína, conocido como marco de lectura abierto u ORF (del inglés Open Reading Frame) y se encuentra flanqueado por dos UTRs denominadas 5´ y 3´ dependiendo de su localización. En el extremo 3´ de los mRNAs celulares, y después de la UTR 3', se encuentra una secuencia de treinta o más adeninas, comúnmente llamada "cola poli(A)", la cual estabiliza el transcrito y participa durante el proceso de traducción. Por otra parte, en el extremo 5´UTR del mRNA se encuentra una estructura llamada cap (caperuza), que consiste de una 7-metilguanosina unida mediante un enlace 5´-5´-trifosfato al primer nucleótido del transcrito naciente (Figura 3). El cap tiene funciones importantes en diferentes procesos del mRNA que incluyen: reclutar factores involucrados en el splicing del pre-mRNA, la exportación del núcleo al citoplasma, el inicio de la síntesis de proteínas de manera dependiente de cap, la estabilidad y protección contra la degradación mediada por exoribonucleasas 5´-3´; además, permite a la célula, discernir entre los mRNAs "propios" y de los provenientes de agentes patógenos principalmente virales, que pueden no tener cap (26)(27).

El cap es añadido al extremo 5´ de los RNAs transcritos por la RNA polimerasa II (RNA pol II) en el núcleo de la célula; la RNA pol II es responsable de la transcripción de los pre-mRNAs, pre-miRNAs (miRNAs), pre-lncRNA (RNAs largos no codificantes), snoRNAs (RNAs pequeños nucleolares) y snRNAs (RNAs pequeños nucleares). Todos estos transcritos contienen cap en su extremo 5´, sin

embargo, algunos como los pre-miRNAs lo pierden durante el proceso de maduración, mientras que los snRNAs y los snoRNAs sufren otras modificaciones como la adición de tri-metilguanosina.

La adición de cap es la primera modificación que se realiza a los RNAs generados por la RNA polimerasa II, que se lleva a cabo co-transcripcionalmente, justo después de agregar los primeros 25 a 30 nucleótidos del transcrito naciente (27).

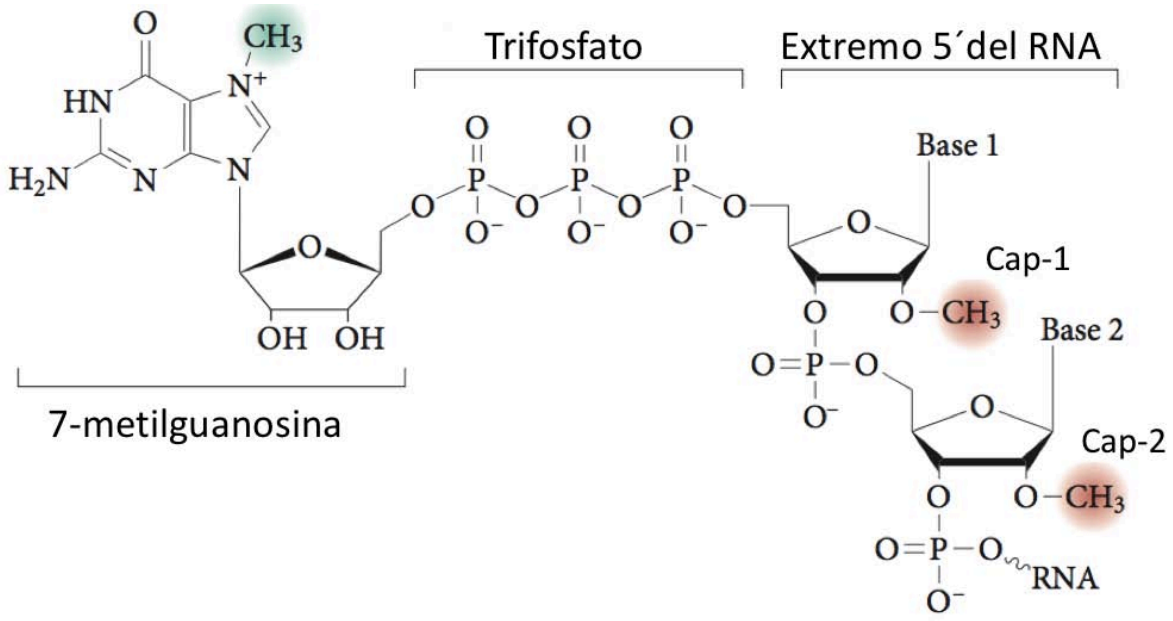

Figura 3. Estructura química del cap presente en los mRNAs. La estructura cap consiste de una 7-metilguanosina unida mediante un enlace 5´-5´-trifosfato al primer nucleótido del transcrito naciente. El grupo metilo en la posición N7 se muestra en verde, mientras que el 2´O metilo en el primer y segundo residuo que forman el cap-1 y cap-2, respectivamente, se muestran en rojo. Modificado de (28).

La vía canónica de adición de cap consiste en la acción secuencial de tres enzimas las cuales convierten el extremo 5´trifosfato del RNA naciente en la

estructura cap tipo 0 (Figura 4). Primero, la RNA 5´trifosfatasa (RTasa) hidroliza el γ-fosfato del extremo 5´trifosfato para generar un RNA 5´di-fosfato. El siguiente paso es la transferencia de una guanosina monofosfato (GMP), tomada de un GTP, al extremo 5´del RNA, esta reacción es catalizada por la RNA guanililtransferasa (GTasa). En el tercer paso, la enzima guanina-N7 metiltransferasa (N7-MTasa) transfiere un grupo metilo proveniente de la S-adenosilmetionina (SAM) a la posición N7 de la guanina terminal, con este paso se completa la síntesis de la estructura cap tipo 0 (29).

Adicionalmente, la m7G RNA 2´-O-ribosa metiltransferasa (2´-O- MTasa) metila la posición 2´O de las ribosas +1 y +2 generando las estructuras cap tipo 1 y tipo 2, respectivamente; mientras que la adición de la 2´O de la ribosa +1 se lleva a cabo en el núcleo, la adición en +2 se realiza tanto en el núcleo como en citoplasma (Figura 3) (30). En el citoplasma de las células eucariontes, el cap tipo 1 presente en los mRNAs es importante en la identificación de RNAs foráneos por parte del sistema inmune innato ya que los RNAs con grupos tri- o di- fosfatos en el extremo 5´ son reconocidos por la proteína RIG-I induciendo la expresión de interferón (IFN) a través de una cascada de señalización (31)(32). Por otra parte, el cap tipo 2 participa en el incremento de la traducción de mRNAs celulares (30).

Recientemente, se han descrito diferentes estructuras de cap no canónicas, las cuales están compuestas de coenzimas, como la nicotinamida adenina dinucleótido (NAD) que inicialmente fueron encontradas en estructuras parecidas al cap en RNAs bacterianos, aunque también han sido encontradas en mRNAs de levaduras y humanos. El nivel de adición de NAD-cap en los mRNAs está

determinado en parte por la concentración celular de NAD y está relacionada con la estabilidad de los mRNAs (33). Aunque se han identificado bajas concentraciones de otros tipos de cap no canónicos tanto en RNAs celulares como virales, su función, mecanismos de adición y relevancia aún no han sido estudiados (34).

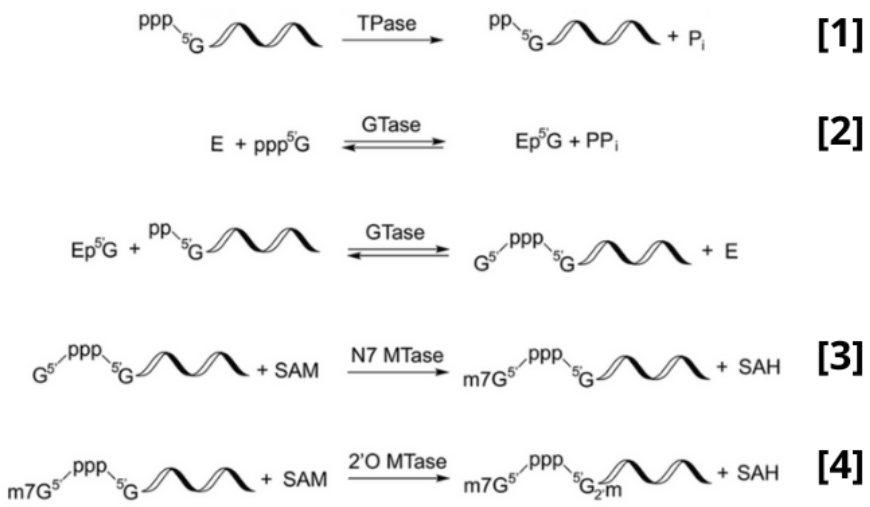

Figura 4. Esquema de las reacciones enzimáticas involucradas en la adición de cap al mRNA. 1) La RNA 5´ trifosfatasa (RTasa) hidroliza el γ-fosfato del extremo 5´trifosfato para generar un RNA 5´difosfato y un fosfato inorgánico. 2) La RNA guanililtransferasa (GTasa) toma una molécula de GTP y forma un intermediario que contiene un enlace lisil-N-5´-fosofoguanosina. En presencia de un RNA con 5´difosfato, la actividad GTasa transfiere la 5´-fosfoguanosina (GMP) a el 5´difosfato, formando un enlace 5´-5´trifosfato entre la primera base del RNA y la base del cap. 3) En presencia de S-adenosilmetionina (SAM), la enzima guanina-N7 metiltransferasa (MTasa) agrega un grupo metilo a la amina N7 de la guanosina del cap, formando la estructura cap 0. 4) Finalmente, la m7G cap-especifica 2´O MTasa modifica el 2´O de la ribosa +1 y genera la estructura cap 1. Modificado de (32).

Proteínas de unión al cap involucradas en la respuesta inmune antiviral

En el citoplasma de las células se encuentran receptores de reconocimiento de patrones (PRRs del inglés Pattern Recognition Receptors), los cuales son componentes del sistema inmune innato que reconocen RNAs producto de infecciones virales. Ejemplo de ello son las proteínas RIG-I (del inglés Retinoic Acid Inducible I; DDX58) y MDA5 (del inglés Melanoma Differentiation-Associated protein 5), las que, al detectar a su ligando, inician una cascada de señalización que culmina con la expresión de citosinas e interferón (IFN) tipo I, induciendo un estado antiviral en las células vecinas.

La proteína MDA-5 reconoce la presencia de fragmentos largos de dsRNA en el citoplasma; mientras que RIG-I reconoce tanto fragmentos cortos de dsRNA como grupos tri- o di-fosfato en el extremo 5´terminal del RNA (35). La estructura cap tipo 1 inhibe la interacción de dsRNA con RIG-I y MDA5 evitando la activación de la vía de señalamiento de IFN (36). La activación de RIG-I estimula la expresión de proteínas IFIT (del inglés IFN- Induced Protein with Tetratricopeptide Repeats), que se unen al mRNA con estructuras cap que no tienen el grupo 2´O metil, inhibiendo la traducción de los RNAs virales. La proteína IFIT1 se une a estructuras cap incompletas, que incluyen: m7G(5´)ppp(5´)G, G(5´)ppp(5´)G y A(5´)ppp(5´)G; pero no se unen a RNAs que tienen el primer o segundo nucleótido con la ribosa O-2 metilada. Por otra parte, IFIT5 se une solamente a RNAs sin cap con grupos trifosfato en el extremo 5´(37)(38). Este conjunto de proteínas sensoras-efectoras del sistema inmune innato tienen como función el reconocer RNAs foráneos, provenientes de infecciones virales que no tienen modificaciones en el extremo 5´.

Síntesis de cap en virus

Algunos virus que infectan células eucarióticas incorporan la estructura cap en el extremo 5´ de sus mRNAs virales para poder incrementar la síntesis de sus proteínas y para enmascarar sus mRNAs de la detección del sistema inmune innato del hospedero. Las enzimas involucradas en la adición del cap se localizan en el núcleo, por lo que los virus que llevan a cabo su ciclo de replicación en el citoplasma han evolucionado diferentes estrategias que les permiten producir y agregar la estructura cap a sus mRNAs sin depender de las proteínas nucleares.

En comparación a la vía canónica de adición de cap, los mecanismos que emplean los virus para agregarlo a sus mRNAs son muy diversos tanto en componentes genéticos, dominio organizacional de las proteínas, estructuras de las enzimas y mecanismos de reacción, aunque en todos los casos culminan en la síntesis de una estructura cap similar a la de los mRNAs del hospedero.

A grandes rasgos, la estructura cap puede ser agregada a los RNAs virales a través de uno de los siguientes tres mecanismos: 1) los utilizan la RNA polimerasa II celular para sintetizar sus mRNAs y en consecuencia son procesados como mRNAs celulares; 2) los que han evolucionado diversas enzimas especializadas en la adición del cap, que se encuentran codificadas en su genoma; y 3) los que se apropian de las estructuras cap de los mRNAs celulares, en un proceso llamado `cap snatching´.

Adición de cap en RNA virales por vías no canonicas

Adición de cap en alfavirus

En los alfavirus (Ej. virus Sindbis y chikungunya) el cap es adicionando por las proteínas virales nsP1 y nsP2, que interaccionan y actúan en conjunto con la proteína viral nsP4 que es la RNA polimerasa dependiente de RNA (RdRp). La proteína nsP1 tiene las actividades enzimáticas de GTasa y N7-guanilil MTasa, mientras que la actividad de RTPasa se encuentra en la proteína nsP2. El mecanismo de adición de cap en alfavirus es diferente al canónico ya que en el primer paso el GTP es metilado y se une a la GTasa como m7GMP, que posteriormente es transferido a un ppRNA para formar m7G-cap (39). Es decir, la metilación de GMP ocurre antes de la formación del enlace 5´-5´trifosfato entre el GMP y el transcrito naciente.

Cap snatching (robo de cap)

Algunos virus no codifican una maquinaria que les permita la adición de cap a sus mRNAs, por lo que estos virus pueden “robar” la estructura cap del RNA del hospedero en un proceso llamado `cap snatching´. Este método fue inicialmente descrito en el virus de influenza, un virus de ss(-)RNA perteneciente a la familia *Ortomixoviridae*. Además de esta familia los virus pertenecientes a las familias *Bunyaviridae* y *Arenaviridae* también emplean este mecanismo para adicionar la estructura cap a sus mRNAs. En el virus de influenza, la RdRp es un complejo formado por tres proteínas: las proteínas básicas de la polimerasa 1 y 2 (PB1 y PB2) y la proteína ácida de la polimerasa (PA). En el núcleo, la subunidad PB2 se une a

mRNAs celulares con cap a través de un dominio de unión al cap que reconoce el 5´ metilo presente en el cap tipo 1 de los mRNAs del hospedero. Posteriormente, la actividad de endonucleasa localizada en el amino terminal de la proteína PA corta los primeros 10-15 nucleótidos (nt) del RNA con cap, este fragmento se une a los mRNAs transcritos por el virus que no contienen cap (40). En los virus de la familia *Arenaviridae,* la endonucleasa genera un RNA mucho más corto, con un tamaño de 4 a 7 nt.

Por otra parte, los arenavirus y bunyavirus codifican por una sola proteína (proteína L), que tiene ambas actividades (polimerasa y cap-snatching), aunque aún no es claro cuáles son los dominios de la proteína involucrados en cada uno de estos procesos. Los RNAs virales con cap “robados” son posteriormente utilizados como iniciadores de la síntesis de mRNA por la RNA polimerasa viral. De esta manera los virus que llevan a cabo esta estrategia bloquean la expresión de RNAs celulares, y a la vez favorecen la expresión de los mRNAs virales. Contrario a lo que se pensaba, recientemente se encontró que el virus de la influenza tiene preferencia por obtener el cap de los RNAs no codificantes como los snRNAs U1 y U2, en lugar de los mRNAs o pre-mRNAs (41).

ANTECEDENTES

Adición de cap en rotavirus por la proteína viral VP3

La proteína viral VP3 es una proteína multifuncional codificada en el segmento 3 del genoma de rotavirus, tiene un peso molecular aproximado de 88 kDa y se encuentra en pocas cantidades en la capa más interna de los viriones (12 a 24 copias de esta proteína por virión). La organización de los dominios de VP3 de diferentes cepas de rotavirus ha sido obtenida mediante estudios funcionales y bioinformáticos (Figura 5) (42). Estructuralmente, esta proteína contiene todos los dominios que le permiten tener actividad de metil-guanilil-transferasa, lo que le permite adicionar la estructura cap en el extremo 5´ de los transcritos virales nacientes y su 2´O metilación.

La actividad de adición del cap de VP3 ha sido ampliamente estudiada mediante diferentes enfoques que incluyen estudios bioquímicos y estructurales, lo que ha permitido caracterizar sus diferentes funciones. Estudios realizados con partículas virales de rotavirus purificadas demostraron que VP3 se une al +RNA de una sola cadena (ss+RNA), presentando una mayor afinidad al RNA sin cap. Además, VP3 se une de manera covalente y reversible a GMP y puede transferir este residuo a pirofosfatos o a GDP, lo que es consistente con la actividad guanililtransferasa. También, en presencia de S-adenosil-metionina (SAM) la VP3 contenida en las partículas virales pueden metilar la estructura cap, es decir VP3 posee la actividad de metil-transferasa la cual depende de la presencia de SAM (43)(44). Recientemente, mediante estudios bioquímicos se demostró que VP3, además, posee las actividades de RTPasa y helicasa. En conjunto estas actividades

presentes en VP3 le permiten adicionar cap tipo 1 a los transcritos virales de rotavirus. La presencia de cap tipo 1 en los mensajeros virales es un mecanismo que permite la evasión de proteínas del sistema inmune innato ya que evita que los transcritos virales sean detectados en el citoplasma por las proteínas MDA-5 y RIG-I (45); además, también evita el reconocimiento de sus proteínas efectoras IFITIM-1 y IFITIM-5 (46).

Además de los dominios responsables de la adición de cap, la proteína VP3 de los rotavirus del grupo A tiene en el dominio carboxilo terminal una actividad de 2´-5´-fosfodiesterasa (PDE), por medio de la cual degrada a los 2´-5´oligoadenilatos (2´-5´ As), que se sintetizan en la célula infectada a través de las oligoadenilato sintetasas (OAS). Los 2´-5´ As activan específicamente a la RNasa L, que es una RNasa inespecífica que degrada RNA celular y viral. La actividad de PDE de VP3 inhibiendo la activación de la vía 2´-5´-oligoadenilato sintetasa (OAS)-RNasa L, ha sido estudiada en sistemas *in vitro* e *in vivo* y se abordará con mayor detalle más adelante (47)(45). Como se puede notar, la multifuncionalidad de la proteína VP3 de los rotavirus del grupo A, puede contribuir a la evasión de la respuesta inmune del hospedero por dos mecanismos; de manera indirecta (mediante la adición de cap) y de manera directa (a través de la degradación de los 2´-5´A).

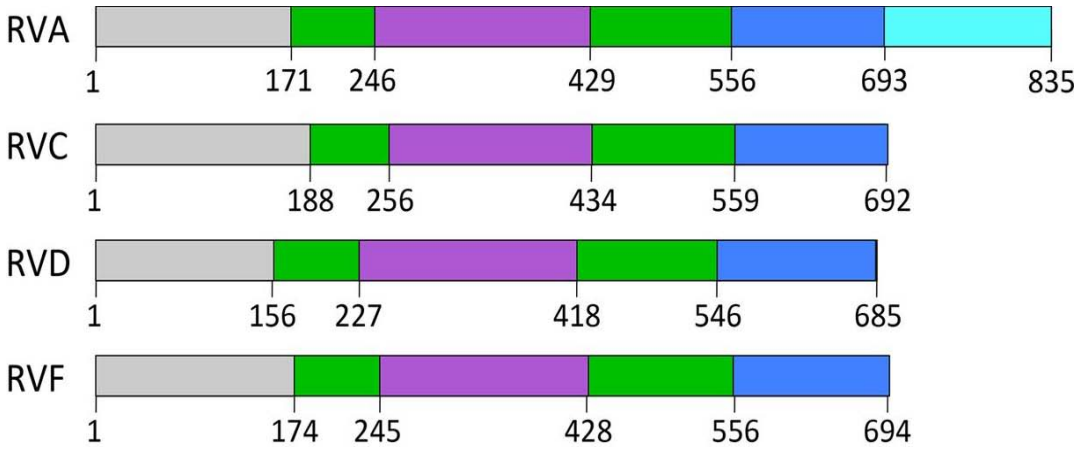

Figura 5. Predicción bioinformática de la organización de dominios de VP3 de diferentes especies de rotavirus. Los diferentes dominios son marcados y coloreados de acuerdo a su función predicha: gris, función no conocida; verde, N7-MTasa; purpura, 2´-O-MTasa; azul, GTasa/RTPasa; turquesa, PDE. Tomado de (42).

Dominios presentes en VP3

Debido a las dificultades en la purificación de la proteína recombinante VP3 y al bajo número de copias presente en las partículas virales, durante mucho tiempo no se contó con su estructura cristalográfica, limitando el estudio de las bases moleculares de sus diferentes actividades enzimáticas.

Recientemente Kumar et al publicaron la estructura cristalográfica de la proteína VP3 (residuos 1 al 835; 98 kDa) y mediante ensayos de cromatografía de exclusión de tamaño y análisis de ultracentrifugación analítica se determinó que esta proteína forma un tetrámero muy estable en diferentes rangos de pH y concentraciones de sales. El monómero de VP3 presenta una organización modular que consta de 5 dominios (Figura 6): el dominio N-terminal cinasa-like [(KL) residuos 1 -181]; el dominio guanina-N7 MTasa [(N7-MTasa) residuos 182 - 255 y 441 - 560],

este dominio está inter-espaciado por el domino ribosa 2´-O-MTasa (residuos 256-440); y el dominio GTasa (residuos 694 al 835), que está unido al domino N-terminal PDE (residuos 694 al 835) (48)(42). Los dominios presentes en VP3 son similares en cuanto a su función y organización a los que tiene la proteína VP4 del virus Bluetongue (BTV), otro miembro de la familia *Reoviridae*, con la excepción del dominio PDE, que no se encuentra en la VP4 de BTV (49).

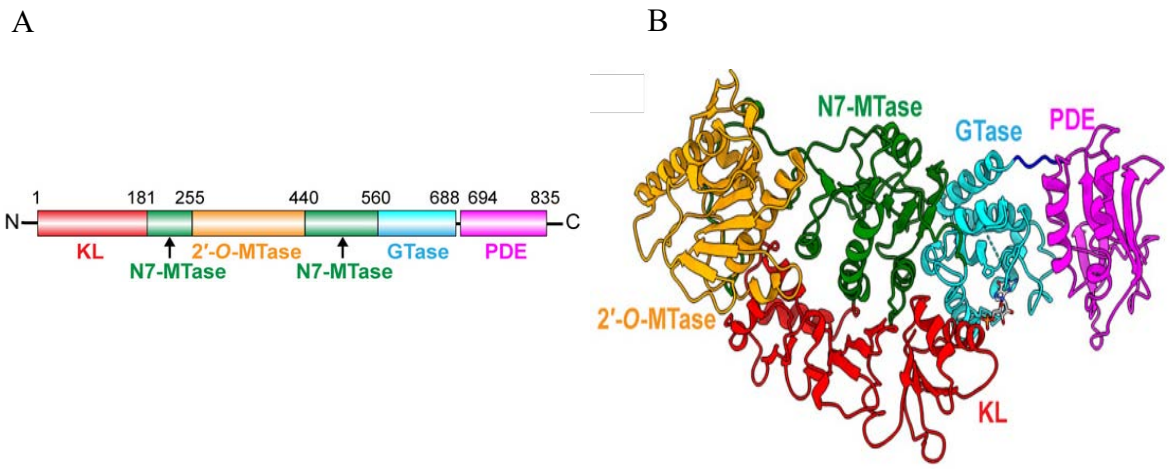

Figura 6. Organización de los dominios presentes en el monómero de VP3 obtenidos a partir de la estructura cristalográfica. A) Localización de los dominios a lo largo de la cadena peptídica de VP3, basada en la anotación estructural. B) Organización modular de los dominios del monómero de VP3. Las actividades que presenta cada dominio se muestran en la figura. Imagen tomada de (48).

El estudio de Kumar et al, permitió encontrar dos nuevas funciones de VP3 que no se habían reportado. La actividad RTPasa/NTPasa, necesaria para la síntesis del cap y la actividad de helicasa. Previamente, la única proteína de rotavirus con actividad RTPasa/NTPasa conocida, era la proteína no estructural NSP2 (50); sin embargo, esta proteína no se encuentra en el core del virus por lo que no se había dilucidado el mecanismo por el cual se removía el γ-fosfato de los

transcritos nacientes, necesario para la adición del cap. Kumar et al, demostraron que VP3 posee una actividad RTPasa en el dominio PDE, que se encarga de remover el γ-fosfato presente en el extremo 5´del mRNA. Además, encontraron que VP3 tiene una actividad de helicasa, que se encarga de separar las cadenas del dsRNA viral para que se pueda agregar el cap, aunque el mecanismo por el cual esta actividad se lleva a cabo, aún no es claro (48).

Modelo de adición de cap en partículas virales

Como se mencionó previamente, el "core" de las partículas virales de rotavirus está formado por las proteínas VP1, VP2 y VP3. La proteína VP1 es la RNA polimerasa dependiente de RNA (RdRp), esta proteína transcribe los +RNAs a partir del dsRNA genómico, y también sintetiza la cadena complementaria -RNA generando el dsRNA genómico que es empacado en los "cores" (51). VP1 interacciona directamente con las proteínas VP2 y VP3; la interacción entre el dominio amino terminal de VP2 con VP1 y VP3 induce su nucleación, permitiendo que sean incorporadas en las partículas virales. Además, la interacción de estas proteínas también es importante para activar la actividad de RdRp de VP1, permitiendo la generación de dsRNA a partir del +RNA (52)(53).

Por otra parte, VP1 también interacciona directamente con VP3, encargada de adicionar la estructura cap a los mRNAs sintetizados por VP1. Aunque aún no se ha reportado la estructura cristalográfica del complejo VP1/VP3, la obtención de la estructura de VP3 y el conocimiento previo del proceso de transcripción ha permitido proponer un mecanismo conjunto de acción de ambas proteínas (2)(48).

En este se sugiere que la proteína VP3 es incorporada a las partículas virales en forma de tetrámero y se encuentra asociada a VP1 dentro del “core”; durante la transcripción, el dúplex formado por la cadena molde y el transcrito naciente generado por VP1 es separado por la actividad de helicasa asociada a VP3. Mientras el transcrito naciente es sometido a la adición del cap, el molde vuelve a formar un dúplex con la cadena positiva para seguir un proceso de transcripción iterativa. En este modelo el transcrito pasa a través del dominio GTasa y después por el dominio MTasa y después continua con el proceso de adición de cap. De manera similar, otro transcrito, generado por la VP1 adyacente al otro extremo del tetrámero de VP3, puede sufrir el mismo proceso enzimático, generando una producción simultánea de transcritos con cap (Figura 7)(48).

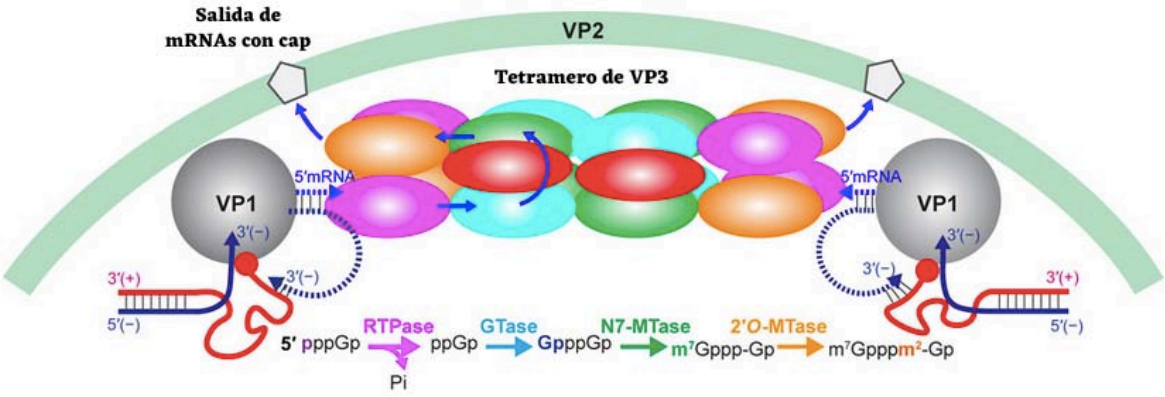

Figura 7. Modelo propuesto de la adición de cap durante la transcripción. Representación de una posible ruta para la salida del transcrito naciente sintetizado por VP1 que emerge a través de los dominios PDE y GTasa de una subunidad de VP3 y el dominio MTasa de la subunidad adyacente de VP3, seguido de su salida a través del canal de salida más cercano de la DLP. Antes de la adición del cap, el dúplex de dsRNA formado por el transcrito naciente y la cadena molde necesitan ser separados. Se sugiere que la

actividad de helicasa de VP3 tiene un papel importante en la separación del dúplex, para posteriormente favorecer la adición de cap en el extremo 5´. Imagen modificada de (48).

En rotavirus la actividad de adición de cap la lleva a cabo la proteína viral VP3, Uzri y colaboradores caracterizaron mediante ensayos enzimáticos el extremo 5´de los RNAs virales. En ese estudio emplearon transcritos sintetizados *in vitro* por las DLPs virales y RNAs purificados de células infectadas a las 6 horas post infección; para determinar el nivel de cap de estos mRNAs, éstos fueron transfectados en células de hepatoma humano Huh7 y se midió la expresión del gen reportero IFN-beta acoplado a luciferasa. Encontraron que ambos tipos de RNAs (sintetizado in vitro o aislado de células infectadas) contienen una población de RNAs sin cap los cuales presentan grupos fosfatos expuestos en el extremo 5´. Por otra parte, se identificó una población de RNAs que si bien presentan cap está carece de la 2´-O-metilación (59). Estos datos sugieren que la proteína VP3 no adiciona el cap de manera eficiente a los transcritos virales. Aunque este trabajo permitió identificar la presencia o ausencia del cap en los RNAs virales, este análisis se limitó a la caracterización de dos tipos de RNAs; los producidos en la transcripción *in vitro* y los purificados a las 6 hpi, además la caracterización se llevó a cabo empleando un método indirecto el cual no permite caracterizar las poblaciones de RNA con o sin cap de manera cuantitativa.

La presencia de cap en los transcritos y el genoma de rotavirus ha sido caracterizada empleando diferentes metodologías que incluyen ensayos de cromatografía de RNAs con marca radiactiva que habían sido tratados química o enzimáticamente (43). Estos estudios permitieron identificar las secuencias del

extremo 5´ terminal, así como el tipo de cap presente en los mRNAs de rotavirus. Sin embargo, mediante estos ensayos no fue posible determinar la abundancia relativa del cap en los RNAs virales. En el presente trabajo caracterizamos de manera cuantitativa la presencia de cap en diversas poblaciones de RNAs virales incluyendo: el dsRNA genómico presente en partículas virales purificadas; el RNA transcrito *in vitro*; el RNA viral sintetizado a diferentes tiempos durante la infección y además la cantidad de cap en RNA viral que se produce en condiciones en las que la expresión de VP3 y RNasa L fueron silenciadas por RNAs de interferencia (RNAi). La caracterización de estas poblaciones de RNA viral nos permitirá explorar si el cap cumple alguna función no tradicional durante el ciclo replicativo de rotavirus.

HIPÓTESIS

La proteína VP3 adiciona de manera eficiente la estructura cap a los extremos 5´ de los transcritos virales.

OBJETIVO GENERAL

Determinar cuantitativamente la presencia de cap en el extremo 5´ del +RNA de rotavirus bajo diferentes condiciones.

OBJETIVOS PARTICULARES

1.- Determinar si el RNA encapsidado en las partículas virales maduras posee cap.

2.- Determinar la eficiencia de adición de cap de la proteína viral VP3.

3.- Evaluar la presencia del cap en los +RNAs virales durante la infección por rotavirus.

4.- Determinar si el silenciamiento o co-silenciamiento de las proteínas VP3 y RNasa L afectan la abundancia del cap en los RNAs virales.

MATERIALES Y MÉTODOS

Cultivo celular y virus

En este estudio se utilizó la línea celular MA104 (ATCC: CRL-2378.1) derivada de epitelio renal de mono verde (Cercopitecus aethiops), la cual fue cultivada en medio mínimo esencial Eagle (MEM) Advance (Thermo Scientific HyClone, Logan, UT) suplementado con 5% V/V de suero fetal bovino (SFB, Biowest, Kansas City, MO) inactivado por calor. Los cultivos fueron incubados en atmosfera húmeda con 5% de CO_2 a 37ºC.

La cepa de rotavirus de simio Rhesus (RRV) proporcionada por H. B. Greenberg (Universidad de Stanford, Stanford, CA) fue utilizada en este trabajo. Para su propagación se utilizaron células MA104 en medio MEM sin SFB, suplementado con 2 μg/mL de glutamina. El lisado viral fue activado durante 30 minutos a 37ºC con tripsina (Gibco Life Technologies, Carlsbad, CA) a una concentración de 10 μg/mL. El virus activado fue adicionado a las células y se incubó durante 1 h a 37ºC, posteriormente el inóculo fue retirado, se agregó medio MEM sin SFB y se incubó por 18 h en atmosfera húmeda con 5% de CO_2 a 37ºC. Las células fueron sometidas a tres ciclos de congelamiento descongelamiento, el lisado celular se centrifugó para eliminar los restos celulares y se almacenó en alícuotas a -70ºC. El titulo viral fue determinado como se describe en la sección de ensayo de inmunoperoxidasa.

Anticuerpos y reactivos

Los anticuerpos primarios empleados en este estudio se resumen en la Tabla 1. Los anticuerpos; cabra anti-ratón y cabra anti-conejo acoplados a la enzima peroxidasa (PerkinElmer Life Sciences [Boston, MA, USA]) fueron utilizados como anticuerpos secundarios.

Tabla 1. Anticuerpos empleados en el estudio.

Anticuerpo	Antígeno	Clonalidad	Especie	Fabricante
α-VP3	VP3 de la cepa RRV	Policlonal	Conejo	GenScript (Nueva Jersey, Estados Unidos)
α-RNasa L	RNasa L recombinante	Monoclonal	Ratón	Abcam (Cambridge, Reino Unido)
α-TLPs	Proteínas estructurales de diferentes cepas de rotavirus	Policlonal	Conejo	Preparado en el laboratorio de la Dra. Susana López y Dr. Carlos Arias (Cuernavaca, Morelos, México)
α-Vimentina	Vimentina humana recombinante	Policlonal	Conejo	Preparado en el laboratorio de la Dra. Susana López y Dr. Carlos Arias (Cuernavaca, Morelos, México)

Determinación de título viral

Células MA104 crecidas a confluencia en placas de 96 pozos se lavaron dos veces con MEM; posteriormente, fueron inoculadas con diluciones seriadas de los lisados virales durante 1 h a 37ºC, se retiró el inóculo viral y se incubó con MEM durante 16 h a 37ºC en atmosfera húmeda con 5% de CO_2 a 37ºC. Previo a la inoculación, los lisados virales fueron activados como se describió en la sección de cultivo celular y virus. Pasadas las 16 horas el medio fue retirado y las células fueron fijadas y permeabilizadas con acetona al 80% en PBS 1X durante 20 minutos a

temperatura ambiente (TA). Finalmente, el título viral fue determinado mediante ensayos de inmunoperoxidasa.

Ensayo de inmunoperoxidasa

Para realizar estos ensayos las células fueron fijadas y permeabilizadas con acetona al 80% durante 20 min, posteriormente se incubaron con el anticuerpo primario α-TLPs diluido 1:3000 en PBS 1X durante 1 h a TA, se retiró el anticuerpo y se lavó con PBS 1X dos veces. Después, se colocó el anticuerpo secundario α-conejo peroxidasa diluido 1:3000 en PBS 1X y se incubó durante 1 h a TA. Transcurrido el tiempo el anticuerpo fue retirado, las células fueron lavadas dos veces con PBS 1X y se procedió a revelar la actividad peroxidasa con 3-amino-9-etil carbazol (AEC) (1 mg/ml) en buffer de acetato de sodio (50 mM), pH 5.0 y 0.04% de H_2O_2. Después de observar la presencia de color la reacción fue detenida lavando con agua en varias ocasiones. El conteo de focos infecciosos se llevó a cabo con el objetivo 20X en un microscopio invertido (Leika, Alemania) recorriendo los campos contenidos a lo largo de una banda central del pozo.

Transfección de siRNAs

Los ensayos de transfección o co-transfección de siRNAs (del inglés “small interfering RNA”) fueron realizados mediante transfección reversa como se describió previamente (16). Las secuencias de los siRNAs y las concentraciones a los que fueron utilizados se describen en la Tabla 2. Como agente transfectante se empleo oligofectamina (Invitrogen, Carlsbad, CA). Las células junto con la mezcla

de transfectante y siRNA fueron incubadas durante 72 h a 37ºC, posteriormente fue retirada y se realizó el tratamiento indicado en el texto.

Tabla 2. Secuencias de siRNAs empleados en el estudio

Nombre	Secuencia en sentido 5´-3´	Concentración empleada [μM]
VP3	GAA GGU AUG UUG UGU UAA AGA UU	2.5
RNase L	SMARTpool: ON-TARGETplus siRNA	2.5
Non-targeting	siGENOME Non-Targeting siRNA #3	La misma concentración que el siRNA de prueba

Análisis de proteínas por Western Blot

Las células obtenidas en las diferentes condiciones fueron lisadas con el buffer Laemli (50 mM Tris-HCl pH 6.8, 2% SDS, 0.1% azul de bromofenol, 10% glicerol, 5% β-mercaptoetanol) y después se hirvieron durante 5 min. Las proteínas fueron separadas mediante electroforesis desnaturalizante en geles de poliacrilamida-SDS (SDS-PAGE) al 10% y transferidas a una membrana Immobilon NC (Millipore Merck KGaA, Darmstadt, Germany) en buffer CAPS 1X (10 mM, pH 11), adicionado con 10% de metanol durante 1 h con una corriente de 130 mA. Posteriormente, la membrana fue bloqueada con solución de bloqueo (5% de leche baja en grasa, 0.1% tween 20 en PBS 1X) en agitación constante durante 1 h a TA o durante toda la noche a 4ºC. El exceso de leche fue retirado y se realizaron 3 lavados rápidos con la solución de lavado (PBS/Tween-20 0.1%). Después, la membrana se incubó con los anticuerpos primarios que se indican a las siguientes concentraciones: α-VP3 (1:3000), α-RNase L (1:2000), α-TLPs (1:3000) o α-vimentina (1:3000). Los anticuerpos fueron diluidos en solución de bloqueo y se

incubaron durante 1 h a TA o durante toda la noche a 4°C en agitación constante. Pasado el tiempo, el anticuerpo primario fue retirado y la membrana se lavó 3 veces durante 10 min con solución de lavado. Después de los lavados, la membrana se incubó con el anticuerpo secundario (α-conejo o α-ratón) o proteína A acoplada a la enzima peroxidasa (1:3000 [GE Healthcare]) durante 1 h a TA. Posteriormente, se lavó 3 veces durante 10 min con solución de lavado. Finalmente, las proteínas se detectaron con el sustrato para peroxidasa Western Lightning®-ECL, Enhanced Chemiluminescence Substrate (Perkin-Elmer, Massachusetts, USA) de acuerdo a las instrucciones del proveedor, empleando la película hipersensible Kodak Medical X-Ray film (Carestream, Jalisco, México).

Purificación de partículas virales de doble y triple capa (DLPs y TLPs)

Células MA104 fueron crecidas a confluencia en placas de 150-cm^2, las monocapas fueron infectadas con la cepa de rotavirus RRV a una multiplicidad de infección (MOI) de 3, a las 12 horas post infección (hpi) las células fueron lisadas mediante 3 ciclos de congelamiento y descongelamiento y posteriormente los lisados fueron sonicados. Las partículas virales fueron concentradas por ultracentrifugación durante 1 h a 30,000 rpm a 4ºC en un rotor SW55Ti (Beckman, Fullerton, CA). Los botones celulares (pellets) obtenidos fueron resuspendidos en buffer TNC frío (10 mM Tris-HCl pH 7.5, 140 mM NaCl, 10 mM $CaCl_2$). Después, se realizaron al menos dos extracciones con triclorofluorometano (Freón), recolectando la fase acuosa.

Para purificar TLPs o DLPs, a las fases acuosas colectadas durante la extracción con freón se les agregó CsCl para obtener una densidad de 1.38 g/cm^3,

esta mezcla fue centrifugada por 18 h a 36,000 rpm en un rotor SW55 Ti (Beckman, Fullerton, CA) a 4ºC. Las bandas opalescentes correspondientes a TLPs o DLPs fueron colectadas mediante punción con la ayuda de una jeringa de 3 mL y fueron almacenadas a 4 ºC. Antes de ser utilizadas en los diferentes ensayos, el ClCs unido a las partículas virales fue eliminado mediante columnas de sephadex G-25 coarse. Para esto, un volumen de 18 μl de partículas virales fue pasado por una columna de resina sephadex G-25 empacada en puntas estériles de 200 μl de micropipeta. La columna de sephadex fue lavada con buffer TNC o TNE (10 mM Tris-HCl pH 7.5, 140 mM NaCl, 10 mM EGTA pH 8) cuando se requería eliminar el ClCs de las fracciones correspondientes a TLPs o DLPs, respectivamente. Para eliminar la posible contaminación de (+)RNAs de origen viral o celular unido a la parte externa de las partículas virales, las TLPs purificadas fueron tratadas con 10 μg de RNasa A por 15 min a 37 ºC, para posteriormente proceder a la purificación del dsRNA genómico con el reactivo TRIzol (Ambion-Life Technologies, Carlsban, CA) como se indica en el manual de usuario.

Para obtener partículas virales a partir de células infectadas en las que VP3 y RNasa L fueron silenciadas o co-silenciadas, células MA104 crecidas en placas de 6 pozos fueron transfectadas con el siRNA indicado como se describió previamente (45). A las 72 h post transfección (hpt), las células fueron infectadas con rotavirus RRV a una MOI de 3. A las 12 hpi las células fueron lisadas mediante 3 ciclos de congelamiento descongelamiento, sonicadas con 4 pulsos de 20s y después se realizaron al menos 2 extracciones con triclorofluorometano (Freón), recolectando la fase acuosa. La suspensión viral fue concentrada utilizando un

colchón de sacarosa al 40% mediante centrifugación por 2 h a 40,000 rpm; rotor SW55Ti (Beckman, Fullerton, CA) a 4ºC. El pellet viral fue resuspendido en buffer TNC, cuando se requerían TLPs o en buffer TNE para remover las proteínas de capa externa de las partículas virales y obtener DLPs.

Ensayos de transcripción *in vitro*

Para realizar estos ensayos se emplearon partículas virales de doble capa (DLPs) obtenidas de las condiciones que se indican en el texto, las DLPs fueron purificadas como se describe en la sección anterior. Las reacciones de transcripción *in vitro* se llevaron acabo de la siguiente manera: 2.4 μg de DLPs purificadas se incubaron con una mezcla de reacción que contiene 8 mM ATP, 2.5 mM GTP, 2.5 mM CTP, 2.5 mM UTP (Ambion, Carlsban, CA), 0.5 mM S-adenosilmetionina (SAM, NEB, Ipswich, MA), 0.5 U/μl RNasin (Thermo Scientific, Waltham, MA), buffer de transcripción (140 mM Tris-HCl pH 8, 200 mM acetato de sodio y 40 mM acetato de magnesio) y 4% de bentonita. La reacción fue incubada por 6 h a 42ºC, después se centrifugó por 1 min a 14,000 rpm para remover la bentonita, inmediatamente después el RNA presente en el sobrenadante fue purificado por extracción fenol:cloroformo y precipitado con 4M de LiCl durante toda la noche a 4ºC. El RNA fue sedimentado por centrifugación durante 15 min a 13,500 rpm a 4ºC, se lavó 2 veces con etanol al 80%, fue secado y resuspendido en agua grado biología molecular libre de RNasas. La concentración de RNA fue determinada por absorbancia empleando el espectrofotómetro NanoDrop. Finalmente, el RNA fue almacenado en alícuotas a -70ºC y descongelado hasta su uso.

Obtención de RNA viral para los ensayos de cuantificación de cap

Monocapas de células MA104 crecidas en placas de 6 pozos se infectaron con RRV a una MOI de 10 durante 1 h a 37ºC; posteriormente, se retiró el inóculo viral y se incubó con MEM en atmosfera húmeda con 5% de CO_2 a 37ºC. A los tiempos indicados, el RNA total fue extraído y purificado con TRIzol como se indica en el manual de usuario. El RNA viral de las reacciones de transcripción *in vitro*, el dsRNA genómico de partículas virales y el RNA total de células infectadas fue obtenido como se indica en el texto. Posteriormente, la concentración de RNA fue determinada por absorbancia empleando el espectrofotómetro NanoDrop, el RNA fue dividido en alícuotas y almacenado a -70 ºC hasta su uso. Con el fin de no comprometer la integridad del RNA, se evitó que las alícuotas se sometieran a más de 2 ciclos de congelamiento y descongelamiento.

Para la caracterización del extremo 5´ de los RNAs virales se emplearon las siguientes cantidades de RNA: 250 ng de RNA purificado a partir de partículas virales u obtenido de las reacciones de transcripción *in vitro*; 1 μg de RNA total obtenido de células infectadas o células infectadas tratadas con el siRNA indicado.

Caracterización de los extremos 5´de los RNAs virales

Para caracterizar el extremo 5´ de la cadena positiva de los RNAs virales de rotavirus (ss+RNAs), se llevó a cabo un procesamiento enzimático seguido del análisis por RT-qPCR como fue descrito previamente (55). El ensayo fue utilizado en la caracterización de la estructura cap del RNA genómico del virus Sindbis (SINV). El protocolo que realizamos presenta modificaciones que se detallan a continuación (Figura 8 A): El primer paso consiste en incubar el RNA con la enzima

Fosfatasa Antártica (NEB, Ipswich, MA) por 1 h a 37ºC para eliminar los grupos fosfatos del extremo 5´. Después, la reacción fue inactivada por calor colocándola por 5 min a 80ºC. Posteriormente, la reacción fue dividida en dos alícuotas del mismo volumen para llevar acabo, en paralelo, el ensayo de presencia o ausencia de ^{7me}GpppG cap en el RNA viral.

Para determinar la cantidad de RNAs sin cap, el RNA en la reacción fue tratado con la enzima T4 Polinucleótido Cinasa (PNK [NEB, Ipswich, MA]) con esté tratamiento se producen dos poblaciones de RNA; una con un grupo monofosfato y otra con ^{7me}GpppGcap en el extremo 5´. La otra alícuota fue tratada con la enzima RNA 5´ Pirofosfohidrolasa (RppH [NEB, Ipswich, MA]) que remueve el ^{7me}GpppG de los RNAs con cap, produciendo una mezcla de RNAs sin grupos fosfato y con grupos monofosfato en el extremo 5´ (60). Ambas reacciones fueron incubadas durante 1 h a 37ºC y después las enzimas fueron inactivadas con calor. Posteriormente, ambas alícuotas fueron usadas en paralelo como sustrato para la ligación de un oligo de RNA, el cual será llamado “linker” (5´-GCUGAUGGCGAUGAAUGAACACUGCGUUUGCUGGCUUUGAUGAAA-3´) (Tabla 2). El RNA linker se unió al grupo monofosfato presente en el extremo 5´ del RNA mediante la acción de la T4 RNA ligasa (NEB, Ipswich, MA), la reacción fue incubada durante 1 h a 37ºC. Después, el RNA presente en las reacciones fue purificado por fenol:cloroformo, precipitado con etanol y resuspendido en agua grado biología molecular libre de RNasas.

Reacción de reversa transcriptasa (RT)

La PCR cuantitativa con reacción reversa (RT-qPCR) se llevó a cabo en dos pasos, como fue descrita por Ayala-Breton *et al* (61). Después de su purificación, los RNAs fueron utilizados como sustratos para la reacción de transcripción reversa (RT) usando oligonucleótidos específicos complementarios a la cadena positiva del segmento 10 del RNA viral (Figura 8 B, paso 1). La síntesis del cDNA fue realizada con la enzima reversa transcriptasa M-MLV (Invitrogen, Waltham, MA) utilizando los siguientes oligonucleotidos; con la finalidad de detectar el amplicón que contiene al linker unido al extremo 5´ se utilizó el oligonucleótido reverso (5´-CGAGGCCTTATGTAATGTAAATAG -3´) que se une el extremo 5´ del gen viral 10 en las posiciones 168 a 191 nt (Figura 8 B, paso 1[a]); mientras que, para cuantificar la cantidad total del segmento 10 del (+)RNA viral presente en cada reacción el siguiente oligonucleótido reverso fue utilizado (YM10-3´, 5´-CAGACCCGGGCCGCGGTCACATTAAGACCGTTC-3´), este oligo se une en las posiciones 241 a 193 nt del segmento viral 10 (Figura 8 B paso 1[a]).

Tabla 3. Secuencias de oligos utilizados.

Nombre	Secuencia en dirección 5´-3´	Gen blanco
YM10-5´	CAGACCCGGGTACCTTTTAAAAGTTCTGTTCC	gen 10
YM10-3´	CAGACCCGGGCCGCGGTCACATTAAGACCGTTC	gen 10
Linker	GCUGAUGGCGAUGAAUGAACACUGCGUUUGCUGGCUUUGAUGAAA	
Linker-5´	CGATGAATGAACACTGCGTTTG	Linker
Reverso-10-3´	CGAGGCCTTATGTAATGTAAATAG	gen 10

Análisis del PCR en tiempo real (qPCR)

Después de la síntesis del cDNA, los siguientes oligonucleótidos fueron utilizados para detectar el amplicón que contiene al linker unido al extremo 5´. El oligonucleótido sentido complementario al linker de RNA (5´-CGATGAATGAACACTGCGTTTG-3´) y el oligonucleótido reverso (5´-CGAGGCCTTATGTAATGTAAATAG -3´) que se une al extremo 5´ del gen viral 10 fueron utilizados como se muestra en la figura 8 B paso 2[a], estos oligos amplifican un amplicón de 228 pb. En reacciones en paralelo, se emplearon oligonucleótidos que reconocen una región interna del gen viral 10, que fueron empleados como control interno de cada amplificación (Figura 8 B paso 2[a]); el oligo sentido (5´-TCCTGGAATGGCGTATTTTC-3´) y el oligo reverso (5´-GAGCAATCTTCATGGTTGGAA-3´) fueron usados en la reacción de qPCR, produciendo un amplicón de 90 pb. Las muestras fueron analizadas en el termociclador de tiempo real ABI 7000 sequence detector system (Applied Biosystem). Para llevar acabo el análisis cuantitativo de los datos, los resultados fueron normalizados con respecto a los niveles del segmento 10 de rotavirus detectado en cada muestra. El cambio de la expresión del gen fue calculado con el método $2^{-\Delta\Delta CT}$, en donde C_T es el ciclo de umbral (62). Finalmente, la abundancia relativa de los RNAs con y sin cap fueron determinados comparándolas cantidades relativas de el amplicón que contiene el linker con la cantidad de +RNA presente usando el método $\Delta\Delta$CT para obtener las proporciones de RNAs con y sin cap dependiendo del tratamiento de la muestra, como se describió previamente (55).

Determinación del número de copias del gen viral 10

Para determinar el número de copias virales presentes en las muestras, se generó una curva estándar utilizando diluciones seriadas de un RNA transcrito *in vitro* bajo el promotor T7 que contiene la secuencia del segmento 10 del genoma de rotavirus cepa RRV. De manera breve, el logaritmo de la concentración de cada dilución fue graficada contra valor de C_T y el número de copias de una muestra cuyo valor no es conocido se determinó extrapolando el valor de C_T en la correspondiente curva estándar.

Análisis estadístico

Los datos reportados en este estudio son las medias de un mínimo de tres replicas biológicas independientes. Las barras de error indican +/- la desviación estándar de la media. El análisis estadístico fue realizado utilizando el programa GraphPad Prism 6.0 (GraphPad Software Inc) como se describe en la sección de Resultados.

RESULTADOS

Las partículas maduras de rotavirus contienen RNA con y sin cap en los extremos 5´.

Los once segmentos de dsRNA que conforman el genoma viral se encuentran protegidos por las proteínas del core o núcleo de la partícula de tres capas (TLP) de rotavirus. En estudios previos se demostró que de las dos cadenas del dsRNA genómico solamente la cadena de RNA de polaridad positiva (+RNA), contiene cap en el extremo 5´, mientras que la cadena de polaridad negativa (-RNA) carece de esta estructura. Sin embargo, aún no es claro si todo el RNA de polaridad positiva contenido en las partículas virales posee cap (2)(63).

Como primer punto decidimos evaluar cuantitativamente la proporción de cap presente en el extremo 5´ del +RNA, encapsidado en las partículas virales maduras. Para ello, empleamos un método enzimático que permite cuantificar la presencia de cap, esté método fue empleado previamente en la caracterización del cap en el RNA genómico del virus Sindbis (SINV)(55). Brevemente, el RNA proveniente de células infectadas o de partículas virales purificadas es tratado con una fosfatasa que elimina los grupos mono-, di- o tri- fosfatos presentes en el extremo 5´ terminal de los RNAs que no tienen cap. A continuación, la muestra se divide en dos alícuotas que son sometidas a diferentes reacciones enzimáticas en paralelo: Para determinar la presencia de RNA sin cap, una alícuota es incubada con la enzima polinucleótido cinasa (PNK), de este tratamiento resulta una mezcla de RNAs con grupos monofosfato y los RNAs con cap en el extremos 5´ que no se modifican con la PNK. Por otra parte, la otra alícuota es incubada con la enzima ribofosfohidrolasa (RppH) que tiene un domino Nudixx que elimina la estructura cap dejando un grupo

monofosfato en el extremo 5´; como producto de esta reacción se generan dos poblaciones de RNA: una monofosfatatada y otra sin fosfatos en el extremo 5´. Después de estos tratamientos las enzimas empleadas son inactivadas por calor. Posteriormente, ambas alícuotas son incubadas con un linker de RNA que es un oligonucleótido de RNA de secuencia definida que en presencia de la enzima T4 RNA ligasa se puede ligar a los extremos 5´ del RNAs monofosfatados (Figura 8 A). En seguida, ambas alícuotas de RNA son empleadas como moldes para la síntesis de DNA complementario (cDNA) a través de la transcriptasa reversa (RT). En esta reacción se emplearon dos cebadores reversos específicos que hibridan en la cadena positiva del segmento 10 de RNA viral: el primero consiste de un cebador el cual hibrida en el extremo 5´del RNA viral y amplifica la región que corresponde al extremo 5´ terminal del gen 10 y el RNA linker (en caso de que este presente); el otro cebador reconoce una región interna del RNA del gen viral 10, este prima una reacción que es independiente de la presencia del linker y es utilizado para cuantificar la cantidad total del gene 10 presente en la reacción. Finalmente, las reacciones de RT son usadas para realizar el ensayo de PCR cuantitativa (qPCR), en este ensayo también se emplean dos pares de cebadores; el primer par detecta la presencia del amplicon RNA-linker y consta de un cebador sentido el cual es complementario a una secuencia en el linker y del mismo oligo reverso que se empleó en la reacción de RT; el segundo par, tanto el oligo sentido como el reverso son complementarios a regiones internas del gen 10 (Figura 8 B).

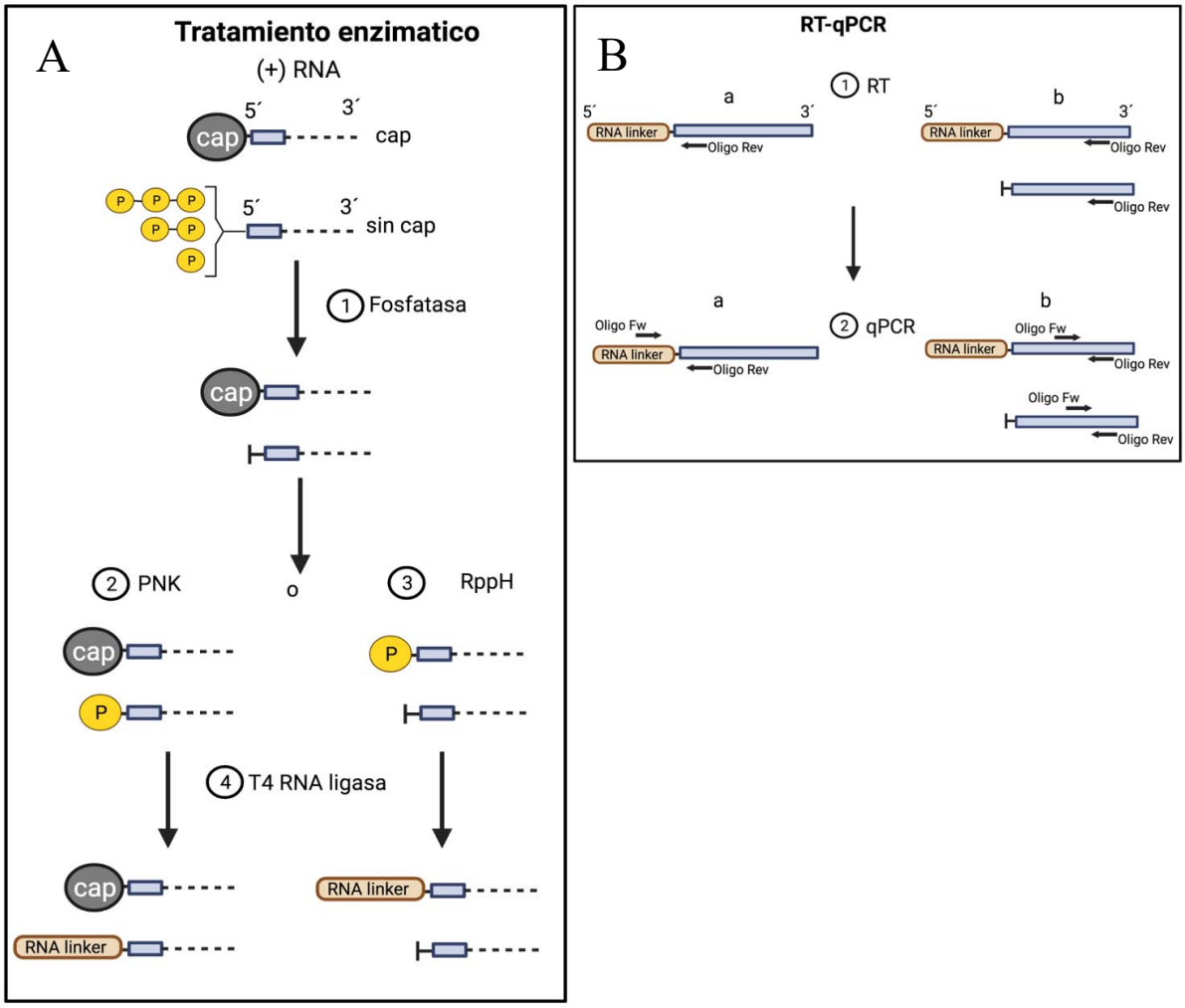

Figura 8. Esquema del ensayo enzimático para la determinación cuantitativa de la presencia o ausencia de ^{7me}GpppGcap en el RNA viral. En los ensayos se empleó dsRNA genómico o +RNA. A) Tratamiento enzimático. 1) El +RNA con o sin cap fue tratado con la enzima Fosfatasa Antártica, después la reacción fue dividida en dos alícuotas. 2) Una alícuota fue tratada con PNK, que adiciona un grupo fosfato al 5´-OH del RNA. 3) La otra alícuota fue tratada con RppH, que elimina el cap de las moléculas de RNA dejando un grupo P en el extremo 5´. 4) Un linker de RNA fue ligado al grupo fosfato presente en el extremo 5´de las moléculas de RNA, utilizando la enzima T4 RNA ligasa. B) RT-qPCR. 1) Se realizaron dos reacciones de RT-qPCR. Oligonucleótidos específicos fueron utilizados para llevar a cabo la reacción de transcripción reversa (RT), para detectar el amplicón producido por la ligación del RNA linker con el gen viral 10 (a) o para detectar la cantidad total del gene viral 10 presente en la reacción (b). 2) El cDNA obtenido fue

empleado en la reacción de qPCR, para esto se utilizaron oligos específicos que detectan el amplicón RNA linker-gene viral 10 (a) y al gen viral 10 (b).

Para determinar la presencia o ausencia de la estructura cap en el extremo 5´ del dsRNA genómico, se purificaron partículas virales de rotavirus a partir de lisados de células infectadas mediante gradientes isopícnicos de CsCl. Estos gradientes permiten separar dos poblaciones virales que corresponden a las partículas de doble y triple capa de proteínas (DLPs y TLPs, respectivamente); en estos ensayos se utilizó la banda correspondiente a las TLPs. Previo a la extracción del RNA contenido en las partículas virales purificadas, éstas fueron tratadas con RNasa A con el objetivo de eliminar cualquier RNA viral o celular que estuviese unido al exterior de las TLPs. Posteriormente, el dsRNA genómico fue extraído y purificado como se indica en materiales y métodos y se utilizó para determinar la fracción de cap presente en esta preparación mediante el método enzimático que permite la cuantificación del ^{7me}GpppGcap como se describió previamente. En este ensayo encontramos que, contrario a lo que se pensaba, en las partículas virales maduras se encuentran ambas poblaciones de +RNA, con y sin cap en el extremo 5´. Los resultados obtenidos muestran que el 40% +/- 8.3% de los +RNAs presentes en las TLPs no tienen cap (Figura 9).

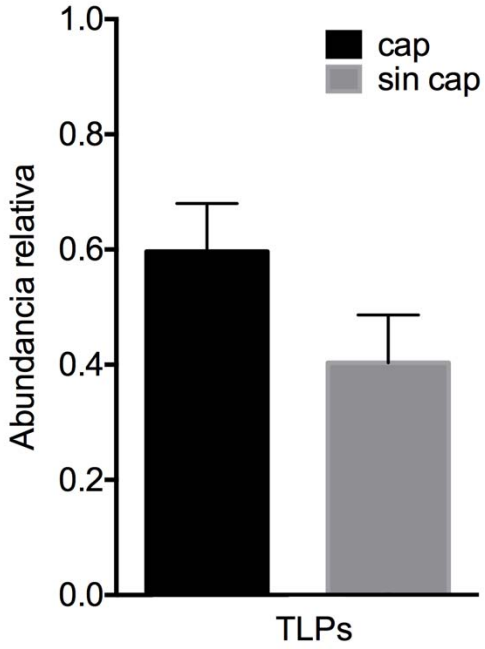

Figura 9. En las partículas virales maduras de rotavirus se encuentran poblaciones de +RNAs con y sin cap. Células MA104 fueron infectadas con RRV a una MOI de 3 y cosechadas a las 12 hpi. Las partículas virales maduras (TLP´s) fueron obtenidas mediante gradientes isopícnicos de CsCl. Previo a la extracción del RNA genómico las partículas fueron tratadas con RNasa A; finalmente, el dsRNA genómico fue purificado y sometido al ensayo de caracterización de cap como se indica en la sección de materiales y métodos. Se muestra la media aritmética +/- la desviación estándar de tres replicas biológicas independientes.

Caracterización de la actividad de adición de cap de la proteína VP3 en un sistema de transcripción *in vitro*.

Dado que encontramos que hay una proporción de RNA genómico dentro de las partículas virales maduras que no presenta cap, decidimos evaluar si esto se debía a una baja eficiencia de la actividad enzimática de la proteína viral VP3, encargada de la adición del cap. Durante el ciclo replicativo del virus, después de la

entrada de rotavirus a la célula, las proteínas que forman la capa externa de las TLPs se desprenden, generando partículas de doble capa (DLPs), que son transcripcionalmente activas e inician la síntesis de mRNAs virales en la célula infectada. En condiciones apropiadas, las DLPs pueden sintetizar grandes cantidades de +RNA viral en un sistema de transcripción *in vitro* (43), sin embargo, se desconoce si todos los transcritos sintetizados en estas condiciones tienen cap en el extremo 5´.

Para caracterizar la eficiencia de adición de cap de VP3 *in vitro*, las partículas virales obtenidas de un lisado de células infectadas se concentraron mediante centrifugación a través de un colchón de sacarosa al 40%. La pastilla obtenida fue resuspendida en un buffer con EDTA (TNE) que al quelar el Ca^{2+}, provoca que las proteínas de la capa externa se liberen, generando así las DLPs. Las partículas así obtenidas se usaron en el ensayo de transcripción *in vitro* como se describe en la sección de materiales y métodos. Posteriormente, el RNA sintetizado en este ensayo fue sometido al tratamiento enzimático para cuantificar la presencia de cap como se describe en materiales y métodos. Como se muestra en la figura 10, encontramos que la proporción de RNA con y sin cap sintetizado *in vitro* fue 1:1 (50% +/- 9.1%), lo que sugiere que en estos ensayos la proteína viral VP3 tiene una eficiencia de adición de cap de alrededor del 50%, similar a la que se encontró en los +RNAs aislados de partículas virales maduras.

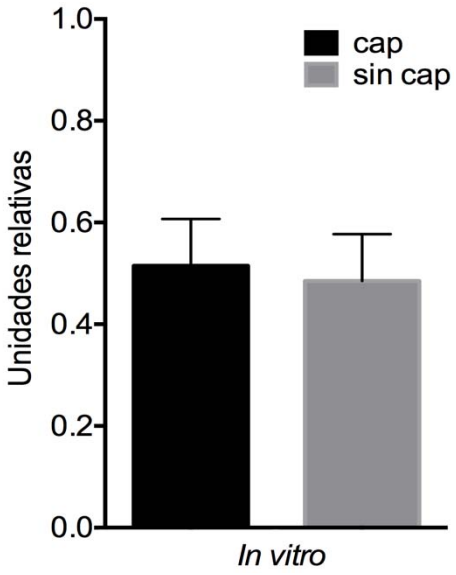

Figura 10. En ensayos de transcripción in vitro no todo el mRNA sintetizado contiene cap en el extremo 5´. Células MA104 fueron infectadas con RRV a una MOI de 3 y cosechadas a las 12 hpi. Las DLPs fueron concentradas mediante colchones de sacarosa al 40% en buffer TNE; posteriormente, se utilizaron en ensayos de transcripción *in vitro* como se describe en la sección de materiales y métodos. El RNA obtenido mediante este método fue sometido al ensayo de caracterización de cap como se indica en el texto. Se muestra la media aritmética +/- la desviación estándar de tres replicas biológicas independientes.

Evaluación de la actividad de adición de cap de VP3 durante el ciclo replicativo de rotavirus.

Para determinar si la actividad de adición de cap de VP3 observada en los ensayos anteriores, en donde se utilizó RNA de partículas virales o sintetizado en un sistema de transcripción *in vitro* se observaba en las mismas proporciones durante la infección, determinamos la cantidad de RNA viral con y sin cap producido en las células infectadas a diferentes horas post infección. Para esto, se infectaron monocapas de células MA104 y se cosecharon a diferentes horas postinfección (0, 3, 6, 9 y 12 hpi). Posteriormente, el RNA total de estos lisados fue extraído y

purificado y se sometió al ensayo enzimático para cuantificar la presencia o ausencia de cap en el RNA viral. Como se muestra en la figura 11 A, encontramos que la cantidad relativa de +RNAs virales con y sin cap cambia durante el ciclo de replicación de rotavirus. Encontramos que la proporción de RNA viral sin cap frente a la que contiene ^{7me}GpppGcap al inicio de la infección (0 hpi) fue 1:1 (50% +/- 1.8%), mientras que a las 3 hpi el RNA con cap fue del 33% +/- 4.2%. Por otra parte, a las 6 hpi la cantidad de RNA viral con ^{7me}GpppGcap incrementó hasta un 73% +/- 4.2%. Finalmente, una proporción similar de RNA con y sin cap, cercano a 50 % +/- 4.6 %, fue detectado en tiempos tardíos de la infección (9 y 12 hpi) (Figura 11 A).

En un ensayo en paralelo, la abundancia relativa del +RNA del gen viral 10 fue cuantificada mediante RT-qPCR como se describe en materiales y métodos. Se cuantificó la abundancia del RNA viral a los mismos tiempos post infección en los que la proporción de cap fue evaluada. En concordancia con lo reportado previamente por nuestro laboratorio (61), la cantidad de +RNA viral se acumula conforme avanza el ciclo replicativo (Figura 11 B.), esto nos sugiere que en nuestro ensayo estamos cuantificando la presencia de RNA con y sin cap partiendo de diferentes cantidades de RNA, ya que como se muestra en la figura la abundancia del RNA viral presente en las células cambia con respecto al tiempo. El incremento de RNA viral detectado a partir de las 6 hpi proviene de los transcritos virales sintetizados en la segunda ronda de replicación, la cual se lleva a cabo en los viroplasmas. En conjunto, estos resultados sugieren que en general la proporción de RNA con y sin cap es dinámica, con cambios principalmente durante tiempos tempranos del ciclo replicativo, mientras que la proporción de RNAs con ^{7me}GpppGcap y sin cap a las 9 y 12 hpi fue muy similar (1:1). De manera interesante,

la proporción de RNA con y sin cap detectada a tiempos tardíos concuerda con los valores encontrados en las partículas virales purificadas (Figura 9).

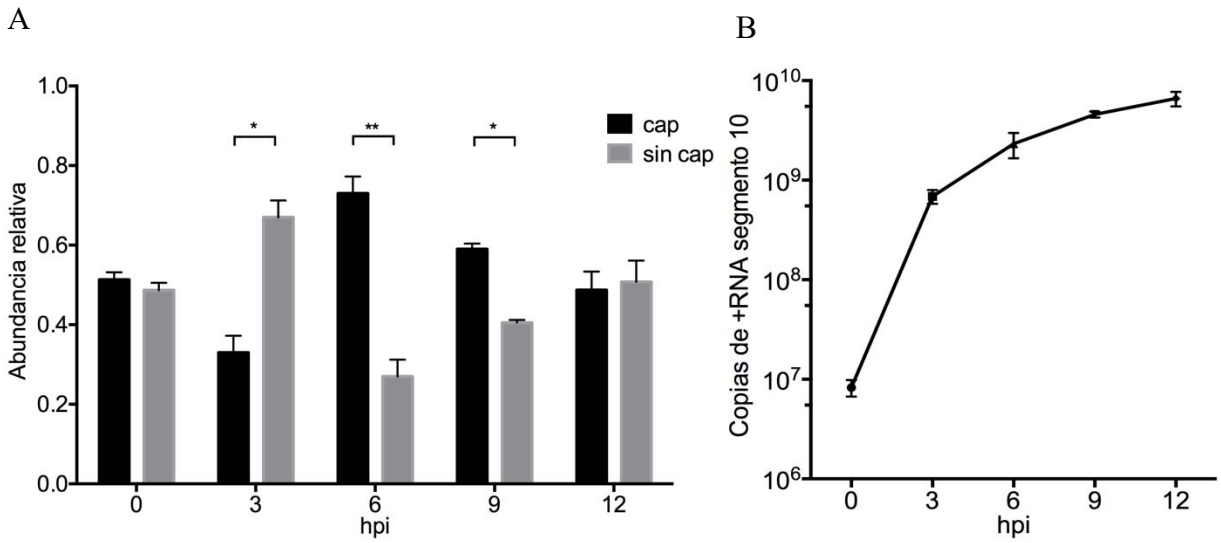

Figura 11. La abundancia del cap cambia durante el ciclo replicativo de rotavirus. A) Células MA104 fueron infectadas con RRV a una MOI de 10 y fueron cosechadas a los tiempos indicados. Posteriormente, el RNA total fue purificado y empleado en el ensayo de caracterización del cap como se describe en materiales y métodos. B) Cuantificación del número de copias de RNA segmento 10 sintetizado en los mismos tiempos que en A. El RNA obtenido en A fue utilizado para cuantificar la abundancia del segmento 10 mediante RT-qPCR. Se muestra la media aritmética +/- la desviación estándar de tres replicas biológicas independientes. Los asteriscos indican las diferencias significativas entre la cantidad de RNA con y sin cap presente en la misma condición. *, $P<0.05$. **, $P<0.01$.

Los virus que se producen en ausencia de VP3 son más infecciosos.

Reportes previos de nuestro laboratorio han mostrado que el silenciamiento de la expresión de VP3 mediante el uso de siRNAs resulta en una disminución de alrededor del 80% del rendimiento de la progenie viral infecciosa y en una reducción

de aproximadamente 10 veces en los niveles de mRNA y dsRNA virales, mientras que en estas condiciones la síntesis de las otras proteínas virales (aparte de VP3) no se ve afectada (61). Sin embargo, no se ha estudiado si la cantidad de cap presente en los transcritos virales cambia cuando la expresión de VP3 es silenciada. Para evaluar el efecto de la ausencia de VP3 en la encapsidación de RNAs virales, purificamos partículas virales producidas en células infectadas en las cuales VP3 fue silenciada por RNA de interferencia y determinamos su infectividad; además, evaluamos la proporción de RNA con y sin cap en las partículas virales producidas en estas condiciones. Para estos ensayos, las partículas virales presentes en los lisados celulares que fueron tratados con un siRNA contra VP3 o un siRNA irrelevante, fueron concentradas a través de un colchón de sacarosa. Para verificar la eficiencia del silenciamiento, la presencia de VP3 y otras proteínas virales estructurales fue analizada mediante ensayos de western blot. Para ello, muestras de lisado total de células infectadas tratadas o no con el siRNA dirigido contra VP3 y de las partículas virales semi-purificadas de cada una de estas condiciones separaron electroforéticamente y se transfirieron a membrana de nitrocelulosa que fue incubada con un anticuerpo monoclonal dirigido contra la proteína VP3 (αVP3) y posteriormente la misma membrana se incubó con un anticuerpo policlonal dirigido contra las TLPs (αTLPs), que reconoce las proteínas estructurales VP4, VP6 y VP7 (Figura 12 A).

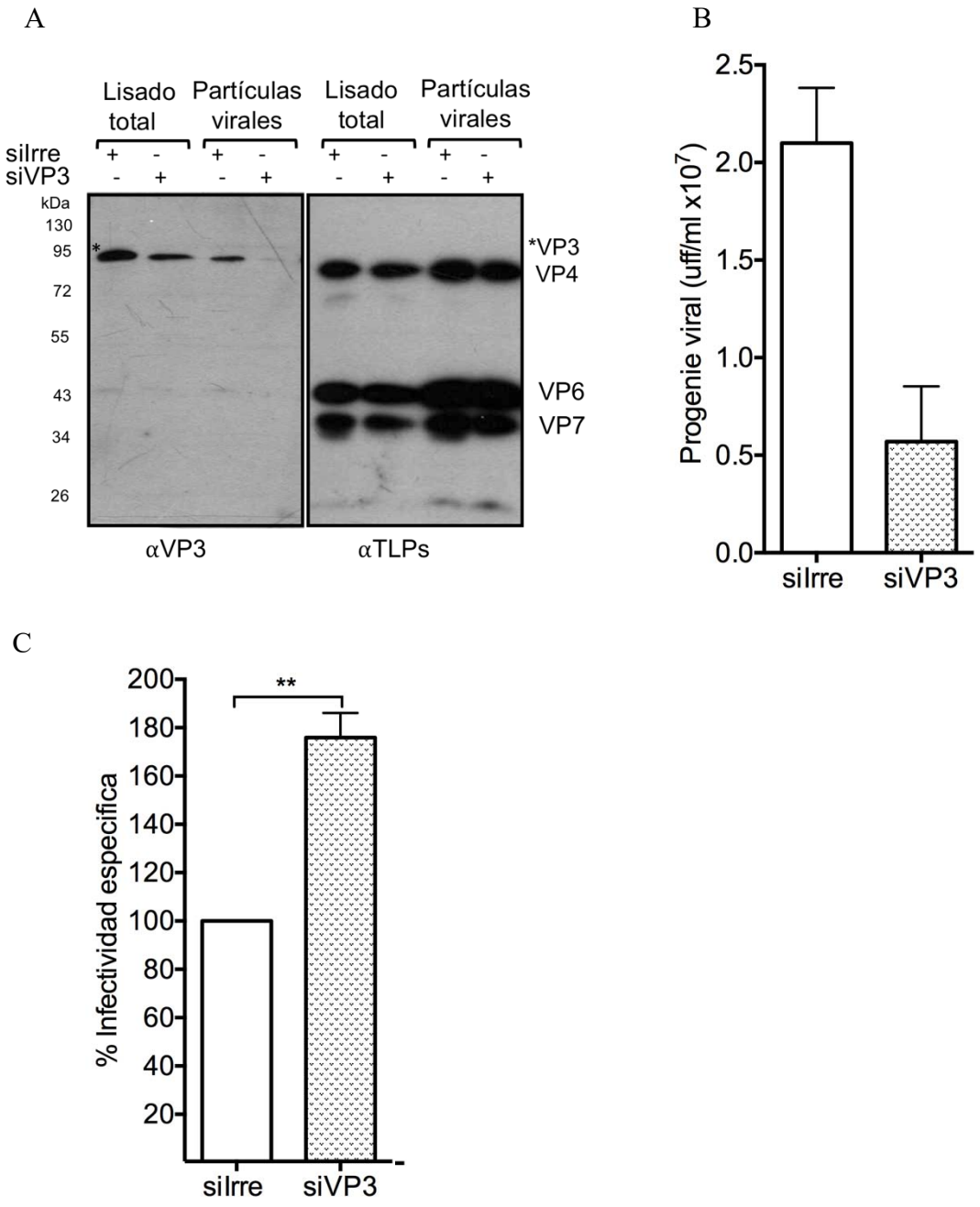

Figura 12. El virus producido en ausencia de VP3 es más infeccioso. A) Análisis del silenciamiento de VP3 de los lisados totales y partículas virales semi-purificadas mediante western blot. Las proteínas presentes en los lisados y en las partículas virales fueron analizadas en un gel SDS-PAGE al 10% y se detectaron mediante western blot empleando el anticuerpo monoclonal dirigido contra VP3. El anticuerpo αTLPs fue empleado como control de carga. B) Titulo viral de los lisados totales obtenidos de células en las que VP3 fue silenciada. Las células fueron transfectadas con el siRNA indicado y a

las 72 h post-transfección las células fueron infectadas con RRV y lisadas a las 12 hpi. El titulo viral fue determinado mediante ensayo inmunoperoxidasa. Los datos son expresados como progenie infecciosa (uff/ml). C) Infectividad especifica de las partículas virales. Las células fueron transfectadas con el siRNA indicado, después de 72 h post-transfección las células fueron infectadas con RRV. A las 12 hpi las células fueron lisadas y las partículas virales fueron concentradas mediante colchón de sacarosa; y el titulo viral de las partículas virales semi-purificadas fue determinado mediante ensayo inmunoperoxidasa. La cantidad de proteína viral VP4 presente en el western blot mostrado en A) fue calculada mediante densitometría utilizando el programa ImageJ (LOCI, Universidad de Wisconsin) y el título viral fue correlacionado con la cantidad de proteína viral VP4. Los datos son expresados como el porcentaje de infectividad específica obtenido cuando las células fueron transfectadas con un siRNA irrelevante (siIrre), el cual fue tomado como 100%. Se muestra la media aritmética +/- la desviación estándar de tres replicas biológicas independientes. Los asteriscos indican las diferencias significativas entre la cantidad de RNA con y sin cap presente en la misma condición. *, $P<0.05$. **, $P<0.01$.

Al evaluar mediante ensayos de western blot la eficiencia del silenciamiento de la proteína viral VP3 en el lisado total de las células infectadas, observamos que la expresión de esta proteína fue menor en la condición en la que las células fueron tratadas con el siVP3, aunque no se logró un abatimiento total de su expresión. Sin embargo, cuando se analizó la presencia de VP3 en las partículas virales semi-purificadas obtenidas de los lisados de células infectadas en donde la expresión de VP3 fue silenciada, se observó una cantidad casi indetectable de dicha proteína (VP3). Posteriormente, decidimos descartar la posibilidad de que este resultado fuera causado por variaciones en la cantidad de proteína cargada en el gel; por lo que evaluamos la presencia de las proteínas estructurales VP4, VP6 y VP7 en la misma membrana en la que la presencia de la proteína VP3 fue evaluada; para esto incubamos la membrana con el anticuerpo policlonal αTLPs. Como podemos

observar en la figura 12 (izq) no encontramos diferencias en la abundancia de las proteínas virales que son reconocidas por el αTLPs (Figura 12 A), tanto en los lisados totales como en las partículas semi-purificadas. En conjunto estos resultados nos permiten confirmar que es posible obtener partículas virales que carecen de la proteína estructural VP3.

Una vez caracterizadas las proteínas presentes en las partículas virales obtenidas de células en las que VP3 fue silenciada, evaluamos su infectividad específica. Para esto, realizamos ensayos de infectividad de la progenie viral presente en los lisados celulares obtenidos de células que fueron tratadas con el siRNA irrelevante o el dirigido contra VP3. Como se puede observar en la figura 12 B, cuando se silenció la expresión de VP3 el titulo viral disminuyó aproximadamente 80%, este resultado concuerda con lo reportado previamente por nuestro laboratorio (61). Sin embargo, de manera sorpresiva al evaluar la infectividad específica de las partículas virales semi-purificadas, expresada como el número de unidades formadoras de focos corregido por la cantidad de proteína viral presente en cada condición, encontramos que, aunque al silenciar VP3 se producen menos partículas, estás fueron aproximadamente 75.8% +/- 7.2% más infecciosas en relación con las partículas virales obtenidas de células control en las que VP3 no fue silenciada (Figura 12 C). Aunque el silenciamiento de proteínas virales o celulares empleando RNAi permite disminuir de manera significativa la abundancia de la proteína blanco, el tratamiento no es 100% eficiente. Esto tiene como consecuencia que dicha proteína aún este presente en pequeñas cantidades, que se pueden encontrar por debajo del límite de detección del western blot. Por lo que,

en nuestros ensayos no esperábamos abatir por completo la expresión de VP3 y por ende la presencia de cap en los transcritos virales, pero si disminuirla de manera significativa.

Posteriormente, caracterizamos la abundancia del ^{7me}GpppGcap presente en el genoma de las partículas virales ensambladas en ausencia de VP3, las cuales presentaban un aumento en la infectividad especifica. Para esto, el dsRNA genómico fue extraído y purificado de las partículas virales obtenidas a partir de células tratadas con el siVP3 o tratadas con un interferente irrelevante. Una vez purificado, el RNA genómico viral se utilizó para determinar la fracción de cap presente mediante el método enzimático que permite la cuantificación del ^{7me}GpppGcap como se describe previamente en la sección de materiales y métodos. En este ensayo esperábamos tres posibles resultados: primero, debido a la ausencia de VP3 se espera una reducción en la cantidad de RNA viral con cap, por lo que las partículas virales podrían tener una mayor cantidad de RNA sin cap; segundo, que el poco RNA viral con cap presente, producto de la actividad residual de VP3, sea encapsidado de manera preferencial, lo que se reflejaría en un incremento de la cantidad de ^{7me}GpppGcap en las partículas virales y finalmente que el RNA sea encapsidado en las misma proporciones independientemente de la abundancia del RNA con y sin cap. Después de realizar la cuantificación de la presencia o ausencia de cap, encontramos que la proporción del RNA con ^{7me}GpppGcap frente al que no tiene cap en las partículas virales que se produjeron en las células en las que se silenció VP3 fue de 1:1 (50% +/- 12.7%), esta proporción fue similar a la del RNA extraído de partículas obtenidas en la condición en la que la proteína VP3 no fue silenciada (Figura 13)

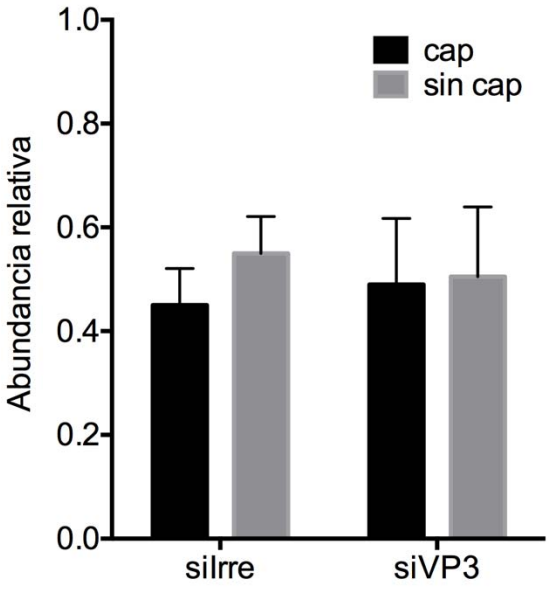

Figura 13. Las partículas virales obtenidas cuando se silencia la expresión de VP3 tienen la misma proporción de RNAs con y sin cap. Células MA104 fueron transfectadas con el interferente indicado, después de 72 h post-transfección (hpt) las células fueron infectadas con RRV a una MOI de 3. A las 12 hpi las partículas virales fueron semi-purificadas mediante colchones de sacarosa al 40% y el RNA de las partículas fue purificado y empleado en el ensayo de determinación de cap. Se muestra la media aritmética +/- la desviación estándar de tres replicas biológicas independientes.

Posteriormente evaluamos la presencia del cap en los transcritos virales producidos *in vitro* por las partículas virales obtenidas en condiciones en las que VP3 se silenció. Utilizamos las DLPs semi-purificadas obtenidas de células en las que VP3 fue silenciada, y estas se utilizaron en el ensayo de transcripción *in vitro* como se describió en la sección de materiales y métodos; el RNA obtenido se utilizó en el ensayo de determinación de cap. Encontramos que estas partículas producen una cantidad significativamente mayor de RNAs sin cap, ya que solo el 15.5 % +/- 12 % del RNA producido tenía ^{7me}GpppGcap, mientras que el 83.5 % +/- 12% del RNA no poseía cap (Figura 14). Este resultado sugiere que estas partículas

contienen una cantidad muy baja de VP3, tal y como se observó en los ensayos de western blot; sin embargo, este resultado contrasta con los valores obtenidos cuando caracterizamos la proporción de cap presente en el +RNA obtenido de las partículas virales (Figura 13), donde encontramos proporciones similares de RNAs con y sin cap.

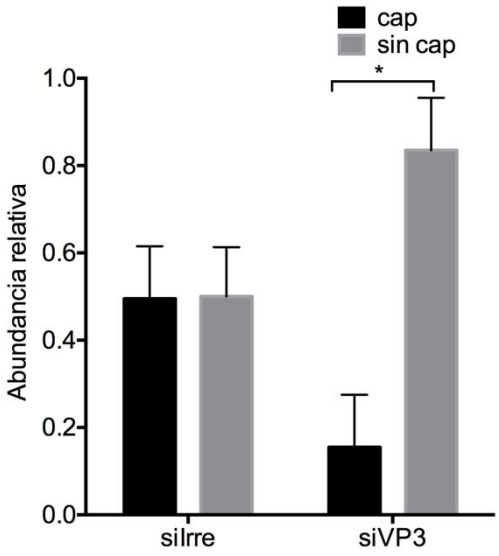

Figura 14. Las DLPs producidas en ausencia de VP3 producen una menor proporción de +RNAs con cap. Células MA104 fueron transfectadas con el RNA interferente indicado, 72 hpt las células fueron infectadas con RRV a una MOI de 3. A las 12 hpi las DLPs fueron purificadas mediante colchones de sacarosa al 40% y se utilizaron en el ensayo de transcripción *in vitro* como se describe en materiales y métodos. El RNA sintetizado fue utilizado para determinar la proporción de RNA con y sin cap empleando el ensayo de determinación de cap. Se muestra la media aritmética +/- la desviación estándar de tres replicas biológicas independientes. Los asteriscos indican las diferencias significativas entre la cantidad de RNA con y sin cap presente en la misma condición. *, $P<0.05$.

En conjunto, los resultados mostrados indican que las partículas virales producidas en células en las que se silenció la expresión de VP3 se ensamblan en

menor cantidad en comparación con las obtenidas en células tratadas con un siRNA irrelevante (Figura 12 B). De manera interesante, estás partículas tuvieron una mayor infectividad especifica, esté incremento en la infectividad parece no estar relacionado con la presencia o ausencia de cap, ya que el +RNA genómico encapsidado en estas partículas presentó una proporción similar (1:1) de RNA con y sin ^{7me}GpppGcap al encontrado en las condiciones control. Sin embargo, encontramos que los +RNAs transcritos por las partículas virales producidas en ausencia de VP3 sintetizaron una cantidad significativamente menor de +RNAs con cap. Los resultados obtenidos sugieren que durante el proceso de encapsidación del dsRNA genómico los RNAs con y sin cap se encapsidan en una proporción similar, independientemente de la abundancia del RNA con ^{7me}GpppGcap presente en las células infectadas.

Efecto del co-silenciamiento de RNasa L y VP3 en la adición de cap.

Como se mencionó previamente, además de la actividad de guanilil-metil transferasa, la proteína VP3 tiene en el domino carboxilo terminal una actividad de 2´-5´-fosfodiesterasa (PDE), por medio de la cual degrada a los 2´-5´ As, impidiendo la activación de la RNasa L, que es una RNasa inespecífica que al activarse establece un estado antiviral en la célula, degradando RNAs celulares y virales (64,65). Reportes previos de nuestro laboratorio mostraron que el co-silenciamiento VP3 y RNasa L mediante RNAi resultó en un incremento del rendimiento de la progenie viral infecciosa y de la integridad del RNA viral (45). Estos resultados sugieren que la actividad de adición de cap de VP3 parece no ser esencial para la producción de progenie viral infecciosa durante el ciclo replicativo de rotavirus. Con

el objetivo de analizar el efecto que tiene el co-silenciamiento de VP3 y RNasa L en la abundancia de RNA viral con cap, células MA104 fueron co-transfectadas con los siRNA indicados y posteriormente, las células fueron infectadas con rotavirus y se colectaron a diferentes horas postinfección (0, 3, 6, 9 y 12 hpi). Para demostrar la eficacia del co-silenciamiento, la presencia de las proteínas VP3 y RNasa L fueron analizadas mediante ensayos de western blot utilizando anticuerpos monoclonales dirigidos contra las proteínas VP3 y RNasa L (Figura 15 A); como control de carga se utilizó un anticuerpo policlonal que reconoce a la proteína celular vimentina. La eficiencia de los silenciamientos fue calculada cuantificando la densitometría de las bandas (Figura 15 B). Posteriormente, la infectividad de la progenie viral producida a las 12 hpi fue analizada mediante ensayos de inmunoperoxidasa como se describe en la sección de materiales y métodos (Figura 15 C). Encontramos que al silenciar la expresión de VP3 hubo una disminución del título viral cercano al 60%; sin embargo, el co-silenciamiento de la expresión de VP3 y RNasa L tuvo como efecto un aumento en la infectividad de aproximadamente 50% en comparación con las células control en las cuales ningún gen, viral o celular, fue silenciado (Figura 15).

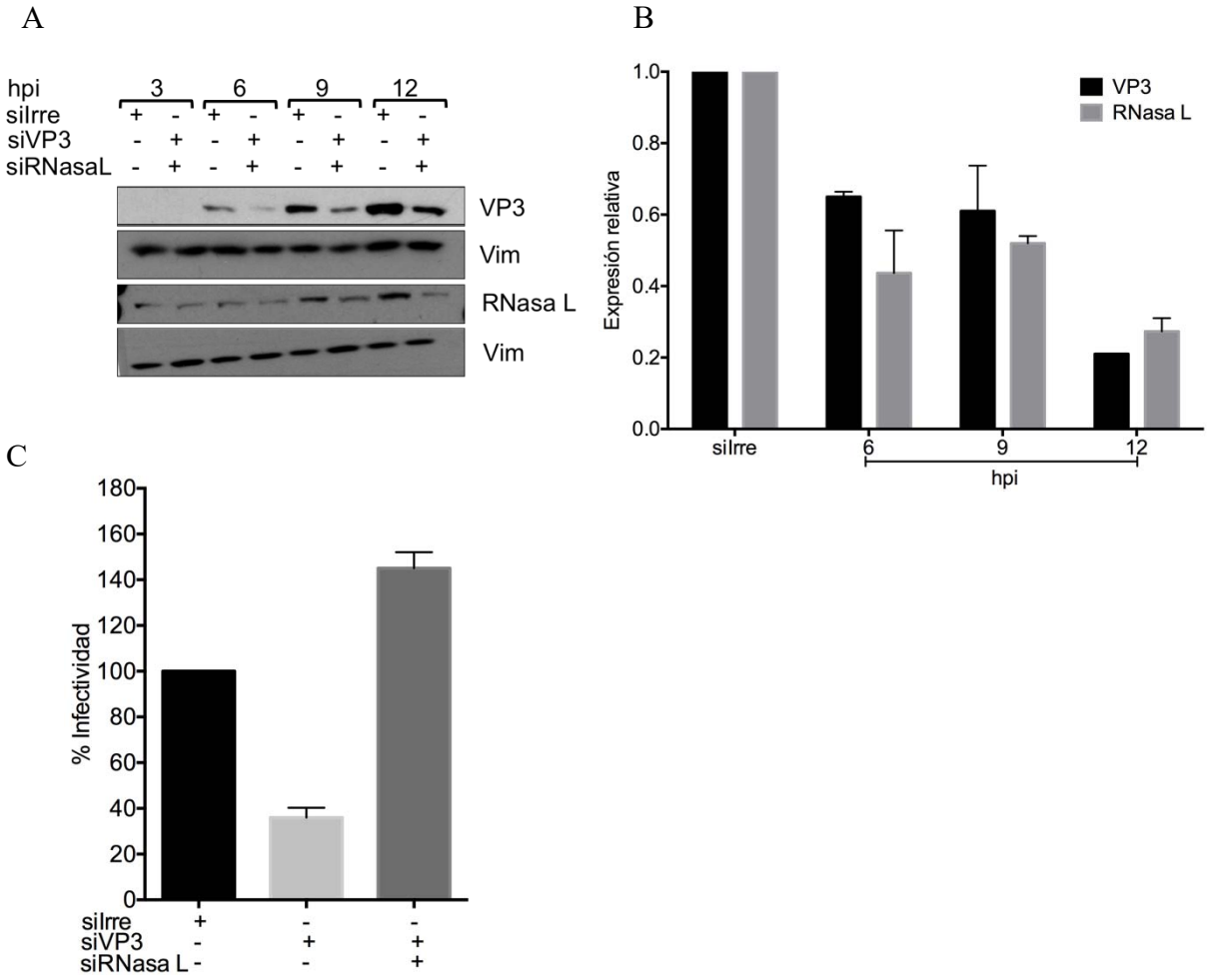

Figura 15. El co-silenciamiento de VP3 y RNasa L incrementa la producción de la progenie viral. A) Células MA104 fueron transfectadas con el interferente indicado como se menciona en la sección de materiales y métodos. A las 72 hpt las células fueron infectadas con RRV a una MOI de 3 y lisadas a los tiempos indicados. Las proteínas fueron separadas en un gel SDS-PAGE al 10% y se detectaron mediante western blot empleando los anticuerpos monoclonales dirigidos contra VP3 y RNasa L. La proteína vimentina (Vim) fue empleada como control de carga. Se muestra una imagen representativa de los lisados celulares de células transfectadas con los siRNAs dirigidos contra VP3 y RNasa L. B) Cuantificación de la eficiencia del silenciamiento de las proteínas VP3 y RNasa L. La cantidad relativa de la proteína indicada fue calculada cuantificando la densitometría de las bandas usando el software ImageJ (LOCI, Universidad de Wisconsin). C) En paralelo, las células fueron infectadas con RRV a una MOI de 3, a las 12 hpi las células fueron lisadas y

el titulo viral fue determinado mediante ensayo inmunoperoxidasa. Los datos son representados como el porcentaje de la infectividad obtenida cuando las células fueron transfectadas con un siRNA irrelevante (siIrre) que fue tomado como 100%. Se muestra la media aritmética +/- la desviación estándar de tres replicas biológicas independientes.

Posterior al análisis de la expresión de las proteínas silenciadas, el RNA total de cada condición fue extraído y purificado en los tiempos indicados y se cuantificó la presencia o ausencia de cap en el +RNA viral. Encontramos que la proporción de +RNA viral sin cap frente a la que contiene cap al inicio de la infección (0 hpi) fue 1:1; esté resultado fue similar al obtenido cuando se analizaron TLP´s purificadas (Figura 9) y en las células control, que fueron tratadas con un siRNA irrelevante. Por otra parte, después de las 6 hpi la cantidad de RNA con ^{7me}GpppGcap fue del 73% +/- 3%, mientras que a las 9 hpi fue de 64% +/- 2%. Finalmente, a las 12 hpi se encontró una proporción de RNA con cap significativamente mayor (83% +/- 2%; Figura 16 A).

Además, se evaluó si el co-silenciamiento de VP3 y RNasa L afecta la abundancia del +RNA viral. Para esto, en un ensayo en paralelo cuantificamos la abundancia relativa del +RNA del gen viral 10 mediante RT-qPCR. Encontramos que en los tiempos evaluados se produjo una cantidad similar de +RNA tanto en las células co-silenciadas como en la condición control (Figura 16 B). Este resultado sugiere que el co-silenciamiento de éstas proteínas no afectó la abundancia del RNA viral durante la infección al igual que en los resultados mostrados previamente (Figura 11). Dado que estamos cuantificando la presencia de RNA con y sin cap de diferentes cantidades de RNA, las diferencias en la proporción de ^{7me}GpppGcap encontradas en las células infectadas que fueron co-silenciadas con los

interferentes dirigidos contra las proteínas VP3 y RNasa L, no fueron debidas a diferencias en la transcripción del RNA viral.

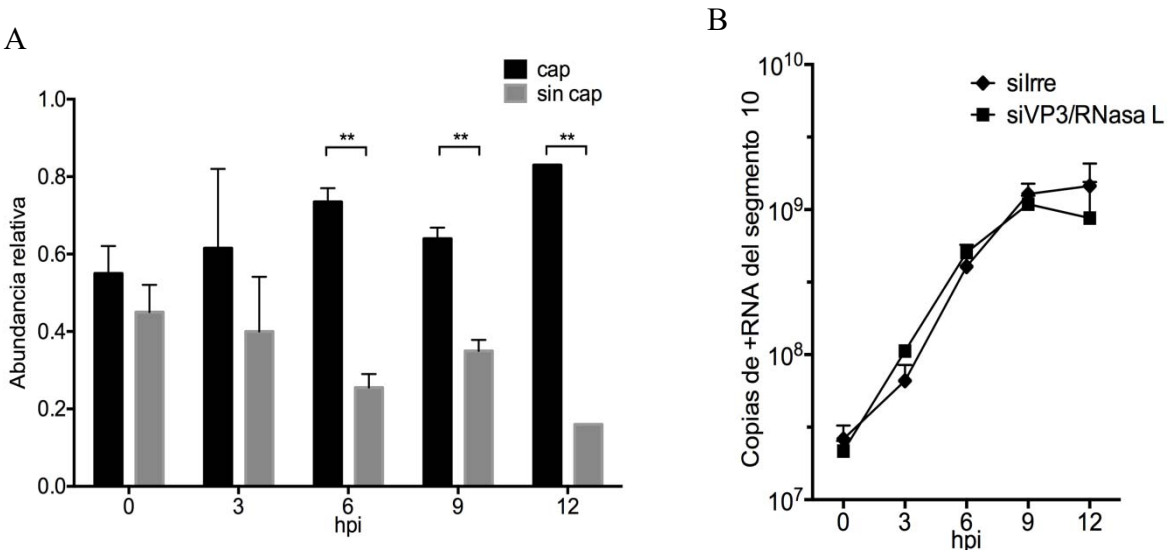

Figura 16. Determinación cuantitativa de +RNAs con y sin cap en células en las que VP3 y RNasa L fueron co-silenciadas. A) Las células fueron transfectadas con el interferente indicado como se menciona en la sección de materiales y métodos. A las 72 hpt las células fueron infectadas con RRV y lisadas a los tiempos indicados. El RNA total fue purificado y usado en el ensayo de determinación de cap como se describe en materiales y métodos. B) Abundancia relativa del segmento 10 del (+)RNA viral. El RNA obtenido en A fue empleado para cuantificar la abundancia del segmento 10 en un ensayo de RT-qPCR como se describe en materiales y métodos. Se muestra la media aritmética +/- la desviación estándar de tres replicas biológicas independientes. Los asteriscos indican las diferencias significativas entre la cantidad de RNA con y sin cap presente en la misma condición. *, $P<0.05$. **, $P<0.01$.

La proporción de RNA con y sin cap en las partículas virales no depende de la proporción presente en las células infectadas

Como mostramos en los resultados anteriores, la proporción de RNA con ^{7me}GpppGcap producida en células infectadas en donde se co-silenciaron las

proteínas VP3 y RNasa L fue significativamente mayor, por lo que decidimos evaluar si bajo estas condiciones la proporción de +RNA con cap presente en las partículas virales también incrementaba. Para ello, células MA104 fueron co-transfectadas con los siRNAs dirigidos contra VP3 y RNasa L; o transfectadas solamente con el siRNA dirigido contra RNasa L o con un siRNA irrelevante; posteriormente, las células fueron infectadas con rotavirus y se cosecharon a las 12 hpi. Las partículas virales presentes en estos lisados celulares fueron concentradas pasándolas a través de un colchón de sacarosa. La eficiencia del silenciamiento de las proteínas VP3 y RNasa L se evaluó mediante ensayos de western blot. Por otra parte, el silenciamiento de la proteína celular RNasa L se evaluó en los lisados totales a partir de los que se purificaron las partículas virales. Como se muestra en la Figura 17 A, se logró silenciar eficientemente ambas proteínas y también se obtuvieron partículas virales sin VP3 en la condición en la que está proteína fue silenciada.

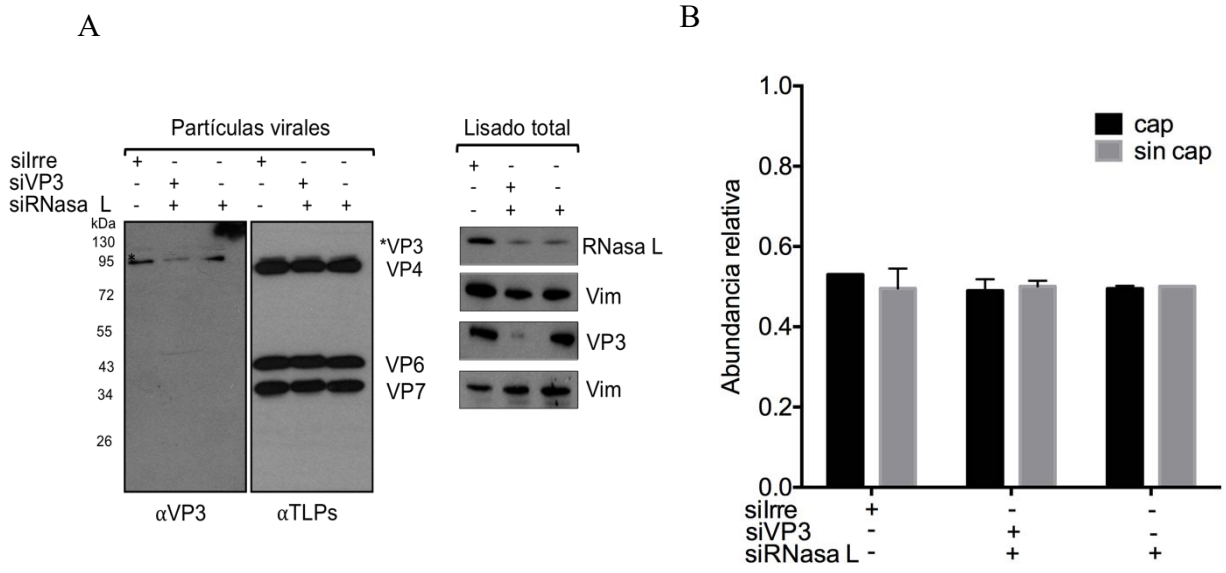

Figura 17. La proporción de RNAs con y sin cap que son encapsidadas en las partículas virales no depende de la abundancia del cap presente en las

células infectadas. A) Células MA104 fueron transfectadas con el interferente indicado como se menciona en la sección de materiales y métodos. A las 72 hpt las células fueron infectadas con RRV a una MOI de 3. A las 12 hpi las partículas virales fueron semi-purificadas mediante colchones de sacarosa al 40%. Las proteínas presentes en los lisados y en las partículas virales fueron analizadas en un gel SDS-PAGE al 10% y se detectaron mediante western blot empleando los anticuerpos monoclonales dirigidos contra VP3 y RNasa L. Los anticuerpos αVim y αTLPs fueron empleados como control de carga. Se muestra una imagen representativa de los lisados celulares de células transfectadas con los siRNAs dirigidos contra VP3 y RNasa L. B) Las partículas virales fueron tratadas con RNasa A y el RNA de estas partículas fue purificado y empleado en el ensayo de determinación de cap. Se muestra la media aritmética +/- la desviación estándar de tres replicas biológicas independientes.

Posteriormente, el dsRNA genómico fue extraído y purificado de las partículas virales semi-purificadas obtenidas de las células que fueron tratadas con el siRNA indicado. Después de ser purificado, el RNA genómico viral se utilizó para determinar la fracción de cap presente. Encontramos que, contrario a lo que esperado, la proporción de RNAs con y sin cap en las partículas virales obtenidas de células en las que VP3 y RNasa L fueron co-silenciadas fue de 1:1 (50% +/- 2.0%), una proporción similar fue encontrada en el RNA extraído de las partículas virales producidas en las condiciones en las que solo RNasa L fue silenciada o en las producidas en la condición control (Figura 17 B). Como mostramos en la figura 17 A, en los lisados de células en las que se co-silenció la expresión de VP3 y RNasa L se encontró una mayor cantidad de RNA con cap, por lo que nuestros datos sugieren que la proporción de RNA viral con o sin cap que es encapsidada en la partícula viral no depende de la abundancia de estas dos especies de +RNAs presente en las células infectadas.

DISCUSIÓN

La presencia del cap en el extremo 5´ de los mRNAs virales tiene funciones importantes que incluyen: protección contra la degradación mediada por 5´-3´ exoribonucleasas, incrementar la síntesis de proteínas virales en los virus que tienen un inicio de la traducción dependiente de cap, además de evitar que los transcritos virales presentes en el citoplasma de la célula infectada sean reconocidos por el sistema inmune innato del hospedero (66)(67). En el citoplasma de las células infectadas, los RNAs sin cap son detectados por las proteínas del sistema inmune innato RIG-I y MDA5, estás proteínas reconocen ligandos específicos (grupos tri- di- o mono- fosfatos) presentes en el extremo 5´ de los transcritos virales que no se encuentran en los RNAs que son sintetizados por la maquinaria de transcripción celular. La unión a sus ligandos inicia una cascada de señalización que culmina con la expresión de interferón α/β (IFN) como respuesta del sistema inmune innato a la infección, induciendo un estado antiviral en la célula infectada y en las células adyacentes (68)(35). Los virus que llevan a cabo su ciclo replicativo en el citoplasma han desarrollado diferentes estrategias que les permiten evadir el reconocimiento de sus transcritos virales por componentes del sistema inmune innato evitando así la activación y expresión de IFN; una de estas estrategias es la adición de cap en el extremo 5´de sus mRNAs (69).

Los rotavirus emplean diferentes estrategias que evitan que su genoma (dsRNA) y los transcritos virales producidos durante el ciclo replicativo sean reconocidos por las proteínas del sistema inmune (46), una de ellas es la adición de cap. El cap es adicionado por la proteína viral VP3 que posee todas las actividades

enzimáticas involucradas en este proceso. En este trabajo caracterizamos la presencia de ^{7me}GpppGcap en uno de los RNAs producidos por rotavirus para ello empleamos un método enzimático que permite cuantificar la presencia del cap, que fue utilizado previamente en la caracterización del cap en el RNA genómico del virus Sindbis (SINV). Al analizar la presencia de cap en las partículas virales infecciosas (TLP´s), encontramos que el dsRNA genómico encapsidado tiene tanto +RNAs con y sin cap. La presencia de +RNA genómico sin cap en partículas virales ya había sido reportado previamente para el virus SINV (55); sin embargo, este es el primer estudio en el que se caracteriza de manera cuantitativa la presencia de RNAs con y sin cap presente en las partículas virales de un miembro de la familia *Reoviridae*.

Dado que detectamos una proporción alta de +RNAs sin cap en las partículas virales, decidimos evaluar si esto era debido a una baja actividad de la guanilil transferasa de VP3 por lo que caracterizamos la presencia de cap en los transcritos virales producidos en un sistema de transcripción *in vitro*. Encontramos que VP3 adiciona de manera poco eficiente el cap, ya que la proporción de +RNAs con y sin cap fue 1:1, sugiriendo que la eficiencia enzimática de VP3 no es del 100%. Este resultado concuerda con lo reportado por Uzri y colaboradores, quienes emplearon un enfoque indirecto para determinar la presencia de +RNAs virales con y sin cap por su habilidad de inducir la secreción de IFN. En este ensayo, el RNA obtenido mediante transcripción *in vitro,* o aislado a las 6 horas post infección fue transfectado en fibroblastos embrionarios murinos (MEFs) y el nivel de IFN-β secretado fue cuantificado mediante ensayo de ELISA (70). Empleando está metodología encontraron que ambas poblaciones de RNAs estudiadas, contenían RNAs con

grupos fosfatos expuestos en el extremo 5´ y estructuras cap que no se encuentran completamente 2´-O-metiladas, y propusieron que no todos los RNA virales contenían cap en su extremo 5´.

Como en nuestros ensayos encontramos que VP3 no adiciona el cap al 100% de los transcritos virales, decidimos caracterizar la presencia de esta estructura durante el ciclo replicativo de rotavirus; encontramos que la abundancia de los +RNAs virales con y sin ^{7me}GpppGcap en las células infectadas con rotavirus es dinámica, ya que las proporciones cambian a los diferentes tiempos post infección, con una mayor cantidad de RNAs con ^{7me}GpppGcap a las 6 hpi. Por otra parte, a tiempos tardíos de la infección (12 hpi) la proporción de RNAs con y sin cap fue 1:1, similar al resultado obtenido en la caracterización del RNA genómico viral encapsidado en las TLP´s (Figura 9). De manera similar, al caracterizar la proporción de RNAs con y sin cap durante el ciclo replicativo de SINV encontraron una mayor proporción de RNAs sin cap a tiempos tempranos de la infección (3 hpi); mientras que a tiempos tardíos (9 y 12 hpi) la proporción de RNAs con cap aumentó hasta llegar a una proporción 1:1 (55). El mecanismo por el cual la abundancia de RNAs con cap incrementa durante la infección de SINV no ha sido elucidada; sin embargo, en nuestro estudio esté incremento puede ser debido a que después de las 4 hpi hay un aumento significativo de la cantidad de los transcritos virales como resultado de la segunda ronda de replicación que es llevada a cabo por las nuevas DLPs ensambladas en los viroplasmas (61)(Figura 11 B). Aunque durante la infección de SINV no se caracterizó la proporción del cap en el RNA a las 0 hpi, en nuestro estudio la proporción de ^{7me}GpppGcap presente a este tiempo fue similar al obtenido en las partículas virales (Figura 11 A). Al inicio de la infección (0 hpi) el

único RNA viral proviene del +RNA genómico presente en las partículas virales se encuentran en el lisado empleado en la infección de las células. Las diferencias en las proporciones de RNAs con y sin ^{7me}GpppGcap obtenidas del RNA proveniente de ensayos *in vitro* y de células infectadas con rotavirus pueden ser debido a que las condiciones en las que se llevaron a cabo los ensayos de transcripción *in vitro* son “óptimas”, mientras que el RNA viral producido durante la infección se encuentra expuesto a un ambiente citoplasmático en el cual existen proteínas celulares que pueden estabilizar o desestabilizar el RNA viral. En este trabajo caracterizamos la presencia o ausencia del cap en el segmento 10 del genoma de rotavirus, esté segmento ha sido empleado en nuestro laboratorio y en otros laboratorios como representativo de todos los segmentos del genoma en diferentes estudios. Sin embargo, con este trabajo no podemos descartar la posibilidad de que la proporción de RNA con y sin cap pueda ser diferente en otros segmentos del genoma viral.

Además de la actividad de adición de cap, la proteína viral VP3 puede contrarrestar la respuesta inmune innata del hospedero a través de diversos mecanismos. En células epiteliales intestinales infectadas con rotavirus, VP3 envía a degradación mediada por proteasoma a la proteína celular MAVS, que es una proteína involucrada en la transducción de señales que permiten la producción de IFN. Al degradar a MAVS se bloquea la producción de IFN-λ, teniendo como consecuencia un incremento en la replicación y en la patogenesis viral de rotavirus (47). Por otra parte, VP3 tiene en el carboxilo terminal un dominio de fosfodiesterasa (PDE) que degrada a los 2´-5´oligoadenilatos que son producidos en respuesta a la detección del dsRNA por OAS, de esta manera se inhibe la activación de RNasa L.

La función y actividad del dominio PDE de VP3 durante la infección de rotavirus ha sido evaluada en diversos estudios y se ha demostrado que la actividad antagonista de VP3 hacia OAS/RNasa L es importante para que los rotavirus puedan replicarse de manera eficiente tanto en modelos de infección *in vivo* e *in vitro* (45)(71). Como demostramos en este trabajo, durante el ciclo replicativo de rotavirus se producen RNAs sin cap, los cuales pueden inducir la activación de la expresión de IFN, sin embargo, VP3 es una proteína multifuncional que puede contrarrestar esta activación a través de diferentes mecanismos aunados a las funciones de la proteína viral NSP1 (46).

Previamente en nuestro laboratorio se reportó el efecto de silenciar la expresión de VP3 sobre la síntesis de proteínas virales y en la producción de partículas virales; sin embargo, no se ha estudiado cómo la ausencia de esta proteína afecta la adición del cap a los RNAs virales (13). En este trabajo encontramos que, de acuerdo a lo reportado, el silenciamiento de VP3 tiene como consecuencia una disminución significativa en la abundancia del RNA y en la formación de partículas virales, aunque paradójicamente la síntesis de las proteínas virales no se afecta. Al caracterizar la presencia de cap en las partículas virales producidas en esta condición encontramos que contenían una proporción 1:1 de +RNAs con y sin cap (1:1), similar a la obtenida cuando caracterizamos las partículas virales obtenidas de células control que fueron tratadas con un siRNA irrelevante. Una posible explicación es que el RNA con ^{7me}GpppGcap detectado en las partículas obtenidas en el silenciamiento de VP3 puede provenir de las partículas virales utilizadas durante la infección, y que este RNA con cap pueda ser suficiente para que se lleve a cabo la síntesis de proteínas virales durante el ciclo replicativo,

y sea encapsidado en las nuevas partículas virales, aunque esta posibilidad es poco probable. Inesperadamente, las partículas virales obtenidas de células en las que VP3 fue silenciada mostraron una infectividad especifica mayor que las obtenidas de las células control. Adicionalmente, las nuevas partículas virales ensambladas en estas condiciones poseen muy poca cantidad de VP3, no solo evidente por la señal en los western blots sino que además encontramos que los transcritos virales sintetizados *in vitro* por las DLPs tienen una cantidad significativamente menor de ^{7me}GpppGcap (Figura 14). El mecanismo por el cual el RNA y las proteínas virales interaccionan para ensamblar las nuevas partículas virales no ha sido caracterizado en detalle. Sin embargo, se ha propuesto un modelo en el que inicialmente monómeros de VP1, que quizá se encuentra formando un complejo con VP3, se unen al extremo 3´de los +RNAs virales, creando complejos de RNA-proteína(25). Posteriormente, a este complejo se une la proteína VP2, la unión de esta proteína es indispensable para la activación de la RdRp de VP1 y la síntesis del dsRNA genómico (52). Aunque la función de VP3 en el ensamblado del “core” viral no ha sido evaluada, nuestros resultados sugieren que, en cultivo celular, VP3 puede ser no esencial en la formación del “core” viral y en la transcripción del RNA viral; sin embargo, la relevancia de VP3 debe de ser evaluada a un segundo ciclo de infección empleando partículas deficientes en VP3 y en un modelo de replicación *in vivo*.

La importancia del dominio PDE de VP3 ha sido evaluada durante el ciclo replicativo de rotavirus, en reportes previos encontraron que el co-silenciamiento de VP3 y RNasa L tiene como efecto, contrario al silenciamiento de VP3, la recuperación de la producción de partículas virales infecciosas; este resultado

sugiere que la actividad de adición de cap de VP3 no es esencial para la producción de progenie viral (45). En este estudio evaluamos la abundancia de ^{7me}GpppGcap en +RNAs purificados a diferentes hpi de células infectadas que fueron co-silenciadas con interferentes dirigidos contra VP3 y RNasa L. Encontramos que después de las 6 hpi hubo un incremento significativo de RNA con cap con respecto al RNA sin cap, con una abundancia mayor al 80% a las 12 hpi. Este resultado fue inesperado, ya que esperábamos detectar una mayor cantidad de RNAs sin cap, debido a la ausencia de la proteína viral involucrada en su adición y la proteína celular encargada de degradar a los RNAs. Como mencionamos VP3 es una proteína multifuncional, el incremento en la abundancia de RNAs con cap a tiempos tardíos nos sugiere que VP3 puede estar modulando (directa o indirectamente) la actividad de otras endonucleasas, además de RNasa L, que degradan a los RNAs sin cap. Por otra parte, cuando analizamos la abundancia de cap en el +RNA contenido en las partículas virales purificadas en estas condiciones encontramos la misma proporción de +RNAs con y sin cap (1:1), este resultado, junto con el obtenido al cuantificar el cap en las partículas virales semi-purificadas de células en las que se silenció VP3, sugieren que existe un mecanismo por el cuál rotavirus controla la proporción de los +RNAs con y sin cap que son encapsidados; además, que el RNA que se encapsida en la partícula viral, no depende de los niveles de RNA con ^{7me}GpppGcap presente en las células infectadas por rotavirus.

El efecto que tiene la abundancia del cap en los transcritos virales en la patogénesis viral ha sido evaluada mediante diferentes enfoques. Los reportes disponibles principalmente se basan en la producción de virus mutantes en los que se incrementa o disminuye la actividad de alguna de las enzimas involucradas en la

adición de cap. De manera interesante, la función del cap durante el ciclo replicativo parece ser dependiente del virus en la que se esté estudiando, ya que mientras para SARS-CoV-2 la presencia del cap con la modificación de N7-metilguanosina es importante para incrementar su virulencia (72), la patogénesis de SINV se ve afectada de manera negativa al incrementarse la proporción de RNAs con cap. En reovirus, otro miembro de la familia *Reoviridae*, recientemente se reportó que el incremento de la presencia de cap en el sistema de genética reversa mediante la incorporación de la proteína fusión C3P3, que contiene a la T7 polimerasa y la proteína viral NP868R encargada de la adición del cap en el virus de la fiebre porcina africana, tuvo como efecto un incremento en la síntesis de proteínas virales de al menos 2 veces, mientras que la producción de viriones infecciosos se vio incrementada al menos 60 veces. Estos resultados sugieren que el cap presente en el RNA viral además de ser importante para incrementar la síntesis de proteínas virales, tiene una función no tradicional que consiste en promover el ensamblado de partículas virales y la incorporación del RNA viral genómico en los nuevos viriones (54).

Otro virus del que se ha caracterizado la importancia del cap durante su ciclo replicativo es el SINV, que a diferencia de rotavirus tiene un genoma de RNA de cadena sencilla de polaridad positiva. Durante la infección de SINV se producen dos subpoblaciones de partículas virales (“SINV light” y “SINV heavy”) que pueden ser separadas por las diferencias en su densidad. La proporción de partículas físicas: infecciosas es 100:1 y 10:1, para “SINV light” y “SINV heavy”, respectivamente (73). De manera interesante, cuando se caracterizó la presencia de cap en el RNA genómico de estas partículas, se encontró que las partículas SINV heavy tienen una

proporción mayor de cap (79%) contrario a SINV light en donde se encontró una mayor cantidad de RNAs sin cap (70%); sin embargo, aún no es claro si el ^{7me}GpppGcap tiene una función durante la encapsidación del RNA genómico (55). Recientemente se reportó la importancia de la adición de cap al 5´de los transcritos virales de SINV, tanto en modelos *in vitro* e *in vivo*. En estos estudios, realizaron mutaciones puntuales en la proteína viral involucrada en la adición de cap (nsP1), con el objetivo de disminuir o incrementar su eficiencia de adición de cap a los transcritos virales. En aquellos ratones que fueron infectados con el virus mutante con actividad de adición de cap disminuida, se encontró una ligera disminución en la mortalidad; por el contrario, cuando se incrementó la eficiencia de adición de cap la mortalidad y morbilidad causada por estos mutantes fue nula (69)(57). También encontraron que la expresión de las citosinas proinflamatorias disminuye significativamente cuando se incrementa la capacidad de adición del cap, sugiriendo que la eficiencia de adición de cap y la producción de RNAs sin cap son importantes para alcanzar niveles patogénicos de inflamación. Estos datos sugieren que la presencia de RNAs sin cap tiene un rol crítico en la patogénesis y virulencia en este virus.

Recientemente, se reportó un método sensible que permite detectar diferentes tipos de cap presentes en el extremo 5´ del RNA, dicha metodología combina la cromatografía liquida de alta resolución (HPLC) con la dilución isotópica acoplada a espectrometría de masas (LC-MS/MS) (74). Con esta técnica se caracterizaron los diferentes tipos de cap presentes en el RNA obtenido de diferentes líneas celulares y microorganismos incluido el virus del dengue (DENV). El DENV tiene un genoma de RNA de cadena sencilla de polaridad positiva que

codifica la maquinaria necesaria para adicionar cap tipo 1 a sus transcritos virales. Al analizar el RNA genómico extraído de viriones purificados se encontró, como era esperado, que el 70% del RNA tenía cap tipo 1, mientras que solo el 14% tenía cap tipo 0. De manera inesperada, también se detectaron estructuras cap no canónicas como UDP-GlcNAc, NAD y FAD (74). La presencia de cap no canónicos en el RNA genómico de DENV resulta interesante; sin embargo, es necesario determinar si estas estructuras tienen alguna relevancia biológica durante el ciclo replicativo de DENV. Está técnica también podría ser utilizada en el estudio de los RNAs de rotavirus con el objetivo de determinar si el genoma encapsidado en las partículas virales o el RNA viral presente en las células infectadas posee en el extremo 5´ algún tipo de cap no canónico.

Con la caracterización de los dominios de VP3 involucrados en la adición de cap (42)(48), y el reciente desarrollo del sistema de genética reversa para rotavirus (11) es posible producir virus con mutaciones puntuales en los diferentes dominios de VP3, particularmente en los involucrados en la actividad RNA guanililtransferasa, con el objetivo de establecer cuál es función de la estructura cap durante la infección de rotavirus y poder determinar si la actividad de adición de cap de VP3 es importante para el ensamble de nuevas partículas virales en modelos de infección *in vitro* e *in vivo*. También esta metodología (genética reversa) nos permitirá superar las limitaciones intrínsecas de los ensayos de silenciamiento usando siRNAs. Actualmente se han desarrollo fármacos que tienen como blanco a las proteínas no estructurales NS5 y NsP1 de los flavivirus y alfavirus, respectivamente(75)(76). Debido a la importancia que tiene la maquinaria de adición del cap para algunos virus, las enzimas involucradas en la biosíntesis del 5´cap pueden ser blanco para

el tratamiento de las infecciones virales. Estos fármacos han demostrado inhibir de manera eficiente la replicación viral en ensayos *in vitro*; sin embargo, aún es necesario evaluar su actividad *in vivo*. Es importante estudiar las modificaciones a las que el RNA viral de rotavirus es sometido, para así poder comprender la función y el impacto que puedan tener durante el ciclo replicativo con el objetivo de poder desarrollar terapias específicas que permitan contender contra la infección viral.

CONCLUSIONES

- Las partículas virales infecciosas de rotavirus contienen una proporción similar de +RNAs con/sin ^{7me}GpppGcap.
- En las células infectadas con rotavirus la abundancia de RNAs virales con y sin ^{7me}GpppGcap cambia durante el ciclo replicativo.
- La eficiencia de adición de cap en los +RNAs en ensayos *in vitro* es muy similar a la encontrada en las partículas virales
- El co-silenciamiento de las proteínas VP3 y RNasa L incrementa significativamente la proporción de +RNAs con cap en tiempos tardíos de la infección.
- La proporción de +RNAs con ^{7me}GpppGcap que se encapsida en las partículas virales maduras no depende de la abundancia de las poblaciones de +RNAs con y sin cap presentes en las células infectadas.

PERSPECTIVAS

- Generar mutantes de VP3 con cambios en los dominios involucrados en la adición de cap, mediante el sistema de genética reversa.
- Determinar si la presencia de cap es importante para la incorporación de +RNA a las partículas virales.
- Determinar si los RNAs sin cap juegan algún papel durante el ciclo replicativo de rotavirus.
- Evaluar la proporción de RNAs con/sin cap en otras cepas de rotavirus.
- Determinar qué factores influyen en el incremento de la infectividad específica de las partículas producidas en células en las que VP3 fue silenciada.

REFERENCIAS

1. Troeger C, Khalil IA, Rao PC, Cao S, Blacker BF, Ahmed T, et al. Rotavirus Vaccination and the Global Burden of Rotavirus Diarrhea Among Children Younger Than 5 Years. JAMA Pediatr. 2018 Oct 1;172(10):958–65.
2. Jenni S, Salgado EN, Herrmann T, Li Z, Grant T, Grigorieff N, et al. In situ Structure of Rotavirus VP1 RNA-Dependent RNA Polymerase. J Mol Biol. 2019/06/21. 2019 Aug 9;431(17):3124–38.
3. Crawford SE, Ramani S, Tate JE, Parashar UD, Svensson L, Hagbom M, et al. Rotavirus infection. Nat Rev Dis Prim. 2017;3(1):17083.
4. Estes M.K KA. Rotaviruses. In: Wilkins WKHW&, editor. Fields Virology. 5th ed. Philadelphia: In Knipe DM, Howley PM, Griffin DE, Lamb RA, Martin MA, Roizman B, Straus SE (ed); 2007. p. 1917–74.
5. Gentsch JR, Laird AR, Bielfelt B, Griffin DD, Bányai K, Ramachandran M, et al. Serotype Diversity and Reassortment between Human and Animal Rotavirus Strains: Implications for Rotavirus Vaccine Programs. J Infect Dis. 2005 Sep 1;192(Supplement_1):S146–59.
6. Santos N, Hoshino Y. Global distribution of rotavirus serotypes/genotypes and its implication for the development and implementation of an effective rotavirus vaccine. Rev Med Virol. 2005 Jan 1;15(1):29–56.
7. Poncet D, Aponte C, Cohen J. Rotavirus protein NSP3 (NS34) is bound to the 3' end consensus sequence of viral mRNAs in infected cells. J Virol. 1993 Jun 1;67(6):3159–65.
8. Maria P, Thierry D, Jeanne G, Didier P. Identification of the RNA-Binding, Dimerization, and eIF4GI-Binding Domains of Rotavirus Nonstructural Protein NSP3. J Virol. 1999 Jul 1;73(7):5411–21.
9. M. OK, N. RH, T. PJ. Residues of the Rotavirus RNA-Dependent RNA Polymerase Template Entry Tunnel That Mediate RNA Recognition and Genome Replication . J Virol. 2011 Mar 1;85(5):1958–69.
10. Patton JT, Vasquez-Del Carpio R, Tortorici MA, Taraporewala ZFBT-A in VR. Coupling of Rotavirus Genome Replication and Capsid Assembly. In Academic Press; 2006. p. 167–201.
11. Kanai Y, Komoto S, Kawagishi T, Nouda R, Nagasawa N, Onishi M, et al. Entirely plasmid-based reverse genetics system for rotaviruses. Proc Natl Acad Sci. 2017 Feb 28;114(9):2349 LP – 2354.
12. Mossel EC, Ramig RF. A lymphatic mechanism of rotavirus extraintestinal spread in the neonatal mouse. J Virol. 2003 Nov;77(22):12352–6.
13. Kapil S, E. BS, Khalil E, Xi-Lei Z, R. BJ, E. CS, et al. Human Intestinal Enteroids: a New Model To Study Human Rotavirus Infection, Host Restriction, and Pathophysiology. J Virol. 2022 Feb 28;90(1):43–56.
14. Arias CF, López S. Rotavirus cell entry: not so simple after all. Curr Opin Virol. 2021;48:42–8.
15. López S, Arias CF. Multistep entry of rotavirus into cells: a Versaillesque dance. Trends Microbiol. 2004 Jun 1;12(6):271–8.
16. Gutiérrez M, Isa P, Sánchez-San Martin C, Pérez-Vargas J, Espinosa R, Arias CF, et al. Different rotavirus strains enter MA104 cells through different endocytic pathways: the role of clathrin-mediated endocytosis. J Virol.

2010/07/14. 2010 Sep;84(18):9161–9.
17. Torres-Flores JM, Silva-Ayala D, Espinoza MA, López S, Arias CF. The tight junction protein JAM-A functions as coreceptor for rotavirus entry into MA104 cells. Virology. 2015;475:172–8.
18. F. AC, Daniela S-A, Susana L, B. T. Rotavirus Entry: a Deep Journey into the Cell with Several Exits. J Virol. 2022 Feb 28;89(2):890–3.
19. A. D-SM, Pedro R, Rafaela E, Yasutaka H, Susana L, F. AC. The Spike Protein VP4 Defines the Endocytic Pathway Used by Rotavirus To Enter MA104 Cells. J Virol. 2013 Feb 1;87(3):1658–63.
20. Eichwald C, Rodriguez JF, Burrone OR. Characterization of rotavirus NSP2/NSP5 interactions and the dynamics of viroplasm formation. J Gen Virol. 2004;85(3):625–34.
21. Garcés Suárez Y, Martínez JL, Torres Hernández D, Hernández HO, Pérez-Delgado A, Méndez M, et al. Nanoscale organization of rotavirus replication machineries. Chakraborty AK, Desselberger U, Kaminski CF, editors. Elife. 2019;8:e42906.
22. Boudreaux CE, Kelly DF, McDonald SM. Electron microscopic analysis of rotavirus assembly-replication intermediates. Virology. 2015;477:32–41.
23. Jourdan N, Maurice M, Delautier D, Quero AM, Servin AL, Trugnan G. Rotavirus is released from the apical surface of cultured human intestinal cells through nonconventional vesicular transport that bypasses the Golgi apparatus. J Virol. 1997 Nov 1;71(11):8268–78.
24. Trejo-Cerro Ó, Eichwald C, Schraner EM, Silva-Ayala D, López S, Arias CF. Actin-Dependent Nonlytic Rotavirus Exit and Infectious Virus Morphogenetic Pathway in Nonpolarized Cells. J Virol. 2018 Feb 26;92(6):e02076-17.
25. Trask SD, McDonald SM, Patton JT. Structural insights into the coupling of virion assembly and rotavirus replication. Nat Rev Microbiol. 2012;10(3):165–77.
26. Furuichi Y. Discovery of m(7)G-cap in eukaryotic mRNAs. Proc Jpn Acad Ser B Phys Biol Sci. 2015;91(8):394–409.
27. Galloway A, Cowling VH. mRNA cap regulation in mammalian cell function and fate. Biochim Biophys acta Gene Regul Mech. 2018/10/09. 2019 Mar;1862(3):270–9.
28. Decroly E, Ferron F, Lescar J, Canard B. Conventional and unconventional mechanisms for capping viral mRNA. Nat Rev Microbiol. 2012;10(1):51–65.
29. Ghosh A, Lima CD. Enzymology of RNA cap synthesis. WIREs RNA. 2010 Jul 1;1(1):152–72.
30. Werner M, Purta E, Kaminska KH, Cymerman IA, Campbell DA, Mittra B, et al. 2'-O-ribose methylation of cap2 in human: function and evolution in a horizontally mobile family. Nucleic Acids Res. 2011/02/09. 2011 Jun;39(11):4756–68.
31. Kasprzyk R, Jemielity J. Enzymatic Assays to Explore Viral mRNA Capping Machinery. ChemBioChem. 2021 Dec 2;22(23):3236–53.
32. Ramanathan A, Robb GB, Chan S-H. mRNA capping: biological functions and applications. Nucleic Acids Res. 2016/06/17. 2016 Sep 19;44(16):7511–26.
33. Kiledjian M. Eukaryotic RNA 5′-End NAD+ Capping and DeNADding. Trends Cell Biol. 2018;28(6):454–64.

34. Wang J, Alvin Chew BL, Lai Y, Dong H, Xu L, Balamkundu S, et al. Quantifying the RNA cap epitranscriptome reveals novel caps in cellular and viral RNA. Nucleic Acids Res. 2019 Nov 18;47(20):e130–e130.
35. Brisse M, Ly H. Comparative Structure and Function Analysis of the RIG-I-Like Receptors: RIG-I and MDA5 . Vol. 10, Frontiers in Immunology . 2019.
36. C. DS, Chen W, T. MM, Anand R, Fuguo J, G. KA, et al. Structural basis for m7G recognition and 2′-O-methyl discrimination in capped RNAs by the innate immune receptor RIG-I. Proc Natl Acad Sci. 2016 Jan 19;113(3):596–601.
37. M. AY, Theres LB, Saúl M-M, Regina C, Matthias H, Andreas P, et al. Structure of human IFIT1 with capped RNA reveals adaptable mRNA binding and mechanisms for sensing N1 and N2 ribose 2′-O methylations. Proc Natl Acad Sci. 2017 Mar 14;114(11):E2106–15.
38. Zhou X, Michal JJ, Zhang L, Ding B, Lunney JK, Liu B, et al. Interferon induced IFIT family genes in host antiviral defense. Int J Biol Sci. 2013/02/11. 2013;9(2):200–8.
39. Ahola T, Kääriäinen L. Reaction in alphavirus mRNA capping: formation of a covalent complex of nonstructural protein nsP1 with 7-methyl-GMP. Proc Natl Acad Sci. 1995;92(2):507–11.
40. Reich S, Guilligay D, Pflug A, Malet H, Berger I, Crépin T, et al. Structural insight into cap-snatching and RNA synthesis by influenza polymerase. Nature. 2014;516(7531):361–6.
41. Gu W, Gallagher GR, Dai W, Liu P, Li R, Trombly MI, et al. Influenza A virus preferentially snatches noncoding RNA caps. RNA. 2015/10/01. 2015 Dec;21(12):2067–75.
42. Ogden KM, Snyder MJ, Dennis AF, Patton JT. Predicted structure and domain organization of rotavirus capping enzyme and innate immune antagonist VP3. J Virol. 2014/06/04. 2014 Aug;88(16):9072–85.
43. Chen D, Luongo CL, Nibert ML, Patton JT. Rotavirus Open Cores Catalyze 5′-Capping and Methylation of Exogenous RNA: Evidence That VP3 Is a Methyltransferase. Virology. 1999;265(1):120–30.
44. Imai M, Akatani K, Ikegami N, Furuichi Y. Capped and conserved terminal structures in human rotavirus genome double-stranded RNA segments. J Virol. 1983;47(1):125–36.
45. Sánchez-Tacuba L, Rojas M, Arias CF, López S. Rotavirus Controls Activation of the 2'-5'-Oligoadenylate Synthetase/RNase L Pathway Using at Least Two Distinct Mechanisms. J Virol. 2015/09/23. 2015 Dec;89(23):12145–53.
46. Morelli M, Ogden KM, Patton JT. Silencing the alarms: Innate immune antagonism by rotavirus NSP1 and VP3. Virology. 2015;479–480:75–84.
47. Ding S, Zhu S, Ren L, Feng N, Song Y, Ge X, et al. Rotavirus VP3 targets MAVS for degradation to inhibit type III interferon expression in intestinal epithelial cells. Elife. 2018 Nov 21;7:e39494.
48. Kumar D, Yu X, Crawford SE, Moreno R, Jakana J, Sankaran B, et al. 2.7 Å cryo-EM structure of rotavirus core protein VP3, a unique capping machine with a helicase activity. Sci Adv. 2020 Apr 1;6(16):eaay6410.
49. Sutton G, Grimes JM, Stuart DI, Roy P. Bluetongue virus VP4 is an RNA-capping assembly line. Nat Struct Mol Biol. 2007;14(5):449–51.
50. Taraporewala ZF, Jiang X, Carpio RV-D, Jayaram H, Prasad BVV, Patton JT.

Structure-Function Analysis of Rotavirus NSP2 Octamer by Using a Novel Complementation System. J Virol. 2006;80(16):7984–94.
51. Ding K, Celma CC, Zhang X, Chang T, Shen W, Atanasov I, et al. In situ structures of rotavirus polymerase in action and mechanism of mRNA transcription and release. Nat Commun. 2019;10(1):2216.
52. McDonald SM, Patton JT. Rotavirus VP2 core shell regions critical for viral polymerase activation. J Virol. 2011 Apr;85(7):3095–105.
53. Zeng CQ-Y, Estes MK, Charpilienne A, Cohen J. The N Terminus of Rotavirus VP2 Is Necessary for Encapsidation of VP1 and VP3. J Virol. 1998;72(1):201–8.
54. Eaton HE, Kobayashi T, Dermody TS, Johnston RN, Jais PH, Shmulevitz M, et al. African Swine Fever Virus NP868R Capping Enzyme Promotes Reovirus Rescue during Reverse Genetics by Promoting Reovirus Protein Expression, Virion Assembly, and RNA Incorporation into Infectious Virions. J Virol. 2017;91(11):e02416-16.
55. Sokoloski KJ, Haist KC, Morrison TE, Mukhopadhyay S, Hardy RW. Noncapped Alphavirus Genomic RNAs and Their Role during Infection. J Virol. 2015/04/01. 2015 Jun;89(11):6080–92.
56. WANG H-L, O'REAR J, STOLLAR V. Mutagenesis of the Sindbis Virus nsP1 Protein: Effects on Methyltransferase Activity and Viral Infectivity. Virology. 1996;217(2):527–31.
57. LaPointe AT, Moreno-Contreras J, Sokoloski KJ. Increasing the Capping Efficiency of the Sindbis Virus nsP1 Protein Negatively Affects Viral Infection. MBio. 2018 Dec 11;9(6):e02342-18.
58. T. LA, Douglas L V, E. WC, J. SK, T. PJ. Production of Noncapped Genomic RNAs Is Critical to Sindbis Virus Disease and Pathogenicity. MBio. 2022 Feb 11;11(6):e02675-20.
59. Uzri D, Greenberg HB. Characterization of Rotavirus RNAs That Activate Innate Immune Signaling through the RIG-I-Like Receptors. PLoS One. 2013 Jul 23;8(7):e69825.
60. Song M-G, Bail S, Kiledjian M. Multiple Nudix family proteins possess mRNA decapping activity. RNA. 2013/01/25. 2013 Mar;19(3):390–9.
61. Ayala-Breton C, Arias M, Espinosa R, Romero P, Arias CF, López S. Analysis of the kinetics of transcription and replication of the rotavirus genome by RNA interference. J Virol. 2009/06/24. 2009 Sep;83(17):8819–31.
62. Livak KJ, Schmittgen TD. Analysis of Relative Gene Expression Data Using Real-Time Quantitative PCR and the 2−ΔΔCT Method. Methods. 2001;25(4):402–8.
63. Hauser M, Dearnaley WJ, Varano AC, Casasanta M, McDonald SM, Kelly DF. Cryo-EM Reveals Architectural Diversity in Active Rotavirus Particles. Comput Struct Biotechnol J. 2019 Jul 31;17:1178–83.
64. Zhou A, Hassel BA, Silverman RH. Expression cloning of 2-5A-dependent RNAase: A uniquely regulated mediator of interferon action. Cell. 1993;72(5):753–65.
65. Schwartz SL, Conn GL. RNA regulation of the antiviral protein 2′-5′-oligoadenylate synthetase. Wiley Interdiscip Rev RNA. 2019;10(4):1–17.
66. Netzband R, Pager CT. Epitranscriptomic marks: Emerging modulators of

RNA virus gene expression. Wiley Interdiscip Rev RNA. 2019;(October):1–25.
67. Helm M, Motorin Y. Detecting RNA modifications in the epitranscriptome: Predict and validate. Nat Rev Genet. 2017;18(5):275–91.
68. Kell AM, Gale M. RIG-I in RNA virus recognition. Virology. 2015;479–480:110–21.
69. Beachboard DC, Horner SM. Innate immune evasion strategies of DNA and RNA viruses. Curr Opin Microbiol. 2016/06/08. 2016 Aug;32:113–9.
70. Uzri D, Greenberg HB. Characterization of Rotavirus RNAs That Activate Innate Immune Signaling through the RIG-I-Like Receptors. PLoS One. 2013;8(7):1–14.
71. Song Y, Feng N, Sanchez-Tacuba L, Yasukawa LL, Ren L, Silverman RH, et al. Reverse Genetics Reveals a Role of Rotavirus VP3 Phosphodiesterase Activity in Inhibiting RNase L Signaling and Contributing to Intestinal Viral Replication *In Vivo*. J Virol. 2020;94(9):e01952-19.
72. Pan R, Kindler E, Cao L, Zhou Y, Zhang Z, Liu Q, et al. N7-Methylation of the Coronavirus RNA Cap Is Required for Maximal Virulence by Preventing Innate Immune Recognition. MBio. 2022;13(1):e03662-21.
73. Sokoloski KJ, Snyder AJ, Liu NH, Hayes CA, Mukhopadhyay S, Hardy RW. Encapsidation of host-derived factors correlates with enhanced infectivity of Sindbis virus. J Virol. 2013/09/04. 2013 Nov;87(22):12216–26.
74. Wang J, Alvin Chew BL, Lai Y, Dong H, Xu L, Balamkundu S, et al. Quantifying the RNA cap epitranscriptome reveals novel caps in cellular and viral RNA. Nucleic Acids Res. 2019;47(20):e130.
75. Delang L, Li C, Tas A, Quérat G, Albulescu IC, De Burghgraeve T, et al. The viral capping enzyme nsP1: a novel target for the inhibition of chikungunya virus infection. Sci Rep. 2016;6(1):31819.
76. Stahla-Beek HJ, April DG, Saeedi BJ, Hannah AM, Keenan SM, Geiss BJ. Identification of a Novel Antiviral Inhibitor of the Flavivirus Guanylyltransferase Enzyme. J Virol. 2012;86(16):8730–9.
77. Pan Y, Zhang D, Yang P, Poon LLM, Wang Q. Viral load of SARS-CoV-2 in clinical samples. Lancet Infect Dis. 2020;20(4):411–2.
78. Wang Y, Kang H, Liu X, Tong Z. Combination of RT-qPCR testing and clinical features for diagnosis of COVID-19 facilitates management of SARS-CoV-2 outbreak. J Med Virol. 2020;92(6):538–9.
79. Khurshid Z, Asiri FYI, Al Wadaani H. Human saliva: Non-invasive fluid for detecting novel coronavirus (2019-nCoV). Int J Environ Res Public Health. 2020;17(7):17–20.
80. Ng K, Poon BH, Kiat Puar TH, Shan Quah JL, Loh WJ, Wong YJ, et al. COVID-19 and the Risk to Health Care Workers: A Case Report. Ann Intern Med. 2020;172(11):766–7.
81. Moreno-Contreras J, Espinoza MA, Sandoval-Jaime C, Cantú-Cuevas MA, Barón-Olivares H, Ortiz-Orozco OD, et al. Saliva sampling and its direct lysis, an excellent option to increase the number of SARS-CoV-2 diagnostic tests in settings with supply shortages. J Clin Microbiol. 2020;58(10):1–6.
82. Morandi P-A, Schockmel GA, Yerly S, Burgisser P, Erb P, Matter L, et al. Detection of Human Immunodeficiency Virus Type 1 (HIV-1) RNA in Pools of Sera Negative for Antibodies to HIV-1 and HIV-2. J Clin Microbiol. 1998 Jun

1;36(6):1534 LP – 1538.
83. Abdalhamid B, Bilder CR, McCutchen EL, Hinrichs SH, Koepsell SA, Iwen PC. Assessment of specimen pooling to conserve SARS CoV-2 testing resources. Am J Clin Pathol. 2020;153(6):715–8.
84. Corman VM, Landt O, Kaiser M, Molenkamp R, Meijer A, Chu DKW, et al. Detection of 2019 novel coronavirus (2019-nCoV) by real-time RT-PCR. Eurosurveillance. 2020;25(3).
85. Quentin O, Sylvie P, Olivier M, Julie G, Charlotte T, Nadine A, et al. Prospective evaluation of the point-of-care use of a rapid antigenic SARS-CoV-2 immunochromatographic test in a pediatric emergency department. Clin Microbiol Infect. 2022 Jan 24;

Los resultado de este trabajo fueron publicado en la revista Journal of Virology:

Mature Rotavirus Particles Contain Equivalent Amounts of 7-meGpppG-Capped and Noncapped Viral Positive-Sense RNAs.

Journal of Virology®

GENOME REPLICATION AND REGULATION OF VIRAL GENE EXPRESSION

Mature Rotavirus Particles Contain Equivalent Amounts of ^{7me}GpppG-Capped and Noncapped Viral Positive-Sense RNAs

Joaquin Moreno-Contreras,[a] Liliana Sánchez-Tacuba,[b,c,d] Carlos F. Arias,[a] Susana López[a]

[a]Departamento de Genética del Desarrollo y Fisiología Molecular, Instituto de Biotecnología, Universidad Nacional Autónoma de México, Cuernavaca, Morelos, México
[b]Department of Medicine, Division of Gastroenterology and Hepatology, Stanford School of Medicine, Stanford, California, USA
[c]Department of Microbiology and Immunology, Stanford School of Medicine, Stanford, California, USA
[d]VA Palo Alto Health Care System, Department of Veterans Affairs, Palo Alto, California, USA

ABSTRACT Viruses have evolved different strategies to overcome their recognition by the host innate immune system. The addition of caps at their 5′ RNA ends is an efficient mechanism not only to ensure escape from detection by the innate immune system but also to ensure the efficient synthesis of viral proteins. Rotavirus mRNAs contain a type 1 cap structure at their 5′ end that is added by the viral capping enzyme VP3, which is a multifunctional protein with all the enzymatic activities necessary to add the cap and also functions as an antagonist of the 2′-5′-oligoadenylate synthetase (OAS)/RNase L pathway. Here, the relative abundances of capped and noncapped viral RNAs during the replication cycle of rotavirus were determined. We found that both classes of rotaviral plus-sense RNAs (+RNAs) were encapsidated and that they were present in a 1:1 ratio in the mature infectious particles. The capping of viral +RNAs was dynamic, since different ratios of capped and noncapped RNAs were detected at different times postinfection. Similarly, when the relative amounts of capped and uncapped viral +RNAs produced in an *in vitro* transcription system were determined, we found that the proportions were very similar to those in the mature viral particles and in infected cells, suggesting that the capping efficiency of VP3, both *in vivo* and *in vitro*, might be close to 50%. Unexpectedly, when the effect of simultaneously knocking down the expression of VP3 and RNase L on the cap status of viral +RNAs was evaluated, we found that, even though at late times postinfection there was an increased proportion of capped viral RNAs in infected cells, the viral particles isolated from this condition contained equal ratios of capped and noncapped viral RNA, suggesting that there might be selective packaging of capped and noncapped RNAs.

IMPORTANCE Rotaviruses have a genome composed of 11 segments of double-stranded RNA. Whether all 5′ ends of the positive-sense genomic RNAs contained in the mature viral particles are modified by a cap structure is unknown. In this work, we characterized the relative proportions of capped and noncapped viral RNAs in rotavirus-infected cells and in viral particles by using a direct quantitative assay. We found that, independent of the relative proportions of capped/noncapped RNAs present in rotavirus-infected cells, there were similar proportions of these two kinds of 5′-modified positive-sense RNAs in the viral particles.

KEYWORDS rotavirus, dsRNA, capping enzymes, VP3, RNA modifications

A signature of cellular mRNAs is the presence of N7-methyl-GTP (cap) at their 5′ end. The cap structure is important for different mRNA cellular processes, including splicing, nuclear-cytoplasmic export, translation initiation, stability, and recognition of self from foreign RNAs (1, 2). The canonical RNA-capping pathway takes place in the nucleus and occurs cotranscriptionally by a sequential enzymatic process that involves three enzymes: an RNA triphosphatase (RTPase) that removes the γ-phosphate from 5′-triphosphate to generate a 5′-diphosphate end, an RNA guanylyltransferase (GTase)

Editor Colin R. Parrish, Cornell University

Address correspondence to Susana López, susana@ibt.unam.mx.
The authors declare no conflict of interest.
Received 27 July 2022
Accepted 3 August 2022

that binds a GMP nucleotide from GTP to the 5′-diphosphate RNA to form a 5′-guanylylated RNA, and a guanine-N7-methyltransferase (N7-MTase) that transfers a methyl group from *S*-adenosylmethionine (SAM) to the N7 position of the terminal guanine base, completing the synthesis of the type 0 cap structure (3). Additionally, the RNA 2′-*O*-ribose methyltransferase adds a methionine to the ribose 2′-hydroxyl (2′-O) of the first nucleotide, forming the type 1 cap structure.

In the cell's cytoplasm, noncapped RNAs are sensed as nonself by cellular cytoplasmic pattern recognition receptors, such as RIG-1 or MDA5, triggering a signaling cascade that ends with the expression of interferon, inducing an antiviral state (1). To overcome the recognition of their transcripts by proteins of the innate immune system, viruses have evolved different strategies to hide the 5′ end of viral mRNAs, including hijacking the cellular capping machinery, acquiring cap structures from cellular RNAs by "cap snatching," or encoding their own capping machinery (4, 5).

Rotaviruses are a leading cause of severe gastroenteritis in young animals, including humans, causing an estimated 258 million episodes of diarrhea and 128,500 deaths of children younger than 5 years annually, mainly in developing countries around the world (6). These nonenveloped viruses belong to the *Reoviridae* family and are formed by three protein layers that surround the genome, which is composed of 11 segments of double-stranded RNA (dsRNA). The structural proteins VP4 and VP7 form the outer layer, the middle layer is composed of VP6, and the innermost layer is formed by VP2, small amounts of the viral RNA-dependent RNA polymerase (RdRp) VP1, and the methyl-guanylyltransferase VP3 (7).

After entering the cell, the viral outer layer is released, yielding a double-layered particle (DLP) that is transcriptionally active and begins the synthesis of the plus-sense, messenger viral RNAs (+RNAs); these mRNAs direct the synthesis of all viral proteins and are also used as templates for the synthesis of the negative-strand RNAs (−RNAs) to form the genomic dsRNA. Once a critical amount of viral proteins is made, the formation of cytoplasmic, electrodense structures called viroplasms begins; in these nonmembranous structures, the replication of the viral genome and the initial steps of the morphogenesis of virions take place (8). The assembly of new transcriptionally active DLPs in viroplasms initiates a second round of transcription, increasing the amount of viral RNAs in the infected cell (9).

Similar to cellular mRNAs, rotavirus mRNAs contain a type 1 cap (m^7GpppGm) at their 5′ end, a structure that is added by the 98-kDa viral protein VP3, encoded in dsRNA segment 3 of the rotavirus genome (10). Recently, Kumar et al. described a detailed cryo-electron microscopy structure of this protein that showed that VP3 forms a stable tetramer with a modular organization of five domains, four of them involved in cap addition (11). While previous studies demonstrated that VP3 had RNA binding and guanylyl- and methyltransferase activities (8, 10), it was not clear whether the helicase and RNA triphosphatase (RTPase) activities were also present in VP3 or were in another viral protein. In their work, Kumar et al. demonstrated that these last two activities were located in the phosphodiesterase (PDE) domain of VP3 (11, 12). The PDE domain is also involved in the degradation of the 2′-5′-oligoadenylates, thus blocking the activation of RNase L and inhibiting the innate immune 2′-5′-oligoadenylate synthetase (OAS)/RNase L pathway (13, 14).

Thus far, it has not been characterized whether the viral +RNAs that are translated (mRNAs) during the replication cycle of rotavirus contain a cap structure while the +RNAs that serve as templates for the negative-strand synthesis are uncapped or whether all +RNAs synthesized in infected cells contain a 5′ cap structure. To address this question, we sought to quantitatively evaluate the relative abundances of capped and noncapped viral RNAs during rotavirus replication. Here, we report that both capped and noncapped rotaviral +RNAs are present in similar proportions in mature infectious particles. We also show that the capping of viral +RNAs is dynamic, since different ratios of capped and noncapped RNAs are found at different times postinfection. Likewise, when the relative amounts of capped and noncapped viral +RNAs produced in an *in vitro* transcription (IVT) system are characterized, their proportions are very similar to those found in infected cells, suggesting that the capping efficiency of VP3 *in vivo* and *in vitro* is close to 50%.

Unexpectedly, in cells where VP3 was silenced, the specific infectivity of the viral particles produced was higher than in control cells, although they contained a similar ratio of capped and noncapped RNAs; as expected, the viral RNA synthesized *in vitro* by the VP3-deficient particles was poorly capped. Finally, when the effect of cosilencing VP3 and RNase L on the cap status of viral +RNA was evaluated, we found that there were increased proportions of capped viral RNAs at late times of infection, but the viral particles isolated from this condition contained an equal ratio of capped and noncapped RNA, suggesting that there might be selective packaging of capped and noncapped viral RNAs.

RESULTS

The genomic RNA segments within the mature rotavirus particles contain capped and noncapped positive-sense RNA strands. The rotavirus genome, formed by 11 dsRNA segments, is enclosed in viral particles; however, whether the positive strand of the genomic dsRNA contained in the mature viral capsid is capped or not has not been characterized (15, 16). To quantitatively evaluate the proportion of the 5′ cap present on rotaviral RNAs, we resorted to an enzymatic method for cap quantification that was previously described for use in determining the presence of cap in the RNA of Sindbis virus (SINV) (17). In this method, total RNA is treated with a phosphatase to remove 5′-terminal phosphates. The sample is then divided into two equal aliquots. One is treated with polynucleotide kinase (PNK), which introduces a phosphate group into the 5′ end of uncapped RNAs, yielding a mixture of 5′-monophosphates and ^{7me}GpppG-capped RNAs that are not affected by the phosphatase or PNK treatments. The other half of the phosphatase-treated RNA is incubated with a decapping enzyme that cleaves off the ^{7me}Gppp, leaving a 5′-terminal monophosphate. Both reaction mixtures are then subjected to an RNA ligation step using a 5′ adaptor RNA oligonucleotide linker. These two treatments result in the specific modification of the original noncapped or ^{7me}GpppG-capped viral RNAs with a 5′ adaptor linker (Fig. 1A). The modified RNAs are then used as templates for the synthesis of cDNA via reverse transcription (RT), using a reverse primer that hybridizes specifically to the positive strand of the viral RNA to be analyzed; afterwards, the RT reaction is used for quantitative PCRs (qPCRs), using oligonucleotides complementary to the 5′ adaptor linker sequence and to the 5′ end of the viral RNA. For our purpose, specific oligonucleotides to detect an internal amplicon on the +RNA viral gene 10 and oligonucleotides for the 5′ adaptor linker sequence and the 5′ end of the same viral RNA were used (Fig. 1B). This assay allows the quantification of the amounts of ^{7me}GpppG-capped and noncapped (capped/noncapped) viral RNAs in a given preparation.

To determine the presence or absence of the 5′ cap structure on the positive strand of the genomic dsRNA, triple layered particles (TLPs; mature infectious particles) obtained from rotavirus-infected MA104 cells were purified by isopycnic CsCl gradients. Before RNA extraction, the purified viral particles were treated with RNase A to remove any possible RNA bound to the exterior of the TLPs. Then, the genomic dsRNA was isolated and used to perform the enzymatic method for ^{7me}GpppGcap quantification. We found that, contrary to what was thought, there was a significant amount of noncapped RNAs present in the purified particles (40% ± 8.3%) (Fig. 1C, TLPs).

The *in vitro* capping activity of VP3. Since there was a proportion of the encapsidated genomic-dsRNA positive strands that was not capped, we evaluated the efficiency of the capping enzyme *in vitro*. After rotavirus entry into cells, the outermost layer of the TLPs is released, generating double-layered particles (DLPs) that are transcriptionally active. Under appropriate conditions, purified DLPs can synthesize large amounts of viral +RNA *in vitro* (10); however, whether all mRNAs synthesized are capped is unknown. To characterize the efficiency of the VP3 capping activity, DLPs were obtained from rotavirus strain RRV-infected MA104 cells, and the viral particles were concentrated by centrifugation through a 40% sucrose cushion and resuspended in TNE buffer (Tris-HCl, NaCl, and EGTA), which contains EDTA and causes the release of the outer-layer proteins VP4 and VP7. These DLPs were used for an *in vitro*

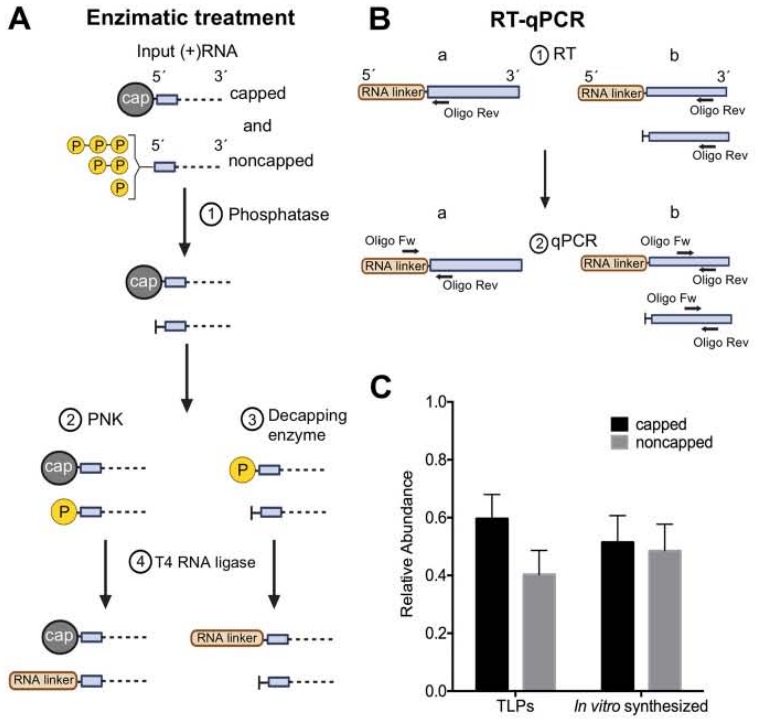

FIG 1 Quantitative determination of capped and noncapped viral RNA. Schematic representation of the method used for the quantitative capping determination on viral 5′ ends. The input RNA consists of either genomic dsRNA or viral single-stranded +RNA. (A) Enzymatic treatment. (1) Capped or noncapped single-stranded +RNAs were treated with Antarctic phosphatase, and then the reaction mixture was split in two. (2) One half was treated with PNK, which adds a phosphate group to the 5′-OH RNA. (3) The other half was treated with RppH, which cleaves the cap from RNA molecules, leaving a 5′-phosphate group. (4) An RNA linker was ligated to the free phosphate groups present at the 5′ ends of RNA molecules, using T4 RNA ligase. (B) RT-qPCRs. Two RT-qPCRs were performed. Specific oligonucleotides were employed to perform the reverse transcription (RT) reaction to detect the amplicon produced by the ligation of the RNA linker with viral segment 10 (a) or to detect the total amount of viral gene 10 in the reaction mixture (b). All reactions were performed as detailed in Materials and Methods. (C) Quantitative determination of capped and noncapped RNAs in mature viral particles (TLPs) and in *in vitro*-synthesized viral RNAs. The arithmetic mean values ± standard deviations from three independent biological replicates are shown.

transcription assay as described in Materials and Methods; after single-stranded RNA (ssRNA) precipitation with LiCl, the proportions of ^{7me}GpppG-capped and noncapped 5′ ends in the *in vitro*-transcribed RNAs was determined as described above. A ratio of capped/noncapped RNA of 1:1 (50% ± 9.1%) (Fig. 1C) was found, suggesting that in this assay, VP3 has a capping efficiency of about 50%.

VP3 capping activity during the infection cycle. To determine the capping activity of VP3 during the replication cycle, we quantitated the amounts of ^{7me}GpppG-capped and noncapped viral RNA produced in infected cells. For this, total RNA was isolated from strain RRV-infected cells at different times postinfection, and the enzymatic assay to quantitate capped/noncapped viral RNAs was performed. As shown by the results in Fig. 2A, we found that the relative amounts of capped versus noncapped viral +RNAs varied during the rotavirus replication cycle. The overall ratio of capped/noncapped viral RNAs at the beginning of the infection (0 hpi) was 1:1 (50% ± 1.8%), probably reflecting the capped/noncapped ratio of the input virus, while at 3 h postinfection (hpi), the capped/noncapped RNA ratio decreased to 33% ± 4.2%. In contrast, at 6 hpi, the amount of ^{7me}GpppG-capped viral RNAs increased up to 73% ± 4.2%, and a ratio of capped/noncapped RNAs close to 50% ± 4.6% was observed at later times postinfection (9 and 12 hpi). In parallel, we quantitated by an

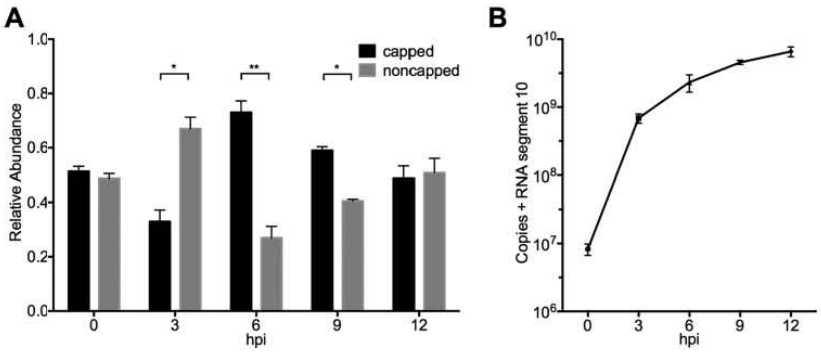

FIG 2 Quantitative determination of capped and noncapped RNAs at different times postinfection. (A) MA104 cells were infected with RRV at an MOI of 3, total RNA was extracted at the indicated times postinfection, and the amounts of capped and noncapped RNA were measured at each time point as described in Materials and Methods. The arithmetic mean values ± standard deviations from three independent biological replicates are shown. (B) The levels of viral +RNA gene 10 synthesized in rotavirus-infected cells were quantitated by an RT-qPCR assay at the indicated times postinfection. The number of viral copies at each time point was determined using a standard curve that was generated using a 10-fold serial dilution of an *in vitro*-T7-transcribed RNA that contains the sequence of rotavirus RRV segment 10. The arithmetic mean values ± standard deviations from three independent biological replicates are shown. Statistical significance was determined by Student's *t* test. *, $P < 0.05$; **, $P < 0.01$.

RT-qPCR assay the abundances of viral +RNA gene 10 at the same times postinfection. In agreement with our previous findings (9), the amounts of viral +RNA accumulated over time, with a clear increase beginning at 3 hpi (Fig. 2B), suggesting that the ratio of capped/noncapped RNA detected after 6 hpi represented mostly newly synthesized viral RNA. Together, these results suggest that the overall ratios of capped/noncapped RNA are dynamic, varying during the early times postinfection, while at 9 and 12 hpi they stabilize to a 1:1 proportion, in agreement with the finding that purified virions and *in vitro*-transcribed +RNAs also have a 1:1 proportion between capped and noncapped RNA molecules.

Virus produced in the absence of VP3 is more infectious. We have previously reported that silencing the expression of VP3 through RNA interference (RNAi) resulted in a decreased yield of infectious progeny and, also, in a 10-fold reduction in the levels of mRNA and dsRNA during the infection, while paradoxically, the synthesis of other viral proteins (besides VP3) was not affected (9). To evaluate the effect of the absence of VP3 on the encapsidation of viral RNAs (with and without cap), we purified viral particles produced in infected cells in which VP3 was silenced by RNAi and determined their infectivity and the proportions of capped/noncapped RNA present in the viral particles. For this, MA104 cells grown in 6-well plates were transfected either with a small interfering RNA (siRNA) to VP3 (siVP3) or with an irrelevant siRNA (siIrre) for 72 h, and the cells were then infected with rotavirus RRV at a multiplicity of infection (MOI) of 3 and harvested at 12 hpi. The viral particles present in the cell lysates were concentrated by sedimentation through a 40% sucrose cushion as indicated in Materials and Methods and resuspended in TNC buffer (Tris-HCl, NaCl, and $CaCl_2$).

The efficiency of VP3 knockdown was analyzed by immunoblot analysis of total infected cell lysates and of semipurified viral particles using a MAb directed to VP3 or a polyclonal antibody directed to TLPs (Fig. 3A). We found that while some VP3 could be detected in total cell lysates obtained from VP3-silenced cells, semipurified particles contained very little, if any, detectable VP3. The same nitrocellulose blot was then stained with an antibody to TLPs, showing that there was a similar amount of viral proteins in the semipurified particles (Fig. 3A). The yield of infectious virus produced under these conditions was determined by an immunoperoxidase focus-forming assay (FFA) assay, where we found that there was about a 4-fold decrease in viral infectivity in the lysate of cells where VP3 was silenced compared to the viral infectivity in the lysate from the control condition (Fig. 3B). We also determined the specific infectivities of the

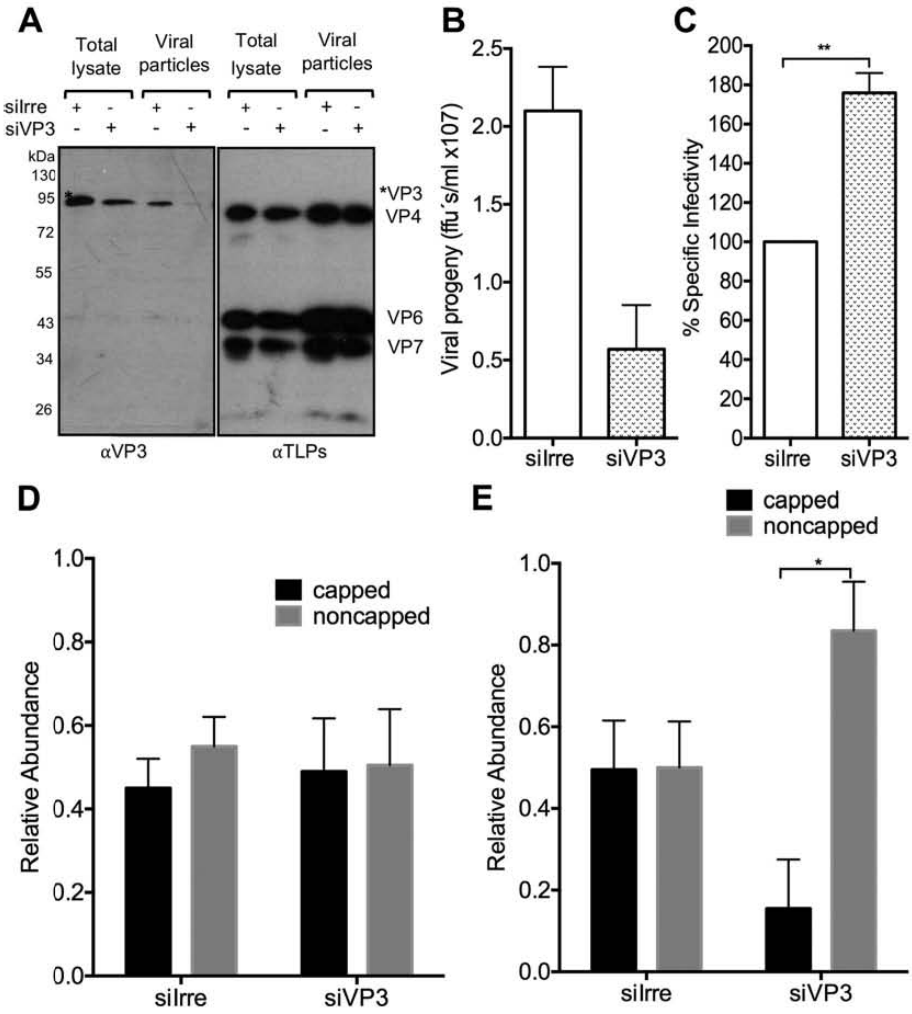

FIG 3 Virus produced in the absence of VP3 is more infectious. MA104 cells were transfected with the indicated siRNAs, infected with rotavirus RRV at an MOI of 3 at 72 h posttransfection, and harvested at 12 hpi. The viral particles present in the cell lysates were concentrated by sedimentation through a 40% sucrose cushion and resuspended in TNC buffer. (A) Representative immunoblots of total cell lysates or semipurified viral particles obtained from cells transfected with the indicated siRNAs. The expression of VP3 and the structural viral proteins VP4, VP6, and VP7 was detected using either an anti-VP3 antibody (αVP3) or an anti-TLP antibody (αTLP), as indicated. (B) The virus titer present in total cell lysates was determined by an immunoperoxidase focus-forming assay as described in Materials and Methods. Data are expressed as focus-forming units (FFUs)/mL $\times$ 10^7. The arithmetic mean values $\pm$ standard deviations from three independent experiments are shown. (C) Specific infectivity of the viral particles obtained in the semipurified viral particles from cells transfected with either siVP3 or an irrelevant siRNA (siIrre). The viral titer of the semipurified viral particles was determined under each condition by an immunoperoxidase focus-forming assay as described in Materials and Methods. The amount of viral protein VP4 present in the Western blots shown in panel A was calculated by densitometry of the band using ImageJ software (LOCI, University of Wisconsin), and the viral titer was correlated with the amount of viral protein VP4. Data are expressed as the percentages of the specific infectivity obtained when the cells were transfected with an irrelevant siRNA (Irre), which was taken as 100% infectivity. The arithmetic mean values $\pm$ standard deviations from three independent experiments are shown. (D) The relative amounts of capped and noncapped RNAs from the semipurified particles treated with the indicated siRNAs were determined as indicated in Materials and Methods. (E) Quantitative determination of capped and noncapped *in vitro*-transcribed RNAs obtained from DLPs produced in infected cells treated with the indicated siRNAs. Values shown represent mean results from three independent biological replicates, with error bars representing standard deviations. Statistical significance was determined by Student's *t* test. *, $P < 0.05$.

semipurified viral particles isolated under these conditions. Figure 3C shows the results of these assays, in which the viral titers of the viral particles obtained from cells in which VP3 was silenced or not were expressed as a function of the amount of viral-protein VP4 present in the semipurified particles from each condition (Fig. 3A), which was calculated by densitometry of the bands in the Western blots using ImageJ software (LOCI, University of Wisconsin). We found that the viral particles in which VP3 was silenced were about 75.8% ± 7.2% more infectious than the viral particles obtained from the nonsilenced control condition.

To evaluate whether the presence of ^{7me}GpppGcap on the RNA correlated with the increased specific infectivity observed, the capped/noncapped RNA ratio in the viral particles after VP3 knockdown was quantitated. For this, genomic dsRNA was purified from particles treated with either siVP3 or silrre and was used for a capping determination assay. Prior to RNA extraction, viral particles were treated with RNase A to eliminate any possible viral +RNA contamination. Unexpectedly, we found that the ratio of capped/noncapped RNA in the particles that were produced in VP3 knockdown cells was 1:1 (50% ± 12.7%), a ratio similar to that found in the RNA extracted from particles obtained from the control condition (Fig. 3D). To corroborate that the semipurified viral particles used in these assays lacked VP3, we explored the capping activity of the same viral particles using an *in vitro* transcription assay that was performed as previously described. After RNA precipitation, the *in vitro*-transcribed RNA was used for a capping determination assay. We found that, in contrast to the 1:1 proportion of capped/noncapped RNA obtained from particles treated with an irrelevant siRNA, only 15.5% ± 12% of the RNA obtained from viral particles where VP3 was silenced had the ^{7me}GpppGcap, while 83.5% ± 12% of the *in vitro*-synthesized RNA was not capped (Fig. 3E), indicating that these particles contained very little, if any VP3.

Together, these results showed that in cells where the expression of VP3 was silenced, the yield of infectious viral particles was decreased compared to the yield in control cells transfected with an irrelevant siRNA (Fig. 3B). Nevertheless, these particles had a higher specific infectivity (Fig. 3C), which did not seem to be related to the presence or absence of capped RNA, since the genomic RNA enclosed in these particles had a similar capped/noncapped RNA ratio (1:1). However, when these particles were used for an *in vitro* transcription assay, a higher proportion of noncapped RNAs was detected, underlining the absence of VP3. These results suggest that during genome encapsidation, RNAs with or without ^{7me}GpppGcap are encapsidated in similar proportions, irrespective of the amount of capped RNAs present in infected cells.

Effect of silencing the expression of RNase L and VP3 on viral RNA capping. It has been previously demonstrated that, in addition to its capping activity, VP3 has a phosphodiesterase (PDE) activity that is involved in the degradation of 2′-5′-oligoadenylates, thus preventing the activation of RNase L, an endoribonuclease that upon activation establishes a cellular antiviral state, cleaving single-stranded regions of cellular and viral RNAs (18, 19). We previously showed that when the expression of VP3 and RNase L was cosilenced by RNAi in rotavirus-infected cells, the yield of infectious virus was higher and the integrity of the viral RNA increased compared to those in control conditions where irrelevant siRNAs were used (13). These results suggest that under conditions where RNase L is silenced (and thus, the PDE activity of VP3 is not needed), the capping activity of VP3 is not essential for the production of infectious progeny virus. To analyze whether the cosilencing of VP3 and RNase L influenced the abundance of capped viral RNA, MA104 cells grown in 48-well plates and cotransfected with the indicated siRNAs were infected with rotavirus strain RRV, and the monolayers were recovered at different times postinfection. The efficiency of cosilencing of VP3 and RNase L was evaluated by Western blotting using specific monoclonal antibodies against these proteins (Fig. 4A), and the infectivity of the viral particles produced under these conditions was determined at 12 hpi (Fig. 4B). As previously reported (13), we found that cosilencing the expression of VP3 and RNase L resulted in an increase in viral infectivity of about 50%, which contrasts with the effect of only silencing VP3, under

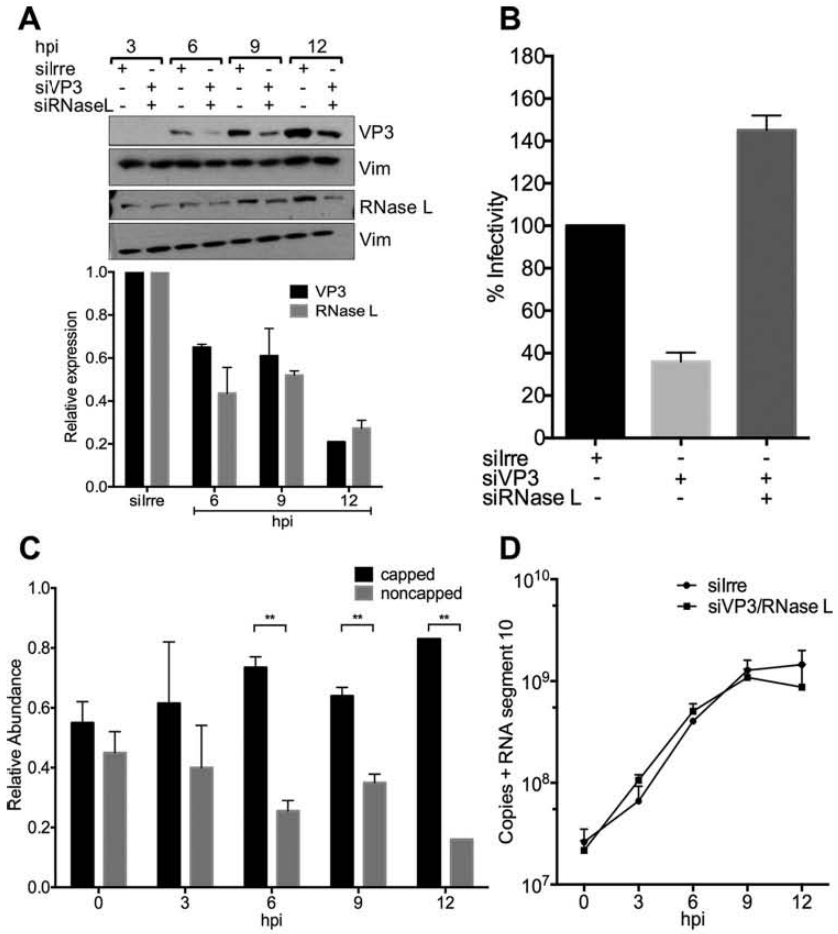

FIG 4 Effect of silencing the expression of RNase L and VP3 on viral RNA capping. MA104 cells were transfected with the indicated siRNAs as described in Materials and Methods. Cells were infected with RRV at an MOI of 3 at 72 h posttransfection and lysed at the indicated times postinfection. (A) A representative immunoblot analysis of total cell lysates from cells transfected with the indicated siRNAs. The expression of VP3 and RNase L was detected with the antibodies indicated to the right, and anti-vimentin (Vim) antibody was used as a loading control. Below the immunoblot, a quantitation of the amount of protein detected under each condition is shown; the relative amounts of the indicated proteins were calculated by densitometry of the bands using ImageJ software (LOCI, University of Wisconsin). Values represent the amount of protein detected as the percentage of the amount of protein detected in control cells treated with the irrelevant siRNA (siIrre) from three independent experiments. (B) In parallel, cells transfected with the indicated siRNAs were infected at an MOI of 3, and at 12 hpi, cells were lysed and the virus titer produced under these conditions was determined by an immunoperoxidase focus-forming assay as described in Materials and Methods. Data are expressed as the percentages of the infectivity obtained when the cells were transfected with an siIrre, which was taken as 100% infectivity. The arithmetic mean values ± standard deviations from three independent experiments are shown. (C) MA104 cells transfected and infected as described for panel A were harvested at the indicated times postinfection, total RNA was extracted, and the amounts of capped and noncapped RNA measured as indicated in Materials and Methods. The arithmetic means ± standard deviations from three independent experiments are shown. (D) The levels of viral +RNA gene 10 synthesized in cells where VP3 and RNase L were cosilenced or in control cells transfected with an siIrre were quantitated by an RT-qPCR assay at the indicated times postinfection. The number of viral copies at each time point was determined using a standard curve that was generated using a 10-fold serial dilution of an *in vitro*-T7-transcribed RNA that contains the sequence of rotavirus RRV segment 10. The arithmetic means ± standard deviations from three independent biological replicates are shown. Statistical significance was determined by Student's *t* test. *, $P < 0.05$; **, $P < 0.01$.

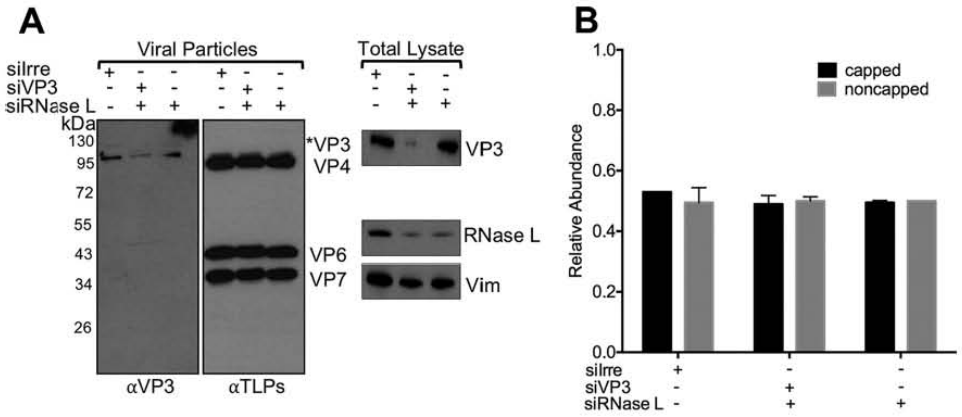

FIG 5 The proportions of capped and noncapped RNA that are encapsidated in viral particles do not depend on the proportions present in infected cells. MA104 cells were transfected with the indicated siRNA as indicated in Materials and Methods. Cells were infected with rotavirus RRV at an MOI of 3 at 72 h posttransfection and harvested at 12 hpi. The viral particles present in the cell lysates were concentrated by sedimentation through a 40% sucrose cushion and resuspended in TNC buffer. (A) The proteins were resolved by 10% SDS-PAGE and detected by immunoblot analysis. A representative immunoblot of viral particles or total cell lysates from cells transfected with the indicated siRNAs is shown. The expression of VP3 and the structural viral proteins VP4, VP6, and VP7 in viral particles was detected with the indicated antibodies, and the expression of VP3, RNase L, and vimentin (Vim) in total cell lysates was detected with the indicated antibodies. (B) The relative amounts of capped and noncapped RNAs from the semipurified particles treated with the indicated siRNAs were determined as indicated in Materials and Methods. The arithmetic mean values ± standard deviations from three independent biological replicates are shown.

which condition a lower total infectious titer was found compared with the virus titer obtained in control infected cells transfected with an irrelevant siRNA (Fig. 4B).

To quantitate the relative abundances of ^{7me}GpppGcap and noncapped viral RNA produced under these conditions, total RNA was purified at different times postinfection and analyzed in the capping assay as previously described. We found that at early times postinfection (0 and 3 hpi), the ratio of capped/noncapped RNA was close to 1:1, which was also observed in control cells treated with an irrelevant siRNA (not shown). In contrast, starting at 6 hpi, higher proportions of capped RNA to noncapped RNA were found (73 ± 3% at 6 hpi, 64 ± 2% at 9 hpi, and 83% ± 2% at 12 hpi) (Fig. 4C). To demonstrate that there was not decreased synthesis of positive-sense viral RNA under these conditions, the amounts of viral RNA produced at the different time points of the assay were measured by RT-qPCR using specific oligonucleotides to detect viral gene 10. We found that at all time points measured, similar amounts of segment 10 were produced under experimental and control conditions (Fig. 4D), suggesting that the differences found in the relative proportions of capped/noncapped RNA in VP3/RNase L-cosilenced infected cells were not due to differences in RNA transcription.

The proportions of capped and noncapped RNA that are encapsidated in viral particles do not depend on the proportions present in infected cells. Since we found that the proportion of capped RNA produced in infected cells where VP3 and RNase L were cosilenced was higher than under control conditions, we investigated whether this proportion was maintained in the newly formed viral particles. For this, viral particles produced in infected cells in which VP3 and RNase L were cosilenced were obtained as previously described (Fig. 3); in these assays, as a control, viral particles were also obtained from cells in which only RNase L was knocked down. The efficiency of silencing VP3 was analyzed by immunoblot analysis of the semipurified viral particles using a monoclonal antibody (MAb) to VP3 or a polyclonal antibody directed to TLPs, and total infected-cell lysates prior to particle isolation were used to demonstrate the silencing of RNase L (Fig. 5A).

The ratio of capped/noncapped genomic positive-sense RNAs present in the viral particles obtained under these cosilencing conditions was quantitated. For this, the genomic dsRNA present in the semipurified particles was extracted and used for a

capping determination assay. Prior to RNA extraction, viral particles were treated with RNase A to eliminate any possible viral +RNA contamination. We found that, contrary to what was expected, the ratio of capped to noncapped RNA in the particles that were produced in VP3/RNase L-cosilenced cells was 1:1 (50% ± 2.0%), similar to the ratio found in the RNA extracted from particles obtained from either of the control conditions, in which an siRNA to RNase L or an irrelevant siRNA was used (Fig. 5B), suggesting that the proportions of capped and noncapped viral RNA that are encapsidated did not depend on the relative abundances of these RNA populations in the infected cells.

DISCUSSION

In the cell's cytoplasm, noncapped RNAs are detected by RIG-I and MDA5, proteins of the innate immune system that recognize specific epitopes present on the 5′ end of non-self RNAs, including the presence of tri-, di- and monophosphate groups. The recognition of these epitopes triggers a signaling cascade that leads to the expression of interferon (IFN) as an initial immune response against viral infection (20, 21). Viruses have evolved different mechanisms to overcome this recognition, thus preventing the induction of IFN (22). Rotaviruses have different strategies to avoid the recognition of the dsRNA genome produced during the replication cycle; however, even though the viral capsid contains a protein (VP3) with all the enzymatic activities required to add the cap structure to the 5′ end of the viral transcripts, here we have found that, during the virus replication cycle, noncapped RNAs are produced and the molecular sensors RIG-I and MDA-5 are activated (23, 24); the continuous production of noncapped RNAs throughout the viral cycle might explain, at least in part, the activation of these cellular sensors.

In this work, we quantitated the presence of ^{7me}GpppGcap on rotavirus viral RNAs by employing a modified version of an enzymatic assay previously used in the characterization of the 5′ ends of Sindbis virus. Counterintuitively, we found a significant proportion of noncapped +RNAs present in the mature infectious particles (TLPs); interestingly, in *in vitro* assays, similar proportions (1:1) of 5′-capped and noncapped RNAs were synthesized, suggesting that the efficiency of the capping enzyme was not 100%, as was previously observed by Uzri and Greenberg, who found that in viral RNA isolated from rotavirus-infected cells and in *in vitro*-transcribed RNA, there was a significant proportion of RNA molecules with exposed 5′ phosphate groups and incompletely 2′-*O*-methylated cap structures (25). In their study, the absence of cap was determined by an indirect approach in which the viral RNAs either obtained from *in vitro* transcription or isolated from infected cells were transfected into murine embryonic fibroblasts (MEFs) and the level of secreted IFN-β was measured by enzyme-linked immunosorbent assay (ELISA) (25). In this work, we found that the abundances of ^{7me}GpppG-capped and noncapped RNAs in rotavirus-infected cells were dynamic, since their proportions varied at different times postinfection, with larger amounts of capped RNAs at 6 and 9 hpi. The increased proportions of capped RNAs found at these times could be the result of the increased transcription observed during the replication cycle (Fig. 2B) (9), while at 12 hpi, the proportions of capped and noncapped RNAs were close to 1:1, which was the same as the proportions of ^{7me}GpppG-capped to noncapped RNA detected in the genomic +RNA present in the mature viral particles (Fig. 1C). In these assays, we characterized the relative abundances of capped and noncapped 5′ ends of RNA segment 10, which was taken as representative of all genome segments. Of course, we cannot discard the possibility that different capped/noncapped ratios could be present in different genome segments.

Interestingly, besides its capping activity, VP3 has several mechanisms to counteract the innate immune response; it has recently been shown that VP3 is involved in the degradation of MAVS, blocking IFN-λ production in rotavirus-infected intestinal epithelial cells and thus evading the host cell immune response (26). It also has a phosphodiesterase (PDE) domain that degrades the 2′-5′-oligoadenylates produced in response to the detection of dsRNA by the OAS/RNase L pathway; this PDE activity prevents the

activation of RNase L, an enzyme that is in charge of degrading cellular and viral RNAs in infected cells to restrain viral infection (18). Thus, apparently VP3 is a multifunctional protein that can counteract the activation caused by the lack of cap in the transcripts synthesized during the infection.

The effect of silencing the expression of VP3 on the synthesis of viral proteins and on the production of viral particles has been reported; however, how the addition of cap on viral RNAs affects these processes had not been characterized (9, 13). We found that even though there was a significantly smaller amount of RNA under conditions where VP3 was silenced, the translation of viral proteins was not affected, and the viral particles produced (although in smaller amounts) contained a ratio of capped and noncapped RNAs similar to the ratio in viral particles obtained from cells treated with an irrelevant siRNA. Most probably, all the ^{7me}GpppGcap-containing viral RNAs produced in the VP3-silenced infected cells originated from the incoming particles and might be enough to direct the synthesis of the viral proteins during the infection cycle and to be encapsidated in newly formed viral particles (although in smaller amounts). On the other hand, the particles produced under these conditions, although less abundant, had a slightly higher specific infectivity than those obtained in control cells. It is tempting to suggest that these particles probably have a better sorting of capped/noncapped RNA segments, as opposed to control infected cells where probably there could be more viral particles assembled containing on average a higher proportion of uncapped RNAs, resulting in a relative lower specific infectivity. As expected, the viral particles assembled in VP3-silenced cells contained very little or no VP3, since the *in vitro*-transcribed RNA from DLPs produced under these conditions had a significantly smaller amount of ^{7me}GpppGcap RNA. It is interesting to note that even though there was little or no VP3 in these particles, viral RNA was encapsidated, suggesting that VP3 might not play a role in this function, contrary to what has been proposed.

We have previously found that in cells where the expression of VP3 and RNase L was cosilenced, the yield of viral infectious particles was similar to that obtained from control cells where no genes were silenced, suggesting that the capping activity of VP3 was not essential for the production of infectious progeny virus under those conditions (13). Here, we found that there was a higher proportion of capped than of uncapped viral RNAs produced in the infected cells where VP3 and RNase L were cosilenced, such that by 12 hpi, more than 80% of the viral +RNA was capped, and yet, the proportions of ^{7me}GpppG-capped and noncapped +RNA found in the viral particles isolated from these conditions were in a 1:1 ratio, suggesting that there should be a mechanism that controls the proportions of capped/uncapped +RNA that are encapsidated, despite the levels of ^{7me}GpppG-capped RNA present in rotavirus-infected cells. These findings also suggest that VP3 might be involved (either directly or indirectly) in blocking the activity of other cellular exonucleases that degrade uncapped RNAs.

In contrast, in reovirus, another member of the family *Reoviridae*, it has recently been shown that the efficient capping of viral RNAs, in addition to its role in enhancing protein translation, has a function in promoting the assembly of particles and the incorporation of genomic RNA into progeny virions (27). These results were obtained in a reverse genetics assay of reovirus in which C3P3, a fusion protein containing the T7 RNA polymerase and the African swine fever virus NP868R capping enzyme, was tested for its ability to rescue reovirus; it remains to be determined whether the activity of the native reovirus capping enzymes during the replication cycle of this virus is similar.

Recently, it was reported that noncapped RNAs had an important relevance during SINV infection in *in vitro* and *in vivo* models, since when the viral protein involved in cap addition (nsP1) was mutated to decrease the amount of cap on viral RNAs, a slight decrease in mortality of infected mice was observed. Conversely, an increased addition of cap resulted in an almost complete abrogation of mortality and morbidity compared to those of mice infected with a wild-type virus (28, 29). Thus, in SINV, noncapped RNAs play a critical role in determining whether the virus is neurovirulent or not; however, whether the cap structure has a role in genome encapsidation is not known.

Whether there is a role of the noncapped viral rotavirus RNAs early during the infection needs to be determined.

Since the domains involved in cap addition by VP3 have recently been defined (11, 12), and taking advantage of the available reverse genetics system for rotavirus (30), it would be interesting to generate VP3 mutants that are impaired in some of the regions involved in the different functions of the methyl-guanylyltransferase activity of this protein and establish whether ^{7me}GpppG-capped and noncapped RNAs have a role during rotavirus infection and whether the capping activity of VP3 is important for particle assembly.

MATERIALS AND METHODS

Cell culture and virus. The rhesus kidney epithelial cell line MA104 (ATCC) was grown in Dulbecco's modified Eagle's medium with reduced serum (DMEM-RS) (HyClone; Thermo Scientific, Logan, UT) supplemented with 5% heat-inactivated fetal bovine serum (FBS; Biowest, Kansas City, MO) at 37°C in a 5% CO_2 atmosphere and was used for all experiments carried out in this work. Simian rotavirus strain RRV was originally obtained from H. B. Greenberg (Stanford University, Stanford, CA) and was propagated in MA104 cells as described previously (31). Prior to infection, the RRV-containing cell lysates were activated with 10 μg/mL of trypsin (Gibco Life Technologies, Carlsbad, CA) for 30 min at 37°C.

Reagents and antibodies. Small interfering RNAs (siRNAs) were purchased from GE Healthcare Dharmacon (Lafayette, CO). The sequences of the siRNAs against rotavirus dsRNA segment 3 that encodes VP3 have been previously reported (32). As an irrelevant control, the siGENOME nontargeting siRNA 4 from Dharmacon was used. The monoclonal antibody (MAb) to RNase L was obtained from Abcam (Cambridge, MA), and the MAb to VP3 was purchased from GenScript. The rabbit anti-rotavirus polyclonal antiserum raised against purified triple-layered particles (TLPs) and the rabbit polyclonal antiserum to human vimentin (Vim) were produced in our laboratory (33). Horseradish peroxidase-conjugated goat anti-rabbit polyclonal and anti-mouse antibodies were purchased from PerkinElmer Life Sciences (Boston, MA).

Infectivity assay. MA104 cells were grown to confluence in 96-well plates and infected with 2-fold serial dilutions of the virus cell lysates for 1 h at 37°C. After this time, the unbound virus was removed, and the cells were incubated in minimal essential medium (MEM) without serum for 14 h at 37°C. Afterwards, the cells were fixed with 80% acetone in phosphate-buffered saline (PBS) for 30 min at room temperature and then washed twice with PBS. The fixed monolayers were then incubated with a rabbit anti-rotavirus polyclonal antiserum, followed by incubation with a secondary anti-rabbit antibody conjugated with horseradish peroxidase. Finally, the cells were washed twice with PBS and stained with a solution of 1 mg/mL of carbazole (3-amino-9-ethylcarbazole [AEC]) in sodium acetate buffer (50 mM, pH 5) with 0.04% H_2O_2. The reaction was stopped by washing in tap water, and the infectious focus-forming units were counted in a Nikon TMS inverted phase-contrast microscope with a 20× objective (34).

siRNA transfection. Transfection and cotransfection of siRNAs into MA104 cells were performed using Oligofectamine reagent (Invitrogen, Carlsbad, CA) in 48- or 6-well plates using a reverse transfection method as described previously (35).

Immunoblot assays. Cells were lysed in Laemmli sample buffer and denatured by boiling for 5 min. Proteins in cell lysates were separated by 10% SDS-PAGE and transferred to Immobilon NC membranes (Millipore Merck KGaA, Darmstadt, Germany). The membranes were blocked by incubation with 5% nonfat dry milk in PBS overnight at 4°C and then incubated with primary antibodies diluted in PBS containing 0.1% nonfat dry milk. The membranes were then incubated with the corresponding secondary antibodies conjugated to horseradish peroxidase. The peroxidase activity was developed using Western Lightning plus chemiluminescence reagent (PerkinElmer Life Sciences, Boston, MA) according to the manufacturer's instructions. The blots were also probed with an anti-vimentin (Vim) antibody, which was used as a loading control.

TLP and DLP purification. MA104 cells grown in 150-cm^2 flasks were infected with RRV at a multiplicity of infection (MOI) of 3, and at 12 h postinfection (hpi), cells were lysed by three cycles of freeze-thaw and the viral particles were concentrated by ultracentrifugation for 1 h at 30,000 rpm at 4°C in an SW40 rotor (Beckman Coulter, Fullerton, CA). Viral pellets were resuspended in TNC buffer (10 mM Tris-HCl [pH 7.5], 140 mM NaCl, 10 mM $CaCl_2$), sonicated three times for 20 s, and extracted with trichloromonofluoromethane as previously described (34). To purify viral TLPs, CsCl was added to the aqueous phase obtained from the trichloromonofluoromethane extraction to obtain a final density of 1.36 g/cm^3, and the mixture was centrifuged for 18 h at 36,000 rpm in an SW55 Ti rotor (Beckman Coulter, Fullerton, CA) at 4°C. The opalescent bands corresponding to TLPs or DLPs were collected by puncture and stored at 4°C. Before use, viral particles were desalted in a Sephadex G-25 spin column and resuspended in TNC buffer. Purified TLPs were treated with 10 μg of RNase A for 15 min at 37°C prior to dsRNA extraction with TRIzol reagent (Invitrogen, Carlsbad, CA) as indicated by the manufacturer.

To obtain viral particles from infected cells in which VP3 and RNase L were either silenced individually or cosilenced, MA104 cells grown in 6-well plates were transfected with the indicated siRNA (13). Cells were infected with rotavirus strain RRV at an MOI of 3 at 72 h posttransfection and were harvested at 12 hpi. Viral lysates were freeze-thawed three times, sonicated, and then extracted with trichloromonofluoromethane as described above. The virus suspension was pelleted through a 40% sucrose cushion by centrifugation for 2 h at 40,000 rpm in an SW55 Ti rotor (Beckman Coulter, Fullerton, CA) at 4°C. The viral pellet was resuspended in TNC buffer (for total viral particles) or in TNE buffer (10 mM Tris-HCl [pH 7.5], 140 mM NaCl, 5 mM EGTA) to remove the outer-layer proteins of the particles to obtain DLPs.

***In vitro* transcription.** *In vitro* transcription (IVT) reactions were carried out as follows: 2.4 μg of purified DLPs was mixed in a reaction mixture containing 8 mM ATP, 2.5 mM GTP, 2.5 mM CTP, 2.5 mM UTP (Ambion, Carlsban, CA), 0.5 mM *S*-adenosylmethionine (SAM) (NEB, Ipswich, MA), 0.5 U/μL RNasin (Thermo Scientific, Waltham, MA), transcription buffer (140 mM Tris-HCl, pH 8, 200 mM sodium acetate, and 40 mM magnesium acetate), and a 4% suspension of bentonite. The reaction mixture was incubated for 6 h at 42°C and centrifuged in an Eppendorf centrifuge for 1 min at 14,000 rpm to remove the bentonite, and the RNA present in the supernatant was immediately isolated by extraction with phenol/chloroform and precipitated with 4 M LiCl overnight at 4°C. Then, the RNA was sedimented by centrifugation, washed with 80% ethanol, dried briefly, and resuspended in RNase-free water. The RNA concentration was determined by absorbance on a NanoDrop spectrophotometer and stored in aliquots at −70°C.

RNA preparation. MA104 cells were grown to confluence in 6-well plates and infected with rotavirus strain RRV at an MOI of 10. At different times postinfection, total RNA was isolated with TRIzol as indicated by the manufacturer. Viral RNA from IVT, genomic dsRNA from viral particles, and RNA from infected cells were obtained as described above. To characterize the 5′ ends of viral RNAs, the following amounts of input RNA were employed: 250 ng of purified RNAs obtained from either genomic dsRNA extracted from viral particles or RNA from IVT reactions and 1 μg of total RNA obtained from infected cells.

Characterization of the 5′ end of viral RNA. To characterize the 5′ ends of the plus-sense rotavirus RNAs (+RNAs), we carried out an enzymatic process followed by RT-qPCR as previously described (17), with the following modifications (Fig. 1A). The input RNAs were treated with Antarctic phosphatase (NEB, Ipswich, MA) for 1 h at 37°C to remove any 5′-end phosphates. Then, the reaction mixture was heat inactivated and split into two equal aliquots to assay the noncapped and ^{7me}GpppG-capped RNAs in parallel. For the noncapped-RNA assay, the RNA in the reaction mixture was treated with T4 PNK (NEB, Ipswich, MA) to produce a pool of 5′-monophosphate RNAs and ^{7me}GpppG-capped RNAs. The other aliquot was treated with RppH (NEB, Ipswich, MA) to remove the ^{7me}GpppG from capped RNAs, producing a pool of 5′-nonphosphorylated and decapped 5′-monophosphate RNAs. Both reaction mixtures were incubated for 1 h at 37°C, and afterwards, the enzymes were heat inactivated. Then, both reaction mixtures were used in parallel as substrates for ligation with an RNA oligonucleotide (named linker RNA; 5′-GCUGAUGGCGAUGAAUGAACACUGCGUUUGCUGGCUUUGAUGAAA-3′), with the 5′-monophosphates available on the treated viral RNAs, using T4 RNA ligase (NEB, Ipswich, MA) for 1 h at 37°C. After the ligation step, samples were extracted with phenol/chloroform, ethanol precipitated, and resuspended in RNase-free H_2O.

Reverse transcriptase reaction. The reverse transcription (RT)-quantitative PCR (RT-qPCR) was performed in two steps as described by Ayala-Breton et al. (9). After purification, the RNAs were used as substrates for an RT reaction using specific oligonucleotides complementary to the positive strand of RNA segment 10 (Fig. 1B, step 1). cDNA was reverse transcribed using Moloney murine leukemia virus (M-MLV) reverse transcriptase (Invitrogen, Waltham, MA) with the following oligonucleotides: to detect the linker-containing amplicon, a reverse oligonucleotide (5′-CGAGGCCTTATGTAATGTAAATAG-3′) complementary to the 5′ end of viral segment 10 at positions 168 to 191 was employed (Fig. 1B, step 1a); meanwhile, to quantify the total amount of viral segment 10 present in the reaction mixture, an inner reverse oligonucleotide (5′-GAGCAATCTTCATGGTTGGAA-3′) that binds at nucleotide positions 214 to 193 of viral segment 10 was used (Fig. 1B, step 1b).

Real-time RT-qPCR analysis. After cDNA synthesis, the following oligonucleotides were used to detect the linker-containing amplicon: a forward oligonucleotide that binds on the RNA linker (5′-CGATGAA TGAACACTGCGTTTG-3′), and a reverse oligonucleotide (5′-CGAGGCCTTATGTAATGTAAATAG-3′) that binds at the 5′ end of gene 10 (Fig. 1B, step 2a). In parallel, primers for the amplification of an inner region of rotavirus RNA segment 10, described previously, were used as an internal control of each amplification (Fig. 1B, step 2b) (9). Forward primer 5′-TCCTGGAATGGCGTATTTTC-3′ and reverse primer 5′-GAGCAATCTTCATGGTT GGAA-3′ were used in the qPCR. Samples were analyzed in an ABI 7000 sequence detector system (Applied Biosystems). To perform quantitative analysis of the data, the results were normalized to the levels of rotavirus segment 10 detected in each RNA sample. The changes in gene expression were calculated by the $2^{-\Delta\Delta CT}$ method, where C_T is the threshold cycle, as previously described (17, 36). Finally, the relative amounts of 5′-capped and noncapped viral RNA were determined by comparing the relative quantities of the linker-containing amplicon with the total amounts of viral +RNA present, using the $\Delta\Delta C_T$ method to obtain the ratios of 5′-capped and noncapped RNAs depending on the sample treated, as previously described (17).

Determination of the viral gene 10 copy number. To determine the number of viral copies in a sample, a standard curve was generated, using a 10-fold serial dilution of an *in vitro*-T7-transcribed RNA that contains the sequence of rotavirus RRV segment 10. Briefly, the logarithm of the concentration of each dilution was plotted against the C_T value, and the viral copy number from unknown samples was determined by extrapolating the C_T value onto the corresponding standard curve.

Statistical analysis. The data reported in this study represent the mean values from a minimum of three independent biological replicates. Error bars in the figures indicate the plus-or-minus standard deviations of the means. Statistical analysis was performed using GraphPad Prism 6.0 (GraphPad Software, Inc.) as described in Results.

ACKNOWLEDGMENTS

We are grateful to J. L. Reyes for providing the 5′ RNA adapter, to R. Espinosa and M. A. Espinoza for their excellent technical assistance, to K. J. Sokolosky for his help with the analysis of the results, and to C. Sandoval-Jaime for his valuable input during the

development of this project. The work of P. Gaytán, E. López, and J. Yañez from the DNA sequencing and synthesis core unit is also acknowledged.

This work was supported by grants number A1-S-15356 and 302965 from CONACyT. J.M.-C. was the recipient of a scholarship (#385106) from CONACyT.

REFERENCES

1. Ramanathan A, Robb GB, Chan S-H. 2016. mRNA capping: biological functions and applications. Nucleic Acids Res 44:7511–7526. https://doi.org/10.1093/nar/gkw551.
2. Galloway A, Cowling VH. 2019. mRNA cap regulation in mammalian cell function and fate. Biochim Biophys Acta Gene Regul Mech 1862:270–279. https://doi.org/10.1016/j.bbagrm.2018.09.011.
3. Furuichi Y. 2015. Discovery of m(7)G-cap in eukaryotic mRNAs. Proc Jpn Acad Ser B Phys Biol Sci 91:394–409. https://doi.org/10.2183/pjab.91.394.
4. Decroly E, Ferron F, Lescar J, Canard B. 2011. Conventional and unconventional mechanisms for capping viral mRNA. Nat Rev Microbiol 10:51–65. https://doi.org/10.1038/nrmicro2675.
5. Jan E, Mohr I, Walsh D. 2016. A cap-to-tail guide to mRNA translation strategies in virus-infected cells. Annu Rev Virol 3:283–307. https://doi.org/10.1146/annurev-virology-100114-055014.
6. Troeger C, Khalil IA, Rao PC, Cao S, Blacker BF, Ahmed T, Armah G, Bines JE, Brewer TG, Colombara DV, Kang G, Kirkpatrick BD, Kirkwood CD, Mwenda JM, Parashar UD, Petri WA, Riddle MS, Steele AD, Thompson RL, Walson JL, Sanders JW, Mokdad AH, Murray CJL, Hay SI, Reiner RC. 2018. Rotavirus vaccination and the global burden of rotavirus diarrhea among children younger than 5 years. JAMA Pediatr 172:958–965. https://doi.org/10.1001/jamapediatrics.2018.1960.
7. Estes MK, Kapikian AZ. 2007. Rotaviruses, p 1917–1974. *In* Knipe DM, Howley PM, Griffin DE, Lamb RA, Martin MA, Roizman B, Straus SE (ed), Fields virology, 5th ed. Lippincott Williams & Wilkins, Philadelphia, PA.
8. Patton JT, Spencer E. 2000. Genome replication and packaging of segmented double-stranded RNA viruses. Virology 277:217–225. https://doi.org/10.1006/viro.2000.0645.
9. Ayala-Breton C, Arias M, Espinosa R, Romero P, Arias CF, López S. 2009. Analysis of the kinetics of transcription and replication of the rotavirus genome by RNA interference. J Virol 83:8819–8831. https://doi.org/10.1128/JVI.02308-08.
10. Chen D, Luongo CL, Nibert ML, Patton JT. 1999. Rotavirus open cores catalyze 5′-capping and methylation of exogenous RNA: evidence that VP3 is a methyltransferase. Virology 265:120–130. https://doi.org/10.1006/viro.1999.0029.
11. Kumar D, Yu X, Crawford SE, Moreno R, Jakana J, Sankaran B, Anish R, Kaundal S, Hu L, Estes MK, Wang Z, Prasad BVV. 2020. 2.7 Å cryo-EM structure of rotavirus core protein VP3, a unique capping machine with a helicase activity. Sci Adv 6:eaay6410. https://doi.org/10.1126/sciadv.aay6410.
12. Ogden KM, Snyder MJ, Dennis AF, Patton JT. 2014. Predicted structure and domain organization of rotavirus capping enzyme and innate immune antagonist VP3. J Virol 88:9072–9085. https://doi.org/10.1128/JVI.00923-14.
13. Sánchez-Tacuba L, Rojas M, Arias CF, López S. 2015. Rotavirus controls activation of the 2′-5′-oligoadenylate synthetase/RNase L pathway using at least two distinct mechanisms. J Virol 89:12145–12153. https://doi.org/10.1128/JVI.01874-15.
14. Zhang R, Jha BK, Ogden KM, Dong B, Zhao L, Elliott R, Patton JT, Silverman RH, Weiss SR. 2013. Homologous 2′,5′-phosphodiesterases from disparate RNA viruses antagonize antiviral innate immunity. Proc Natl Acad Sci U S A 110:13114–13119. https://doi.org/10.1073/pnas.1306917110.
15. Jenni S, Salgado EN, Herrmann T, Li Z, Grant T, Grigorieff N, Trapani S, Estrozi LF, Harrison SC. 2019. In situ structure of rotavirus VP1 RNA-dependent RNA polymerase. J Mol Biol 431:3124–3138. https://doi.org/10.1016/j.jmb.2019.06.016.
16. Hauser M, Dearnaley WJ, Varano AC, Casasanta M, McDonald SM, Kelly DF. 2019. Cryo-EM reveals architectural diversity in active rotavirus particles. Comput Struct Biotechnol J 17:1178–1183. https://doi.org/10.1016/j.csbj.2019.07.019.
17. Sokoloski KJ, Haist KC, Morrison TE, Mukhopadhyay S, Hardy RW. 2015. Noncapped alphavirus genomic RNAs and their role during infection. J Virol 89:6080–6092. https://doi.org/10.1128/JVI.00553-15.
18. Zhou A, Hassel BA, Silverman RH. 1993. Expression cloning of 2-5A-dependent RNAase: a uniquely regulated mediator of interferon action. Cell 72:753–765. https://doi.org/10.1016/0092-8674(93)90403-D.
19. Schwartz SL, Conn GL. 2019. RNA regulation of the antiviral protein 2′-5′-oligoadenylate synthetase. Wiley Interdiscip Rev RNA 10:e1534. https://doi.org/10.1002/wrna.1534.
20. Kell AM, Gale M. 2015. RIG-I in RNA virus recognition. Virology 479-480:110–121. https://doi.org/10.1016/j.virol.2015.02.017.
21. Brisse M, Ly H. 2019. Comparative structure and function analysis of the RIG-I-like receptors: RIG-I and MDA5. Front Immunol 10:1586. https://doi.org/10.3389/fimmu.2019.01586.
22. Beachboard DC, Horner SM. 2016. Innate immune evasion strategies of DNA and RNA viruses. Curr Opin Microbiol 32:113–119. https://doi.org/10.1016/j.mib.2016.05.015.
23. Broquet AH, Hirata Y, McAllister CS, Kagnoff MF. 2011. RIG-I/MDA5/MAVS are required to signal a protective IFN response in rotavirus-infected intestinal epithelium. J Immunol 186:1618–1626. https://doi.org/10.4049/jimmunol.1002862.
24. Sen A, Pruijssers AJ, Dermody TS, García-Sastre A, Greenberg HB. 2011. The early interferon response to rotavirus is regulated by PKR and depends on MAVS/IPS-1, RIG-I, MDA-5, and IRF3. J Virol 85:3717–3732. https://doi.org/10.1128/JVI.02634-10.
25. Uzri D, Greenberg HB. 2013. Characterization of rotavirus RNAs that activate innate immune signaling through the RIG-I-like receptors. PLoS One 8:e69825. https://doi.org/10.1371/journal.pone.0069825.
26. Ding S, Zhu S, Ren L, Feng N, Song Y, Ge X, Li B, Flavell RA, Greenberg HB. 2018. Rotavirus VP3 targets MAVS for degradation to inhibit type III interferon expression in intestinal epithelial cells. Elife 7:e39494. https://doi.org/10.7554/eLife.39494.
27. Eaton HE, Kobayashi T, Dermody TS, Johnston RN, Jais PH, Shmulevitz M, López S. 2017. African swine fever virus NP868R capping enzyme promotes reovirus rescue during reverse genetics by promoting reovirus protein expression, virion assembly, and RNA incorporation into infectious virions. J Virol 91:e02416-16. https://doi.org/10.1128/JVI.02416-16.
28. LaPointe AT, Landers VD, Westcott CE, Sokoloski KJ, Patton JT. 2020. Production of noncapped genomic RNAs is critical to Sindbis virus disease and pathogenicity. mBio 11:e02675-20. https://doi.org/10.1128/mBio.02675-20.
29. LaPointe AT, Moreno-Contreras J, Sokoloski KJ. 2018. Increasing the capping efficiency of the Sindbis virus nsP1 protein negatively affects viral infection. mBio 9:e02342-18. https://doi.org/10.1128/mBio.02342-18.
30. Kanai Y, Komoto S, Kawagishi T, Nouda R, Nagasawa N, Onishi M, Matsuura Y, Taniguchi K, Kobayashi T. 2017. Entirely plasmid-based reverse genetics system for rotaviruses. Proc Natl Acad Sci U S A 114:2349–2354. https://doi.org/10.1073/pnas.1618424114.
31. Pando V, Isa P, Arias CF, López S. 2002. Influence of calcium on the early steps of rotavirus infection. Virology 295:190–200. https://doi.org/10.1006/viro.2001.1337.
32. Montero H, Arias CF, Lopez S. 2006. Rotavirus nonstructural protein NSP3 is not required for viral protein synthesis. J Virol 80:9031–9038. https://doi.org/10.1128/JVI.00437-06.
33. López T, Camacho M, Zayas M, Nájera R, Sánchez R, Arias CF, López S. 2005. Silencing the morphogenesis of rotavirus. J Virol 79:184–192. https://doi.org/10.1128/JVI.79.1.184-192.2005.
34. Martínez JL, Arnoldi F, Schraner EM, Eichwald C, Silva-Ayala D, Lee E, Sztul E, Burrone ÓR, López S, Arias CF. 2019. The guanine nucleotide exchange factor GBF1 participates in rotavirus replication. J Virol 93:e01062-19. https://doi.org/10.1128/JVI.01062-19.
35. Gutiérrez M, Isa P, Sánchez-San Martin C, Pérez-Vargas J, Espinosa R, Arias CF, López S. 2010. Different rotavirus strains enter MA104 cells through different endocytic pathways: the role of clathrin-mediated endocytosis. J Virol 84:9161–9169. https://doi.org/10.1128/JVI.00731-10.
36. Livak KJ, Schmittgen TD. 2001. Analysis of relative gene expression data using real-time quantitative PCR and the $2^{-\Delta\Delta CT}$ method. Methods 25:402–408. https://doi.org/10.1006/meth.2001.1262.

Como parte de mi doctorado, hice una estancia de 3 meses en la escuela de medicina en el departamento de microbiología e inmunología en la Universidad de Louisville, Kentucky, USA, bajo la supervisión del Dr. Kevin J Sokoloski. El propósito de la estancia fue para capacitarme en la metodología de detección de RNA +/- cap, desarrollada por el Dr. Sokoloski. Como producto de mi estancia se publico el siguiente articulo en la revista mBio:

Increasing the Capping Efficiency of the Sindbis Virus nsP1 Protein Negatively Affects Viral Infection.

RESEARCH ARTICLE
Molecular Biology and Physiology

Increasing the Capping Efficiency of the Sindbis Virus nsP1 Protein Negatively Affects Viral Infection

Autumn T. LaPointe,[a] Joaquín Moreno-Contreras,[b] Kevin J. Sokoloski[a,c]

[a]Department of Microbiology and Immunology, University of Louisville School of Medicine, Louisville, Kentucky, USA

[b]Departamento de Génetica del Desarrollo y Fisiología Molecular, Instituto de Biotecnología, Universidad Nacional Autónoma de México, Cuernavaca, Morelos, Mexico

[c]The Center for Predictive Medicine for Biodefense and Emerging Infectious Diseases, University of Louisville School of Medicine, Louisville, Kentucky, USA

ABSTRACT Alphaviruses are arthropod-borne RNA viruses that are capable of causing severe disease and are a significant burden to public health. Alphaviral replication results in the production of both capped and noncapped viral genomic RNAs (ncgRNAs), which are packaged into virions during infections of vertebrate and invertebrate cells. However, the roles that the ncgRNAs play during alphaviral infection have yet to be exhaustively characterized. Here, the importance of the ncgRNAs to alphaviral infection was assessed by using mutations of the nsP1 protein of Sindbis virus (SINV), which altered the synthesis of the ncgRNAs during infection by modulating the protein's capping efficiency. Specifically, point mutations at residues Y286A and N376A decreased capping efficiency whereas a point mutation at D355A increased the capping efficiency of the SINV genomic RNA during genuine viral infection. Viral growth kinetics levels were significantly reduced for the D355A mutant relative to wild-type infection, whereas the Y286A and N376A mutants showed modest decreases in growth kinetics. Overall genomic translation and nonstructural protein accumulation were found to correlate with increases and decreases in capping efficiency. However, genomic, minus-strand, and subgenomic viral RNA synthesis were largely unaffected by the modulation of alphaviral capping activity. In addition, translation of the subgenomic alphaviral RNA (vRNA) was found not to be impacted by changes in capping efficiency. The mechanism by which the decreased presence of ncgRNAs reduced viral growth kinetics levels operated through the impaired production of viral particles. Collectively, these data illustrate the importance of ncgRNAs to viral infection and suggest that they play an integral role in the production of viral progeny.

IMPORTANCE Alphaviruses have been the cause of both localized outbreaks and large epidemics of severe disease. Currently, there are no strategies or vaccines which are either safe or effective for preventing alphaviral infection or treating alphaviral disease. This deficit of viable therapeutics highlights the need to better understand the mechanisms behind alphaviral infection in order to develop novel antiviral strategies for treatment of alphaviral disease. In particular, this report details a previously uncharacterized aspect of the alphaviral life cycle: the importance of noncapped genomic viral RNAs for alphaviral infection. This offers new insights into the mechanisms of alphaviral replication and the impact of the noncapped genomic RNAs on viral packaging.

KEYWORDS RNA processing, RNA virus, alphavirus, molecular biology

Alphaviruses are positive-sense, single-stranded RNA viruses which are capable of being transmitted between sylvatic vertebrate reservoir hosts and competent mosquito vectors in an enzootic cycle. During epizootic events, these viruses are

Received 23 October 2018 **Accepted** 8 November 2018 **Published** 11 December 2018

Citation LaPointe AT, Moreno-Contreras J, Sokoloski KJ. 2018. Increasing the capping efficiency of the Sindbis virus nsP1 protein negatively affects viral infection. mBio 9: e02342-18. https://doi.org/10.1128/mBio.02342-18.

Editor Jaisri R. Lingappa, University of Washington

Address correspondence to Kevin J. Sokoloski, kevin.sokoloski@louisville.edu.

capable of causing severe disease and are broadly categorized into two groups based on symptomology. Diseases caused by the encephalitic alphaviruses, such as Venezuelan equine encephalitis virus, are characterized by neurological symptoms and are capable of causing severe encephalitis, which may result in the death of the vertebrate host (1, 2). In contrast, the arthritogenic alphaviruses, such as Sindbis virus (SINV), Ross River virus (RRV), and chikungunya (CHIKV), cause disease ranging in severity from mild febrile illness to debilitating polyarthritis, which may persist for several months to years past the acute phase of infection (3–7). Despite the burden to public health posed by the alphaviruses, there are currently no effective and safe antiviral treatments for alphaviral disease.

During alphaviral infection, three viral RNA species are produced: the genomic strand, which encodes the nonstructural polyprotein, which is processed proteolytically to form the replication machinery; a minus-strand RNA template; and a subgenomic RNA, which encodes the structural proteins. The positive-sense alphaviral RNAs (vRNAs), namely, the genomic and subgenomic vRNAs, have a type 0 cap structure cotranscriptionally added to their 5′ ends during RNA synthesis in order to protect the 5′ end of the transcript and to facilitate translation after entry into the host cell (8–10). The addition of the 5′ cap structure to the positive-sense vRNAs is a multistep process involving at least two alphaviral nonstructural proteins. Briefly, the methyltransferase domain of the alphaviral nsP1 protein catalyzes the addition of a methyl group from S-andenosylmethionine to a GTP molecule, forming a covalent m^7GMP-nsP1 intermediate (11). Following the removal of the 5′ γ-phosphate on the nascent vRNA molecule by nsP2, the m^7GMP moiety is then transferred to the vRNA molecule by the guanylyltransferase activities of nsP1, resulting in the formation of the type 0 cap structure, ^{7me}GpppA (12, 13). Importantly, biochemical studies of alphaviral nsP1 proteins have found that both the methyltransferase activity and guanylyltransferase activity of nsP1 can be altered either negatively or positively via point mutations *in vitro* (14–16).

The presence of the type 0 cap structure on the alphaviral genomic and subgenomic vRNAs was first observed by paper electrophoresis, or thin-layer chromatography, of metabolically labeled vRNAs that were chemically and enzymatically degraded (8, 9, 17). Those studies further identified the sequences of the 5′ termini of the alphaviral genomic and subgenomic vRNAs, which provided the first evidence for independent promoter initiation for the two positive-sense vRNA species (9). While those studies were able to identify the presence of the 5′ type 0 cap structure, they were, by the nature of their design and technological limitations, unable to determine the relative frequencies with which the positive-sense vRNAs were capped.

Recently, we reported findings that indicated that the alphaviral genomic vRNAs are not ubiquitously capped and that a significant proportion of the genomic vRNAs produced during SINV and RRV infection lack the 5′ type 0 cap structure (18). Furthermore, analyses of infectious and noninfectious viral particles demonstrated that both the capped and noncapped genomic vRNAs are packaged into viral particles throughout the course of infection. Through the use of tissue culture models of alphaviral infection, the presence of the noncapped vRNAs was found to correlate with the activation of a type I interferon (IFN) response. Moreover, an attenuated RRV mutant was found to produce fewer noncapped genomic RNAs than were produced by wild-type (WT) virulent RRV (18, 19). Collectively, these data were highly suggestive of an important biological role for the noncapped genomic vRNAs during infection; however, the precise functions of the noncapped genomic vRNAs during infection remained unknown.

The goal of this study was to determine the importance of noncapped vRNAs to SINV infection of tissue culture cells. Here, we show that the capping activity of SINV nsP1 is capable of being modulated, both positively and negatively, via the mutation of specific residues within the Iceberg region, a structurally organized region of cryptic function that is conserved among many viral capping enzymes (21). In addition, SINV infection was determined to be more detrimentally impacted by increasing the capping efficiency of SINV nsP1 than by decreasing the efficiency. Specifically, increasing the

rate of alphaviral capping negatively impacted viral growth kinetics by negatively affecting viral particle production. Collectively, our findings indicate that the noncapped vRNAs do play an important role during viral infection, and that decreasing the presence of noncapped vRNA impacts the viral life cycle at a fundamental level.

RESULTS

SINV vRNA capping can be modulated by point mutations in the nsP1 protein. As described above, we recently reported that a significant number of the SINV genomic vRNAs produced during infection lack the type 0 5′ cap structure. Despite being noninfectious, the noncapped viral genomic RNAs (ncgRNAs) are produced in a temporally dependent manner and are packaged into viral particles throughout the course of infection (18). Given the evolutionary conservation of the production of the ncgRNAs during alphaviral infection, we hypothesized that they must be biologically important to viral infection. This led us to question how modulating capping activity, which would alter the production of capped viral genomic RNAs and ncgRNAs, impacts viral infection. In order to determine the biological importance of the ncgRNAs during viral infection, we modulated the methyltransferase and guanylyltransferase activities of the alphaviral nsP1 protein to generate mutant SINV strains with either increased or decreased rates of viral capping. These mutations were based on previous work done in VEEV by Li et al. (14), where alanine substitutions at specific residues affected the nsP1 protein's methyltransferase and guanylyltransferase activities, as well as cap formation as a whole. Specifically, the previous study found that alanine substitutions at Y286 and N376 decreased RNA capping efficiencies, although to different extents, whereas an alanine substitution at D355 increased RNA cap formation. All three residues are highly conserved across multiple alphaviruses, including the model alphavirus SINV (Fig. 1A). Modeling of the SINV nsP1 protein using ITASSER indicated that residues D355 and N376 are likely close to one another, in parallel alpha helices proximal to the catalytic site within the Iceberg domain (Fig. 1B) (20). Nonetheless, Y286 is located at a distal site far from the putative active sites, as identified by prior mutational analyses (11, 12, 16). Admittedly, the ITASSER-predicted structure is unlikely to be a wholly accurate representation of the true structure of the SINV nsP1 protein. Despite the inherent inaccuracy of protein folding prediction algorithms in the absence of a closely related crystal structure, secondary and tertiary structural elements reminiscent of methyltransferase and guanylyltransferase enzymes may be detected, including a Rossmann fold-like structure surrounding the key residues involved in methyltransferase activity (16, 21). In addition, the overall arrangements of the core region and Iceberg regions are largely intact, and the known membrane anchoring domains face outward from the globular body of the protein (21). The differential abilities of Y286, D355, and N376 to affect VEEV nsP1 capping activity as well as their locations in highly conserved domains, which play integral roles in cap formation, made them strong candidates for testing how modulating the capping activity of nsP1 affects SINV infection.

In order to verify that the SINV nsP1 mutations altered the rate of vRNA capping, we assessed what proportion of viral particles contained capped RNA genomes. We have shown previously that both capped genomic RNAs and ncgRNAs are packaged and released during viral infection (18). Thus, knowing what proportion of capped viral RNA is being packaged into viral particles gives insight into the general capping efficiency of nsP1 during viral infection. To this end, the comparative assessment of viral capping efficiencies was accomplished by comparing the relative sensitivities of the mutants to RNase degradation using XRN-1, a 5′–3′ exoribonuclease which preferentially degrades RNAs lacking a protective 5′ cap structure, in particular, 5′ monophosphate RNAs (22, 23). By measuring the amount of RNA resistant to XRN-1 degradation, we were able to determine what proportion of the total input RNA was capped relative to that seen with wild-type SINV, as the predominant noncapped 5′ end was previously determined to be a 5′ monophosphate (18). As shown in Fig. 1C, both SINV N376A and SINV Y286A had significantly lower proportions of XRN-1-resistant genomic RNAs than the WT strain,

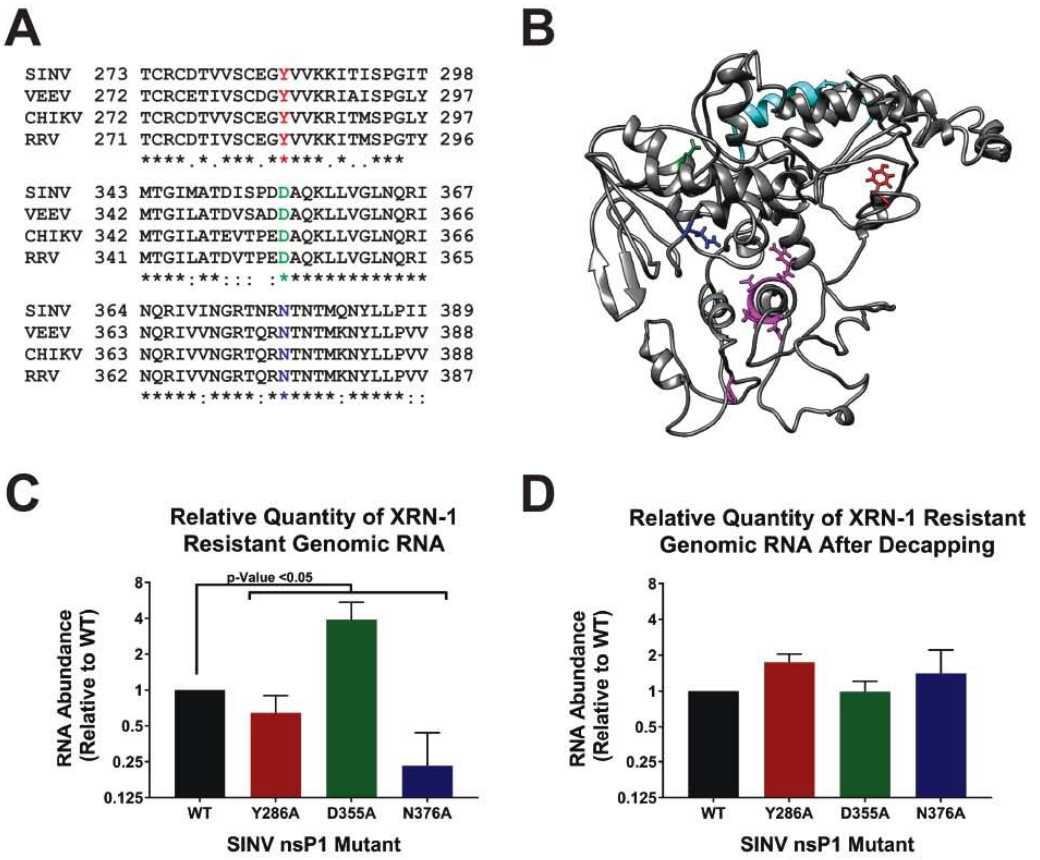

FIG 1 Point mutations in the nsP1 protein of SINV alter 5′ vRNA capping efficiency. (A) Amino acid sequence alignment of selected alphavirus nsP1 proteins. The individual nsP1 protein sequences of Sindbis virus (ViPR accession no. U38305), Venezuelan equine encephalitis virus (VEEV; ViPR accession no. L01443), chikungunya virus (CHIKV; ViPR accession no. DQ443544), and Ross River virus (RRV; ViPR accession no. GQ433359) were aligned by the use of Clustal Omega. (B) An ITASSER-predicted structure of the SINV nsP1 protein. Amino acid residues of importance are highlighted as follows: red, Y286; green, D355; blue, N376; cyan, amphipathic helix; pink, residues involved in methyltransferase activities (including H39, which binds to the ^{m7}GMP residue). (C) Graph depicting the relative quantities of XRN-1-resistant vRNA isolated from viral particles produced by BHK-21 cells infected with wild-type SINV or the individual capping mutants at 24 hpi. (D) Identical to panel C, with the exception that the viral genomic RNAs were enzymatically decapped concurrently with XRN-1 treatment. All quantitative data shown represent means of data from a minimum of three independent biological replicates utilizing 3 independent particle preparations, with the error bars indicating standard deviations of the means. The *P* values indicated on the figure were determined by Student's *t* test.

with SINV Y286A having approximately 25% less XRN-1-resistant RNA than WT and SINV N376A having approximately 75% less XRN-1-resistant RNA. In contrast, and as expected from the previous study by Li et al. (14), SINV D355A was found to have a significantly greater proportion of XRN1-resistant RNA, with a mean approximately 4-fold greater than that observed for WT SINV. To confirm that the observed resistance of the SINV D355A genomic RNAs was due to a cap structure, the genomic RNAs were subjected to XRN-1 nuclease treatment in the presence of an established decapping enzyme (18, 24, 25). As shown in Fig. 1D, enzymatic removal of the 5′ cap structure eliminated the resistance of the D355A-derived genomic RNAs to XRN-1 treatment, resulting in XRN-1 resistance levels comparable to those seen with WT SINV.

From these data, we were able to conclude that the point mutations engineered into the SINV nsP1 protein can indeed alter capping activity, both negatively, in the case of Y286A and N376A, and positively, as with D355A. Therefore, the individual nsP1 mutants can be used to assess the impact of the ncgRNAs by modulating the capping activity of nsP1 in tissue culture models of infection in a controlled manner.

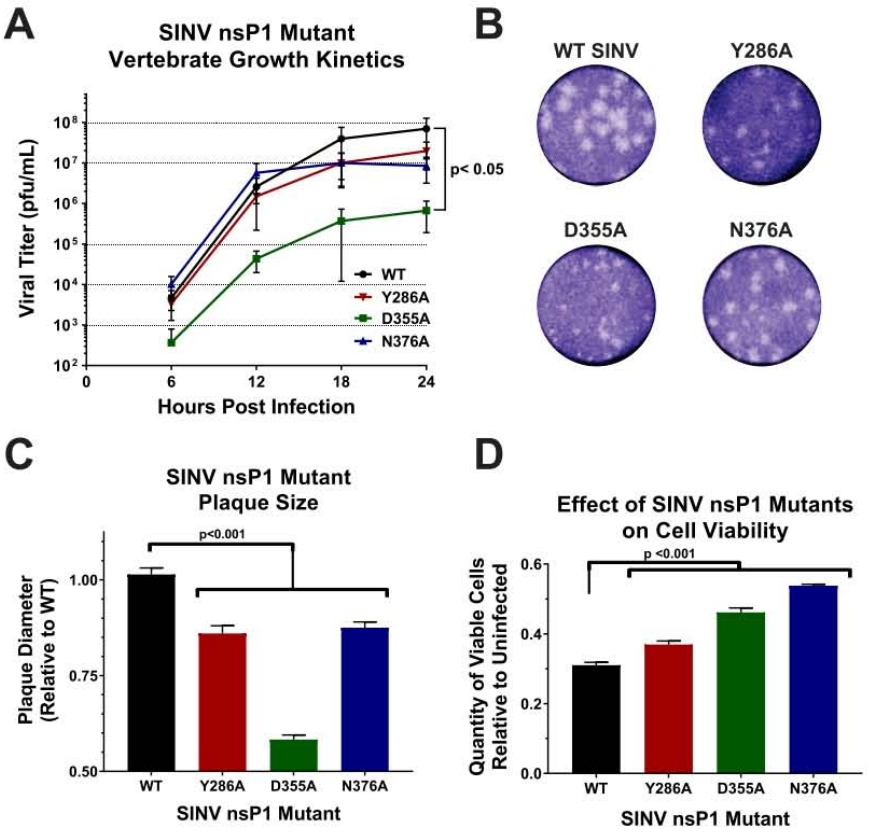

FIG 2 Altering viral capping efficiency negatively impacts viral infection. (A) Multi-step growth kinetics of the individual capping mutants and parental wild-type SINV as observed in BHK-21 cells infected at an MOI of 0.5 PFU/cell. Statistical significance was determined by analysis of the area under the curve. (B) Plaque morphology of wild-type SINV and capping mutant viruses in BHK-21 cells overlaid with 0.5% solution of Avicel at 24 h post-infection. (C) Graph indicating the average plaque diameter of the mutant viruses relative to wild-type SINV. Size was determined by ImageJ software (NIH). (D) Cell viability of BHK-21 cells infected with the individual capping mutants at 24 hpi relative to mock-infected BHK-21 cells. All quantitative data shown represent means of results from at least three independent biological replicates, with error bars representing standard deviations of the means. Statistical significance, as indicated within each panel, was determined by Student's *t* test.

Increased capping decreases SINV growth kinetics in mammalian cells. While the effects of synonymous point mutations on nsP1 capping efficiency have been previously characterized for VEEV at the enzymatic level (14), the effects of modulating capping activity on viral infection as a whole have not yet been studied in detail. Given the molecular function of the 5′ cap structure, one could expect that the SINV nsP1 mutants that showed decreased vRNA capping would show impaired viral growth kinetics relative to wild-type virus. Likewise, if the ncgRNAs were truly nonfunctional, a mutant that increased capping would show enhanced viral growth kinetics with regard to wild-type infection. As demonstrated by the data presented in Fig. 2A, decreasing SINV capping modestly decreased viral growth kinetics levels, as observed for the SINV Y286A and SINV N376A mutants. However, the SINV D355A mutant, which showed increased vRNA capping relative to the WT, exhibited significantly decreased titers over the course of infection (Fig. 2A). In addition to a 2-log decrease in viral titer, the SINV D355A mutant produced plaques approximately half the size of those produced by wild-type SINV (Fig. 2B and C). Despite not showing significantly decreased viral growth kinetics, both the SINV Y286A and SINV N376A mutants also exhibited a small-plaque

phenotype, albeit not to the same extent as the SINV D355A mutant. In addition, all three capping mutants were found to have decreased induction of cell death compared to WT SINV (Fig. 2D).

Collectively, these data indicate that changing the efficiency of vRNA capping negatively impacted viral growth kinetics, illustrating that a step in the viral life cycle had been detrimentally affected. Furthermore, the viral growth kinetics data suggest that SINV is more sensitive to increased vRNA capping efficiency than it is to decreased capping efficiency. Thus, the ncgRNAs produced during infection are indeed biologically important. Nevertheless, despite the clear negative impact on viral infection, the precise nature of the molecular consequences of increased vRNA capping and decreased presence of ncgRNAs cannot be determined from these data alone. As such, the viral gene expression and vRNA synthesis profiles of each of the SINV nsP1 mutants were next assessed to determine if they were negatively affected by modulation of vRNA capping.

Translation of the SINV genomic RNA correlates with capping efficiency. For the majority of mRNAs, a key factor for determining whether or not an mRNA is translated is the presence or absence of a functional 5′ cap structure (26–28). Therefore, changing the ncgRNAs to capped genomic RNAs or vice versa by altering viral capping efficiency should impact the amount of protein being produced by viral RNA during infection. To investigate the effect(s) that modulating nsP1 capping efficiency has on viral gene expression, a SINV reporter which contained the open reading frame of nanoluciferase in frame with the nsP3 nonstructural protein (18) was used to measure viral genomic RNA translation (Fig. 3A). Nanoluciferase expression was measured at regular intervals over the course of viral infection (Fig. 3B). As expected, the SINV D355A mutant, which showed increased capping relative to the wild type, exhibited increased genomic vRNA translation compared to WT SINV for every time point measured (Fig. 3C). Similarly, SINV N376A, which showed decreased capping relative to the wild type, showed decreased translation (Fig. 3C). Curiously, the SINV Y286A mutant showed differential nanoluciferase expression levels during infection, with translation levels being slightly increased very early during infection, decreased at 8 h post-infection (hpi), and similar to wild-type levels at later times post-infection.

While the use of the SINV nanoluciferase reporter virus allows the accurate quantification of viral gene expression during infection, it does not measure the sum accumulation of the nonstructural proteins. To measure the relative accumulations of the viral nonstructural proteins, the levels of SINV nsP2 protein were assessed via Western blotting at 8, 12, and 16 hpi. As shown in Fig. 4A and quantified in Fig. 4B, at 8 hpi, the accumulation of the SINV nsP2 proteins seen in SINV D355A and SINV N376A differed to a statistically significant extent from WT SINV. The abundance of nsP2 increased ~2.5-fold during SINV D355A infection relative to wild-type SINV infection. In contrast, nsP2 levels during SINV N376A infections were decreased ~2-fold relative to wild-type SINV infections. The levels seen with the SINV Y86A mutant were more or less equivalent to the wild-type nsP2 levels. Similar trends were observed at later times during infection. As depicted in Fig. 4C and D, the SINV D355A nsP2 levels at 12 hpi were statistically increased relative to those seen with the wild-type infection; however, given the low magnitude of the effect, these differences are unlikely to be biologically significant. In contrast, SINV D355A nsP2 levels at 16 hpi were increased to an extent that is likely biologically meaningful (Fig. 4E and F).

Overall, the levels of genomic translation for the SINV nsP1 mutants nicely reflect their differences in capping efficiency, with increased vRNA capping resulting in increased translation of the nonstructural proteins and decreased vRNA capping resulting in decreased translation at 8 hpi. These data are consistent with the conversion of the ncgRNAs to translationally competent capped genomic vRNAs. Furthermore, Western blotting confirmed the differences in translational activity detected during SINV nanoluciferase reporter infections. Taken together, the nanoluciferase and Western blot data indicate that the increased translation of the genomic vRNAs continues

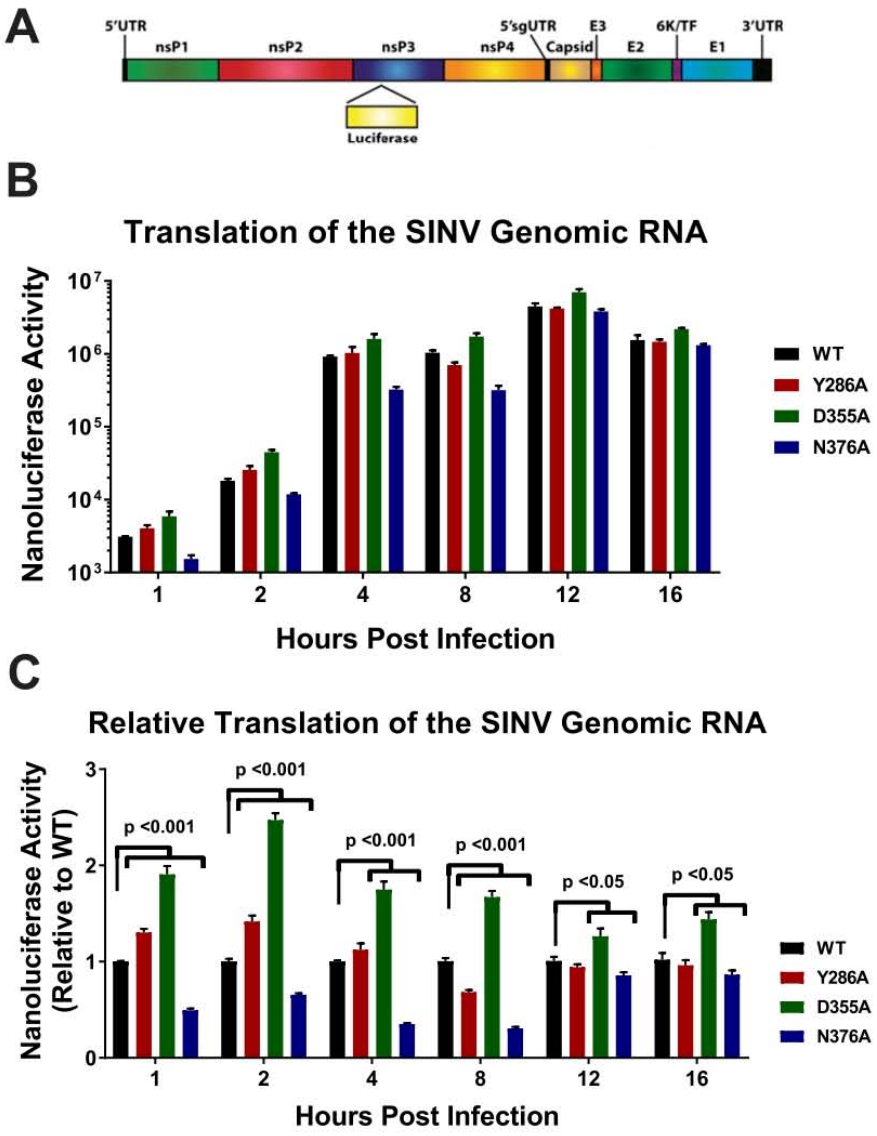

FIG 3 Translation of the genomic vRNA correlates with viral capping efficiency. (A) Schematic diagram of the SINV nanoluciferase reporter used in this study. UTR, untranslated region. (B) BHK-21 cells were infected with either the parental wild-type strain or an individual SINV capping mutant nanoluciferase reporter strain. The level of nanoluciferase activity was quantified at the indicated times post-infection. (C) The nanoluciferase activity, as reported in panel B, normalized to wild-type expression at each individual time point to enable readers to identify differences in translation. All the quantitative data shown represent means of results from three independent biological replicates, with the error bars representing standard deviations of the means. Statistical significances, as indicated in the figure, were first determined using analysis of variance (ANOVA) followed by *post hoc* statistical analyses by Student's *t* test.

during infection with SINV D355A beyond what is observed for wild-type SINV. Nonetheless, the biological differences in translational activity observed between the SINV D355A mutant and the corresponding parental wild-type strain fail to explain the approximately 200-fold reduction in viral titer.

Modulating SINV capping does not alter overall RNA synthesis or accumulation. Since differences in viral gene expression failed to explain outright the observed

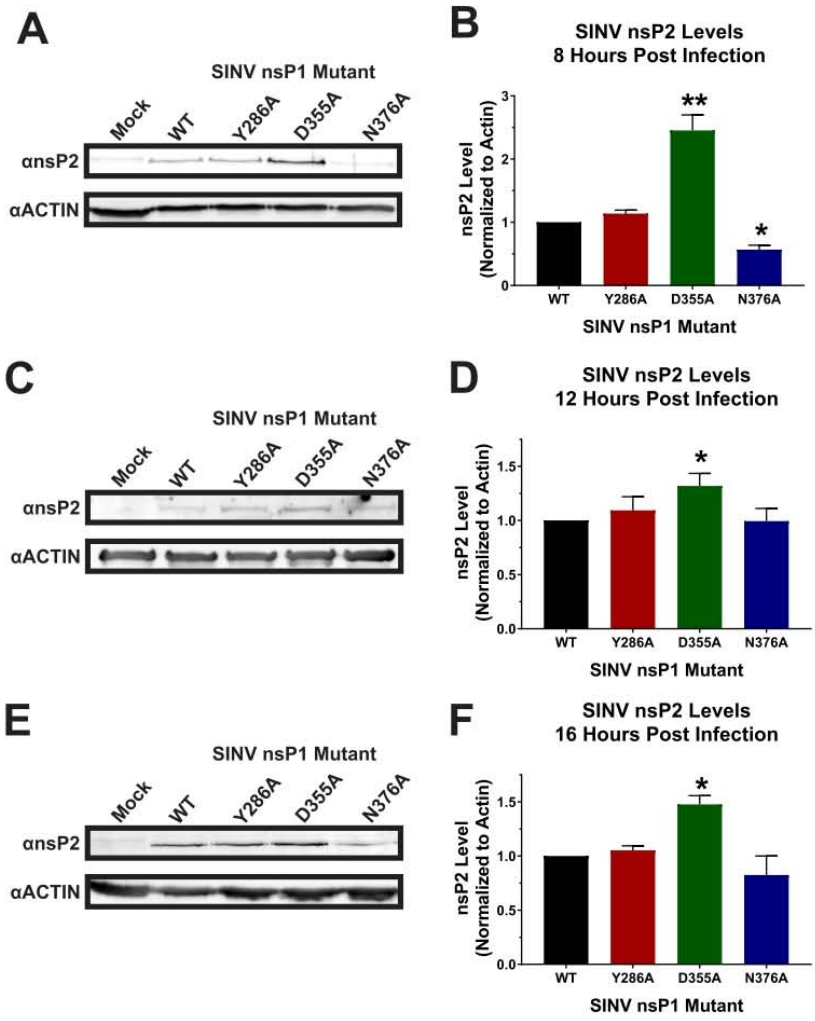

FIG 4 nsP2 protein levels are impacted by mutation of the nsP1 protein. (A) BHK-21 cells were infected with wild-type SINV or an individual capping mutant at an MOI of 5 PFU/cell and assessed by Western blotting to determine the abundance of nsP2 at 8 hpi. Actin is shown as a loading control. (B) Densitometric quantification of the nsP2 protein normalized to actin levels at 8 hpi. (C and D) Western blots and densitometry analyses identical to those described for panels A and B, respectively, with the exception that the timing of the assay coincided with 12 hpi. (E and F) Western blots and densitometry analyses identical to those described for panels A and B, respectively, with the exception that the timing of the assay coincided with 16 hpi. The Western blot images shown are representative of results of at least three independent biological replicates. All the quantitative data shown represent means of results from three independent biological replicates, with the error bars representing standard deviations of the means. Statistical significances, as indicated in the figure, were first determined using ANOVA followed by *post hoc* statistical analyses by Student's *t* test.

decreased viral titers associated with the SINV D355A mutant, we next sought to identify if vRNA synthesis was impaired as a result of nsP1 mutation. To determine what impact alteration of viral capping efficiency has on vRNA synthesis, the genomic, subgenomic, and minus-strand vRNAs were quantitatively assessed at 2, 4, and 8 h post-infection via quantitative reverse transcription-PCR (qRT-PCR). At 2 hpi, the SINV D355A mutant, which has increased vRNA capping relative to wild-type SINV, produced slightly more SINV genomic and subgenomic RNAs, whereas the SINV N376A mutant,

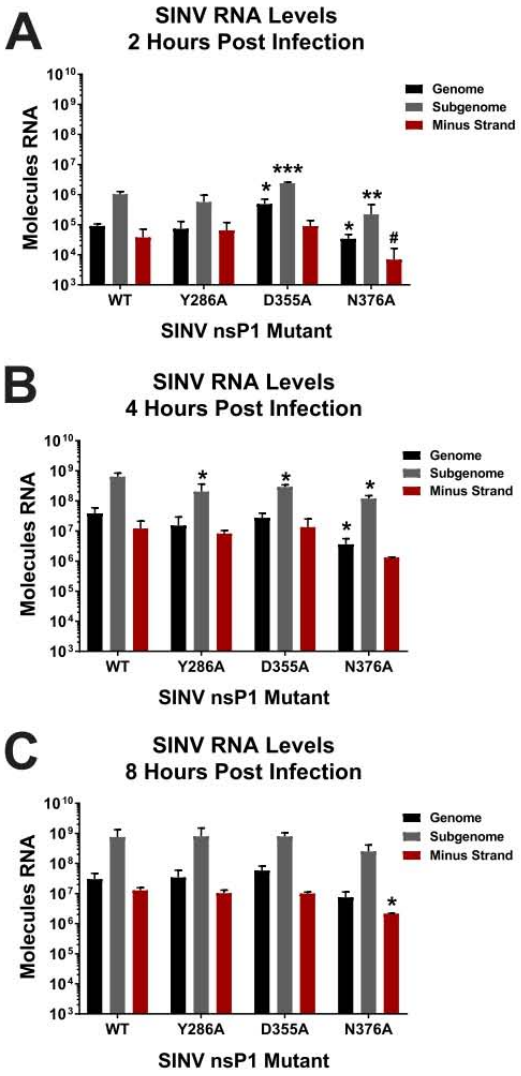

FIG 5 Altering vRNA capping efficiency impacts early RNA synthesis. (A) BHK-21 cells were infected with either wild-type parental SINV or an individual capping mutant virus at an MOI of 5 PFU/cell. At 2 h post-infection, the total cellular RNA was extracted and assessed for the absolute quantities of the genomic, subgenomic, and minus-strand vRNAs by qRT-PCR. (B and C) Identical to panel A, with the exception that the time points represent 4 and 8 h post-infection, respectively. All the quantitative data shown represent means of results from three independent biological replicates, with the error bars representing standard deviations of the means. Statistical significance data, as indicated in the figure, were first determined using ANOVA followed by *post hoc* statistical analyses by Student's *t* test. The *P* values determined by Student's *t* test are represented as follows: *, $P < 0.05$; **, $P < 0.01$; ***, $P < 0.001$. #, one of the biological replicates was below limit of detection, precluding meaningful statistical analysis.

which exhibits decreased vRNA capping, produced slightly fewer genomic and subgenomic RNAs compared to WT infection (Fig. 5A). In general, the differences in the amounts of genomic and subgenomic RNAs being produced by these two capping mutants are reflective of the differences observed in the synthesis of their replication machinery (Fig. 3 and 4). At 4 hpi, all three SINV nsP1 mutants showed a statistically significant deficit in the amount of subgenomic RNA present (Fig. 5B). Nonetheless,

these deficits are unlikely to be biologically meaningful due to their overall magnitude of effect relative to wild-type SINV. By 8 hpi, however, all three capping mutants showed levels of all three RNA species similar to the WT levels, with the exception of N376A, which had lower levels of minus-strand template than WT (Fig. 5C).

Altogether, these data demonstrate that altering the capping activity of nsP1 may have impacts on RNA synthesis very early during viral infection, but that these differences become muted as infection progresses. Importantly, these data indicate that vRNA synthesis on the whole had not been disrupted, precluding the possibility that the point mutations made in nsP1 had disrupted the function of the other nonstructural proteins. Moreover, similarly to that described above regarding viral gene expression in the previous section, the ~2-log reduction in viral growth kinetics observed for the SINV D355A mutant was not due to decreased vRNA accumulation or defective vRNA synthesis.

Translation of the SINV subgenomic RNA is largely unaffected by viral capping. Given that neither the differences in nonstructural gene expression nor the differences in vRNA synthesis were sufficient to explain the negative impact of the SINV nsP1 D355A mutation, we next sought to determine whether the function of the subgenomic vRNAs had been impacted. As both the genomic and subgenomic vRNAs are capped by nsP1, it was hypothesized that mutations which increased capping of the genomic vRNAs might impact subgenomic vRNA function. As such, it could be expected that these vRNAs would exhibit responses similar to those seen with altered capping in terms of translation. In order to determine whether translation of the subgenomic vRNAs had been impacted similarly to results seen with the genomic vRNAs, the amount of protein produced late during infection was measured using metabolic labeling (Fig. 6A). Curiously, both the SINV D355A and SINV N376A mutants exhibited a modest decrease in viral capsid production (Fig. 6B). In addition, none of the SINV nsP1 mutants exhibited differences with regard to the shutoff of host translation (a hallmark of alphaviral infection, as reviewed in reference 29), as evidenced by the labeling of the cellular actin protein, relative to WT SINV (Fig. 6C). Interestingly, however, ongoing synthesis of a high-molecular-weight protein consistent with the characteristics of the nonstructural polyprotein was reproducibly detected during the metabolic labeling of SINV D355A mutant infections.

Collectively, these data indicate either that changes in the capping efficiency of the genome might not lead to equivalent changes in capping of the subgenomic vRNA, or alternatively, that SINV, and likely other alphaviruses, regulates the translation of the structural proteins differently from the nonstructural proteins (30). Regardless, these data suggest that subgenomic translation and host translational shutoff are not impacted to a biologically significant degree by modulating the efficiency of vRNA capping and thus are not responsible for the decreased viral titer associated with increased capping efficiency.

Increasing SINV capping decreases viral particle production. Given that the molecular characterizations of the SINV nsP1 mutants had so far failed to identify the molecular defect leading to decreased viral growth kinetics of the SINV D355A mutant, we expanded our analyses beyond the life cycle events most obviously affected by the 5′ cap structure. Since vRNA synthesis and viral gene expression were unaffected, we next sought to determine whether viral particle assembly was negatively impacted by increases in the capping efficiency of the SINV nsP1 protein.

To determine whether increases in capping efficiency affected viral particle production, we quantified the total number of particles produced by each mutant as well as by wild-type SINV after 24 h of infection. Similarly to what was observed during the kinetic analyses of viral infection, increased vRNA capping was associated with the production of significantly fewer particles, with the SINV D355A mutant producing ~25-fold-fewer particles (as measured by genome equivalents per milliliter) than wild-type SINV (Fig. 7A). In contrast, particle production was largely unaffected during infections of the SINV Y286A and SINV N376A mutants, which decreased vRNA capping.

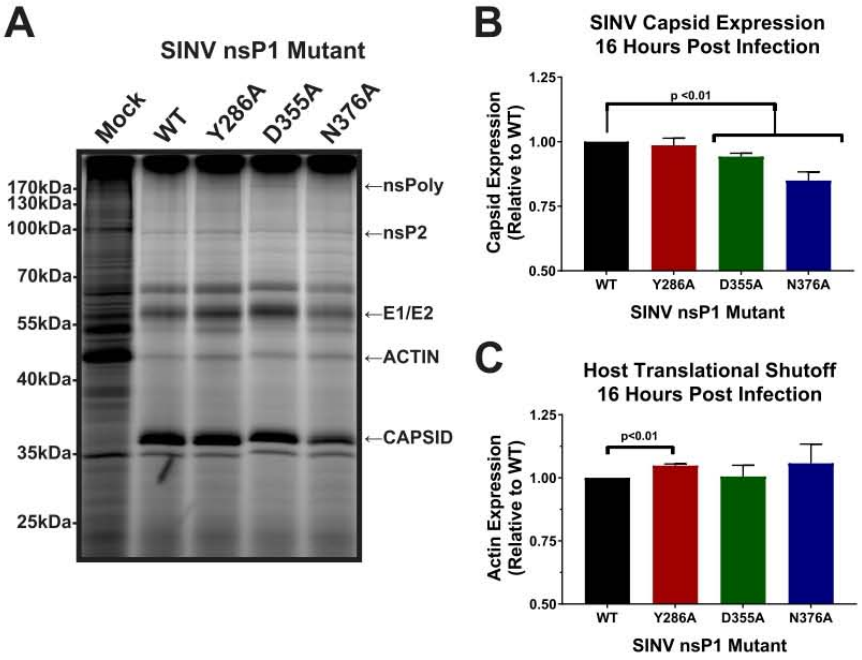

FIG 6 Subgenomic gene expression is unaffected by altering SINV vRNA capping. (A) BHK-21 cells were either mock treated or infected with wild-type SINV or an individual capping mutant at an MOI of 10 PFU/cell. At 14 hpi, the cells were pulsed with L-AHA for a period of 2 h. The cells were then harvested, and equal cell volumes of cell lysate were analyzed by SDS-PAGE and fluorescent imaging. The data shown are representative of results from three independent biological replicates. (B) Densitometric quantification of the SINV capsid protein, with intensity relative to wild-type SINV shown. (C) Densitometric quantification of the host actin protein, with intensity relative to wild-type SINV shown. All the quantitative data shown represent means of results from three independent biological replicates, with the error bars representing standard deviations of the means. Statistical significance was determined by Student's *t* test.

The point mutations utilized in this study are located within, or closely adjacent to, the SINV packaging signal (31). Previous characterizations of the alphaviral packaging signals have indicated the importance of stem-loop structures which contained a guanosine triplet in the loop region. Mutational analyses of the alphaviral packaging elements determined that mutation of the guanosine triplets, or deletion of the packaging element altogether, significantly reduced viral titer due to nonselective particle assembly leading to the production of alphaviral particles containing the subgenomic vRNAs (31). Further experiments revealed that a minimum of two guanosine triplet stem loops was sufficient to impart wild-type particle production with selectivity for the genomic RNA. Even though none of the point mutations used in this study impact either the guanosine triplets or the general secondary structures (as predicted by *in silico* analysis), the potential for the inhibition of assembly by a noncapping mechanism existed, warranting further assessment of particle production during SINV nsP1 mutant infections. As mentioned earlier, disruption of the alphaviral packaging signal leads to the production of viral particles containing predominantly subgenomic RNAs (31). As shown in Fig. 7B, quantitative determinations performed to identify which specific vRNAs were packaged into wild-type and SINV nsP1 mutant viral particles indicated no aberrant packaging of the SINV subgenomic RNA, consistent with an intact functional packaging signal.

The high degree of similarity between the relative magnitude of effect regarding decreased viral titer and viral particle production during SINV D355A infection indicates that particle assembly, and not the slight perturbations in vRNA synthesis or structural gene expression, is primarily responsible for decreased viral growth kinetics. Impor-

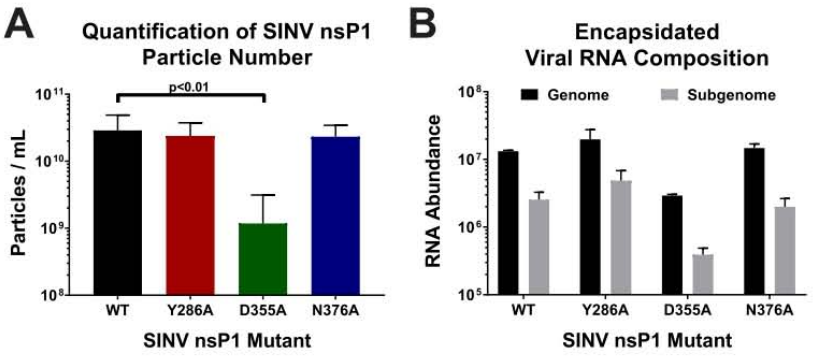

FIG 7 Analysis of SINV particle production. (A) BHK-21 cells were infected with either wild-type SINV or an individual capping mutant at an MOI of 5 PFU/cell. At 24 hpi, the total number of viral particles produced was measured using qRT-PCR. Data shown represent means of results from at least 6 independent biological samples. (B) Quantitative determination of the composition of the encapsidated viral RNAs in mature extracellular viral particles. Samples of virus-containing supernatants were assessed to determine the absolute quantities of the genomic and subgenomic RNAs via standard curve qRT-PCR. All the quantitative data shown represent means of results from three independent biological replicates, with the error bars representing standard deviations of the means. Statistical significance data, as indicated in the figure, were first determined using ANOVA followed by *post hoc* statistical analyses by Student's *t* test.

tantly, these data suggest that SINV, on the whole, was much more tolerant of mutations which decreased capping efficiency than of those that increased capping efficiency and that, by increasing the capped-to-noncapped viral RNA ratio, viral particle production had been detrimentally affected. Moreover, these data validate the idea that the packaging signal remains functional in the presence of the nsP1 point mutations described in this study.

DISCUSSION

The capping of SINV genomic vRNAs can be modulated by point mutations in nsP1. The data shown in Fig. 1 indicate that, in SINV, 5′ capping of the genomic vRNA can be modulated via single-point mutations in the nsP1 protein. This is true for both increases in vRNA capping, as seen with SINV D355A, and decreases in capping, as seen with SINV Y286A and SINV N376A. Moreover, vRNA capping can also be modulated to different extents, as seen with SINV Y286A and SINV N376A, which decreased vRNA capping by 25% and 75%, respectively. The ability to change nsP1 capping efficiency in a controllable manner opened up new avenues to explore the molecular and biological importance of both the capped genomic vRNAs and the ncgRNAs during infection in tissue culture models of infection and *in vivo*.

From the data above, we may conclude that a primary consequence of mutating the SINV nsP1 protein is the alteration of vRNA capping. Nonetheless, the alphaviral nonstructural proteins interact with one another during infection (32–35). Previous studies have shown that disrupting these interactions by mutation results in poorer viral infection and, more specifically, leads to severe defects in vRNA synthesis (32–34). However, the disruption of nonstructural protein interactions is unlikely with the nsP1 mutants reported in this study, as the phenotypes described for situations where the interactions between the nonstructural proteins have been disrupted are inconsistent with what is reported here. For example, several residues in nsP4 have been reported as important for interactions with nsP1, such as G38L in nsP4 (32). When that residue was mutated in nsP4, viral infection exhibited decreased growth kinetics and a small-plaque phenotype. However, a hallmark of disruption of the nonstructural protein interactions was the severely decreased synthesis of minus-strand vRNA throughout the course of infection (32, 34). As shown in Fig. 5, none of the nsP1 mutants examined in this study exhibited a significant deficit in production of any viral RNA species, with the exception of a minor decrease in minus-strand vRNA synthesis by N376A. It is of

note that the nsP4 G38L mutant was able to be rescued by an additional mutation in nsP1 at N374 (32). The nsP1 N374 mutation resulted in complete restoration of viral titer and partial restoration of minus-strand vRNA synthesis in the nsP4 G83L background compared to the wild type. While the effect of mutating nsP1 N374 on capping efficiency is not known, one could speculate that, given its proximity to other residues which we have shown to alter capping activity, modulating the capping efficiency of nsP1 could be a way of coping with the detrimental nsP4 G38L mutation, which creates a severe defect in RNA synthesis. In addition to this, a previous report noted that the region in nsP1 encompassing the SINV point mutations utilized here exhibits little to no interaction with the nsP2 protein (35). Thus, for the reasons described above, the nsP1 residues mutated during this study are likely not involved in mediating nonstructural protein interactions, and the resulting deficits in the viral life cycle are not due to disrupted nonstructural protein interactions.

SINV infection is more sensitive to increased capping than to decreased capping. Multiple studies have shown that polymorphisms in nsP1 have profound effects on virulence. Mutations in regions of nsP1 have been shown to alter vRNA synthesis, viral titer, viral sensitivity to IFN, and disease severity *in vivo* (19, 32, 36). Certain residues, such as nsP1 H39 in SINV, completely abrogate viral infection when mutated by eliminating the methyltransferase activity of the nsP1 protein (15, 16, 37). Therefore, we expected that incorporating the point mutations which alter viral capping would have an impact on viral infection. However, we were surprised to find that while the mutant associated with increased capping was found to have decreased viral growth kinetics, the results seen with the mutants associated with decreased capping were not significantly different from those seen with wild-type SINV (Fig. 2A). This result was especially surprising given that it was found that all three capping mutants had small-plaque phenotypes and decreased cell death, yet D355A was the only mutant to show altered growth kinetics (Fig. 2B, C, and D). Serial passaging of the mutants used in this study indicated that they were stable for at least 4 subpassages, as no reversion events (based on plaque phenotype) were observed for any of the SINV nsP1 mutants. This suggests that SINV is more detrimentally impacted by changes which increase the amount of capped vRNA present than by those which decrease capping efficiency. Thus, increases in the capping efficiency of the SINV nsP1 protein, which effectively reduced the production of the ncgRNAs, indicate that the ncgRNAs are biologically important to viral infection.

Altering capping leads to changes in genomic translation but not RNA synthesis or subgenomic translation. As would be expected, changes in nsP1 capping efficiency correlated with changes in genomic vRNA translation. In addition, the reduced presence of the ncgRNAs correlated with increased translation of the viral genomic RNA throughout infection, as can be seen with the SINV D355A increased-capping mutant. Furthermore, decreasing the capping efficiency of the nsP1 protein, as evidenced by the SINV N376A mutant, modestly decreased translation. Admittedly, the second decreased-capping mutant, SINV Y286A, did not follow the same pattern as the SINV N376A mutant. This may have been due to the comparatively minor decrease in capping efficiency caused by SINV Y286A not having been significant enough to consistently alter the vRNA population, leading to dysregulated genomic translation.

However, the increased translation exhibited by the SINV D355A mutant did not lead to lasting compounding biological effects, at least in tissue culture models of infection. For instance, despite more replication machinery having been produced early during SINV D355A infection, there were no overt differences in the levels of synthesis of any of the viral RNA species at the time points tested (Fig. 5). This suggests that increasing or decreasing the production of the nonstructural proteins alone is not enough to alter RNA synthesis over the long term in highly permissive tissue culture models of infection. Nonetheless, due to technical limitations we were unable to accurately assess vRNA synthesis earlier than 2 h post-infection. Hence, the possibility that vRNA synthesis is enhanced very early during infection remains unaddressed.

Another unexpected result was that changes in capping efficiency seemed to affect subgenomic translation differently than genomic translation. The data presented in Fig. 6 show that both the increased-capping and decreased-capping mutants SINV D355A and SINV N376A demonstrated slight, biologically nonsignificant decreases in capsid production at 16 hpi, despite showing notable differences in nonstructural gene expression (Fig. 3 and 4). This suggests either that capping efficiency is regulated differently for the subgenomic RNA than for the genomic RNA, resulting in no differences in capping efficiency for the subgenomic RNA, or that translation of the subgenomic RNA is less dependent on the presence of a 5′ cap than that of the genomic RNA during infection. The latter speculation is supported by previous studies which demonstrated that the eukaryotic initiation factor 4F (eIF4F) complex, which includes cap-binding eIF4E, is not needed to initiate translation of the alphaviral subgenomic RNA (30, 38). Those previous studies, along with the data presented here, suggest that translation of the subgenomic RNA is unaffected, at least in part, by modulation of vRNA capping.

In addition to there being little effect on subgenomic translation, there were also shown to be no differences in terms of host translational shutoff between any of the capping mutants and WT SINV (Fig. 6C). This further supports the idea that the point mutations made in nsP1 were not negatively affecting interactions between nonstructural proteins, because disruptions between nsP1 and nsP4 have been previously found to negatively affect host translational shutoff (32). Host translational shutoff, at least for SINV, has been largely attributed to the translation of the structural proteins (39). Therefore, it is unsurprising that there is no difference in host shutoff between the capping mutants and the WT SINV given that there is little difference in subgenomic expression.

Decreased titer due to changes in capping caused by interference with particle production. The decreased viral growth kinetics observed during SINV D355A infection correlated remarkably with decreased particle production. However, the congruence of the decreases in the levels of infectious units and viral particles indicates that the levels of viral infectivity are more or less identical for all of the viral strains. The discrepancy between the two magnitudes of effect (an approximate 5-fold difference) is likely due to confounding variations in the accuracy and precision of the two measurements. Nonetheless, it remains possible that the viral particles have differences in their basal infectivity characteristics. Studies examining earlier effects of the ncgRNAs are ongoing and will be presented in a follow-up study.

The observation that decreased particle production was the primary molecular defect during SINV D355A infections suggests that increasing the amount of capped genomic RNAs, thereby decreasing the number of ncgRNAs, negatively impacts the assembly of nascent viral particles. Whether the increased capping activity is directly or indirectly responsible for the packaging phenotype is not definitively known. Characterizations of SINV packaging have indicated that selectivity remains intact during the SINV D355A assembly process despite decreased particle production overall, as packaging of subgenomic vRNAs was not observed. This is indicative of a functional alphaviral packaging signal despite the incorporation of minor point mutations into the region defined as the packaging signal for SINV. Moreover, the SINV Y286A mutation which also resides within the SINV packaging element lacks an appreciable packaging phenotype. Thus, the assembly phenomena associated with the SINV D355A mutant cannot be simply explained by disruption of the alphaviral packaging signal.

While the underlying mechanism is unclear, the data presented above indicated that nonstructural protein expression is increased relative to the level seen with the wild-type parental virus and remains increased well into the late stages of infection during SINV D355A infections. Collectively, these data indicate that decreasing the production of the ncgRNAs perturbs viral genomic RNA function beyond the individual RNA level, as apparent compounding effects on the genomic RNA population are observed. Precisely how the translationally inactive ncgRNAs serve to modulate genomic vRNA function as a whole, leading to efficient particle assembly, is unknown.

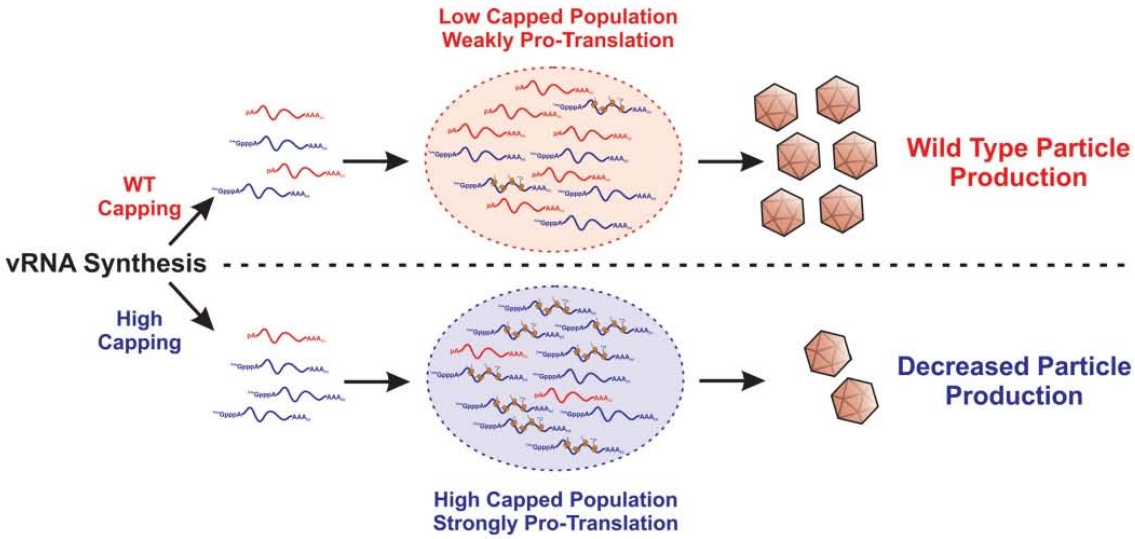

FIG 8 Proposed model of how increasing genomic vRNA capping negatively impacts viral infection.

We propose that, as diagrammed in Fig. 8, during wild-type infections, the translationally inactive ncgRNAs temper the molecular activities of the translationally active, capped genomic vRNA population, allowing the temporal progression of infection to lead to the assembly and release of viral particles. We postulate that the ncgRNAs, due to their lack of translational capacity, interact with a unique set of host factors relative to the capped translationally competent genomic RNAs. Collectively, these interactions lead to the development of a proassembly microenvironment by excluding host factors that either inhibit the assembly process or promote nucleocapsid disassembly. For instance, if the ncgRNAs foster a nontranslational environment through the interaction of host factors, such as those found within stress granules, the 60S ribosomal subunit, which is implicated in nucleocapsid disassembly, would be excluded from the local microenvironment, allowing assembly to occur unimpeded (40, 41). However, when the genomic RNA population was altered by increasing the efficiency of genomic RNA capping, such as was observed with the SINV D355A mutant, the increased and continuous translational activity of the genomic vRNA culminated in the formation of a protranslational vRNA "pool" that is refractory to encapsidation and particle assembly. Work examining such possibilities is ongoing in the laboratory of K. J. Sokoloski and will be reported in the future.

Conclusions. Collectively, these data affirm the existence and biological importance of the ncgRNAs during SINV infection. This assertion is directly supported by the capacity to modulate the capping activities of nsP1 protein via site-directed mutagenesis, resulting in increased production of XRN-1-resistant genomic vRNAs without increased overall genomic RNA numbers. Moreover, the preponderance of gene expression data indicating increased translation brought about by increasing the capping of the genomic vRNA supports the existence of the alphaviral ncgRNAs at a functional level. Finally, the molecular characterizations of SINV nsP1 mutant infections provide insight into the biological importance of the ncgRNAs with regard to the regulation of alphaviral infection at the molecular level.

MATERIALS AND METHODS

Tissue culture cells. BHK-21 cells (a gift from R. W. Hardy, Indiana University—Bloomington) were maintained in minimal essential media (MEM; Cellgro) containing 10% fetal bovine serum (FBS; Atlanta Biologicals), 1% antibiotic-antimycotic solution (Cellgro), 1% nonessential amino acids (Cellgro), and 1%

L-glutamine (Cellgro). Cells were cultured at 37°C and 5% CO_2 in a humidified incubator. Low-passage stocks were maintained via regular passaging using standard subculturing techniques.

Generation of SINV capping mutants. The SINV nsP1 mutants used in this study were generated either by site-directed mutagenesis or by Gibson assembly reactions. In particular, the SINV p389 Y286A and D355A mutants were generated via site-directed mutagenesis according to the instructions supplied with a Q5 site-directed mutagenesis kit (NEB). To this end, the parental wild-type strain consisting of the p389 SINV nsP3-GFP (nsP3-green fluorescent protein) reporter strain was PCR amplified with high-fidelity Q5 DNA polymerase using primer sets that incorporated the indicated alanine substitutions individually. Due to technical limitations that prevented the successful use of site-directed mutagenesis, the N376A mutant was generated by Gibson assembly via the use of a Gibson Ultra kit (SGI) through the use of restriction-digested p389 cDNA plasmid and a synthetic DNA fragment, according to the instructions of the manufacturers. SINV nanoluciferase reporter mutants, similarly to those previously described, were generated either by site-directed mutagenesis or by conventional restriction enzyme cloning schemes which swapped the GFP coding region of the existing p389 site mutants with a nanoluciferase coding region in a modular fashion (18).

In all cases, individual mutants were verified by whole-genome sequencing before subsequent analyses were performed. Full-genome sequences are available upon request. Highly similar phenotypes were observed for any given mutant in all virus backgrounds evaluated.

Production of SINV wild-type and mutant virus stocks. Wild type, Y286A, D355A, and N376A SINV p389 (a derivative of the Toto1101 strain containing GFP in frame with nsP3 [42]), as well as SINV pToto1101-nanoluc (a derivative of the Toto1101 strain containing nanoluciferase in frame with nsP3 [18]), were prepared by electroporation as previously described (43, 44). Briefly, 2.8×10^6 BHK-21 cells were electroporated with 10 μg of *in vitro*-transcribed RNA using a single pulse at 1.5 kV, 25 mA, and 200 Ω from a Gene Pulser Xcell system (Bio-Rad) as previously described (44). Cells were then incubated under normal incubation conditions until a cytopathic effect became apparent, at which point the supernatant was collected and clarified by centrifugation at $8,000 \times g$ for 10 min at 4°C. The clarified supernatant was then aliquoted into small-volume stocks, which were then stored at −80°C for later use.

Analysis of viral growth kinetics. To determine if mutation of the SINV nsp1 protein negatively affected infection, the viral growth kinetics of each of the individual strains described above were assayed in tissue culture models of infection. Essentially, BHK-21 cells were seeded in a 24-well plate and incubated under normal conditions. Once cell monolayers were 80% to 90% confluent, they were infected with either the wild-type parental virus or the individual capping mutant viruses at a multiplicity of infection (MOI) of 5 infectious units (IU) per cell. After a 1-h adsorption period, the inoculum was removed and the cells were washed twice with 1× phosphate-buffered saline (PBS) to remove unbound viral particles. Whole medium was added, and the cells were incubated at 37°C in a humidified incubator in the presence of 5% CO_2. At the indicated times post-infection, tissue culture supernatants were harvested (and the media replaced), and viral titer was determined via plaque assay.

Quantification of infectious virus by plaque assay. Standard virological plaque assays were used to determine the infectious titer of all viral samples produced during these studies. Briefly, BHK-21 cells were seeded in a 24-well plate and incubated under normal conditions. Once the cell monolayers were 80% to 90% confluent, they were inoculated with 10-fold serial dilutions of virus-containing samples. After a 1-h adsorption period, cells were overlaid with a solution of 0.5% Avicel (FMC Corporation) in 1× media for 28 to 30 h (45). The monolayers were fixed with formaldehyde solution (3.8% formaldehyde–1× PBS) for a period of no less than 1 h. Plaques were visualized via staining with crystal violet after removal of the overlay and quantified by manual counting.

XRN1 protection assay/RppH assay. Viral genomic RNAs were extracted from purified viral particles harvested at 24 hpi. After extraction, the RNA samples were subjected to enzymatic degradation via use of the 5′ to 3′ exonuclease XRN-1, which is capable of degrading 5′ monophosphate and RNAs *in vitro* but is unable to effectively degrade RNA substrates that are 5′ capped (22, 23). Briefly, equivalent amounts of viral genomic RNAs were incubated in the presence of 0.25 units of XRN-1 (NEB) in a final volume of 20 μl for a period of 5 min at 37°C prior to being quenched via the addition of high-salt column buffer (25 mM Tris-HCl [pH 7.6]–400 mM NaCl–0.1% [wt/vol] sodium dodecyl sulfate [SDS]). After the termination of the reaction, the RNAs were purified via phenol-chloroform extraction and ethanol precipitation with linear acrylamide carrier. The resulting precipitate was resuspended and utilized as the substrate for the synthesis of cDNA via the use of ProtoScript II reverse transcriptase (NEB). The resulting cDNAs were quantified via quantitative PCR (qPCR) analysis of an amplicon located in the nsP1 region, as described below, to determine the sensitivity of a sample relative to wild-type viral genomic vRNAs (44, 46).

To confirm that the nature of the 5′ end, in particular, the presence of a 5′ cap structure, was responsible for the differences in XRN-1 sensitivity, the extracted RNAs were coincubated with XRN-1 in the presence of the decapping enzyme RppH (18, 24, 25). To this end, the reaction mixtures described above were supplemented with 1.25 units of RppH (NEB) and processed as described above.

Metabolic labeling of protein synthesis. To determine the rates of host and viral protein synthesis during infection, BHK-21 cells were seeded in a 12-well tissue culture dish and grown to 80% to 90% confluence prior to being infected with either the wild-type parental virus or one of the individual capping mutant viruses at an MOI of 10 IU/cell. After a 1-h adsorption period, fresh medium was added to each well, and the cells were incubated under the normal incubation conditions. Thirty minutes before the indicated times post-infection, the medium was removed and replaced with methionine- and cysteine-free Dulbecco's modified Eagle's medium (DMEM; Cellgro) to starve the cells of methionine. After a 30-min incubation period, the starvation medium was removed and replaced with methionine-

and cysteine-free DMEM supplemented with 50 μM L-azidohomoalanine (L-AHA), a methionine analogue (47, 48). After 2 h, the labeling medium was removed, and the cells were washed with 1× PBS and then harvested with radioimmunoprecipitation assay (RIPA) buffer (50 mM Tris-HCl [pH 7.5]–150 mM NaCl–1% [vol/vol] Nonidet P-40 [NP-40]–0.5% [wt/vol] SDS–0.05% [wt/vol] sodium deoxycholate–1 mM EDTA). Cell lysates were labeled with DIBO-Alexa 648 (Invitrogen) at a final concentration of 5 μM and incubated at room temperature in the dark for at least 1 h. The labeled lysates were then loaded onto a 12% SDS-PAGE gel, and the proteins were separated by electrophoresis. Fluorescence was then imaged using a Pharos FX Plus Molecular Imager (Bio-Rad), and the densitometry of individual protein species was used to quantify viral and host protein expression.

Western blot detection of SINV nsP2 protein expression. Whole-cell lysates were generated from BHK-21 cells infected with either the wild-type virus or the individual SINV nsP1 capping mutant viruses by resuspension in RIPA buffer at 12 and 16 hpi. Equivalent amounts of protein were loaded onto 10% acrylamide gels, and the individual protein species were resolved using standard SDS-PAGE practices. After sufficient resolution of the protein species, the proteins were transferred to polyvinylidene difluoride (PVDF) membranes, which were rinsed in methanol and thoroughly dried after transfer. After drying, the blots were probed with anti-SINV nsP2 polyclonal sera (a gift from R.W. Hardy at Indiana University—Bloomington) or with anti-actin (clone mAbGEa; Thermo Fisher Scientific) antibodies diluted in 1× PBS–1.0% (vol/vol) Tween (PBST) for a period of at least 1 h at 25°C with gentle rocking. The blots were washed three times with 1× PBST and were probed with fluorescent anti-rabbit (A32732; Thermo Fisher Scientific) and anti-mouse secondary (A32723; Thermo Fisher Scientific) antibodies. Protein detection was achieved using a Pharos FX Plus Molecular Imager (Bio-Rad), and the densitometry of individual protein species was used to quantify viral and protein expression.

qRT-PCR detection of SINV vRNAs. The quantitative detection of the SINV vRNAs was accomplished as previously described, with minor modifications (43). Briefly, to quantify the SINV genomic, subgenomic, and negative-sense vRNAs, BHK-21 cells were infected at an MOI of 5 IU/cell and cells were harvested at 2, 4, and 8 hpi via the addition of Ribozol (VWR). Total RNA was then isolated via extraction, and 1 μg was reverse transcribed using Protoscript II reverse transcriptase (NEB) and a cocktail of specific RT primers based on the intended amplification targets. To detect the positive-sense RNA species, the RT primer cocktail consisted of nsP1, E1, and 18S reverse primers; to detect the minus-strand RNA species, the RT primer cocktail consisted of nsP1 forward and 18S reverse primers. The individual vRNA species were detected via the use of TaqMan probes and the following primer sets: for SINV nsP1, 5′-AAGGAT CTCCGGACCGTA-3′ forward (F) and 5′-AACATGAACTGGGTGGTGTCGAAG-3′ (reverse [R]); for SINV E1, 5′-TCAGATGCACCACTGGTCTCAACA-3′ (F) and 5′-ATTGACCTTCGCGGTCGGATACAT-3′ (R); for mammalian 18S, 5′-CGCGGTTCTATTTTGTTGGT-3′ (F) and 5′-AGTCGGCATCGTTTATGGTC-3′ (R). The sequences of the TaqMan detection probes used were as follows: SINV nsP1 probe, 5′-ACCATCGCTCTGCTTTCACAAC GA-3′; SINV E1 probe, 5′-ACTTATTCAGCAGACTTCGGCGGG-3′; mammalian 18S probe, 5′-AAGACGGACC AGAGCGAAAGCAT-3′.

To quantify the total number of viral particles present in a sample, BHK-21 cells were infected at an MOI of 5 IU/cell and supernatant was collected at 24 hpi. As previously described, 5 μl of supernatant was reverse transcribed (43). Reverse transcription and qPCR reactions were performed identically to those described above with the exception of the mammalian 18S primer and probes not being used. Absolute quantities of viral genomic RNAs were determined via the use of a standard curve of known concentrations.

Cell viability assay. To determine the effect of SINV infection on cell viability, BHK-21 cells were seeded in a 96-well plate and were infected with the wild-type parental virus or the individual capping mutant viruses at an MOI of 10 IU/cell. After a 1-h adsorption period, whole medium was added and the cells were incubated under normal incubation conditions for the indicated times. Afterward, the cells were washed with 1× PBS and a solution of 1/6 CellTiter 96 AQ_{ueous} One Solution reagent (Promega)–1× PBS was added to each well. The cells were then allowed to incubate at 37°C and 5% CO_2 for 2 h. Absorbance at 490 nm was then recorded using a Synergy H1 microplate reader (BioTek).

Quantification of viral gene expression via nanoluciferase assays. To quantify genomic translation during infection, BHK-21 cells were infected at an MOI of 5 IU/cell with the wild-type parental virus or the individual capping mutants containing the nanoluciferase gene within the nsP3 protein (18). After a 1-h period of adsorption on ice, the inoculum was removed and the medium was replaced with prewarmed whole medium. The infected cells were incubated under normal conditions, and at the indicated times post-infection, the medium was removed and the tissue culture cells were washed with 1× PBS. The cells were then harvested into a crude lysate by the addition of 1× PBS supplemented with 0.5% (vol/vol) Triton X-100. The lysate was transferred to a microcentrifuge tube and frozen until the completion of the experimental time course. The samples were thawed and clarified by centrifugation at 16,000 × *g* for 5 min, and equal cell volumes of the nanoluciferase samples were processed using a Nano-Glo nanoluciferase assay system (Promega) according to the manufacturer's instructions. Luminescence was then recorded using a Synergy H1 microplate reader (BioTek).

Statistical analysis. The quantitative data reported in this study represent means of data from a minimum of three independent biological replicates, unless specifically noted otherwise. The growth curve data presented in Fig. 2 were statistically assessed using an area-under-the-curve approach to determine differences in viral growth kinetics throughout the course of the assay. The statistical analysis of comparative samples was performed as previously described (43), using variable bootstrapping where appropriate. The error bars indicate standard deviations of the means. The *P* values associated with individual quantitative data sets were determined using Student's *t* test for the corresponding quantitative data.

ACKNOWLEDGMENTS

We thank the members of the laboratories of K. J. Sokoloski, D. Chung, and I. S. Lukashevich for their input during the development of the project and the preparation/editing of the manuscript. In addition, we thank Susana Lopez for the opportunity to host Joaquín Moreno-Contreras during the course of this work.

This work was funded by a grant from the National Institute of Allergy and Infectious Diseases, specifically, grant R21 AI121450 (to K.J.S. and Richard W. Hardy), and by a pilot grant supported by a COBRE program from the National Institute of General Medical Sciences, specifically grant P20 GM125504 (to K.J.S. and R. Lamont). Additional support for this research consisted of a generous startup package from the University of Louisville (to K.J.S.), support from the Integrated Programs in Biomedical Sciences (IPIBS; to A.T.L.), and funds from the Department of Microbiology and Immunology of the School of Medicine at the University of Louisville (to K.J.S.). A.T.L. was supported by an NIH-NIAID funded predoctoral fellowship, T32 AI132146.

The research efforts of J.M.-C. were supported by funds received from the Scientific Short Visit program sponsored by CONACyT and PAEP/UNAM.

REFERENCES

1. Calisher CH. 1994. Medically important arboviruses of the United States and Canada. Clin Microbiol Rev 7:89–116. https://doi.org/10.1128/CMR.7.1.89.
2. de la Monte S, Castro F, Bonilla NJ, Gaskin de Urdaneta A, Hutchins GM. 1985. The systemic pathology of Venezuelan equine encephalitis virus infection in humans. Am J Trop Med Hyg 34:194–202. https://doi.org/10.4269/ajtmh.1985.34.194.
3. Adouchief S, Smura T, Sane J, Vapalahti O, Kurkela S. 2016. Sindbis virus as a human pathogen-epidemiology, clinical picture and pathogenesis. Rev Med Virol 26:221–241. https://doi.org/10.1002/rmv.1876.
4. Kurkela S, Helve T, Vaheri A, Vapalahti O. 2008. Arthritis and arthralgia three years after Sindbis virus infection: clinical follow-up of a cohort of 49 patients. Scand J Infect Dis 40:167–173. https://doi.org/10.1080/00365540701586996.
5. Kurkela S, Manni T, Myllynen J, Vaheri A, Vapalahti O. 2005. Clinical and laboratory manifestations of Sindbis virus infection: prospective study, Finland, 2002–2003. J Infect Dis 191:1820–1829. https://doi.org/10.1086/430007.
6. Harley D, Sleigh A, Ritchie S. 2001. Ross River virus transmission, infection, and disease: a cross-disciplinary review. Clin Microbiol Rev 14:909–932. https://doi.org/10.1128/CMR.14.4.909-932.2001.
7. Rulli NE, Suhrbier A, Hueston L, Heise MT, Tupanceska D, Zaid A, Wilmes A, Gilmore K, Lidbury BA, Mahalingam S. 2005. Ross River virus: molecular and cellular aspects of disease pathogenesis. Pharmacol Ther 107:329–342. https://doi.org/10.1016/j.pharmthera.2005.03.006.
8. Pettersson RF. 1981. 5′-Terminal nucleotide sequence of Semliki forest virus 18S defective interfering RNA is heterogeneous and different from the genomic 42S RNA. Proc Natl Acad Sci U S A 78:115–119. https://doi.org/10.1073/pnas.78.1.115.
9. Pettersson RF, Soderlund H, Kaariainen L. 1980. The nucleotide sequences of the 5′-terminal T1 oligonucleotides of Semliki-Forest-virus 42-S and 26-S RNAs are different. Eur J Biochem 105:435–443. https://doi.org/10.1111/j.1432-1033.1980.tb04518.x.
10. Cancedda R, Shatkin AJ. 1979. Ribosome-protected fragments from Sindbis 42-S and 26-S RNAs. Eur J Biochem 94:41–50. https://doi.org/10.1111/j.1432-1033.1979.tb12869.x.
11. Mi S, Stollar V. 1991. Expression of Sindbis virus nsP1 and methyltransferase activity in Escherichia coli. Virology 184:423–427. https://doi.org/10.1016/0042-6822(91)90862-6.
12. Ahola T, Kaariainen L. 1995. Reaction in alphavirus mRNA capping: formation of a covalent complex of nonstructural protein nsP1 with 7-methyl-GMP. Proc Natl Acad Sci U S A 92:507–511. https://doi.org/10.1073/pnas.92.2.507.
13. Vasiljeva L, Merits A, Auvinen P, Kaariainen L. 2000. Identification of a novel function of the alphavirus capping apparatus. RNA 5′-triphosphatase activity of Nsp2. J Biol Chem 275:17281–17287. https://doi.org/10.1074/jbc.M910340199.
14. Li C, Guillen J, Rabah N, Blanjoie A, Debart F, Vasseur JJ, Canard B, Decroly E, Coutard B. 2015. mRNA capping by Venezuelan equine encephalitis virus nsP1: functional characterization and implications for antiviral research. J Virol 89:8292–8303. https://doi.org/10.1128/JVI.00599-15.
15. Wang HL, O'Rear J, Stollar V. 1996. Mutagenesis of the Sindbis virus nsP1 protein: effects on methyltransferase activity and viral infectivity. Virology 217:527–531. https://doi.org/10.1006/viro.1996.0147.
16. Ahola T, Laakkonen P, Vihinen H, Kaariainen L. 1997. Critical residues of Semliki Forest virus RNA capping enzyme involved in methyltransferase and guanylyltransferase-like activities. J Virol 71:392–397.
17. Hefti E, Bishop DH, Dubin DT, Stollar V. 1975. 5′ nucleotide sequence of Sindbis viral RNA. J Virol 17:149–159.
18. Sokoloski KJ, Haist KC, Morrison TE, Mukhopadhyay S, Hardy RW. 2015. Noncapped alphavirus genomic RNAs and their role during infection. J Virol 89:6080–6092. https://doi.org/10.1128/JVI.00553-15.
19. Stoermer Burrack KA, Hawman DW, Jupille HJ, Oko L, Minor M, Shives KD, Gunn BM, Long KM, Morrison TE. 2014. Attenuating mutations in nsP1 reveal tissue-specific mechanisms for control of Ross River virus infection. J Virol 88:3719–3732. https://doi.org/10.1128/JVI.02609-13.
20. Yang J, Yan R, Roy A, Xu D, Poisson J, Zhang Y. 2015. The I-TASSER Suite: protein structure and function prediction. Nat Methods 12:7–8. https://doi.org/10.1038/nmeth.3213.
21. Ahola T, Karlin DG. 2015. Sequence analysis reveals a conserved extension in the capping enzyme of the alphavirus supergroup, and a homologous domain in nodaviruses. Biol Direct 10:16. https://doi.org/10.1186/s13062-015-0050-0.
22. Stevens A, Poole TL. 1995. 5′-Exonuclease-2 of Saccharomyces cerevisiae. Purification and features of ribonuclease activity with comparison to 5′-exonuclease-1. J Biol Chem 270:16063–16069. https://doi.org/10.1074/jbc.270.27.16063.
23. Jinek M, Coyle SM, Doudna JA. 2011. Coupled 5′ nucleotide recognition and processivity in Xrn1-mediated mRNA decay. Mol Cell 41:600–608. https://doi.org/10.1016/j.molcel.2011.02.004.
24. Song MG, Bail S, Kiledjian M. 2013. Multiple Nudix family proteins possess mRNA decapping activity. RNA 19:390–399. https://doi.org/10.1261/rna.037309.112.
25. Hetzel J, Duttke SH, Benner C, Chory J. 2016. Nascent RNA sequencing reveals distinct features in plant transcription. Proc Natl Acad Sci U S A 113:12316–12321. https://doi.org/10.1073/pnas.1603217113.
26. Shatkin AJ. 1976. Capping of eucaryotic mRNAs. Cell 9:645–653. https://doi.org/10.1016/0092-8674(76)90128-8.
27. Banerjee AK. 1980. 5′-Terminal cap structure in eucaryotic messenger ribonucleic acids. Microbiol Rev 44:175–205.
28. Sonenberg N, Gingras AC. 1998. The mRNA 5′ cap-binding protein eIF4E and control of cell growth. Curr Opin Cell Biol 10:268–275. https://doi.org/10.1016/S0955-0674(98)80150-6.
29. Fros JJ, Pijlman GP. 2016. Alphavirus infection: host cell shut-off and

ESTRATEGIAS DE ROTAVIRUS CONTRA EL SISTEMA ANTIVIRAL INNATO.

En este artículo se describen las diferentes estrategias que el virus ha desarrollado para evadir la respuesta del sistema inmune innato del hospedero permitiéndole replicarse de manera eficiente. Además, se presenta un resumen de lo que se conoce acerca de las proteínas que conforman el sistema inmune innato del hospedero, el cual es empleado por la célula hospedera para contender contra la infección de rotavirus. Los rotavirus han desarrollado diferentes estrategias que le permiten evadir estas defensas antivirales. De manera breve, se sabe que los rotavirus emplean al menos dos proteínas virales que le permiten interactuar directamente o indirectamente con el sistema de interferón, con el fin de prevenir su activación, además emplean al menos otra proteína viral que le permite modular la actividad de la maquinaria de síntesis de proteínas celulares de esta manera previene la expresión de la mayor parte del programa antiviral de la célula. Los diferentes mecanismos empleados por rotavirus para evadir la respuesta inmune del hospedero se detallan en la siguiente revisión “Rotavirus Strategies Against the Innate Antiviral System”.

Artículo publicado en la revista Annual Review of Virology:

Rotavirus Strategies Against the Innate Antiviral System

Rotavirus Strategies Against the Innate Antiviral System

Susana López, Liliana Sánchez-Tacuba, Joaquin Moreno, and Carlos F. Arias

Departamento de Génetica del Desarrollo y Fisiología Molecular, Instituto de Biotecnología, Universidad Nacional Autónoma de México, Cuernavaca, Morelos 62210, México; email: susana@ibt.unam.mx

Annu. Rev. Virol. 2016. 3:591–609

First published online as a Review in Advance on July 29, 2016

The *Annual Review of Virology* is online at virology.annualreviews.org

This article's doi: 10.1146/annurev-virology-110615-042152

Keywords

innate immune response, host range restriction, type I IFN, type III IFN, *Reoviridae*, dsRNA

Abstract

"Rotaviruses represent the most important etiological agents of acute, severe gastroenteritis in the young of many animal species, including humans." This statement, variations of which are a common beginning in articles about rotaviruses, reflects the fact that these viruses have evolved efficient strategies for evading the innate immune response of the host and for successfully replicating in the population. In this review, we summarize what is known about the defense mechanisms that host cells employ to prevent rotavirus invasion and the countermeasures that these viruses have successfully developed to surpass cellular defenses. Rotaviruses use at least two viral multifunctional proteins to directly interact with, and prevent the activation of, the interferon system, and they use at least one other protein to halt the protein synthesis machinery and prevent the expression of most of the transcriptional antiviral program of the cell. Characterization of the confrontation between rotaviruses and their host cells has allowed us to learn about the virus–host coevolution that prevents the damaging effects of the innate immune response.

INTRODUCTION

TLR: Toll-like receptor

RLR: RIG1-like receptor

IRF: interferon regulatory factor

IFN: interferon

Rotaviruses are one of the most important causes of acute, severe gastroenteritis in children under 5 years of age. They are responsible for approximately 200,000 deaths each year, particularly in developing countries (1–3), despite the recent introduction of two safe and effective vaccines (4). Rotaviruses have also been isolated from a wealth of avian and mammalian species and represent an important veterinary problem in terms of health and economic impact (5).

Rotaviruses have a specific cell tropism, infecting primarily the mature epithelial cells of the small intestine. They also show marked host range restriction; most viral strains isolated from one animal species tend to have diminished virulence and replication capacity in heterologous species. The basis of this host range restriction is probably multifactorial (6–14). The viral spike protein VP4, which interacts with cell receptors during cell entry (15–18), has been identified as a major determinant of the cell and host tropism of the virus, although its precise function in host restriction is still undefined (7, 11–13). NSP1, a nonstructural viral protein, has also been identified as an independent factor that influences host range restriction. Of interest, host range restriction has been used as the basis for the development of rotavirus vaccines. Of the two licensed vaccines, RotaTeq (Merck) is based on genetic reassortants in which a naturally attenuated bovine virus strain is used as the genetic backbone for rotavirus genes encoding the surface proteins (VP7 and VP4) of the most common human serotypes (19).

Rotaviruses, members of the *Reoviridae* family, are nonenveloped viruses formed by three concentric layers of protein that surround a genome composed of 11 segments of dsRNA, which encode six structural (VP1–6) and six nonstructural (NSP1–6) proteins (5). The replication cycle of these viruses is summarized in **Figure 1**.

A well-established model for studying rotavirus infection is the mouse model. It mimics several aspects of rotavirus infection in humans: Suckling mice are susceptible to rotavirus infection and develop diarrhea, but in adult mice rotavirus infection does not cause disease, although the virus replicates in intestinal epithelial cells (IECs). In this model, as well as in cultured epithelial cells, it has been found that part of the restriction in the ability of rotaviruses to replicate efficiently is mediated by the innate immune response. Accordingly, the characterization of rotavirus strains grown in homologous and heterologous animal models and in cultured cells has allowed the identification of several defense mechanisms that the virus uses to evade the antiviral host response.

INNATE IMMUNE RESPONSE, INTERFERONS, AND VIRAL INFECTIONS

As a first line for detecting and preventing the invasion of viral pathogens, host cells have developed a series of membrane-bound and cytosolic receptors that sense various molecules of the invading pathogen. Viral nucleic acids are recognized by the membrane-anchored Toll-like receptors (TLRs), the RIG1-like receptors (RLRs), the dsRNA-dependent protein kinase PKR (20, 21), and the viral DNA sensors (22). Ligand-activated sensors mediate the assembly of signaling complexes that promote the activation of the antiviral program. The TLRs use MyD88 and TRIF as adaptors (23); the RLRs (RIG1 and MDA5) signal through MAVS (24–26); and the DNA sensors depend on STING (27). These signaling cascades trigger the activation of protein kinases, which subsequently phosphorylate transcription factors, including the interferon regulatory factors (IRFs) and NFκB (28), which in turn translocate to the cell nucleus and upregulate the expression of proinflammatory molecules, chemokines, cytokines, and interferons (IFNs) to activate antiviral responses and alert neighboring cells (**Figure 2**) (29, 30).

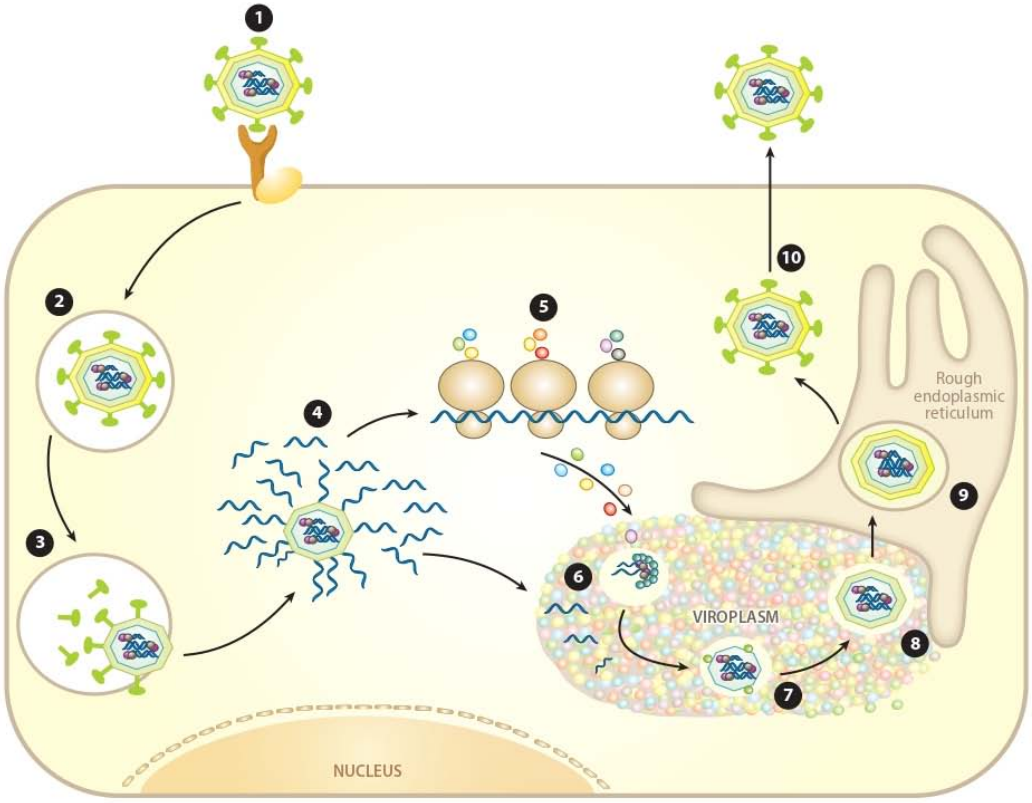

Figure 1

Rotavirus replicative cycle. The viral replication cycle starts with (❶) the binding of the virion to the cell surface and (❷) its internalization by endocytosis. Inside the cell, (❸) the outer protein layer is shed and (❹) the double-layered particle becomes transcriptionally active, giving rise to 11 RNA transcripts that encode 12 viral proteins. (❺) Once a critical mass of viral protein is accumulated, the mRNA transcripts also serve as templates for the synthesis of the genomic dsRNA, which occurs in replication intermediate particles within electron-dense structures called viroplasms that are composed of viral proteins, viral RNA, and some cellular proteins. (❻–❽) Newly synthesized single- and double-layered particles assemble concurrently with genome replication, and (❾) the double-layered particles then bud through an NSP4- and VP7-modified endoplasmic reticulum membrane into the lumen of the rough endoplasmic reticulum, where the final maturation of the viral particle takes place. (❿) Triple-layered infectious particles exit the cell either by lysis or through a nonlytic process, depending on the cell line.

There are three distinct types of IFNs: I, II, and III. Although type II IFNs have been associated mainly with resistance against different types of intracellular microorganisms, type I and III IFNs seem to be primarily committed to antiviral protection (28). Type I IFNs are key components of the host defense against viruses (28), and type III IFNs also represent an important innate immune barrier against viral infections (31, 32). In humans, type I IFNs are encoded by 13 genes for IFNα and one each for IFNβ, IFNε, IFNκ, and IFNω (although the roles for the last three have been less well characterized) (33); the type III IFNs are encoded by four genes for IFNλ1–4 (34). Type I IFNs (IFNα and IFNβ) and type III IFNs (IFNλ) produced in infected cells are secreted and act in

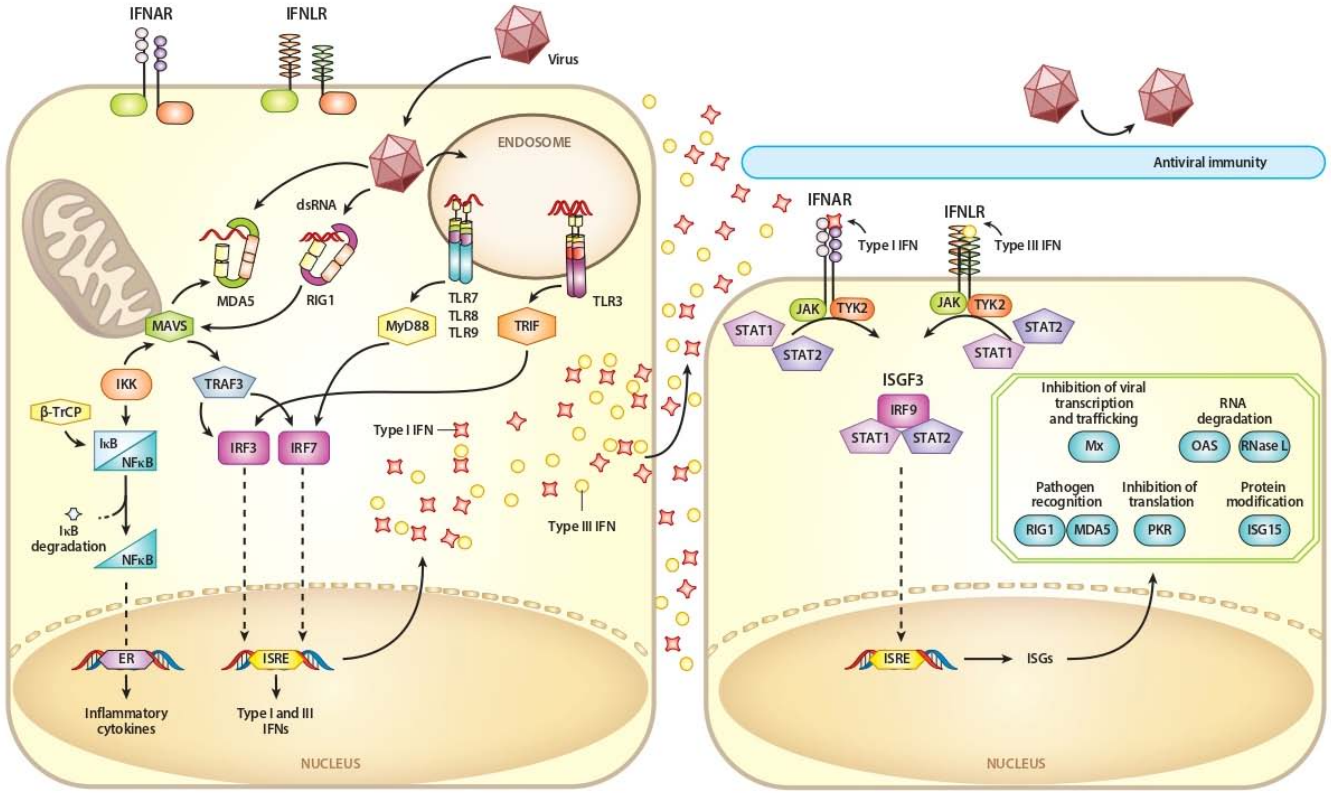

Figure 2

IFN response. Viral infections elicit a variety of cellular responses that are initiated by signals from virus-sensing receptors (RLRs or TLRs) present in the host cell. Ligand-activated sensors mediate the assembly of signaling complexes that promote the activation of the antiviral program. The TLRs use MyD88 and TRIF as adaptors; the RLRs RIG1 and MDA5 signal through MAVS, located in the outer mitochondrial membrane. These signaling cascades trigger the activation of host transcription factors, including IRF3, IRF7, and NFκB, and their translocation to the nucleus. Type I and III IFNs, proinflammatory molecules, and cytokines are expressed and secreted from infected cells and act on neighboring cells. Type I and III IFNs are recognized by IFNARs and IFNLRs present on the surface of the cells, and the JAK/STAT pathway is then activated. The phosphorylated forms of STAT1 and STAT2 associate with IRF9 to form the heterotrimeric complex ISGF3, which translocates to the nucleus, leading to the downstream transcription and expression of ISGs, whose products inhibit viral infection and alter other cellular functions. Abbreviations: IFN, interferon; IFNAR, type I IFN receptor; IFNLR, type III IFN receptor; IRF, interferon regulatory factor; ISG, interferon-stimulated gene; ISRE, interferon-stimulated response element; OAS, 2′,5′-oligoadenylate synthetase; RLR, RIG1-like receptor; TLR, Toll-like receptor.

both an autocrine and a paracrine manner through their interaction with their membrane-bound receptors to signal the activation and transcription of IFN-stimulated genes (ISGs) that promote the antiviral response.

Type I and III IFNs bind to unrelated heterodimeric receptors. The receptor for type I IFNs (IFNAR) is formed by the subunits IFNAR1 and IFNAR2, which are ubiquitously expressed (35), whereas type III IFNs bind to a receptor (IFNLR) formed by the specific IFNλ receptor chain 1 and the shared IL-10 receptor chain 2 (32, 36). Although type I and III IFNs and their receptors are distantly related, they show almost identical signaling pathways. After engaging with their ligands, both receptors induce the same JAK/STAT pathway (32, 37, 38). The phosphorylation and activation of JAK1 and TYK2 kinases, which are associated with the IFN receptors, lead to the phosphorylation of the transcription factors STAT1 and STAT2. The phosphorylated forms of STAT1 and STAT2 associate with IRF9 to form a heterotrimeric transcription complex, called ISGF3, that translocates to the nucleus to induce the expression of more than 300 ISGs, whose encoded protein products act in concert to restrict viral replication (**Figure 2**) (28, 39).

Even though both type I and type III IFNs are induced by and protect from viral infections, their receptors are differentially expressed among different tissues, which results in their different roles in vivo. In general, most cell types are thought to respond to type I IFNs, whereas type III IFN responses are largely confined to epithelial cells (40–42).

ISG: interferon-stimulated gene

MEF: mouse embryo fibroblast

ROTAVIRUS INFECTION TRIGGERS THE INNATE IMMUNE RESPONSE

Role of RIG1-Like Receptors and MAVS

Much of our current understanding of the host response to rotavirus infection has come from in vivo studies in suckling and adult mice using homologous (murine) and heterologous (human, simian, porcine, or bovine) rotavirus strains, from in vitro studies using human (Caco2, HT29) and simian (MA104, Cos7) cell lines that are permissive to rotavirus replication, and from studies using wild-type or knockout mouse embryo fibroblasts (MEFs).

Both RIG1 and MDA5 have been implicated in the detection of rotavirus in infected intestinal cells in mice and in MEFs. Early during infection, rotaviruses activate RIG1 and MDA5, alone or in combination, in a replication-dependent manner. The absence of either of these two factors decreases, but does not abolish, the magnitude of IFNβ activation, which is mediated through MAVS, their common adaptor protein (43–45). Rotavirus-infected adult mice lacking MAVS produced less IFNβ and shed increasing amounts of virus compared with wild-type mice (43). Similar findings have recently been reported in rotavirus-infected mouse $MAVS^{-/-}$ macrophages in which the production of IFN and antiviral cytokines had been abolished (46), underscoring the importance of this adaptor protein. Additionally, neither JNK and p38 kinases nor the NLRP3 inflammasome was triggered in rotavirus-infected macrophages, suggesting that these components might not have an important role in the innate immune response to rotavirus in these cells (46).

The characteristics of the RNA molecules present in a viral infection determine which RLR is activated. In general, RIG1 is activated by uncapped 5′-triphosphorylated RNAs or by monophosphates at the 5′ or 3′ ends of RNA (20, 47), whereas MDA5 preferentially recognizes dsRNAs or highly structured RNA molecules (20, 48). The length of the RNA molecules also determines RLR recognition: Short RNA molecules are preferentially recognized by RIG1, but longer fragments (more than 2 kb) are sensed by MDA5 (49). It is not clear how rotavirus dsRNA is detected by RIG1 and MDA5 in the cytoplasm of infected cells because replication of the viral genome

takes place in intermediate viral particles within viroplasms (50), hidden from host sensors. Nevertheless, the activation of RLRs early during infection suggests that it is likely that nascent viral transcripts are readily detected by RIG1 and MDA5. The size range of the viral transcripts, the recent observation that the capping activity of VP3 during mRNA synthesis is not very efficient (51, 52), and the detection of highly structured viral mRNA in the cytoplasm of infected cells (53, 54) strongly suggest that viral RNA molecules, probably different from genomic dsRNA, could elicit the activation of RIG1 and MDA5 and could also be detected by TLRs.

Role of Toll-Like Receptors and Their Adaptors TRIF and MyD88

In addition to RLRs, membrane-anchored TLRs have been implicated in the detection of viral RNA and activation of the innate immune response to rotavirus infection. However, contradictory data and results have been reported by several groups, most likely due to the use of different rotavirus strains, cell types, or biological systems to characterize the effect of these molecules on rotavirus replication, which emphasizes the need for unifying assays to achieve more definitive conclusions.

There is an important age-dependent susceptibility to symptomatic rotavirus infection in humans as well as in animals; however, the mechanisms involved in this differential susceptibility have not been completely elucidated. A marked reduction of virus shedding (approximately 100-fold) has been observed after infection in adult mice compared with infection in suckling mice (55, 56). The age-dependent expression of TLR3 might be one of the explanations for age-dependent susceptibility. TLR3 is an endosomal TLR that recognizes dsRNA and signals through TRIF to activate NFκB. The production of type III IFNs mediated by TLR3 could contribute to limiting rotavirus replication in adult mice, and the absence of TLR3 in the intestinal epithelium of suckling mice could favor rotavirus replication (57). However, although diarrhea is not induced in adult mice, rotaviruses can replicate in their intestines, suggesting that TLR3 signaling is not enough to prevent infection and that other innate immune responses might be important in preventing the disease. Indeed, $TLR3^{-/-}$ or $TRIF^{-/-}$ adult mice orally infected with rotavirus were found to show neither increased IFNβ production nor augmented rotavirus replication, supporting the observation that TLR3 might not play an essential role in defending against rotavirus infection (43). These conflicting results most likely stem from the different rotavirus strains characterized, because homologous and heterologous strains were studied in these two reports (43, 57).

Other TLRs have also been implicated in stimulating the innate response to rotavirus infection. In human plasmacytoid dendritic cells, TLR7, TLR9, or both play a role in rotavirus recognition. Even though these cells are poorly permissive to rotavirus infection, they are an important source of IFN and represent an important link between the adaptive and innate immune systems (58). More recently, the role of MyD88 signaling during rotavirus infection was studied (MyD88 mediates signaling for all TLRs except TLR3, as well as for the receptors of cytokines IL-1 and IL-18), and it was found that MyD88-mediated TLR signaling protects against acute rotavirus infection in suckling and adult mice, suggesting that TLRs (TLR7, TLR8, and TLR9) that recognize nucleic acids and induce antiviral cytokines could be targets for controlling and preventing rotavirus disease. This MyD88-mediated protection suggests a role for TLRs in the initial control of rotavirus infection, although the mechanism of this signaling and the TLR involved have not been identified (59).

SUSCEPTIBILITY OF ROTAVIRUS REPLICATION TO INTERFERONS

To be able to successfully replicate, rotavirus has coevolved with its host. It has been shown in experimental models that less than 10 infectious units of a homologous rotavirus are able to

ISRE: IFN-stimulated response element

wild-type mice, demonstrating the importance of the IFN system in modulating viral replication (68). Type III IFN production by IECs was not enough to limit rotavirus replication; for effective control of rotavirus replication the concerted action of IL-22 (produced by group 3 innate lymphoid cells) and type III IFNs was necessary. Following rotavirus infection, IECs produced and released alarmin IL-1α, which in turn enhanced the production of IL-22 by group 3 innate lymphoid cells, and type III IFNs and IL-22 were proposed to synergistically activate STAT1 for optimal transcription of ISGs to limit rotavirus replication (74). In addition, treating mice with bacterial flagellin was found to prevent rotavirus infection and cure chronically infected mice. Interestingly, the ability of flagellin to prevent or clear rotavirus infection was recapitulated by the administration of IL-22 and IL-18 to mice, leading to a reduction in viral load in an effect that was independent of type I and type III IFNs (75). Thus, it seems that the antiviral response of the host cell is more complicated than previously thought, and the participation of IFNs and cytokines produced by IECs, immune cells, or both is necessary to control rotavirus replication and spreading.

More information is needed to clarify the relative effects of type I and type III IFNs on the replication of rotaviruses; however, the signaling pathways that are responsible for their induction (IRFs, NFκB) are common, and type I and III IFNs also share activation and signaling through the JAK/STAT pathway, which triggers the expression of ISGs and secondary IFN subtypes. Interestingly, several studies have shown that rotaviruses have developed mechanisms to interfere with these common transcription activators to suppress their function (see below). Thus, irrespective of the IFN type, rotaviruses have evolved strategies to counteract the cellular innate response to successfully replicate in their hosts (60, 61, 76, 77).

VIRAL MEASURES TO COUNTERACT HOST CELL RESPONSES

Rotavirus NSP1, a Multi-Interactor Protein

Activation signals from TLRs and RLRs induce the phosphorylation of the IRF-association domain present in most IRFs and/or the dimerization of the IRFs, leading to their translocation to the nucleus and binding to IFN-stimulated response elements (ISREs) present in the promoters of IFNs and ISGs (**Figure 2**). Like many other viruses (28), rotaviruses have evolved multiple mechanisms to counteract the innate immune response of the host, one of which is to produce proteins capable of antagonizing the IFN response. The best characterized of these proteins is NSP1, an ~57-kDa protein encoded by rotavirus gene segment 5, which is the least conserved among rotavirus proteins and shows extreme sequence diversity (78). NSP1 has a conserved N-terminal RING domain and a variable C-terminal domain that allows the direct interaction of this protein with several host proteins to induce their proteasome-mediated degradation (reviewed in 77), features that suggest NSP1 might function as an E3 ubiquitin ligase (79, 80), although direct evidence demonstrating this activity is lacking.

The first suggestion that NSP1 was involved in modulating the IFN pathway came from a yeast two-hybrid assay in which the interaction between IRF3 and NSP1 was detected (81). Later, this interaction was validated, and it was subsequently shown that, depending on the viral strain and the host species, NSP1 can send to proteasome-mediated degradation several IRFs in addition to IRF3, such as IRF5, IRF7, and IRF9, but not IRF1 (82–84). It has also been shown that the IRF-associated domain of these IRFs, which mediates homodimer and heterodimer formation (85), is the region that interacts with the C terminus of NSP1, which leads to its subsequent proteasome-mediated degradation (**Figure 3*a***); this mechanism is conserved among many animal rotavirus strains (82).

In contrast to most NSP1 proteins from animal rotavirus strains, the NSP1 of most human and porcine rotaviruses blocks the expression of IFN by inducing the proteasomal degradation of

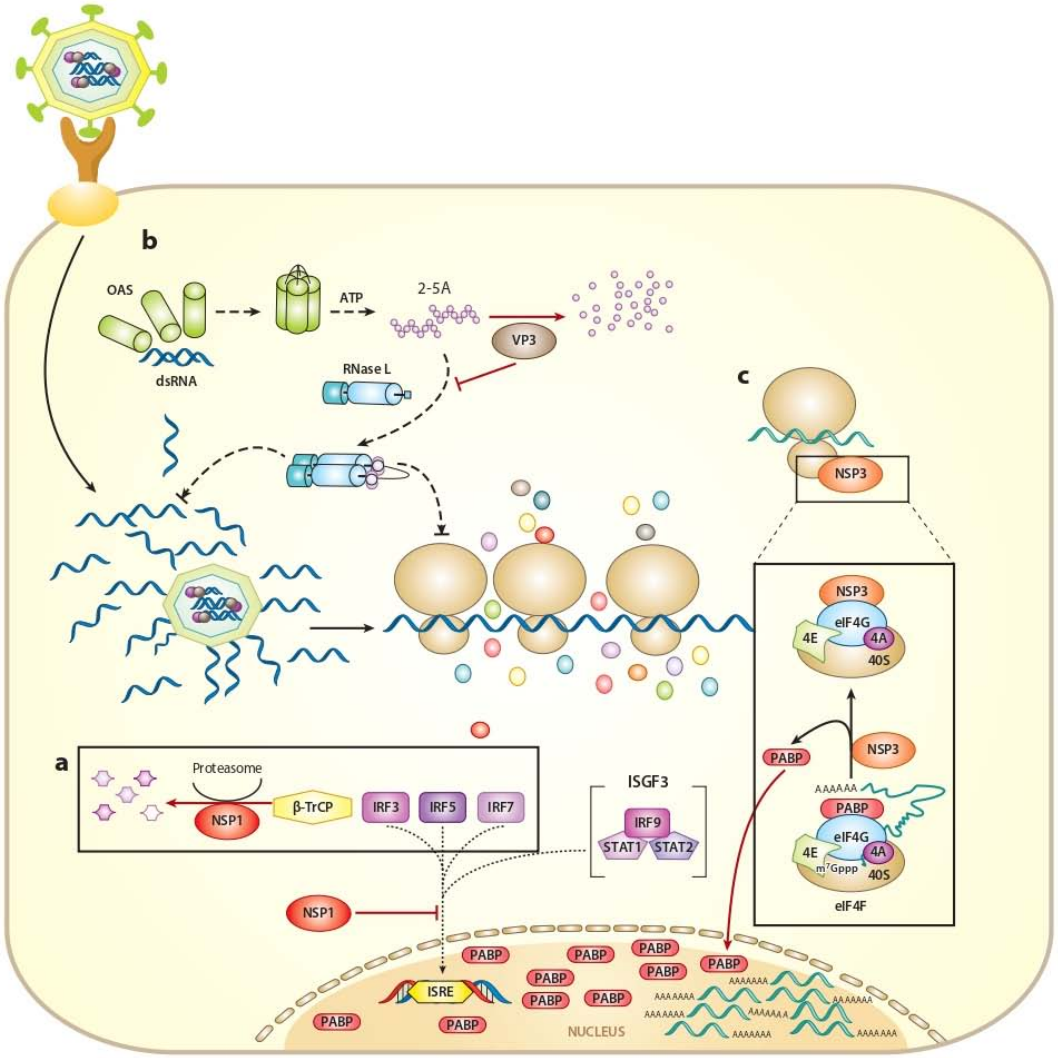

Figure 3

Rotavirus measures to counteract the host response. (*a*) During infection, NSP1 interacts with, and causes the proteasome-dependent degradation of, IRF3, IRF5, IRF7, and β-TrCP, and also prevents the activation and translocation of ISGF3 in a proteasome-independent manner. (*b*) In the presence of dsRNA, OAS oligomerizes and synthesizes 2′,5′-oligoadenylates (2-5As), which in turn interact with RNase L, causing its dimerization and activation. The phosphodiesterase activity of VP3 degrades the 2-5As, preventing RNase L activation. (*c*) NSP3 interacts specifically with eIF4G, displacing PABP and preventing the translation of poly(A)-containing mRNAs. Also during infection, PABP and poly(A)-containing mRNAs accumulate in the cell nucleus. Abbreviations: 2-5A, 2′-5′-oligoadenylate; IRF, interferon regulatory factor; ISRE, interferon-stimulated response element; OAS, 2′,5′-oligoadenylate synthetase.

β-TrCP, a cellular E3 ligase that is essential for NFκB activation (80, 86). In uninfected cells, NFκB is retained in the cell cytoplasm through its interaction with IκB (87). Signaling from TLRs, RLRs, and other receptors activates the IκB kinase that phosphorylates IκB in the two serine residues present in a six-residue region known as a phosphodegron motif (88). This motif is recognized by β-TrCP, leading to the ubiquitination and degradation of IκB, thus releasing NFκB, which translocates to the nucleus and activates the transcription of IFNs and ISGs (89). Interestingly, the C-terminal domains of some human and porcine NSP1 proteins have a degron-like motif that upon phosphorylation by kinases in rotavirus-infected cells mimics a phosphodegron that recruits β-TrCP and induces its proteasomal degradation, thus preventing the activation of NFκB (80). Notably, this seems to be a strategy shared by viruses belonging to different families (90–94), underscoring the importance of the NFκB pathway in pathogen surveillance and signaling and the need for different viruses to inhibit its activation. β-TrCP also mediates the degradation of other proteins involved in the activation of NFκB, such as IFNAR (95) and IRAK1 (96). Thus, it is expected that the NSP1 proteins that direct the degradation of β-TrCP will also impact the half-lives of these other proteins.

In addition to the well-characterized proteasomal degradation of IRFs and β-TrCP, other studies have found that NSP1 has also evolved several strain-specific strategies to target and induce the proteasome-mediated degradation of other immunomodulatory factors. For example, some rotavirus NSP1 proteins interact with and mediate the degradation of TRAF2 (97), a member of the TRAF family that is involved in mediating signaling from several cellular receptors, among which are those that activate the NFκB pathway (98). Additionally, it has also been shown that some NSP1 proteins can induce the degradation of p53, a cellular factor that promotes apoptosis in stressed cells (99).

Furthermore, it has been found that the NSP1 protein of some animal rotaviruses can block the transcriptional activity of IRF3 without inducing its degradation (100) or prevent the signaling of RIG1 (101) and MAVS (102) in a proteasome-independent manner. This suggests that this viral nonstructural protein has several mechanisms for preventing the activation of IFNs and ISGs in the host cell (reviewed in 60, 77) and also for preventing the signaling of IFNs in neighbor cells (see below). Unraveling the antiviral functions of NSP1 is a work in progress, and it is relevant to determine how many more host interactors of NSP1 exist and the consequences of these interactions in preventing the antiviral responses of the cell.

Blocking the Activation of STATs

Any type of IFN (I, II, or III) secreted from infected cells binds to its receptors, which may be present in infected cells, bystander cells, or both, and activates a signaling cascade that results in the expression of hundreds of ISGs. As previously mentioned, once IFNs interact with their receptors, the JAK/STAT pathway becomes activated; phosphorylated STAT1 and STAT2 form a heterodimer that associates with IRF9, forming the ISGF3 complex that is then translocated to the nucleus, where it upregulates ISG expression (**Figure 2**) (103). The activation of this complex is central to the IFN transduction signaling pathway; thus, several viruses have developed different strategies to prevent its activation (28). Rotaviruses are not the exception; it has been observed that during rotavirus infection, the nuclear translocation of STAT1 and STAT2 is blocked, thus preventing its transcriptional activity (104). In addition, the ability to prevent STAT nuclear translocation was found to be conserved in several rotavirus strains, and this is independent of the interaction of this complex with IMPα5, which is necessary for its nuclear translocation (105). The degradation of IRFs mediated by NSP1, including IRF9, was not found to be relevant for this phenotype (105). Additionally, a recent report has shown that at a late stage of infection,

rotaviruses are able to prevent the phosphorylation, and thus the activation, of STAT1 in infected and bystander cells. Furthermore, the heterologous expression of NSP1 alone could prevent the phosphorylation of STAT1, but interestingly, this effect was independent of the proteasome. In this study, however, the nuclear localization of STATs was not analyzed (106). Whether the inhibition of STAT transcriptional activity depends on NSP1 is still controversial; differences reported could be due to different experimental approaches being used (single-cell analysis versus whole-cell culture), the time frame analyzed, and the cell lines employed. Nevertheless, these studies support the fact that during rotavirus infection, the activation of STATs is hampered and the transcriptional activation of ISGs is prevented (**Figure 3*a***). The mechanism by which this inhibition occurs involves blocking the phosphorylation of STAT1 and inhibiting STAT1 and STAT2 translocation into the nucleus. Whether these two processes are needed or depend on each other, the mechanism by which STAT1 and STAT2 are retained in the cytoplasm, and the role that NSP1 or other viral proteins might play in this viral countermeasure remain to be determined.

OAS: 2′,5′-oligoadenylate synthetase

VP3, a Multifunctional Enzyme

VP3 is an ~98-kDa structural protein encoded by rotavirus RNA segment 3. This is an ssRNA-binding protein present in 12 copies in the nucleocapsid of the viral particles, where it associates with VP1, the RNA-dependent RNA polymerase of the virus (107, 108). Until recently, the main functions attributed to VP3 were its activities as the guanylyltransferase and methyltransferase responsible for the 5′-capping and 2′-*O*-methylation of the 5′-cap structures of the viral transcripts (109, 110). Apparently, these activities are not very efficient, because a fraction of the synthesized viral transcripts are noncapped and could therefore be recognized as RNA patterns to activate the immune signaling pathway through RLR or TLR sensors (52, 111). The presence of cytoplasmic dsRNA also triggers the activation of the 2′,5′-oligoadenylate synthetase (OAS)/RNase L pathway, which catalyzes the degradation of cellular and viral RNAs, contributing to (among other things) a general shutoff of protein synthesis. The presence of dsRNA induces the oligomerization of the OAS that is present in small amounts in the cytoplasm, thus activating it. Once active, OAS synthesizes 2′,5′-oligoadenylates (2-5As) using ATP as a substrate; these 2-5A molecules bind with high specificity and affinity to monomers of RNase L, inducing its dimerization and its activation (**Figure 3*b***) (112). Activated RNase L degrades viral and cellular RNAs, inducing cellular autophagy and apoptosis and inhibiting viral replication (112–114).

The C-terminal domain of VP3 from a simian rotavirus strain contains a 2′,5′-phosphodiesterase motif similar to that of the ns2 protein of the mouse hepatitis virus, which has been shown to antagonize the antiviral activity of RNase L by degrading 2-5As (114, 115). The C-terminal domain of rotavirus VP3 has a phosphodiesterase activity in vitro and can functionally substitute for the equivalent domain in ns2 during mouse hepatitis virus infection (115). This domain of VP3 has been cocrystallized with its substrate 2-5A, and its activity in vitro has been corroborated (116). The role of this protein during rotavirus infection of cultured MA104 cells has recently been demonstrated; even though the OAS/RNase L pathway became activated during infection, rotavirus was able to counteract this pathway through the phosphodiesterase activity of VP3, which prevented the activation of RNase L (**Figure 3*b***) (51). The recent finding that the C-terminal domain of VP3 contains 2′,5′-phosphodiesterase activity that degrades the activators of RNase L, in addition to its role as a capping enzyme, makes this protein a multifunctional enzyme that contributes to the virulence and the innate immune evasion mechanisms of rotaviruses. It remains to be seen how common this countermeasure is among different rotavirus strains and whether it is functional in vivo in rotavirus-infected animals.

Rotavirus NSP3 and Inhibition of Cellular Protein Synthesis

In addition to the elegant mechanisms by which viral proteins target a specific group of antiviral responses, a bolder and less specific strategy takes place during infection. Early in the infection process, rotaviruses take over the host translation machinery, shutting off cell protein synthesis, which, among other consequences, prevents the translation of the mRNAs induced during the IFN response of the cell. The two main checkpoints for controlling the cell translation apparatus are the initiation of polypeptide synthesis, in particular the activity of the eukaryotic initiation factor (eIF) eIF2, and the formation of the eIF4F complex, both of which are frequent targets of control by viruses (reviewed in 117, 118).

Rotavirus mRNAs are capped at their 5′ end but do not contain a poly(A) tail at the 3′ end; instead, they have at their 3′ end a consensus sequence (GACC) that is conserved in all 11 viral genes and is specifically recognized by the N-terminal domain of the nonstructural protein NSP3 (119). This viral protein also binds through its C-terminal domain to eIF4GI, a component of the eIF4F complex, in the same region used by the poly(A)-binding protein (PABP) but with higher affinity (120, 121). Thus, it has been proposed that, during rotavirus infection, NSP3 evicts PABP from eIF4G, impairing the translation of cellular mRNAs and enhancing the translation of rotavirus mRNAs (120–122). But this story might not be so straightforward. Silencing NSP3 in infected cells by RNA interference can restore cellular protein synthesis, as expected; however, and unexpectedly, it does not decrease the synthesis of viral protein but rather increases the amount of infectious virus produced (123). Furthermore, it has been reported that, in rotavirus-infected cells, PABP (123–125) and poly(A)-containing mRNAs accumulate in the nucleus through a still undefined mechanism that depends on the presence of NSP3 (126). The direct interaction of NSP3 with eIF4G and its involvement in the relocalization of PABP and poly(A)-containing mRNAs to the nucleus clearly have an inhibitory effect on the synthesis of cellular proteins (**Figure 3*c***).

The shutoff of cell protein synthesis induced by rotaviruses is also mediated by a second mechanism; early in the infection, the α subunit of eIF2 (eIF2α) becomes phosphorylated and is maintained in this state throughout the viral replication cycle (125). The continuous phosphorylated status of eIF2α might be beneficial for the virus because under these conditions the viral mRNAs are efficiently translated but the synthesis of most cellular proteins is arrested. The dsRNA-dependent protein kinase PKR has been identified as the kinase responsible for the phosphorylation of eIF2α in rotavirus-infected MA104 cells (54), as well as in IECs (127). In $PKR^{-/-}$ MEFs, or in cells in which the expression of PKR had been knocked down by RNA interference, the phosphorylation of eIF2α was prevented, but neither viral protein synthesis nor viral replication was affected (**Figure 3*c***) (54). In addition to PKR's role in inhibiting translation, it might have an additional role during rotavirus infection. It has been found that in $PKR^{-/-}$ MEFs there was no secretion of IFNβ despite the presence of several antiviral genes induced by IRF3and NFκB, and it was proposed that PKR could play a direct or indirect part in the secretory phase of IFNβ (45). In contrast, a different study using adult $PKR^{-/-}$ knockout mice infected with a simian rotavirus showed that IFNβ levels and viral replication were not different from those in infected wild-type mice. Again, differences in the experimental models, as well as in the viral strains used, might account for the different conclusions reached, thus emphasizing the need to further explore the role of PKR during rotavirus infection.

CONCLUDING REMARKS

There is no doubt that rotaviruses have found ways to successfully replicate in their hosts, evading the innate immune response that is deployed against them. It is not a simple task to escape the

multiple branches of the innate immune response, but rotaviruses have developed several specific measures on several fronts to dodge antiviral cell strategies. And yet it is also clear that host cells manage to keep the infection under control, because in many cases, a defect in any of the factors involved in controlling viral replication appears to result in a more aggressive infection. Close coevolution between rotaviruses and their hosts has occurred over a very long time, and this is clearly evidenced when homologous versus heterologous infections are compared. Indeed, several of the molecules of the innate immune response used against these viruses have been unraveled through the characterization of the replication of rotavirus strains in cells of an origin different from the species from which the virus was isolated.

At least three viral proteins are committed to thwarting the innate immune response of the cell. NSP1 interacts with several members of the IFN signaling cascade, preventing the activation of transcription factors that, in turn, activate the synthesis of IFNs and cytokines in a proteasome-dependent or -independent manner and inhibiting the activity of ISGF3, thus blocking the activation of ISGs. The activity of VP3 as a capping enzyme protects viral mRNAs from being detected by RLRs early in the infection, and then its 2′,5′-phosphodiesterase activity inactivates the unique molecules (2-5As) that turn on the activity of the harmful RNase L. Finally, NSP3, by preventing the interaction of cellular mRNAs with the initiation complex eIF4F, and by causing the accumulation of PABP and poly(A)-containing mRNAs in the cell nucleus, prevents the translation of most cellular mRNAs, thus blocking the translation of many of the transcripts induced during the IFN response of the cell.

There is still a long way to go to completely understand the defense components of the host response to rotaviruses, in particular in the human host. Years of work using animal models and susceptible cells have provided preliminary and interesting picture of host–rotavirus struggles, but the elements that restrict virus replication and the ways in which the virus contends with them remain obscure. The use of different rotavirus strains and study models has partly complicated comparisons between studies; moreover, methodological advances that make possible the analysis of the host cell response at a single-cell level, instead of characterizing the response of pooled and usually heterogeneous cells, will allow us to have a clearer picture of the details of the virus–cell battle. Clearly, characterization of the innate immune response of cells to invading rotaviruses is a work in progress, in which new host and viral defense components and activities will be discovered.

DISCLOSURE STATEMENT

The authors are not aware of any affiliations, memberships, funding, or financial holdings that might be perceived as affecting the objectivity of this review.

ACKNOWLEDGMENTS

Work in our laboratory relevant to this article was supported by grants 153639 and 221019 from the National Council for Science and Technology (CONACyT), Mexico, and grant IG-200114 from Dirección General de Asuntos del Personal Académico–Universidad Nacional Autónoma de México (DGAPA-UNAM).

LITERATURE CITED

1. Lee LA, Franzel L, Atwell J, Datta SD, Friberg IK, et al. 2013. The estimated mortality impact of vaccinations forecast to be administered during 2011–2020 in 73 countries supported by the GAVI alliance. *Vaccine* 31(Suppl. 2):B61–72

2. Tate JE, Burton AH, Boschi-Pinto C, Steele AD, Duque J, et al. 2008. Estimate of worldwide rotavirus-associated mortality in children younger than 5 years before the introduction of universal rotavirus vaccination programmes: a systematic review and meta-analysis. *Lancet Infect. Dis.* 12:136–41
3. Walker CL, Rudan I, Liu L, Nair H, Theodoratou E, et al. 2013. Global burden of childhood pneumonia and diarrhoea. *Lancet* 381:1405–16
4. Babji S, Kang G. 2012. Rotavirus vaccination in developing countries. *Curr. Opin. Virol.* 2:443–48
5. Estes MK, Greenberg HB. 2013. Rotaviruses and their replication. In *Fields Virology*, ed. DN Knipe, PM Howley, pp. 1347–401. Philadelphia: Wolters Kluwer
6. Bridger JC, Dhaliwal W, Adamson MJ, Howard CR. 1998. Determinants of rotavirus host range restriction—a heterologous bovine NSP1 gene does not affect replication kinetics in the pig. *Virology* 245:47–52
7. Bridger JC, Tauscher GI, Desselberger U. 1998. Viral determinants of rotavirus pathogenicity in pigs: evidence that the fourth gene of a porcine rotavirus confers diarrhea in the homologous host. *J. Virol.* 72:6929–31
8. Broome RL, Vo PT, Ward RL, Clark HF, Greenberg HB. 1993. Murine rotavirus genes encoding outer capsid proteins VP4 and VP7 are not major determinants of host range restriction and virulence. *J. Virol.* 67:2448–55
9. Ciarlet M, Estes MK, Barone C, Ramig RF, Conner ME. 1998. Analysis of host range restriction determinants in the rabbit model: comparison of homologous and heterologous rotavirus infections. *J. Virol.* 72:2341–51
10. Feng N, Sen A, Wolf M, Vo P, Hoshino Y, Greenberg HB. 2011. Roles of VP4 and NSP1 in determining the distinctive replication capacities of simian rotavirus RRV and bovine rotavirus UK in the mouse biliary tract. *J. Virol.* 85:2686–94
11. Feng N, Yasukawa LL, Sen A, Greenberg HB. 2013. Permissive replication of homologous murine rotavirus in the mouse intestine is primarily regulated by VP4 and NSP1. *J. Virol.* 87:8307–16
12. Hoshino Y, Saif LJ, Kang SY, Sereno MM, Chen WK, Kapikian AZ. 1995. Identification of group A rotavirus genes associated with virulence of a porcine rotavirus and host range restriction of a human rotavirus in the gnotobiotic piglet model. *Virology* 209:274–80
13. Offit PA, Blavat G, Greenberg HB, Clark HF. 1986. Molecular basis of rotavirus virulence: role of gene segment 4. *J. Virol.* 57:46–49
14. Wang W, Donnelly B, Bondoc A, Mohanty SK, McNeal M, et al. 2011. The rhesus rotavirus gene encoding VP4 is a major determinant in the pathogenesis of biliary atresia in newborn mice. *J. Virol.* 85:9069–77
15. Arias CF, Silva-Ayala D, Lopez S. 2015. Rotavirus entry: a deep journey into the cell with several exits. *J. Virol.* 89:890–93
16. Baker M, Prasad BV. 2010. Rotavirus cell entry. *Curr. Top. Microbiol. Immunol.* 343:121–48
17. Lopez S, Arias CF. 2004. Multistep entry of rotavirus into cells: a Versaillesque dance. *Trends Microbiol.* 12:271–78
18. Lopez S, Arias CF. 2006. Early steps in rotavirus cell entry. *Curr. Top. Microbiol. Immunol.* 309:39–66
19. Heaton PM, Goveia MG, Miller JM, Offit P, Clark HF. 2005. Development of a pentavalent rotavirus vaccine against prevalent serotypes of rotavirus gastroenteritis. *J. Infect. Dis.* 192(Suppl. 1):S17–21
20. Kato H, Takeuchi O, Sato S, Yoneyama M, Yamamoto M, et al. 2006. Differential roles of MDA5 and RIG-I helicases in the recognition of RNA viruses. *Nature* 441:101–5
21. Takeuchi O, Akira S. 2009. Innate immunity to virus infection. *Immunol. Rev.* 227:75–86
22. Kawasaki T, Kawai T, Akira S. 2011. Recognition of nucleic acids by pattern-recognition receptors and its relevance in autoimmunity. *Immunol. Rev.* 243:61–73
23. O'Neill LA, Bowie AG. 2007. The family of five: TIR-domain-containing adaptors in Toll-like receptor signalling. *Nat. Rev. Immunol.* 7:353–64
24. Kawai T, Takahashi K, Sato S, Coban C, Kumar H, et al. 2005. IPS-1, an adaptor triggering RIG-I- and Mda5-mediated type I interferon induction. *Nat. Immunol.* 6:981–88
25. Seth RB, Sun L, Ea CK, Chen ZJ. 2005. Identification and characterization of MAVS, a mitochondrial antiviral signaling protein that activates NF-κB and IRF 3. *Cell* 122:669–82

26. Xu LG, Wang YY, Han KJ, Li LY, Zhai Z, Shu HB. 2005. VISA is an adapter protein required for virus-triggered IFN-β signaling. *Mol. Cell* 19:727–40
27. Ishikawa H, Ma Z, Barber GN. 2009. STING regulates intracellular DNA-mediated, type I interferon-dependent innate immunity. *Nature* 461:788–92
28. Randall RE, Goodbourn S. 2008. Interferons and viruses: an interplay between induction, signalling, antiviral responses and virus countermeasures. *J. Gen. Virol.* 89:1–47
29. O'Neill LA, Bowie AG. 2010. Sensing and signaling in antiviral innate immunity. *Curr. Biol.* 20:R328–33
30. Takeuchi O, Akira S. 2010. Pattern recognition receptors and inflammation. *Cell* 140:805–20
31. Donnelly RP, Kotenko SV. 2010. Interferon-λ: a new addition to an old family. *J. Interferon Cytokine Res.* 30:555–64
32. Kotenko SV, Gallagher G, Baurin VV, Lewis-Antes A, Shen M, et al. 2003. IFN-λs mediate antiviral protection through a distinct class II cytokine receptor complex. *Nat. Immunol.* 4:69–77
33. Pestka S. 2007. The interferons: 50 years after their discovery, there is much more to learn. *J. Biol. Chem.* 282:20047–51
34. Wack A, Terczynska-Dyla E, Hartmann R. 2015. Guarding the frontiers: the biology of type III interferons. *Nat. Immunol.* 16:802–9
35. Uze G, Schreiber G, Piehler J, Pellegrini S. 2007. The receptor of the type I interferon family. *Curr. Top. Microbiol. Immunol.* 316:71–95
36. Sheppard P, Kindsvogel W, Xu W, Henderson K, Schlutsmeyer S, et al. 2003. IL-28, IL-29 and their class II cytokine receptor IL-28R. *Nat. Immunol.* 4:63–68
37. Dumoutier L, Tounsi A, Michiels T, Sommereyns C, Kotenko SV, Renauld JC. 2004. Role of the interleukin (IL)-28 receptor tyrosine residues for antiviral and antiproliferative activity of IL-29/interferon-λ1: similarities with type I interferon signaling. *J. Biol. Chem.* 279:32269–74
38. Kotenko SV. 2011. IFN-λs. *Curr. Opin. Immunol.* 23:583–90
39. Schoggins JW. 2014. Interferon-stimulated genes: roles in viral pathogenesis. *Curr. Opin. Virol.* 6:40–46
40. Durbin RK, Kotenko SV, Durbin JE. 2013. Interferon induction and function at the mucosal surface. *Immunol. Rev.* 255:25–39
41. Hermant P, Michiels T. 2014. Interferon-λ in the context of viral infections: production, response and therapeutic implications. *J. Innate Immun.* 6:563–74
42. Mahlakoiv T, Hernandez P, Gronke K, Diefenbach A, Staeheli P. 2015. Leukocyte-derived IFN-α/β and epithelial IFN-λ constitute a compartmentalized mucosal defense system that restricts enteric virus infections. *PLOS Pathog.* 11:e1004782
43. Broquet AH, Hirata Y, McAllister CS, Kagnoff MF. 2011. RIG-I/MDA5/MAVS are required to signal a protective IFN response in rotavirus-infected intestinal epithelium. *J. Immunol.* 186:1618–26
44. Hirata Y, Broquet AH, Menchen L, Kagnoff MF. 2007. Activation of innate immune defense mechanisms by signaling through RIG-I/IPS-1 in intestinal epithelial cells. *J. Immunol.* 179:5425–32
45. Sen A, Pruijssers AJ, Dermody TS, Garcia-Sastre A, Greenberg HB. 2011. The early interferon response to rotavirus is regulated by PKR and depends on MAVS/IPS-1, RIG-I, MDA-5, and IRF3. *J. Virol.* 85:3717–32
46. Di Fiore IJ, Holloway G, Coulson BS. 2015. Innate immune responses to rotavirus infection in macrophages depend on MAVS but involve neither the NLRP3 inflammasome nor JNK and p38 signaling pathways. *Virus Res.* 208:89–97
47. Hornung V, Ellegast J, Kim S, Brzozka K, Jung A, et al. 2006. 5′-triphosphate RNA is the ligand for RIG-I. *Science* 314:994–97
48. Pichlmair A, Schulz O, Tan CP, Naslund TI, Liljestrom P, et al. 2006. RIG-I-mediated antiviral responses to single-stranded RNA bearing 5′-phosphates. *Science* 314:997–1001
49. Kato H, Takeuchi O, Mikamo-Satoh E, Hirai R, Kawai T, et al. 2008. Length-dependent recognition of double-stranded ribonucleic acids by retinoic acid-inducible gene-I and melanoma differentiation-associated gene 5. *J. Exp. Med.* 205:1601–10
50. Silvestri LS, Taraporewala ZF, Patton JT. 2004. Rotavirus replication: plus-sense templates for double-stranded RNA synthesis are made in viroplasms. *J. Virol.* 78:7763–74
51. Sanchez-Tacuba L, Rojas M, Arias CF, Lopez S. 2015. Rotavirus controls activation of the 2′-5′-oligoadenylate synthetase/RNase L pathway using at least two distinct mechanisms. *J. Virol.* 89:12145–53

52. Uzri D, Greenberg HB. 2013. Characterization of rotavirus RNAs that activate innate immune signaling through the RIG-I-like receptors. *PLOS ONE* 8:e69825
53. Li W, Manktelow E, von Kirchbach JC, Gog JR, Desselberger U, Lever AM. 2010. Genomic analysis of codon, sequence and structural conservation with selective biochemical-structure mapping reveals highly conserved and dynamic structures in rotavirus RNAs with potential *cis*-acting functions. *Nucleic Acids Res.* 38:7718–35
54. Rojas M, Arias CF, Lopez S. 2010. Protein kinase R is responsible for the phosphorylation of eIF2α in rotavirus infection. *J. Virol.* 84:10457–66
55. Kordasti S, Istrate C, Banasaz M, Rottenberg M, Sjovall H, et al. 2006. Rotavirus infection is not associated with small intestinal fluid secretion in the adult mouse. *J. Virol.* 80:11355–61
56. Vancott JL, McNeal MM, Choi AH, Ward RL. 2003. The role of interferons in rotavirus infections and protection. *J. Interferon Cytokine Res.* 23:163–70
57. Pott J, Stockinger S, Torow N, Smoczek A, Lindner C, et al. 2012. Age-dependent TLR3 expression of the intestinal epithelium contributes to rotavirus susceptibility. *PLOS Pathog.* 8:e1002670
58. Deal EM, Jaimes MC, Crawford SE, Estes MK, Greenberg HB. 2010. Rotavirus structural proteins and dsRNA are required for the human primary plasmacytoid dendritic cell IFNα response. *PLOS Pathog.* 6:e1000931
59. Uchiyama R, Chassaing B, Zhang B, Gewirtz AT. 2015. MyD88-mediated TLR signaling protects against acute rotavirus infection while inflammasome cytokines direct Ab response. *Innate Immun.* 21:416–28
60. Arnold MM, Sen A, Greenberg HB, Patton JT. 2013. The battle between rotavirus and its host for control of the interferon signaling pathway. *PLOS Pathog.* 9:e1003064
61. Holloway G, Coulson BS. 2013. Innate cellular responses to rotavirus infection. *J. Gen. Virol.* 94:1151–60
62. Sen A, Rothenberg ME, Mukherjee G, Feng N, Kalisky T, et al. 2012. Innate immune response to homologous rotavirus infection in the small intestinal villous epithelium at single-cell resolution. *PNAS* 109:20667–72
63. De Boissieu D, Lebon P, Badoual J, Bompard Y, Dupont C. 1993. Rotavirus induces α-interferon release in children with gastroenteritis. *J. Pediatr. Gastroenterol. Nutr.* 16:29–32
64. La Bonnardiere C, Cohen J, Contrepois M. 1981. Interferon activity in rotavirus infected newborn calves. *Ann. Rech. Vétérinaires* 12:85–91
65. Frias AH, Vijay-Kumar M, Gentsch JR, Crawford SE, Carvalho FA, et al. 2010. Intestinal epithelia activate anti-viral signaling via intracellular sensing of rotavirus structural components. *Mucosal Immunol.* 3:622–32
66. Feng N, Kim B, Fenaux M, Nguyen H, Vo P, et al. 2008. Role of interferon in homologous and heterologous rotavirus infection in the intestines and extraintestinal organs of suckling mice. *J. Virol.* 82:7578–90
67. Angel J, Franco MA, Greenberg HB, Bass D. 1999. Lack of a role for type I and type II interferons in the resolution of rotavirus-induced diarrhea and infection in mice. *J. Interferon Cytokine Res.* 19:655–59
68. Pott J, Mahlakoiv T, Mordstein M, Duerr CU, Michiels T, et al. 2011. IFN-λ determines the intestinal epithelial antiviral host defense. *PNAS* 108:7944–49
69. Feng N, Sen A, Nguyen H, Vo P, Hoshino Y, et al. 2009. Variation in antagonism of the interferon response to rotavirus NSP1 results in differential infectivity in mouse embryonic fibroblasts. *J. Virol.* 83:6987–94
70. Bass DM. 1997. Interferon γ and interleukin 1, but not interferon α, inhibit rotavirus entry into human intestinal cell lines. *Gastroenterology* 113:81–89
71. Egli A, Santer DM, O'Shea D, Tyrrell DL, Houghton M. 2014. The impact of the interferon-λ family on the innate and adaptive immune response to viral infections. *Emerg. Microbes Infect.* 3:e51
72. Lasfar A, Zloza A, Cohen-Solal KA. 2016. IFN-λ therapy: current status and future perspectives. *Drug Discov. Today* 21:167–71
73. Sommereyns C, Paul S, Staeheli P, Michiels T. 2008. IFN-lambda (IFN-λ) is expressed in a tissue-dependent fashion and primarily acts on epithelial cells in vivo. *PLOS Pathog.* 4:e1000017

74. Hernandez PP, Mahlakoiv T, Yang I, Schwierzeck V, Nguyen N, et al. 2015. Interferon-λ and interleukin 22 act synergistically for the induction of interferon-stimulated genes and control of rotavirus infection. *Nat. Immunol.* 16:698–707
75. Zhang B, Chassaing B, Shi Z, Uchiyama R, Zhang Z, et al. 2014. Prevention and cure of rotavirus infection via TLR5/NLRC4-mediated production of IL-22 and IL-18. *Science* 346:861–65
76. Lopez S, Arias CF. 2012. Rotavirus–host cell interactions: an arms race. *Curr. Opin. Virol.* 2:389–98
77. Morelli M, Ogden KM, Patton JT. 2015. Silencing the alarms: innate immune antagonism by rotavirus NSP1 and VP3. *Virology* 479:75–84
78. Dunn SJ, Cross TL, Greenberg HB. 1994. Comparison of the rotavirus nonstructural protein NSP1 (NS53) from different species by sequence analysis and northern blot hybridization. *Virology* 203:178–83
79. Graff JW, Ewen J, Ettayebi K, Hardy ME. 2007. Zinc-binding domain of rotavirus NSP1 is required for proteasome-dependent degradation of IRF3 and autoregulatory NSP1 stability. *J. Gen. Virol.* 88:613–20
80. Morelli M, Dennis AF, Patton JT. 2015. Putative E3 ubiquitin ligase of human rotavirus inhibits NF-κB activation by using molecular mimicry to target β-TrCP. *mBio* 6:e02490
81. Graff JW, Mitzel DN, Weisend CM, Flenniken ML, Hardy ME. 2002. Interferon regulatory factor 3 is a cellular partner of rotavirus NSP1. *J. Virol.* 76:9545–50
82. Arnold MM, Barro M, Patton JT. 2013. Rotavirus NSP1 mediates degradation of interferon regulatory factors through targeting of the dimerization domain. *J. Virol.* 87:9813–21
83. Barro M, Patton JT. 2005. Rotavirus nonstructural protein 1 subverts innate immune response by inducing degradation of IFN regulatory factor 3. *PNAS* 102:4114–19
84. Barro M, Patton JT. 2007. Rotavirus NSP1 inhibits expression of type I interferon by antagonizing the function of interferon regulatory factors IRF3, IRF5, and IRF7. *J. Virol.* 81:4473–81
85. Yanai H, Negishi H, Taniguchi T. 2012. The IRF family of transcription factors: inception, impact and implications in oncogenesis. *Oncoimmunology* 1:1376–86
86. Graff JW, Ettayebi K, Hardy ME. 2009. Rotavirus NSP1 inhibits NFκB activation by inducing proteasome-dependent degradation of β-TrCP: a novel mechanism of IFN antagonism. *PLOS Pathog.* 5:e1000280
87. Hinz M, Arslan SC, Scheidereit C. 2012. It takes two to tango: IκBs, the multifunctional partners of NF-κB. *Immunol. Rev.* 246:59–76
88. Kanarek N, Ben-Neriah Y. 2012. Regulation of NF-κB by ubiquitination and degradation of the IκBs. *Immunol. Rev.* 246:77–94
89. Hayden MS, Ghosh S. 2012. NF-κB, the first quarter-century: remarkable progress and outstanding questions. *Genes Dev.* 26:203–34
90. Bour S, Perrin C, Akari H, Strebel K. 2001. The human immunodeficiency virus type 1 Vpu protein inhibits NF-κB activation by interfering with βTrCP-mediated degradation of IκB. *J. Biol. Chem.* 276:15920–28
91. Mangeat B, Gers-Huber G, Lehmann M, Zufferey M, Luban J, Piguet V. 2009. HIV-1 Vpu neutralizes the antiviral factor Tetherin/BST-2 by binding it and directing its β-TrCP2-dependent degradation. *PLOS Pathog.* 5:e1000574
92. Mansur DS, Maluquer de Motes C, Unterholzner L, Sumner RP, Ferguson BJ, et al. 2013. Poxvirus targeting of E3 ligase β-TrCP by molecular mimicry: a mechanism to inhibit NF-κB activation and promote immune evasion and virulence. *PLOS Pathog.* 9:e1003183
93. Margottin F, Bour SP, Durand H, Selig L, Benichou S, et al. 1998. A novel human WD protein, h-βTrCP, that interacts with HIV-1 Vpu connects CD4 to the ER degradation pathway through an F-box motif. *Mol. Cell* 1:565–74
94. Tang W, Pavlish OA, Spiegelman VS, Parkhitko AA, Fuchs SY. 2003. Interaction of Epstein-Barr virus latent membrane protein 1 with SCFHOS/β-TrCP E3 ubiquitin ligase regulates extent of NF-κB activation. *J. Biol. Chem.* 278:48942–49
95. Kumar KG, Krolewski JJ, Fuchs SY. 2004. Phosphorylation and specific ubiquitin acceptor sites are required for ubiquitination and degradation of the IFNAR1 subunit of type I interferon receptor. *J. Biol. Chem.* 279:46614–20

96. Cui W, Xiao N, Xiao H, Zhou H, Yu M, et al. 2012. β-TrCP-mediated IRAK1 degradation releases TAK1–TRAF6 from the membrane to the cytosol for TAK1-dependent NF-κB activation. *Mol. Cell. Biol.* 32:3990–4000
97. Bagchi P, Bhowmick R, Nandi S, Kant Nayak M, Chawla-Sarkar M. 2013. Rotavirus NSP1 inhibits interferon induced non-canonical NFκB activation by interacting with TNF receptor associated factor 2. *Virology* 444:41–44
98. Xie P. 2013. TRAF molecules in cell signaling and in human diseases. *J. Mol. Signal.* 8:7
99. Bhowmick R, Halder UC, Chattopadhyay S, Nayak MK, Chawla-Sarkar M. 2013. Rotavirus-encoded nonstructural protein 1 modulates cellular apoptotic machinery by targeting tumor suppressor protein p53. *J. Virol.* 87:6840–50
100. Sen A, Feng N, Ettayebi K, Hardy ME, Greenberg HB. 2009. IRF3 inhibition by rotavirus NSP1 is host cell and virus strain dependent but independent of NSP1 proteasomal degradation. *J. Virol.* 83:10322–35
101. Qin L, Ren L, Zhou Z, Lei X, Chen L, et al. 2011. Rotavirus nonstructural protein 1 antagonizes innate immune response by interacting with retinoic acid inducible gene I. *Virol. J.* 8:526
102. Nandi S, Chanda S, Bagchi P, Nayak MK, Bhowmick R, Chawla-Sarkar M. 2014. MAVS protein is attenuated by rotavirus nonstructural protein 1. *PLOS ONE* 9:e92126
103. Stark GR, Darnell JE Jr. 2012. The JAK–STAT pathway at twenty. *Immunity* 36:503–14
104. Holloway G, Truong TT, Coulson BS. 2009. Rotavirus antagonizes cellular antiviral responses by inhibiting the nuclear accumulation of STAT1, STAT2, and NF-κB. *J. Virol.* 83:4942–51
105. Holloway G, Dang VT, Jans DA, Coulson BS. 2014. Rotavirus inhibits IFN-induced STAT nuclear translocation by a mechanism that acts after STAT binding to importin-α. *J. Gen. Virol.* 95:1723–33
106. Sen A, Rott L, Phan N, Mukherjee G, Greenberg HB. 2014. Rotavirus NSP1 protein inhibits interferon-mediated STAT1 activation. *J. Virol.* 88:41–53
107. Desselberger U. 2014. Rotaviruses. *Virus Res.* 190:75–96
108. Ogden KM, Snyder MJ, Dennis AF, Patton JT. 2014. Predicted structure and domain organization of rotavirus capping enzyme and innate immune antagonist VP3. *J. Virol.* 88:9072–85
109. Chen D, Luongo CL, Nibert ML, Patton JT. 1999. Rotavirus open cores catalyze 5′-capping and methylation of exogenous RNA: evidence that VP3 is a methyltransferase. *Virology* 265:120–30
110. Spencer E, Garcia BI. 1984. Effect of *S*-adenosylmethionine on human rotavirus RNA synthesis. *J. Virol.* 52:188–97
111. Imai M, Akatani K, Ikegami N, Furuichi Y. 1983. Capped and conserved terminal structures in human rotavirus genome double-stranded RNA segments. *J. Virol.* 47:125–36
112. Silverman RH. 2007. Viral encounters with 2′,5′-oligoadenylate synthetase and RNase L during the interferon antiviral response. *J. Virol.* 81:12720–29
113. Chakrabarti A, Jha BK, Silverman RH. 2011. New insights into the role of RNase L in innate immunity. *J. Interferon Cytokine Res.* 31:49–57
114. Silverman RH, Weiss SR. 2014. Viral phosphodiesterases that antagonize double-stranded RNA signaling to RNase L by degrading 2-5A. *J. Interferon Cytokine Res.* 34:455–63
115. Zhang R, Jha BK, Ogden KM, Dong B, Zhao L, et al. 2013. Homologous 2′,5′-phosphodiesterases from disparate RNA viruses antagonize antiviral innate immunity. *PNAS* 110:13114–19
116. Ogden KM, Hu L, Jha BK, Sankaran B, Weiss SR, et al. 2015. Structural basis for 2′-5′-oligoadenylate binding and enzyme activity of a viral RNase L antagonist. *J. Virol.* 89:6633–45
117. Dever TE. 2002. Gene-specific regulation by general translation factors. *Cell* 108:545–56
118. Walsh D, Mohr I. 2011. Viral subversion of the host protein synthesis machinery. *Nat. Rev. Microbiol.* 9:860–75
119. Poncet D, Aponte C, Cohen J. 1993. Rotavirus protein NSP3 (NS34) is bound to the 3′ end consensus sequence of viral mRNAs in infected cells. *J. Virol.* 67:3159–65
120. Groft CM, Burley SK. 2002. Recognition of eIF4G by rotavirus NSP3 reveals a basis for mRNA circularization. *Mol. Cell* 9:1273–83
121. Piron M, Vende P, Cohen J, Poncet D. 1998. Rotavirus RNA-binding protein NSP3 interacts with eIF4GI and evicts the poly(A) binding protein from eIF4F. *EMBO J.* 17:5811–21

122. Vende P, Piron M, Castagne N, Poncet D. 2000. Efficient translation of rotavirus mRNA requires simultaneous interaction of NSP3 with the eukaryotic translation initiation factor eIF4G and the mRNA 3′ end. *J. Virol.* 74:7064–71
123. Montero H, Arias CF, Lopez S. 2006. Rotavirus nonstructural protein NSP3 is not required for viral protein synthesis. *J. Virol.* 80:9031–38
124. Harb M, Becker MM, Vitour D, Baron CH, Vende P, et al. 2008. Nuclear localization of cytoplasmic poly(A)-binding protein upon rotavirus infection involves the interaction of NSP3 with eIF4G and RoXaN. *J. Virol.* 82:11283–93
125. Montero H, Rojas M, Arias CF, Lopez S. 2008. Rotavirus infection induces the phosphorylation of eIF2 α but prevents the formation of stress granules. *J. Virol.* 82:1496–504
126. Rubio RM, Mora SI, Romero P, Arias CF, Lopez S. 2013. Rotavirus prevents the expression of host responses by blocking the nucleocytoplasmic transport of polyadenylated mRNAs. *J. Virol.* 87:6336–45
127. Vijay-Kumar M, Gentsch JR, Kaiser WJ, Borregaard N, Offermann MK, et al. 2005. Protein kinase R mediates intestinal epithelial gene remodeling in response to double-stranded RNA and live rotavirus. *J. Immunol.* 174:6322–31

IMPLEMENTACIÓN DEL DIAGNÓSTICO DE SARS-COV-2 EN MUESTRAS DE SALIVA

Debido a la emergencia de salud mundial causada por la COVID-19, surgió la necesidad de generar e implementar métodos diagnósticos rápidos y confiables para poder detectar la presencia del virus del síndrome respiratorio agudo severo 2 (SARS-CoV-2). Durante la elaboración del proyecto, nuestro laboratorio participó en la implementación del diagnóstico para la detección de SARS-CoV-2 mediante la capacitación de diferentes laboratorios de la academia, esta actividad la realizamos en coordinación con el Instituto de Diagnóstico y Referencia Epidemiológicos (InDRE). Por otra parte, en colaboración con los Servicios de Salud del Estado de Morelos llevamos a cabo, mediante RT-qPCR, la detección de SARS-CoV-2 en muestras de pacientes provenientes de diferentes centros de salud del Estado y en muestras de miembros de la comunidad de la UNAM campus Morelos. El tener acceso a estos especímenes nos permitió explorar diferentes metodologías que nos permitieron optimizar el diagnóstico de SARS-CoV-2, logrando disminuir el tiempo y el costo del procesamiento.

El método diagnóstico considerado estándar de oro para la detección de SARS-CoV-2 es la amplificación de regiones específicas del genoma viral mediante PCR cuantitativo de transcripción reversa (RT-qPCR) a partir de muestras provenientes de hisopados nasofaríngeos y orofaríngeos (NPS y OPS, respectivamente)(77)(78). Sin embargo, durante la pandemia hubo un incremento en la demanda de los reactivos que se emplean para colectar muestras biológicas y para purificar el RNA viral, provocando escases de los reactivos necesarios para realizar el diagnóstico. Los hisopos, el medio de transporte viral y los kits de

extracción de RNA viral fueron los reactivos que más escasearon, comprometiendo el número de pruebas diagnosticas que se podían realizar.

La saliva es un espécimen clínico que ha sido aprobado por la FDA para el diagnóstico de SARS-CoV-2. La toma de muestra empleando saliva tiene múltiples beneficios, ya que al ser colectada por el propio paciente se disminuye el riesgo de contagio del personal de salud encargado de tomar el hisopado; además, no se requiere el uso de equipo de protección personal el cual también escaseo durante este periodo(79)(80). Debido a que los kits de extracción de RNA también escasearon, evaluamos la lisis directa de las salivas como método de obtención de RNA viral empleando el reactivo Quick Extract DNA solution (QE, Lucigen). En este trabajo comparamos los resultados obtenidos por RT-qPCR de 253 muestras de saliva e hisopado obtenidas del mismo paciente. Para realizar la comparación, las muestras de hisopado fueron procesadas utilizando un kit de extracción, mientras que las salivas se trataron directamente con el buffer de lisis QE; posteriormente, se analizó la presencia o ausencia de SARS-CoV-2 mediante RT-qPCR en ambos grupos. En estos ensayos encontramos una buena correlación al comparar ambos tipos de muestras, esto nos permitió proponer a la saliva y su lisis directa como una alternativa para el diagnóstico de SARS-CoV-2. Además, al no requerir hisopos, kits de extracción y medio de transporte viral, el tiempo de procesamiento y su costo se reducen en más del 60%. Esto permite incrementar la capacidad de diagnóstico de los laboratorios y reduce el tiempo de espera de los resultados. Los resultados de este trabajo fueron publicados en el artículo “Saliva sampling and Its Direct Lysis, an Excellent Option To Increase the Number of SARS-CoV-2 Diagnostic Test in Settings with Supply Shortages”. Además, también se publicó el artículo de

divulgación “Un método sensible, rápido y económico para detectar el SARS-CoV-2 en saliva”.

Artículo publicado en la revista Journal of Clinical Microbiology:

Saliva Sampling and Its Direct Lysis, an Excellent Option To Increase the Number of SARS-CoV-2 Diagnostic Test in Settings with Supply Shortages

AMERICAN SOCIETY FOR MICROBIOLOGY | Journal of Clinical Microbiology®

VIROLOGY

Saliva Sampling and Its Direct Lysis, an Excellent Option To Increase the Number of SARS-CoV-2 Diagnostic Tests in Settings with Supply Shortages

Joaquín Moreno-Contreras,[a] Marco A. Espinoza,[a] Carlos Sandoval-Jaime,[a] Marco A. Cantú-Cuevas,[b] Héctor Barón-Olivares,[c] Oscar D. Ortiz-Orozco,[c] Asunción V. Muñoz-Rangel,[c] Manuel Hernández-de la Cruz,[c] César M. Eroza-Osorio,[c] Carlos F. Arias,[a] Susana López[a]

[a]Departamento de Genética del Desarrollo y Fisiología Molecular, Instituto de Biotecnología Universidad Nacional Autónoma de México, Cuernavaca, Morelos, Mexico
[b]Secretaría de Salud del Estado de Morelos, Cuernavaca, Morelos, Mexico
[c]Servicios de Salud del Estado de Morelos, Cuernavaca, Morelos, Mexico

ABSTRACT As part of any plan to lift or ease the confinement restrictions that are in place in many different countries, there is an urgent need to increase the capacity of laboratory testing for severe acute respiratory syndrome coronavirus 2 (SARS-CoV-2). Detection of the viral genome through reverse transcription-quantitative PCR (RT-qPCR) is the gold standard for this virus; however, the high demand of the materials and reagents needed to sample individuals, purify the viral RNA, and perform the RT-qPCR has resulted in a worldwide shortage of several of these supplies. Here, we show that directly lysed saliva samples can serve as a suitable source for viral RNA detection that is less expensive and can be as efficient as the classical protocol, which involves column purification of the viral RNA. In addition, it bypasses the need for swab sampling, decreases the risk of the health care personnel involved in the testing process, and accelerates the diagnostic procedure.

KEYWORDS COVID-19, diagnostic tools, RT-qPCR, SARS-CoV-2

With the worldwide COVID-19 health emergency, there is an urgent need for rapid and reliable methods of diagnosis for severe acute respiratory syndrome coronavirus 2 (SARS-CoV-2). The accepted gold standard for detection of this virus is the amplification of regions of the viral genome by reverse transcription-quantitative PCR (RT-qPCR) in nasopharyngeal and oropharyngeal swabs (1, 2). Unfortunately, given the enormous demand for the reagents needed to collect the biological samples and to purify the viral RNA, there have been shortages of many of the reagents needed for the diagnostic tests. Swabs, viral transport media, and kits for viral RNA extraction are among the most common consumables that have become scarce, compromising the number of tests that can be done in many parts of the world.

Recently, several reports have demonstrated the possibility of using saliva instead of oral and nasal swabs to detect the genome of SARS-COV-2 (3–5). Saliva collection also has many collateral benefits, including self-collection, which decreases the risk to health care workers in charge of taking the swabs and does not require the use of personal protective equipment (PPE), which has also become a scarce item in this pandemic (6, 7). In addition, the methods to extract the RNA from biological samples require the use of purification kits, whose availability has also become limited due to the heavy worldwide demand.

In this study, we compared the RT-qPCR results from 253 paired samples obtained from saliva and swabs of ambulatory patients; the RNA in the swab samples was

Citation Moreno-Contreras J, Espinoza MA, Sandoval-Jaime C, Cantú-Cuevas MA, Barón-Olivares H, Ortiz-Orozco OD, Muñoz-Rangel AV, Hernández-de la Cruz M, Eroza-Osorio CM, Arias CF, López S. 2020. Saliva sampling and its direct lysis, an excellent option to increase the number of SARS-CoV-2 diagnostic tests in settings with supply shortages. J Clin Microbiol 58:e01659-20. https://doi.org/10.1128/JCM.01659-20.

Editor Angela M. Caliendo, Rhode Island Hospital

Address correspondence to Susana López, susana@ibt.unam.mx.

Received 28 June 2020
Returned for modification 17 July 2020
Accepted 21 July 2020
Accepted manuscript posted online 23 July 2020
Published 22 September 2020

extracted using a commercial RNA purification kit, and the saliva samples were directly mixed with a lysis buffer, boiled, and used for the RT-qPCR protocol. We found a very good correlation of results between the two types of samples, and we propose that saliva sampling and direct lysis, which together simplify the sampling of patients and accelerate the preparation of RNA for RT-qPCR, represent an excellent alternative that will facilitate sampling and diagnosis of a larger number of persons at a reduced cost.

MATERIALS AND METHODS

Sample collection. A total of 253 paired samples from oropharyngeal and nasopharyngeal swabs (OPSs and NPSs, respectively) and saliva were collected during a span of 30 days (from 2 May to 31 May) by health care workers from the epidemiology department of the health ministry of the state of Morelos, Mexico (Secretaría de Salud Morelos [SSM]). All but 3 samples were from ambulatory patients; the 3 exceptions were collected from hospitalized patients.

Swab sampling. Oropharyngeal and nasopharyngeal swabs were taken from 71 patients, while a single oropharyngeal swab was taken from each of 182 patients. After their collection, swabs were placed in 2.5 ml of viral transport medium.

Saliva collection. Saliva was self-collected by patients that were asked to spit on several occasions into sterile urine cup containers until completing roughly 2 to 3 ml of saliva. No viral transport media, or stabilizing agents, were added to the saliva samples.

After collection, both swab and saliva samples were stored at 4°C until transported to the Institute of Biotechnology/UNAM for their analysis, which was within 24 to 36 h after sample collection.

Nucleic acid extraction and SARS-CoV-2 detection by RT-qPCR. Total RNA was extracted from swab samples using the QIAamp viral RNA minikit (Qiagen) following the manufacturer's protocol, using 140 μl of viral transport medium from each swab, and the purified RNA was eluted in 60 μl of elution buffer.

Saliva samples were treated with Quick Extract DNA extraction solution (QE; Lucigen) by mixing 50 μl of saliva with 50 μl of the QE reagent and heating for 5 min at 95°C; the mixture was then cooled on ice and kept at 4°C until use (within 1 h of QE treatment). For saliva samples that had high viscosity, 1 volume of sterile phosphate-buffered saline (PBS) was added and mixed by repeated pipetting, and the diluted saliva sample was extracted as mentioned above.

SARS-CoV-2 detection was performed using the Berlin protocol, using the reported oligonucleotides and probes for viral gene E and for human RNase P (8). The RT-qPCRs were performed using the StarQ one-step RT-qPCR (Genes 2 Life) kit, using 5 μl of the column-extracted total RNA in 20 μl of reaction mixture or 2.5 μl of the QE-treated saliva in 22.5 μl of reaction mixture. Samples were analyzed in an ABI Prism 7500 sequence detector system (Applied Biosystems) with the following thermal protocol: 50°C for 15 min, 95°C for 2 min, and then 45 cycles of 95°C for 15 s and 60°C for 30 s. All samples with a threshold cycle (C_T) value equal to or less than 38 were classified as positive.

Determination of viral copy number. To determine the viral copy number in a sample, a standard curve was generated using a 10-fold serial dilution of an *in vitro* T7 RNA transcript that carries the sequence recognized by oligonucleotides and probe for gene E. Briefly, the logarithm of concentration of each dilution was plotted against the C_T and the viral copy number from unknown samples was determined by extrapolating the C_T value onto the corresponding standard curve.

Statistical analysis. Statistical analysis was performed using GraphPad Prism 6.0 (GraphPad Software Inc.) as described in Results.

RESULTS

Detection of SARS-CoV-2 in paired swab and saliva samples. To evaluate if saliva is a good source of viral RNA for the RT-qPCR, we determined the presence of the SARS-CoV-2 genome in paired saliva and swab samples from 253 ambulatory patients. All patients had two or more symptoms related to COVID-19 (8, 9); 116 (45.4%) were male and 137 (54.1%) female, with a median age of 41 ($\pm$14.4) years. Samples were taken from ambulatory patients in the respiratory triage of the Tlaltenango health center in Cuernavaca, Morelos, Mexico. The RT-qPCR Berlin protocol was used to detect SARS-CoV-2, using only the primers and probe for gene E, since previous studies have shown a weak detection of viral RNA when the RNA-dependent RNA polymerase (RdRp) gene is probed (9, 10). As an internal control of RNA content in the samples, the RNase P gene was detected. Total RNA was purified from swabs using the QIAamp viral RNA minikit; the RNA in saliva was directly obtained using the QE lysis buffer (Lucigen) and boiling for 5 min, as reported previously (11).

During the course of the study, and due to the shortage of swabs, the health center shifted temporarily from collecting two swabs per person (nasopharyngeal swab [NPS] plus oropharyngeal swab [OPS]) to only one swab (OPS) per individual. For the 253 patients included in this study, two swabs were used in 71 (28%) of the cases, while a

TABLE 1 Summary of results obtained from parallel testing of swab and saliva samples from patients suspected of having COVID-19

	No. of patients with indicated result for single swab (OPS)			No. of patients with indicated result for double swabs (OPS + NPS)		
Result for saliva	Positive	Negative	Total	Positive	Negative	Total
Positive	41	28	69	19	6	25
Negative	11	102	113	9	37	46
Total	52	130	182	28	43	71

single OPS was taken from the other 182 (72%) irrespective of the number of swabs collected, saliva samples were taken from all patients.

Of the 182 patients with a single swab collected, 80 (43.9%) were positive for SARS-CoV-2 as determined by either the swab or saliva samples. Of these, 41 (51.2%) were positive as determined by both types of samples, while 28 (35%) were positive only by saliva and not by the swab sample and 11 (13.7%) were positive only by the OPS. In total, out of the 80 individuals found to be positive for the virus, 69 (86.2%) were correctly identified using saliva, while only 52 (65%) were identified with the OPS (Table 1 and Fig. 1).

On the other hand, 34 (47.8%) of the 71 patients with two swabs collected were found to be positive for SARS-CoV-2 by either the swabs or the saliva samples. Of these, 19 (55.8%) were positive by both swabs and saliva, while 6 (17.6%) were positive only by saliva and 9 (26.4%) were positive only by the two swab samples. In total, in this group of patients, of the 34 individuals identified as positive for the virus, 25 (73.5%) were identified by testing saliva, while 28 (82.3%) were positive by the swabs (Table 1 and Fig. 1).

Quantitation of viral RNA. When the numbers of viral genome copies in the single OPS and saliva samples were compared, a significant difference in the geometric mean was detected, with saliva samples having a titer 1.9 $\log_{10}$ higher than that observed in the swabs ($P < 0.0024$ [Fig. 2A]). This can be better appreciated when the viral copy numbers in paired swabs and saliva from the same patient are plotted and represented

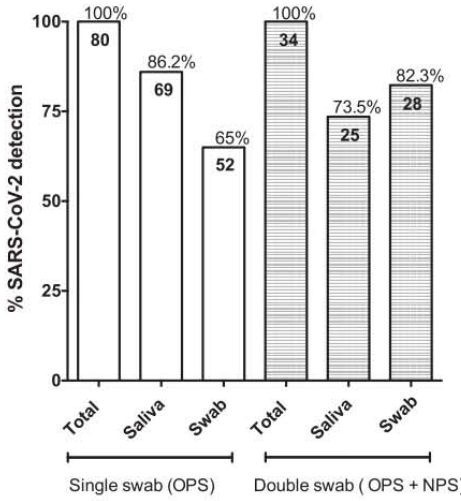

FIG 1 Detection of SARS-CoV-2 in paired swab and saliva samples. Percentages and numbers of positive samples detected among single OPSs and saliva, or double swabs (OPS plus NPS) and saliva, as indicated, are shown. Data are extracted from Table 1.

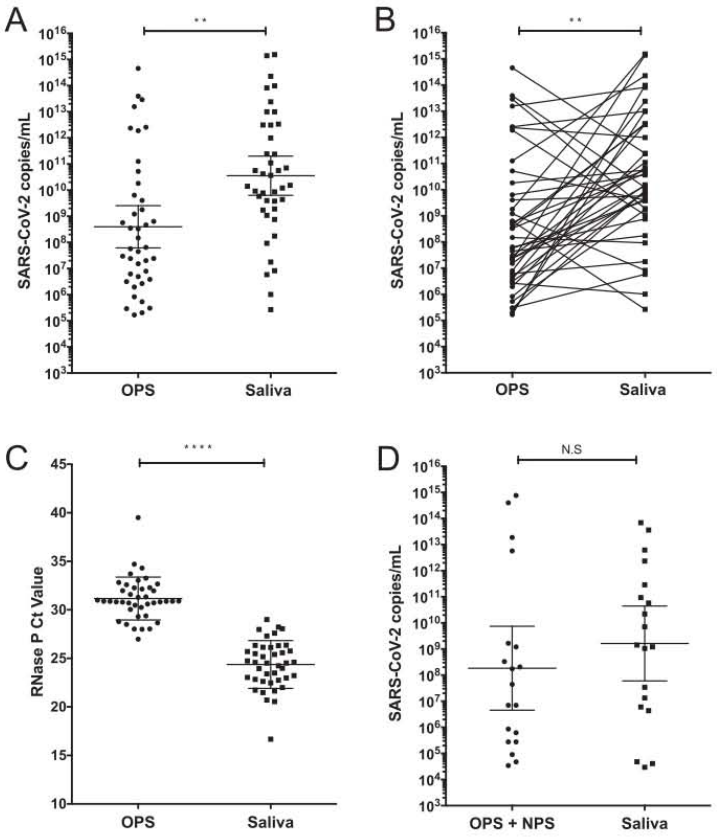

FIG 2 A high SARS-CoV-2 genome copy number is detected in saliva samples. (A) Viral titer detected in paired OPS and saliva samples. (B) Viral titer detected in paired OPS and saliva samples are represented by lines connecting both samples. Data were compared by a Wilcoxon test (**, $P < 0.0024$). (C) RT-PCR cycle C_T values for RNase P detected in OPS and saliva samples. Data were compared by Wilcoxon test (****, $P < 0.0001$). (D) Viral titer detected in paired double (NPS plus OPS) and saliva samples. Data were compared by Wilcoxon test; no statistical significance (N.S) was found ($P < 0.6226$). Bars represent the geometric medians and 95% confidence intervals.

as connecting lines (Fig. 2B); for 31 of the paired samples, the number of viral copies was higher in saliva samples than in swabs. Human RNase P was used as an internal control of sampling quality; of interest, the comparison between the mean of C_T values obtained from OPS and saliva samples showed a difference of at least 6.8 C_T units between both types of samples (Fig. 2C), indicating that there is more cellular material in saliva, as reported in other studies (12). The viral genome copy numbers in the double-swab and saliva samples were not statistically different, although a larger set of data would be needed to confirm these results (Fig. 2D).

DISCUSSION

In this study, we analyzed 253 paired samples from either a single OPS compared to saliva or a double OPS and NPS and saliva. RNA purified from swabs using commercial column kits was compared with saliva samples directly lysed with QE buffer (surpassing the RNA extraction protocol) as a source for the RT-qPCR assay. Although the coincidence rate between the single OPS and saliva samples was relatively low (51.2%), the saliva samples were clearly more efficient in detecting the virus than single OPS samples (86.2% versus 65%). On the other hand, the efficiency of detection of the virus

in saliva compared to the double OPS and NPS was slightly lower (73.5% versus 82.3%), with a coincidence rate of 55.8%.

Taken together, these results suggest that that saliva is a good source for SARS-CoV-2 detection, especially compared with a single OPS. Furthermore, it can be implemented for diagnostic tests using a simple QE buffer-based sample preparation in place of the column-based RNA purification method that is currently employed for swab analyses.

The reason for the low coincidence in the positive results obtained with swab and saliva samples is not clear. The failure of identification of SARS-CoV-2 in swabs when the saliva samples were positive for the virus could be due to bad swab sampling, what can be corroborated by the higher C_T values of RNase P detected in these samples (Fig. 2C), with the consequent low viral copy number. This is a major concern, since the medical personnel in charge of taking the samples frequently do not do it correctly for the risk associated with this process. It has been reported that oropharyngeal swabs have a lower viral titer than nasopharyngeal swabs (1); thus, this could contribute to the discrepancies observed. Furthermore, it has also been previously reported that nasopharyngeal swabs have a lower viral titer than saliva samples (12), which could also contribute to explain our findings. On the other hand, the false negatives in saliva could be due either to the absence or undetectable levels of virus in the saliva samples or to unknown problems during the collection, transport, and/or storage of the sample before its arrival to the laboratory.

SARS-CoV-2 has been detected in saliva at higher titers during the first days after the onset of symptoms, with the viral titer declining over time. It is not clear how long after symptom onset the viral RNA can be detected in saliva, although some reports suggest a short period of detection (~13 days) compared with that for nasopharyngeal swabs (~19 days) (13). However, other reports have recently demonstrated the detection of viral RNA in saliva for longer periods (~20 days or longer) (4, 14). The patients included in this study were ambulatory and according to their clinical interviews were between 1 and 7 days (median of 4 days) of the onset of symptoms. We did not find a significant difference between the onset of symptoms and the cases in which positivity was determined only with saliva versus those that were detected only with swabs.

Direct lysis of nasopharyngeal or oropharyngeal swab samples in viral transport medium using the QE buffer has been reported as a suitable method for direct RT-qPCR for SARS-CoV-2 detection, with rates similar to those of methods based on column purification (11, 15). However, we have found a great variability in the results obtained using the QE lysis protocol when applied to swab samples, most likely due to variations in the material of the swabs used and to variations in the preparation of the viral transport medium employed (data not shown). In this regard, it has recently been reported that the composition of viral transport media can affect the detection of RNA from SARS-CoV-2 and other viruses (16), and due to the scarcity of these media, several laboratories have started to prepare their own transport media, introducing an additional confusion factor. A similar situation occurs with swabs, since in view of the scarcity of suitable materials, other materials are being employed, despite the fact that some of them are known to inhibit RT-PCR (17).

The use of saliva samples offers the advantage that no additives or transport media need to be used for their preservation or analysis if stored in cold temperatures and analyzed up to 36 h after their collection. Our results indicate that a rapid processing of saliva using direct lysis with QE buffer offers an excellent alternative to the current swab analysis that uses RNA column purification, since it is a sensitive, fast, and inexpensive method that can be used for massive screening, in particular in those settings where common supplies needed for the classical methods are in shortage.

ACKNOWLEDGMENTS

We are grateful to the health care workers of Servicios Estatales de Salud de Morelos for their invaluable help in collecting the samples and to the personnel of the Laboratorio Estatal de Salud Pública del Estado de Morelos for their support in the

preparation and transport of the samples. The work of P. Gaytán, E. López, and J. Yañez from the DNA sequencing and synthesis unit is also acknowledged.

Some of the reagents used in this study were provided by the Instituto Nacional de Diagnóstico y Referencia Epidemiológica, supported by INSABI. This work was supported by grant 314343 from CONACyT. J.M.-C. was the recipient of a scholarship from CONACyTs.

REFERENCES

1. Pan Y, Zhang D, Yang P, Poon LLM, Wang Q. 2020. Viral load of SARS-CoV-2 in clinical samples. Lancet Infect Dis 20:411–412. https://doi.org/10.1016/S1473-3099(20)30113-4.
2. Wang Y, Kang H, Liu X, Tong Z. 2020. Combination of RT-qPCR testing and clinical features for diagnosis of COVID-19 facilitates management of SARS-CoV-2 outbreak. J Med Virol 92:538–539. https://doi.org/10.1002/jmv.25721.
3. Kojima N, Turner F, Slepnev V, Bacelar A, Deming L, Kodeboyina S, Klausner JD. 2020. Self-collected oral fluid and nasal swabs demonstrate comparable sensitivity to clinician collected nasopharyngeal swabs for Covid-19 detection. medRxiv https://doi.org/10.1101/2020.04.11.20062372.
4. To KK, Tsang OT, Chik-Yan Yip C, Chan KH, Wu TC, Chan JMC, Leung WS, Chik TS, Choi CY, Kandamby DH, Lung DC, Tam AR, Poon RW, Fung AY, Hung IF, Cheng VC, Chan JF, Yuen KY. 12 February 2020. Consistent detection of 2019 novel coronavirus in saliva. Clin Infect Dis https://doi.org/10.1093/cid/ciaa149.
5. Williams E, Bond K, Zhang B, Putland M, Williamson DA. 23 July 2020. Saliva as a non-invasive specimen for detection of SARS-CoV-2. J Clin Microbiol https://doi.org/10.1128/JCM.00776-20.
6. Khurshid Z, Asiri FYI, Al Wadaani H. 2020. Human saliva: non-invasive fluid for detecting novel coronavirus (2019-nCoV). Int J Environ Res Public Health 17:2225. https://doi.org/10.3390/ijerph17072225.
7. Ng K, Poon BH, Kiat Puar TH, Shan Quah JL, Loh WJ, Wong YJ, Tan TY, Raghuram J. 2020. COVID-19 and the risk to health care workers: a case report. Ann Intern Med 172:766–767. https://doi.org/10.7326/L20-0175.
8. Corman VM, Landt O, Kaiser M, Molenkamp R, Meijer A, Chu DK, Bleicker T, Brunink S, Schneider J, Schmidt ML, Mulders DG, Haagmans BL, van der Veer B, van den Brink S, Wijsman L, Goderski G, Romette JL, Ellis J, Zambon M, Peiris M, Goossens H, Reusken C, Koopmans MP, Drosten C. 2020. Detection of 2019 novel coronavirus (2019-nCoV) by real-time RT-PCR. Euro Surveill 25:2000045. https://doi.org/10.2807/1560-7917.ES.2020.25.3.2000045.
9. Nalla AK, Casto AM, Huang MW, Perchetti GA, Sampoleo R, Shrestha L, Wei Y, Zhu H, Jerome KR, Greninger AL. 2020. Comparative performance of SARS-CoV-2 detection assays using seven different primer-probe sets and one assay kit. J Clin Microbiol 58:e00557-20. https://doi.org/10.1128/JCM.00557-20.
10. Ramirez JD, Munoz M, Hernandez C, Florez C, Gomez S, Rico A, Pardo L, Barros EC, Paniz-Mondolfi A. 2020. Genetic diversity among SARS-CoV2 strains in South America may impact performance of molecular detection. medRxiv https://doi.org/10.1101/2020.06.18.20134759.
11. Ladha A, Joung J, Abudayyeh O, Gootenberg J, Zhang F. 2020. A 5-min RNA preparation method for COVID-19 detection with RT-qPCR. medRxiv https://doi.org/10.1101/2020.05.07.20055947.
12. Wyllie AL, Fournier J, Casanovas-Massana A, Campbell M, Tokuyama M, Vijayakumar P, Geng B, Muenker MC, Moore AJ, Vogels CBF, Petrone ME, Ott IM, Lu P, Lu-Culligan A, Klein J, Venkataraman A, Earnest R, Simonov M, Datta R, Handoko R, Naushad N, Sewanan LR, Valdez J, White EB, Lapidus S, Kalinich CC, Jiang X, Kim DJ, Kudo E, Linehan M, Mao T, Moriyama M, Oh JE, Park A, Silva J, Song E, Takahashi T, Taura M, Weizman EO, Wong P, Yang Y, Bermejo S, Odio C, Omer SB, Dela Cruz CS, Farhadian S, Martinello RA, Iwasaki A, Grubaugh ND, Ko AI. 2020. Saliva is more sensitive for SARS-CoV-2 detection in COVID-19 patients than nasopharyngeal swabs. medRxiv https://doi.org/10.1101/2020.04.16.20067835.
13. Iwasaki S, Fujisawa S, Nakakubo S, Kamada K, Yamashita Y, Fukumoto T, Sato K, Oguri S, Taki K, Senjo H, Sugita J, Hayasaka K, Konno S, Nishida M, Teshima T. 2020. Comparison of SARS-CoV-2 detection in nasopharyngeal swab and saliva. J Infect https://doi.org/10.1016/j.jinf.2020.05.071.
14. To KK, Tsang OT, Leung WS, Tam AR, Wu TC, Lung DC, Yip CC, Cai JP, Chan JM, Chik TS, Lau DP, Choi CY, Chen LL, Chan WM, Chan KH, Ip JD, Ng AC, Poon RW, Luo CT, Cheng VC, Chan JF, Hung IF, Chen Z, Chen H, Yuen KY. 2020. Temporal profiles of viral load in posterior oropharyngeal saliva samples and serum antibody responses during infection by SARS-CoV-2: an observational cohort study. Lancet Infect Dis 20:565–574. https://doi.org/10.1016/S1473-3099(20)30196-1.
15. Sentmanat M, Kouranova E, Cui X. 2020. One-step RNA extraction for RT-qPCR detection of 2019-nCoV. bioRxiv https://doi.org/10.1101/2020.04.02.022384.
16. Kirkland PD, Frost MJ. 2020. The impact of viral transport media on PCR assay results for the detection of nucleic acid from SARS-CoV-2 and other viruses. bioRxiv https://doi.org/10.1101/2020.06.09.142323.
17. Hedman J, Radstrom P. 2013. Overcoming inhibition in real-time diagnostic PCR. Methods Mol Biol 943:17–48. https://doi.org/10.1007/978-1-60327-353-4_2.

Artículo publicado en la revista de divulgación Biotecnología en Movimiento:

Un método sensible, rápido y económico para detectar el SARS-CoV-2 en saliva

GENERANDO **CONOCIMIENTO EN EL IBt**

Sección a cargo de Claudia Díaz Camino (*claudia@ibt.unam.mx*)

Mediante la aplicación del método científico, investigadores y estudiantes plantean hipótesis y obtienen evidencias experimentales en cuestiones básicas y también respuestas que ayudan a entender problemas específicos en la naturaleza y alternativas para varios procesos productivos. Los resultados obtenidos en líneas y proyectos de investigación del IBt, son publicados en revistas científicas arbitradas —alrededor de 200 anualmente— para compartir los hallazgos con la comunidad académica e industrial de todo el mundo. En esta sección, se presentan resúmenes de publicaciones selectas y recientes del IBt, que permiten mostrar el panorama del trabajo académico que desarrollan investigadores, asociados, técnicos y estudiantes de nuestro instituto.

Un método sensible, rápido y económico para detectar el SARS-CoV-2 en saliva

Joaquín Moreno-Contreras y Marco A. Espinoza

Ante la emergencia mundial generada por la COVID-19 y la ausencia de un tratamiento efectivo, existe una necesidad urgente de métodos de diagnóstico rápidos y confiables que permitan identificar a las personas portadoras del virus para poder aislarlos y de esta manera romper la cadena de contagios. En el laboratorio donde realizamos nuestro trabajo experimental, hemos desarrollado y aplicado uno de ellos, el cual se ha publicado recientemente.

A finales de diciembre de 2019 en la ciudad Wuhan, provincia de Hubei, China, se reportó la presencia de una serie de casos de neumonía atípica de origen desconocido. Poco tiempo después, mediante el uso de técnicas moleculares se determinó que el agente infeccioso que estaba afectando a la población era un virus, específicamen-

te un coronavirus. Este nuevo coronavirus es similar al causante del llamado Síndrome Respiratorio Agudo Severo (SARS, por sus siglas en inglés), y presenta variaciones suficientes en su información genética como para ser considerado un virus nuevo y distinto que ha sido nombrado SARS-CoV-2. El virus SARS-CoV-2 es el causante de una variedad de afecciones, agrupadas como COVID-19, acrónimo del inglés *Coronavirus Disease* 2019 (Enfermedad por coronavirus 2019). El 11 de marzo del año en curso, la Organización Mundial de la Salud declaró a la COVID-19 como una pandemia, esto después de que se habían registrado más de 118 mil casos en 114 países alrededor del mundo.

¿De qué manera se puede diagnosticar el SARS-CoV-2?

Existen diferentes pruebas moleculares que permiten la detección del virus SAR-CoV-2: algunas identifican de manera directa ya sea a través de la presencia de alguna proteína viral y el uso de anticuerpos (pruebas antigénicas), o aquellas que detectan el genoma viral a través del reconocimiento de sus secuencias (RT-PCR). Existen otro tipo de pruebas que detectan de manera indirecta la presencia del virus, por ejemplo, mediante la detección de anticuerpos producidos como parte de la respuesta inmune de una persona que ha sido expuesta al virus (pruebas inmunológicas), éstas últimas —también referidas como pruebas serológicas o 'rápidas'— permiten evidenciar si alguna persona ya ha sido infectada previamente, haya o no presentado síntomas; pero no detectan una infección activa al realizarla. Cada una de las pruebas mencionadas presenta diferentes grados de sensibilidad, la cual depende entre otros factores, de la ventana de tiempo posterior al inicio de la aparición de síntomas y la toma de muestras. En general, la prueba más confiable para la detección de SARS-CoV-2 es la amplificación de regiones del genoma viral mediante la *reacción en cadena de la polimerasa con transcripción inversa (RT-PCR) en tiempo real* (ver "Capacidades y avances del IBt para enfrentar la pandemia de la COVID-19", en *Biotecnología en Movimiento* No. 21).

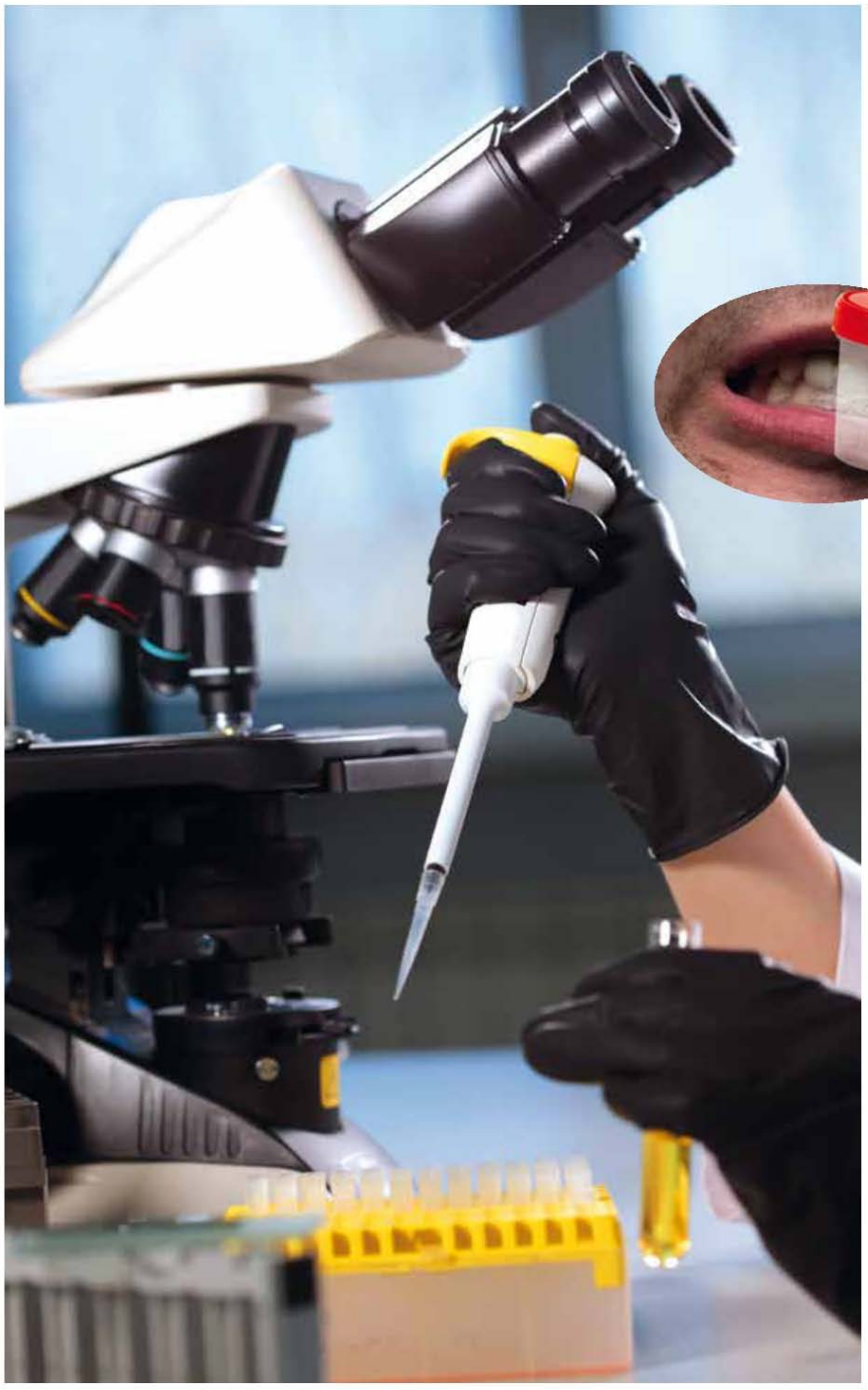

De el total de muestras positivas a SARS-CoV-2, el 86% fue detectado en salivas, mientras que en muestras de un solo hisopo solo el 65% fue positivo

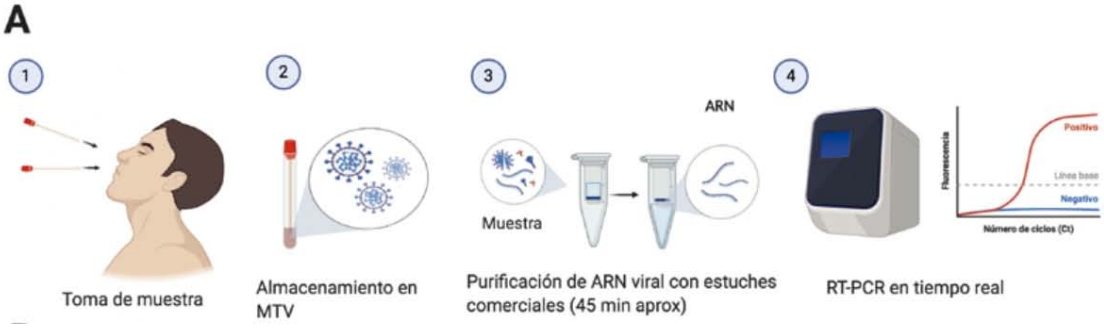

Figura 1. Diagnóstico de SARS-CoV-2 en muestras biológicas obtenidas de: (A) hisopos y (B) saliva. MTV: Medio de transporte viral, RT-PCR: reacción en cadena de la polimerasa con transcripción inversa en tiempo real. Los resultados de la prueba se muestran en las gráficas de las señales que emite el equipo utilizado para este proceso (derecha).

¿Cómo se lleva a cabo el diagnóstico molecular de SARS-CoV-2?

En esta revista se ha relatado sobre varias capacidades y actividades del IBt-UNAM, y del laboratorio de la Dra. Susana López y del Dr. Carlos Arias, para contender con la pandemia a través de la realización de pruebas diagnósticas formales y su optimización; aquí explicamos un método alternativo desarrollado y evaluado en nuestro instituto. Para llevar a cabo el diagnóstico molecular se requiere de la obtención de una muestra biológica, para lo cual se emplean dos hisopos para tomar muestras de la mucosa faríngea: uno a través de la boca (orofaríngeo) y el otro por nariz (nasofaríngeo). Los hisopos utilizados deben de ser de materiales sintéticos como el *rayón* o *dacrón*, ya que las fibras naturales como el algodón pueden afectar la reacción de la RT-PCR. Este paso debe de ser realizado por personal de salud capacitado, el cual utiliza Equipo de Protección Personal (EPP) especial, ya que al ser un procedimiento invasivo, en muchas ocasiones los pacientes tosen o estornudan, por lo que el uso de EPP adecuado (careta y/o anteojos, cubrebocas y/o mascarillas, guantes y bata quirúrgica), minimiza el riesgo de contagio para estas personas. Posteriormente, los dos hisopos son colocados en un tubo que contiene un Medio de Transporte Viral (MTV), con componentes que preservan la integridad de la muestra evitando su degradación y/o contaminación. El siguiente paso, ya en el laboratorio bajo medidas de bioseguridad, es la extracción del ácido ribonucleico (ARN) del virus a partir del MTV, para lo que se emplean estuches comerciales (*kits* de extracción). El ARN obtenido es utilizado como templado o plantilla en la reacción de la RT-PCR en tiempo real, en la cual mediante el uso de iniciadores y probadores moleculares específicos, se detecta la presencia o ausencia del virus [Figura 1.A]. Debido a la enorme demanda de los insumos necesarios para realizar la toma de muestras biológicas, así como para la extracción del ARN viral, ha habido escasez de muchos de los reactivos utilizados para las pruebas diagnósticas. Tanto los hisopos, el MTV, los estuches de extracción de ARN viral y el EPP se encuentran entre los insumos más difíciles de obtener, lo cual ha comprometido el número de pruebas que se pueden realizar en muchas partes del mundo.

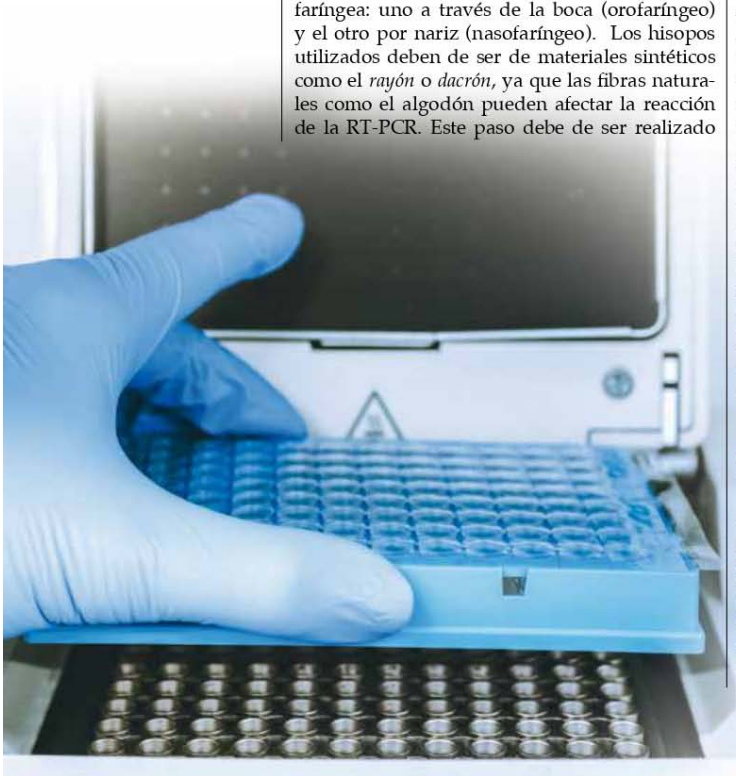

¿Cómo podemos mejorar el diagnóstico molecular de SARS-CoV-2?

En este trabajo evaluamos la detección de SARS-CoV-2 en saliva, comparando la eficiencia de detección del ARN viral entre muestras de un hisopado y la saliva del mismo paciente. Para esto, evaluamos un protocolo de extracción (lisis) directa como un método para obtener el ARN viral, sustituyendo los estuches comerciales; ade-

más, redujimos el tiempo de procesamiento de las muestras de aproximadamente 45 minutos, a solo 5 minutos por muestra. En reportes previos al nuestro, se había demostrado la factibilidad de usar saliva para el diagnóstico de varios virus, incluido SARS-CoV-2 [1]. El uso de saliva en lugar de hisopados orales o nasales para la detección del genoma de SARS-CoV-2 tiene múltiples ventajas: la toma de muestra la realiza el mismo individuo, es decir es una 'auto-toma'; esto reduce de manera considerable el riesgo de infección del personal de salud encargado de realizar dicho proceso y también, por no ser un proceso invasivo, no requiere usar EPP, que ha escaseado debido a la pandemia. Entonces, para obtener la muestra biológica se pide al paciente que concentre la saliva en la boca durante al menos dos minutos; posteriormente la saliva es depositada en un vaso para muestras clínicas, escupiendo repetidamente hasta alcanzar un volumen de alrededor de 2 a 3 mL. Las muestras son almacenadas en refrigeración (4ºC) hasta su procesamiento. Como alternativa al uso de estuches comerciales, el ARN viral presente en la muestra de saliva, se extrae utilizando una 'solución amortiguadora' a los cambios del pH (llamada solución *buffer* de lisis), que contiene enzimas que degradan proteínas (proteasas) y detergentes en solución. Al final, el ARN aislado se analiza directamente mediante la prueba RT-PCR en tiempo real, usando los mismos reactivos (iniciadores, probadores moleculares y enzimas), que para la muestra obtenida con hisopo [Figura 1.B].

¿Qué tan ventajoso es este método diagnóstico?

Para validar este método, se analizaron 253 muestras en pares de hisopados y saliva tomados del mismo paciente. La toma de muestras fue realizada por personal de la Secretaría de Salud del Estado de Morelos (SSEM) y del Laboratorio Estatal de Salud Pública Morelos (LESP). Es importante notar que, durante el período en el que se realizó el estudio, hubo gran escasez de los hisopos utilizados para realizar la toma de muestras nasofaríngeas, por lo que en este período solo se tomaron muestras de hisopado orofaríngeo. Para comparar las pruebas, las muestras de hisopados fueron procesadas utilizando estuches comerciales de extracción, mientras que las salivas se trataron directamente con la solución *buffer* de lisis y, como se mencionó, se analizó posteriormente la presencia o ausencia de SARS-CoV-2 mediante RT-PCR en tiempo real en ambos grupos. A partir de este análisis, queríamos determinar la efectividad que tiene la saliva para ser utilizada como un medio de detección, en lugar de hisopados, y encontramos que de el total de muestras positivas a SARS-CoV-2, el 86% fue detectado en salivas, mientras que en muestras de un solo hisopo solo el 65% fue positivo; por otra parte, las muestras negativas fueron similares en ambas pruebas. Este resultado nos ha permitido publicar un artículo científico [2], para proponer que la saliva es una alternativa al uso de hisopos, que representa ventajas por su sensibilidad, rapidez y accesibilidad. Además, al no requerirse hisopos especiales, ni MTV, ni estuches de extracción de ARN, el tiempo de procesamiento por muestra se reduce en alrededor del 80%, mientras que el costo disminuye aproximadamente 40%. Esto permite incrementar al doble la capacidad diagnóstica del laboratorio, lo que reduce el tiempo de espera de los resultados.

Ante el desconfinamiento e incremento gradual de actividades en espacios públicos, laborales y escolares, lograr un aumento de la cantidad de pruebas diagnósticas realizables —utilizando muestras de saliva como sustrato para su detección— podría ser de vital importancia para detectar, rastrear y/o aislar a las personas infectadas, frenando la cadena de contagios para evitar la propagación continua del nuevo coronavirus.

Contacto: *mcj@ibt.unam.mx*

Referencias

1. To, KK, OT Tsang, CC Yip, et al. (2020), Consistent Detection of 2019 Novel Coronavirus in Saliva, *Clin Infect Dis*, **71** (15): 841-843. *doi:10.1093/cid/ciaa149*

2. Moreno-Contreras J, MA Espinoza, C Sandoval-Jaime, MA Cantú-Cuevas, H Barón-Olivares, OD Ortiz-Orozco, AV, Muñoz-Rangel, M Hernández-de la Cruz, CM Eroza-Osorio, CF Arias, S López (2020), Saliva Sampling and Its Direct Lysis, an Excellent Option To Increase the Number of SARS-CoV-2 Diagnostic Tests in Settings with Supply Shortages, *J Clin Microbiol* **58**:10 e01659-20, *doi:10.1128/JCM.01659-20*

El M.C. Joaquín Moreno-Contreras es estudiante del Doctorado en Ciencias Bioquímicas; el M.C. Marco A. Espinoza es técnico académico en el grupo de la Dra. Susana López, todos en el Departamento de Genética del Desarrollo y Fisiología Molecular del IBt.

DETECCIÓN DE SARS-COV-2 EN POOLS DE MUESTRAS DE SALIVA

Ante el desconfinamiento e incremento gradual de las actividades en espacios públicos, laborales y escolares, lograr aumentar la cantidad de pruebas diagnosticas realizables utilizando muestras de saliva para su detección es de vital importancia para detectar, rastrear y/o aislar a las personas infectadas, frenando la cadena de contagios para evitar la propagación de SARS-CoV-2. Después de demostrar que la lisis directa de saliva puede ser empleada para obtener RNA y detectar el genoma de SARS-CoV-2 y que es tan eficiente como los métodos en los que se emplean kits de extracción(81), decidimos evaluar la posibilidad de realizar la detección de SARS-CoV-2 en pools de muestras de saliva. Los pools de muestras clínicas han sido empleados en el diagnóstico de otros virus; si un pool es negativo, todas las muestras se consideran negativas mientras que, si un pool es positivo, las muestras son evaluadas individualmente(82)(83). Esta estrategia permite diagnosticar un gran número de muestras de manera eficiente a un costo reducido. En nuestro estudio, evaluamos 1,086 muestras de salivas de pacientes ambulatorios en pools de cinco o diez muestras. Lo primero que realizamos fue evaluar la detección de muestras positivas, con un valor de C_T conocido, mezcladas con 4 o 9 muestras negativas. El RNA de estos pools fue obtenido empleando el método de lisis directa y posteriormente se utilizó en la reacción de RT-qPCR. Después, comparamos los valores de C_T obtenidos en los pools con el valor de C_T de la muestra individual. En este estudio encontramos que la sensibilidad del método es menor cuando se analizan pools de 10 muestras, mientras que en los pools de 5 muestras la sensibilidad no es afectada de manera significativa. Los

resultados de este estudio fueron publicados en el artículo “Pooling saliva samples as an excellent option to increase the surveillance for SARS-CoV-2 when re-opening community settings”.

Artículo publicado en la revista PLoS One:

Pooling saliva samples as an excellent option to increase the surveillance for SARS-CoV-2 when re-opening community settings

PLOS ONE

RESEARCH ARTICLE

Pooling saliva samples as an excellent option to increase the surveillance for SARS-CoV-2 when re-opening community settings

Joaquín Moreno-Contreras[1], Marco A. Espinoza[1], Carlos Sandoval-Jaime[1], Marco A. Cantú-Cuevas[2], Daniel A. Madrid-González[2], Héctor Barón-Olivares[3], Oscar D. Ortiz-Orozco[3], Asunción V. Muñoz-Rangel[3], Cecilia Guzmán-Rodríguez[3], Manuel Hernández-de la Cruz[3], César M. Eroza-Osorio[3], Carlos F. Arias[1], Susana López[1]*

1 Departamento de Genética del Desarrollo y Fisiología Molecular, Instituto de Biotecnología UNAM, Cuernavaca, Morelos, México, **2** Secretaría de Salud del Edo. de Morelos, Cuernavaca, Morelos, México, **3** Servicios de Salud del Edo. de Morelos, Cuernavaca, Morelos, México

* susana@ibt.unam.mx

OPEN ACCESS

Citation: Moreno-Contreras J, Espinoza MA, Sandoval-Jaime C, Cantú-Cuevas MA, Madrid-González DA, Barón-Olivares H, et al. (2022) Pooling saliva samples as an excellent option to increase the surveillance for SARS-CoV-2 when re-opening community settings. PLoS ONE 17(1): e0263114. https://doi.org/10.1371/journal.pone.0263114

Editor: Purvi Purohit, All India Institute of Medical Sciences, INDIA

Received: June 30, 2021

Accepted: January 13, 2022

Published: January 25, 2022

Peer Review History: PLOS recognizes the benefits of transparency in the peer review process; therefore, we enable the publication of all of the content of peer review and author responses alongside final, published articles. The editorial history of this article is available here: https://doi.org/10.1371/journal.pone.0263114

Data Availability Statement: All relevant data are within the paper.

Abstract

In many countries a second wave of infections caused by the severe acute respiratory syndrome coronavirus 2 (SARS-CoV-2) has occurred, triggering a shortage of reagents needed for diagnosis and compromising the capacity of laboratory testing. There is an urgent need to develop methods to accelerate the diagnostic procedures. Pooling samples represents a strategy to overcome the shortage of reagents, since several samples can be tested using one reaction, significantly increasing the number and speed with which tests can be carried out. We have reported the feasibility to use a direct lysis procedure of saliva as source for RNA to SARS-CoV-2 genome detection by reverse transcription quantitative-PCR (RT-qPCR). Here, we show that the direct lysis of saliva pools, of either five or ten samples, does not compromise the detection of viral RNA. In addition, it is a sensitive, fast, and inexpensive method that can be used for massive screening, especially considering the proximity of the reincorporation of activities in universities, offices, and schools.

Introduction

After more than one year of the COVID-19 global health emergency, the early detection of severe acute respiratory syndrome coronavirus 2 (SARS-CoV-2) remains a key factor to decrease community virus spreading. Although several antigenic and immunologic assays have been developed, the amplification of specific regions of the viral genome by reverse transcription quantitative-PCR (RT-qPCR) in nasopharyngeal swabs (NPS) remains the golden standard for SARS-CoV-2 diagnosis [1–3]. However, due to the pandemic there has been a shortage of reagents used for testing, including swabs, viral transport medium, and kits for viral RNA extraction, limiting test capabilities in many countries with an active viral propagation.

Recently, we demonstrated that a direct lysis procedure to prepare RNA from saliva samples is a feasible method to detect the SARS-CoV-2 genome, and as efficient as column-based

Funding: Part of the reagents used in this study were provided by the Instituto Nacional de Diagnóstico y Referencia Epidemiológica, supported by INSABI. This work was supported by grant 314343 from CONACyT to SL. JMC was a recipient of a scholarship from CONACyT. The funders had no role in study design, data collection and analysis, decision to publish, or preparation of the manuscript.

Competing interests: The authors have declared that no competing interests exist.

methods, with a significant reduction in costs and time of sample processing [4]. Saliva is a clinical specimen that has been approved for emergency use by the Food and Drug Administration (FDA) for SARS-CoV-2 diagnosis; since it can be self-collected, there is a reduced risk of healthcare workers involved in sampling, making it a good candidate to increase the amount of tests performed in regions with shortages of personal protection equipment (PPE) supplies [5,6]. Pooling of samples has been implemented as a diagnostic tool for other viruses; if a pool is negative, all samples are considered to be below the limit of detection of the test, whereas when a pool is positive, the samples are evaluated individually. This strategy allows to test large number of samples more efficiently and with a reduced cost. For SARS-CoV-2 detection, pooling of samples has been evaluated using NPS and oropharyngeal swabs (OPS), as well as saliva samples, allowing to save reagents, increasing the amount of tests performed and reducing costs, especially in regions with a low prevalence of the virus [7–10]. Even though pooling offers some advantages, sensitivity can be compromised by several factors, including pool size, amount of sample analyzed, and RNA extraction. In this study, we evaluated 1,086 saliva specimens of ambulatory patients in pools of five or ten samples by RT-qPCR. Initially, positive individual samples with a known C_T value were mixed with either 4 or 9 negative samples, and the RNA in the pools was obtained by a lysis protocol as previously reported [4], and used directly for the RT-qPCR test. The C_T value obtained for each pool was compared with that of the positive sample used in the pool. We found that the sensitivity decreased in pools of ten samples, while in pools of five samples the sensitivity was not significantly affected. We propose that saliva pooling and its direct lysis is a good method to detect SARS-CoV-2 that will help to increase the amount of tests performed and accelerate diagnosis at a reduced cost, particularly now, that several public spaces and schools are reopening.

Materials and methods

Sample collection

1,086 saliva samples were collected from August 7th to October 30th 2020 by healthcare workers from the Epidemiology Department of the Health Ministry of the State of Morelos (Secretaría de Salud Morelos, SSM). All samples were taken from ambulatory patients as part of the government program "Pruebas COVID-19 en tu comunidad", aiming to bring SARS-CoV-2 tests into communities located far apart from Cuernavaca, the capital city.

Saliva collection

Saliva was self-collected as previously described [4]. Briefly, patients were asked to spit 2–3 ml of saliva into sterile urine cup containers containing 1 ml of viral transport medium (MTV). After collection, samples were stored and kept at 4˚C until transported to the Instituto de Biotecnología/UNAM (IBT/UNAM) for their analysis, within the next 24–48 h after sample collection.

Saliva pooling, RNA extraction and RT-qPCR

Five or ten saliva samples were pooled by mixing 50 μl of each sample reaching a final volume of 250 or 500 μl, respectively. Pools were mixed homogeneously by pipetting several times and kept at room temperature (RT) until processing. Saliva pools or individual samples were either treated with Quick Extract^{TM} DNA Extraction Solution (QE; Lucigen) by mixing 50 μl of saliva samples with 50 μl of the QE reagent, as reported [4], or with 15 μl of Proteinase K (20 mg/ml, Invitrogen) when using the SalivaDirect protocol [11]. The mixtures were heated for 5 min at 95˚C; and then cooled on ice and kept at 4˚C until use (within 1 h of QE, or proteinase K treatment).

SARS-CoV-2 detection was performed using the Berlin protocol, using the reported oligonucleotides and probes for viral gene E and for human RNase P [12]. The RT-qPCRs were performed using the StartQ one-step RT-qPCR (Genes2 life) kit, using 2.5 μl of the QE- treated saliva in 22.5 μl of RT-qPCR reaction mixture, or 5 μl of proteinase K-treated saliva in 20 μl of RT-qPCR reaction mixture. Samples were analyzed in an ABI 7500 sequence detector system (Applied Biosystem) with the following thermal protocol: 50˚C for 15 min, 95˚C for 2 min and then 45 cycles of 95˚C for 15 s and 60˚C for 30 s. Individual and pools of five samples with a threshold cycle (C_T) equal to or less than 38 were classified as positive. Pools of ten samples with a C_T equal to or less than 41 were classified as positive. The change of C_T between pooled and unpooled samples was calculated by subtracting the C_T of viral gene E in the pool from the C_T of the individual unpooled sample ($C_{T\ change} = C_{T\ pool}$-$C_{T\ unpooled}$). In pools with more than one positive sample, the highest C_T value of the individual unpooled sample was taken.

Statistical analysis

Statistical analysis was performed using GraphPad Prism 6.0 (GraphPad Software Inc.) as described in Results.

Ethical considerations

The protocol used in this study was conducted under the ethical principles and approval of the Bioethics Committee of the Instituto de Biotecnología (Project # 393) of the National University of Mexico (UNAM). Verbal informed consent was obtained from all individuals enrolled in this study and was witnessed by personnel of the Health Ministry of the State of Morelos, who were in charge of collecting the samples.

Results

Effect of saliva sample pooling on the sensitivity of the assay

To evaluate the effect of pooling samples on the C_T value for detection of SARS-CoV-2, positive saliva samples with different C_T values (ranging from 24.2 to 37) for viral gene E were mixed either with four, or nine virus-negative saliva samples. Equal amounts of each sample were homogenously mixed to prepare the pools, and the RNA was directly obtained from a 50 μl aliquot of the pooled samples using the QE lysis buffer (Lucigen) and boiling for 5 min, as reported [13].

A slight decrease in the C_T value of the positive saliva samples was observed when it was determined in the context of the pools of five samples, with a mean change in C_T of 1.7 units (95% C.I: 0.8, 2.6, lineal regression, R^2:0.9388, $p<0.0001$). In the pools of ten samples the C_T value decreased in average 2.6 units (95% C.I: 1.7, 3.5, lineal regression, $R^2 = 0.9214$, $p<0.0001$). In the five-sample pools, 100% (10/10) of the positive samples were detected, while in the pools of ten samples, a sample with a $C_T = 37$ was not detected (Fig 1A). As a control, negative saliva samples were tested in pools of five or ten.

Evaluation of saliva sample pools from ambulatory patients

To evaluate saliva pooling and its direct lysis as a diagnostic tool, the presence of SARS-CoV-2 genome was determined in 1,075 saliva specimens from patients having two or more symptoms related to COVID-19 [14,15]. Samples were collected from ambulatory patients on eleven mobile medical units in 89 locations that belong to the Jurisdicción Sanitaria N.2 in Morelos, México. The presence or absence of SARS-CoV-2 genome was detected by RT-qPCR, as

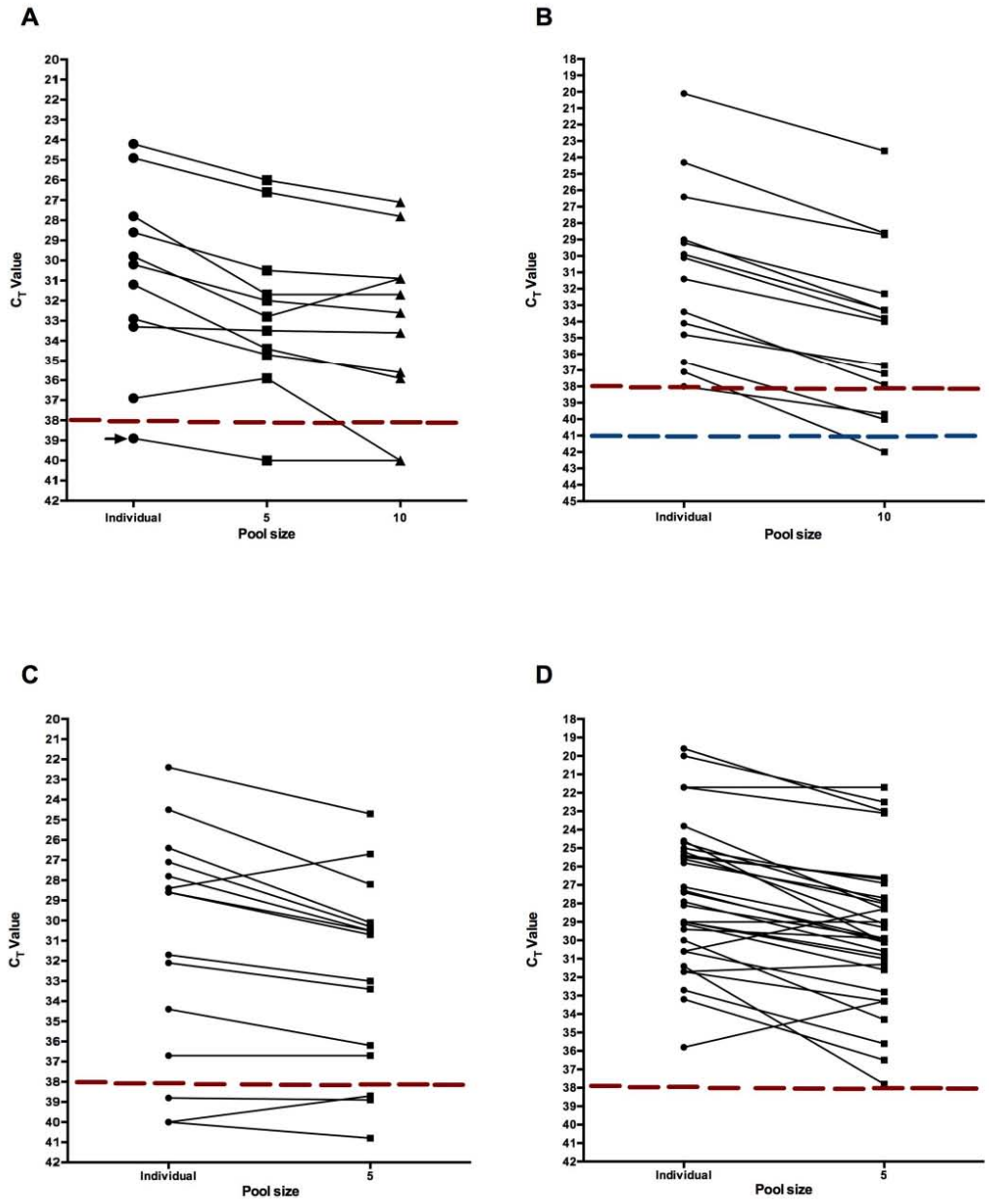

Fig 1. Detection of SARS-CoV-2 in pools of five and ten saliva samples. A) SARS-CoV-2 positive saliva samples were mixed with either four or nine negative samples. The C_T value of the individual samples was compared to that obtained in the pooled samples; the mean change of C_T was +1.7 (95% C.I:

0.8, 2.6, lineal regression, R^2:0.9388, $p<0.0001$), and +2.6 (95% C.I: 1.7, 3.5, lineal regression, $R^2 = 0.9214$, $p<0.0001$) units for pools of 5 and 10, respectively. RNA was obtained from pools of ten (B) or five (C) previously undiagnosed patient saliva samples using QE lysis buffer; positive pools were analyzed as individual samples (C_T mean change for pool of ten, +3.2 C_T, 95% C.I: 2.7, 3.9; pool of five +1.8 C_T, 95% C.I: 0.5, 2.3). D) As an alternative method of RNA extraction, pools of five undiagnosed saliva samples were treated with proteinase K, and positive pools were analyzed individually (C_T mean change + 2.2 C_T, 95% C.I: 1.4, 2.7). In all figures, the C_T value of the viral gene E obtained in individual, or pools of five or ten saliva specimens are represented by lines connecting each condition. Dotted red lines represent C_T cut-off value = 38; for pools of ten samples this value is represented by blue dotted lines, with a C_T cut-off value = 41. Negative control in panel A is shown with an arrow.

https://doi.org/10.1371/journal.pone.0263114.g001

described in the Materials and Methods section. Positive pools were deconvoluted and analyzed as individual samples.

From the total saliva specimens collected, 260 were analyzed in pools of ten; 12 of the 26 pools resulted negative, having a C_T value equal or higher than 41. Since we had previously observed that pooling 10 samples decreased the C_T value by approx. 2.7 units, pools with a $C_T <= 41$, in which a smooth sigmoidal amplification curve was additionally obtained, were taken as positive. Amplification of the viral gene E was detected in the remaining 14 pools, and individual saliva samples were then tested from these pools. Seven pools contained one positive sample, two pools contained two positive samples, four pools contained 3 positive samples, and 1 pool contained 4 positive samples. Comparing the C_T value of the pools with that obtained with individual samples, the mean change of C_T was +3.2 (95% C.I: 2.7, 3.9, Fig 1B).

Subsequently, 235 saliva samples were analyzed in pools of 5; 32 of the 47 pools analyzed were negative. Of the 15 positive pools, 10 had one positive sample, and 5 contained 2 positive samples. When the C_T of the individual samples was compared to that obtained in the pooled samples, the mean difference of C_T was +1.8 units (95% C.I: 0.5, 2.3, Fig 1C).

To test an alternative method of RNA extraction that has been recently described for this purpose [11], 580 saliva specimens grouped in 116 pools of 5 samples were treated with proteinase K and boiled for 5 min, as described [11]. In this assay, we found 84-negative, pools, and the remaining 32 pools were positive. When these pools were analyzed individually, 23 pools contained one positive sample, 6 had 2 positive samples and 3 contained 3 positive samples. Comparing the C_T values of the pools with those obtained with individual samples, the mean change was +2.2 C_T units (95% C.I: 1.4, 2.7, Fig 1D). When the change in C_T values obtained with the QE buffer or proteinase K treatments were compared, no significant differences were found. Accordingly, when the samples in pools of 5 with a C_T value between 38.8 and 41 were analyzed individually, a $C_T > 38$ was found in the samples (Fig 1C).

Using the strategy of saliva pooling, samples with a C_T value close to the cut-off (>35) could be lost; however, an analysis of the distribution of the C_T values obtained from 436 positive samples detected in our laboratory, showed that less than 8.5% of the samples analyzed had a $C_T > 35$ (6% had a $C_T = 37$, and 2.5% had a $C_T = 38$), while the majority of the samples analyzed (66.9%) had C_T values between 26 and 35 (Fig 2).

As part of the re-opening activities of our Institute (Instituto de Biotecnología), asymptomatic students and workers were tested for SARS-COV-2 in a pilot study from the 4th to the 15th of January, prior to their incorporation to work, using pooled saliva specimens. For this, 910 saliva samples were analyzed in 182 pools of five samples each and RNA was obtained by QE-direct lysis. We detected 177-negative, and 5-positive pools, allowing the detection of 6 positive samples (representing a positivity of 0.6%). This enabled the isolation the of positive individuals, preventing the spread of the virus in our community. Additionally, using this protocol 77.9% of reactions were saved.

Discussion

Vaccines against SARS-CoV-2 are a key factor to control viral transmission, but even though several programs of vaccination are being implemented around the world, their cost,

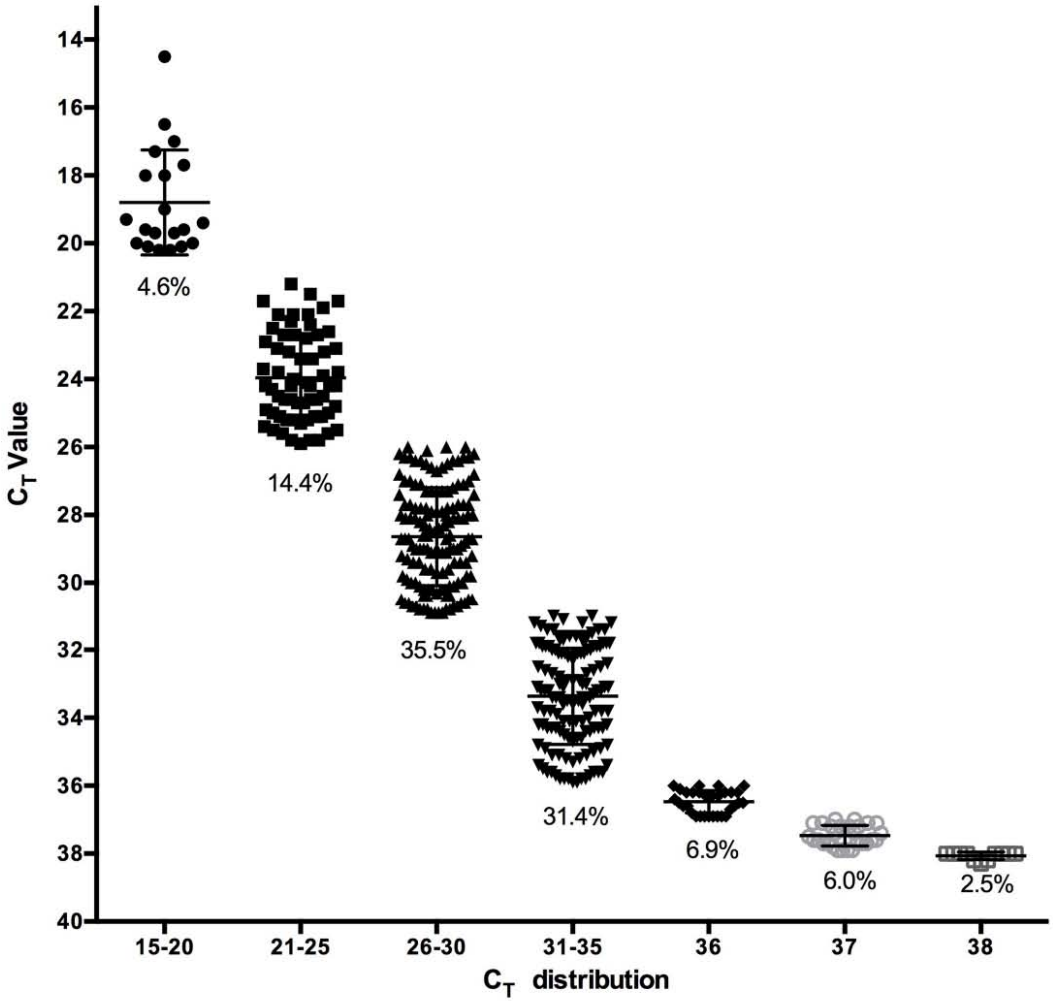

Fig 2. Distribution of C_T values in positive samples. C_T value of viral gene E from 436 positive samples are represented in intervals of five C_Ts, with exception of C_T = 36, 37 and 38. The percentage from the total number of samples analyzed is indicated in the figure.

https://doi.org/10.1371/journal.pone.0263114.g002

availability, and distribution are a bottleneck, especially for developing countries. As long as susceptible populations are not covered by vaccination, detection of infected people needs to be continued to prevent spreading of the virus. Saliva pooling represents a viable strategy to increase testing capabilities with a reduced cost, and unlike antigen tests, the specificity and sensibility are not compromised. In our study, when using pools of ten samples 36.1% of reactions were saved, while 51.1% of reactions were saved in pools of five samples (Table 1). These results were obtained from symptomatic patients with a positivity of 9.5%, however in

Table 1. Summary of results obtained from pools of five and ten saliva samples from patients suspected to have COVID-19.

Pooled samples						
Pool Size	**Extraction Reagent**	**Samples (#)**	**Negative pools**	**Positive pools**	**Reactions used**	**Saved reactions**
5	QE/Proteinase K	815	116	47	398	417 (51.1%)
10	QE	260	12	14	166	94(36.1%)
	Total	1,075				

QE, Quick Extract™ DNA Extraction Solution; #, number.

https://doi.org/10.1371/journal.pone.0263114.t001

populations with a positivity < = 1% a reduction of approximately 80% in the cost of the assays is expected [16].

Saliva is a good specimen for SARS-CoV-2 detection in symptomatic and asymptomatic patients [17]. Sample pooling has been implemented to diagnose viruses like HIV, and influenza, among others [18,19]; this strategy allows to screen the prevalence of different infections in large populations, decreasing diagnostic costs and saving supplies. Detection of SARS-CoV-2 in pools has been characterized using viral RNA obtained from either NPS or OPS, or in combination; saliva samples have also been used. Different strategies for pooling have been tested, including pooling RNAs extracted from individual samples, or pooling the samples before RNA extraction [9,20,21]. In either case, column-based, commercial RNA purification kits have been used. In this work, we showed the feasibility of obtaining good quality RNA from pooled samples by a direct lysis protocol using either the QE buffer (Lucigen) or a proteinase K treatment [11], reducing time and costs of sample processing.

An important factor to consider is the number of samples to pool, which depends on the prevalence of SARS-CoV-2 in the population to study [16]. Different programs to calculate the optimal pool size have been reported [16,22], but the number of infected individuals detected in a short period of time previous to the sampling is a key factor to determine the appropriate pool size. Pools of 32, 20, 15, 10 and 5 samples have been used [20], however, pools of 5 and 10 specimens seem to affect minimally the C_T value of a single positive sample in the pool; the maximum change detected in these assays was an increase of 3 C_T units [10]. In this study, we found C_T changes of ~2 units for five-sample pools, in accordance with previous studies [9,23]. Problems in the detection of samples with C_T values higher that 35 have been reported for ten-sample pools [23,24], however, here we found that our method allowed to detect positive samples with C_T values equal or higher than 35.

It is interesting to note that when a correlation between viral load (expressed as C_T) and infectiousness (as determined by cell-culture of the samples) has been studied, it has been found that detection of SARS-CoV-2 in cell culture decreases to 20% for samples with $C_T >$ 30, and to 3% for $C_T = 35$, suggesting that positive patients with values of $C_T > 35$ have a very low viral load, and most probably are not infectious [25].

When a ten-fold dilution of a positive viral control used in our assays was evaluated by RT-qPCR, an increase of approximately 3.3 C_T units was observed compared to the undiluted control, as expected [26]; thus, we propose to rise the C_T cut-off value (from 38 to 41) when pools of ten samples are analyzed, to increase the detection of samples with C_T values = > 35.

Saliva sampling is a noninvasive method with several advantages for patients and health care workers compared with NPS and OPS, and suitable for the screening of healthy individuals [8,17]. Several studies have compared the efficiency of detection of SARS-CoV-2 in saliva versus OPS and NPS and it is clear that saliva samples contain similar levels of SARS-CoV-2 genome copies as those found in NPS, and perform better than OPS [4,27,28]. In conclusion, saliva pooling and its direct lysis of the samples offers a sensitive, fast, and inexpensive method

for massive screening in the gradual de-escalation of lockdown, especially in the reincorporation of activities in universities, offices, and schools.

Acknowledgments

We are grateful to the healthcare workers of Servicios Estatales de Salud de Morelos for their invaluable help in collecting the samples, and to the personnel of the Laboratorio Estatal de Salud Pública del Estado de Morelos, for their support in the preparation and transporting of the samples. The work of P. Gaytán, E. López and J. Yañez from the DNA sequencing and synthesis unit is also acknowledged.

Author Contributions

Conceptualization: Joaquín Moreno-Contreras, Carlos F. Arias, Susana López.

Formal analysis: Carlos F. Arias.

Investigation: Joaquín Moreno-Contreras, Marco A. Espinoza, Carlos F. Arias.

Methodology: Joaquín Moreno-Contreras, Marco A. Espinoza, Carlos Sandoval-Jaime, Manuel Hernández-de la Cruz.

Resources: Carlos Sandoval-Jaime, Marco A. Cantú-Cuevas, Daniel A. Madrid-González, Héctor Barón-Olivares, Oscar D. Ortiz-Orozco, Asunción V. Muñoz-Rangel, Cecilia Guzmán-Rodríguez, Manuel Hernández-de la Cruz, César M. Eroza-Osorio.

Supervision: Héctor Barón-Olivares, Asunción V. Muñoz-Rangel, Cecilia Guzmán-Rodríguez, César M. Eroza-Osorio, Susana López.

Validation: Marco A. Cantú-Cuevas, Daniel A. Madrid-González, Susana López.

Writing – original draft: Joaquín Moreno-Contreras, Susana López.

Writing – review & editing: Carlos F. Arias, Susana López.

References

1. WHO. Laboratory testing strategy recommendations for COVID-19. World Heal Organ. 2020; (March):1–5.
2. Pan Y, Zhang D, Yang P, Poon LLM, Wang Q. Viral load of SARS-CoV-2 in clinical samples. Lancet Infect Dis. 2020; 20(4):411–2. https://doi.org/10.1016/S1473-3099(20)30113-4 PMID: 32105638
3. Kevadiya BD, Machhi J, Herskovitz J, Oleynikov MD, Blomberg WR, Bajwa N, et al. Diagnostics for SARS-CoV-2 infections. Nat Mater. 2021; 20(5):593–605. https://doi.org/10.1038/s41563-020-00906-z PMID: 33589798
4. Moreno-Contreras J, Espinoza MA, Sandoval-Jaime C, Cantú-Cuevas MA, Barón-Olivares H, Ortiz-Orozco OD, et al. Saliva sampling and its direct lysis, an excellent option to increase the number of SARS-CoV-2 diagnostic tests in settings with supply shortages. J Clin Microbiol. 2020; 58(10):1–6. https://doi.org/10.1128/JCM.01659-20 PMID: 32703816
5. Khurshid Z, Asiri FYI, Al Wadaani H. Human saliva: Non-invasive fluid for detecting novel coronavirus (2019-nCoV). Int J Environ Res Public Health. 2020; 17(7):17–20.
6. Ng K, Poon BH, Kiat Puar TH, Shan Quah JL, Loh WJ, Wong YJ, et al. COVID-19 and the Risk to Health Care Workers: A Case Report. Ann Intern Med. 2020; 172(11):766–7. https://doi.org/10.7326/L20-0175 PMID: 32176257
7. Hogan CA, Sahoo MK, Pinsky BA. Sample Pooling as a Strategy to Detect Community Transmission of SARS-CoV-2. JAMA. 2020 May 19; 323(19):1967–9. https://doi.org/10.1001/jama.2020.5445 PMID: 32250394
8. Denny TN, Andrews L, Bonsignori M, Cavanaugh K, Datto MB, Deckard A, et al. Implementation of a Pooled Surveillance Testing Program for Asymptomatic SARS-CoV-2 Infections on a College Campus

—Duke University, Durham, North Carolina, August 2–October 11, 2020. MMWR Morb Mortal Wkly Rep. 2020; 69(46):1743–7. https://doi.org/10.15585/mmwr.mm6946e1 PMID: 33211678

9. Watkins AE, Fenichel EP, Weinberger DM, Vogels CBF, Brackney DE, Casanovas-Massana A, et al. Increased SARS-CoV-2 testing capacity with pooled saliva samples. Emerg Infect Dis. 2021; 27 (4):1184–7. https://doi.org/10.3201/eid2704.204200 PMID: 33755009
10. Abdalhamid B, Bilder CR, McCutchen EL, Hinrichs SH, Koepsell SA, Iwen PC. Assessment of specimen pooling to conserve SARS CoV-2 testing resources. Am J Clin Pathol. 2020; 153(6):715–8. https://doi.org/10.1093/ajcp/aqaa064 PMID: 32304208
11. Vogels CBF, Watkins AE, Harden CA, Brackney DE, Shafer J, Wang J, et al. SalivaDirect: A simplified and flexible platform to enhance SARS-CoV-2 testing capacity. Med. 2021; 2(3):263–280.e6. https://doi.org/10.1016/j.medj.2020.12.010 PMID: 33521748
12. Corman VM, Landt O, Kaiser M, Molenkamp R, Meijer A, Chu DKW, et al. Detection of 2019 novel coronavirus (2019-nCoV) by real-time RT-PCR. Eurosurveillance. 2020; 25(3).
13. Ladha A, Joung J, Abudayyeh OO, Gootenberg JS, Zhang F. A 5-min RNA preparation method for COVID-19 detection with RT-qPCR. Medrxiv. 2020;1–3.
14. Wang D, Hu B, Hu C, Zhu F, Liu X, Zhang J, et al. Clinical Characteristics of 138 Hospitalized Patients with 2019 Novel Coronavirus-Infected Pneumonia in Wuhan, China. JAMA—J Am Med Assoc. 2020; 323(11):1061–9. https://doi.org/10.1001/jama.2020.1585 PMID: 32031570
15. Chang T, Wu J, Chang L. Clinical features of patients infected with 2019 novel coronavirus in Wuhan, China. J Formos Med Assoc. 2020;(January):19–21. https://doi.org/10.1183/13993003.00544-2020 PMID: 32366488
16. Lyng GD, Sheils NE, Kennedy CJ, Griffin DO, Berke EM. Identifying optimal COVID-19 testing strategies for schools and businesses: Balancing testing frequency, individual test technology, and cost. PLoS One. 2021; 16(3 March):1–13.
17. Yokota I, Shane PY, Okada K, Unoki Y, Yang Y, Inao T, et al. Mass screening of asymptomatic persons for SARS-CoV-2 using saliva. Clin Infect Dis. 2020 Sep 25.
18. Morandi P-A, Schockmel GA, Yerly S, Burgisser P, Erb P, Matter L, et al. Detection of Human Immunodeficiency Virus Type 1 (HIV-1) RNA in Pools of Sera Negative for Antibodies to HIV-1 and HIV-2. J Clin Microbiol. 1998 Jun 1; 36(6):1534 LP– 1538. https://doi.org/10.1128/JCM.36.6.1534-1538.1998 PMID: 9620372
19. Van TT, Miller J, Warshauer DM, Reisdorf E, Jernigan D, Humes R, et al. Pooling Nasopharyngeal/ Throat Swab Specimens To Increase Testing Capacity for Influenza Viruses by PCR. J Clin Microbiol. 2012 Mar 1; 50(3):891 LP– 896. https://doi.org/10.1128/JCM.05631-11 PMID: 22205820
20. Yelin I, Aharony N, Tamar ES, Argoetti A, Messer E, Berenbaum D, et al. Evaluation of COVID-19 RT-qPCR Test in Multi sample Pools. Clin Infect Dis. 2020 Nov 19; 71(16):2073–8. https://doi.org/10.1093/cid/ciaa531 PMID: 32358960
21. Pasomsub E, Watcharananan SP, Watthanachockchai T, Rakmanee K, Tassaneetrithep B, Kiertiburanakul S, et al. Saliva sample pooling for the detection of SARS-CoV-2. J Med Virol. 2021; 93(3):1506–11. https://doi.org/10.1002/jmv.26460 PMID: 32841429
22. Bilder CR, Tebbs JM, McMahan CS. Informative group testing for multiplex assays. Biometrics. 2019 Mar 1; 75(1):278–88. https://doi.org/10.1111/biom.12988 PMID: 30353548
23. Ira Praharaj AJ, Singh M, Anukumar Balakrishnan RD, Borkakoty B, Biswas D, Kalawat U, et al. Pooled testing for COVID-19 diagnosis by real-time RT-PCR: A multi-site comparative evaluation of 5- & 10-sample pooling. Indian J Med Res. 2020; 76(11):88–94. https://doi.org/10.4103/ijmr.IJMR_2304_20 PMID: 32893844
24. Torres I, Albert E, Navarro D. Pooling of nasopharyngeal swab specimens for SARS-CoV-2 detection by RT-PCR. J Med Virol. 2020; 92(11):2306–7. https://doi.org/10.1002/jmv.25971 PMID: 32369202
25. Jaafar R, Aherfi S, Wurtz N, Grimaldier C, Van Hoang T, Colson P, et al. Correlation Between 3790 Quantitative Polymerase Chain Reaction–Positives Samples and Positive Cell Cultures, Including 1941 Severe Acute Respiratory Syndrome Coronavirus 2 Isolates. Clin Infect Dis. 2020 Sep 28.
26. Tom MR, Mina MJ. To Interpret the SARS-CoV-2 Test, Consider the Cycle Threshold Value. Clin Infect Dis. 2020 Nov 19; 71(16):2252–4. https://doi.org/10.1093/cid/ciaa619 PMID: 32435816
27. Herrera LA, Hidalgo-Miranda A, Reynoso-Noverón N, Meneses-García AA, Mendoza-Vargas A, Reyes-Grajeda JP, et al. Saliva is a reliable and accessible source for the detection of SARS-CoV-2. Int J Infect Dis. 2021; 105:83–90. https://doi.org/10.1016/j.ijid.2021.02.009 PMID: 33581365
28. To KK-W, Tsang OT-Y, Yip CC-Y, Chan K-H, Wu T-C, Chan JM-C, et al. Consistent Detection of 2019 Novel Coronavirus in Saliva. Clin Infect Dis. 2020 Jul 28; 71(15):841–3. https://doi.org/10.1093/cid/ciaa149 PMID: 32047895

Por otra parte, en colaboración con el grupo de la Dra. Laura Gómez-Romero investigadora del Instituto Nacional de Medicina Genómica, se desarrolló un software que permite a partir de los datos crudos obtenidos del ensayo de RT-qPCR, catalogar de manera automática las muestras como positivas, negativas o indeterminadas a SARS-CoV-2, estó mediante el análisis de las curvas de amplificación obtenidas. Además, evalúa la calidad del experimento y genera reportes de manera automática. Este trabajo fue publicado en la Revista de Investigación Clínica.

Automated Reverse Transcription Polymerase Chain Reaction Data Analysis for SARS-COV-2 Detection.

REVISTA DE INVESTIGACIÓN CLÍNICA

Contents available at **PubMed**
www.clinicalandtranslationalinvestigation.com

Check for updates

Rev Invest Clin. 2021;73(6):339-46 BRIEF COMMUNICATION

Automated Reverse Transcription Polymerase Chain Reaction Data Analysis for Sars-CoV-2 Detection

Laura Gómez-Romero[1]*, Hugo Tovar[1], Joaquín Moreno-Contreras[3], Marco A. Espinoza[3], and Guillermo de-Anda-Jáuregui[1,2,4]*

[1]Division of Computing/Systems Genomics, Instituto Nacional de Medicina Genómica, Mexico City; [2]Cátedras CONACyT for Young Researchers, Consejo Nacional de Ciencia y Tecnología (CONACyT), Mexico City; [3]Department of Developmental Genetics and Molecular Physiology, Instituto de Biotecnología-Universidad Nacional Autónoma de México (UNAM), Cuernavaca, Mor.; [4]Centro de Ciencias de la Complejidad, UNAM, Mexico City, Mexico

ABSTRACT

Background: The severe acute respiratory syndrome coronavirus 2 (SARS-CoV-2) pandemic is a current public health concern. Rapid diagnosis is crucial, and reverse transcription polymerase chain reaction (RT-PCR) is presently the reference standard for SARS-CoV-2 detection. **Objective:** Automated RT-PCR analysis (ARPA) is a software designed to analyze RT-PCR data for SARS-CoV-2 detection. ARPA loads the RT-PCR data, classifies each sample by assessing its amplification curve behavior, evaluates the experiment's quality, and generates reports. **Methods:** ARPA was implemented in the R language and deployed as a Shiny application. We evaluated the performance of ARPA in 140 samples. The samples were manually classified and automatically analyzed using ARPA. **Results:** ARPA had a true-positive rate = 1, true-negative rate = 0.98, positive-predictive value = 0.95, and negative-predictive value = 1, with 36 samples correctly classified as positive, 100 samples correctly classified as negative, and two samples classified as positive even when labeled as negative by manual inspection. Two samples were labeled as invalid by ARPA and were not considered in the performance metrics calculation. **Conclusions:** ARPA is a sensitive and specific software that facilitates the analysis of RT-PCR data, and its implementation can reduce the time required in the diagnostic pipeline. (REV INVEST CLIN. 2021;73(6):339-46)

Key words: Severe acute respiratory syndrome coronavirus-2 detection. Reverse transcription polymerase chain reaction. Automatic analysis. Amplification curves.

INTRODUCTION

The coronavirus disease 2019 (COVID-19) pandemic, caused by the severe acute respiratory syndrome coronavirus 2 (SARS-CoV-2), is a worldwide priority. Accurate quantitative data are needed to implement efficient and adequate clinical and public health measures[1]. Although several diagnostic tests have been

***Corresponding author:**
Guillermo de Anda-Jáuregui
E-mail: gdeanda@inmegen.edu.mx
Laura Gómez-Romero
E-mail: lgomez@inmegen.gob.mx

Received for publication: 07-04-2021
Approved for publication: 21-06-2021
DOI: 10.24875/RIC.21000189

developed, real-time reverse transcription-polymerase chain reaction (RT-PCR) remains a gold standard diagnostic tool to identify SARS-CoV-2-positive patients[2] due to its sensitivity and specificity.

In RT-PCR, short regions of the SARS-CoV-2 viral genome are amplified in successive cycles, in the presence of a fluorescent reporter probe that emits fluorescence only when the PCR occurs[3]. This fluorescence is proportional to the amount of genetic material of interest (i.e., the number of amplicons) in the sample[4]. An amplification curve is generated by measuring fluorescence (reported as the normalized reporter value ΔRn) after each amplification cycle[3].

The amplification curve of a typical RT-PCR experiment starts with a no-amplification region, in which the measurement of the fluorescence lies below the detection threshold. In the presence of the target genetic material, a region showing exponential growth of the fluorescent signal due to exponential growth in the number of amplicons is observed. Finally, a stationary phase is reached when (and if) the detection limit is reached. The number of initial target molecules in the sample can be determined from the number of cycles required to reach the exponential phase; this threshold is called the cycle threshold (Ct)[4].

Positive and negative controls are used to guarantee the high quality and reproducibility of the experiment and the integrity of the results[5]. A negative control will include all reagents without any target, whereas a specific target of interest will be present in the positive control. A positive amplification in the negative control will occur if there is any type of contamination, and an absence of amplification in the positive control will expose a deficient sample preparation or the presence of PCR inhibitors[3,5].

Diagnostic protocols for SARS-CoV-2 testing using RT-PCR include several steps, from sample collection to diagnosis. First, a sample must be obtained, generally from the upper respiratory tract, from a probable COVID-19 case through a nasopharyngeal swab. Then, viral RNA is extracted by technicians and RT-PCR is performed to quantify specific regions of the viral genome, which have been previously validated for diagnostic use. The quality of the extracted RNA influences the success of the amplification process[5]. Finally, the RT-PCR data along with the experimental controls are analyzed, and a test result is generated.

Since the start of the pandemic, the Institute for Epidemiologic Diagnosis and Reference (Instituto de Diagnóstico y Referencia Epidemiológicos, InDRE) has certified hundreds of clinical and research facilities around Mexico for SARS-CoV-2 diagnosis using RT-PCR. As the demand for testing increases, these laboratories must increase their efforts to provide reliable and timely results. Having shorter turnaround time's helps to reduce the transmission of infectious diseases[6]; the World Health Organization suggests that new cases should be identified and reported within 24 h (https://apps.who.int/iris/bitstream/handle/10665/332073/WHO-2019-nCoV-Adjusting_PH_measures-Criteria-2020.1-eng.pdf).

Here, we present automated RT-PCR analysis (ARPA) software, designed to automatically examine RT-PCR amplification curves, quantifying the Ct per test or quality control (QC) sample. Engineered for COVID-19 diagnostic applications, ARPA provides diagnostic labels per sample and a final QC label per analysis plate. ARPA's performance is similar to that of a trained human analyst; however, it requires only a fraction of the time to label samples accurately.

ARPA provides a user-friendly graphic interface. It can be installed on any MacOS or Linux server, desktop, or laptop computer. Furthermore, ARPA provides templates to generate reports automatically, further reducing the workload of laboratory personnel. ARPA is a free and open software that is ready for use in COVID-19 diagnostic laboratories. ARPA can be downloaded from https://github.com/INMEGEN/ARPA.

METHODS

Sample collection and manual analysis

A total of 140 saliva samples were collected by healthcare workers from the epidemiology department of the Health Ministry of the State of Morelos (Secretaría de Salud Morelos, SSM). Briefly, the

patients were asked to provide 2-3 mL of saliva in sterile urine cup containers (containing 1 mL of viral transport medium [VTM]). After collection, samples were stored at 4°C until transported to the Institute of Biotechnology/UNAM (IBT/UNAM) for their analysis, which was within 24-48 h after sample collection. Saliva samples were treated with the Quick Extract™ DNA Extraction Solution (QE, Lucigen) by mixing 50 µL of saliva with 50 µL of the QE reagent and heating for 5 min at 95°C, cooled on ice, and kept at 4°C until use (within 1 h of QE treatment) as previously described[7]. Total RNA was extracted using the QIAamp viral RNA mini kit (QIAGEN) following the manufacturer's protocol, using 140 µL of V™ from each swab, and the purified RNA was eluted in 60 µL of elution buffer. SARS-CoV-2 detection was performed using the Charité-Berlin protocol[3]. Some studies have found that the degree of sequence variability in the region targeted by the RdRp probes is higher than that observed in the region targeted by the E probes[8,9]. Considering the recommendations made by the local authorities (InDRE), detection of SARS-CoV-2 was performed using primers and probes only for the *E* gene, in addition to a probe to amplify a constitutive human gene, such as RNase P (probe RP). The RT-qPCRs were performed using the StarQ One-Step RT-qPCR (Genes 2 Life) kit, using 5 µL of the column-extracted total RNA in 20 µL of reaction mix. Samples were analyzed using an ABI Prism 7500 Sequence Detector System (Applied Biosystems) with the following thermal protocol: 50°C for 15 min, 95°C for 2 min, followed by 45 cycles of 95°C for 15 s and 60°C for 30 s. All samples with a Ct value ≤ 40 were classified as positive.

QC experimental design

In-house QCs were designed to be used with the implemented Charité-Berlin protocol. The positive control contained *in vitro* transcribed RNA to monitor primer and probe integrity. Nuclease-free water was used as a negative control, and to detect any reagent contamination. Any of the components of the extraction kit handled in the same area as the test samples were used as the extraction control; this was used to monitor any contamination in the extraction kit or any mishandling during the extraction process.

Automatic analysis of PCR data

The process to analyze automatically data from a SARS-CoV-2 diagnostic RT-PCR requires three steps. First, a signal threshold must be determined for the analyzed plate. Second, ARPA must detect and quantify amplification by determining the cycle in which the curve crosses the signal threshold. Third, for each sample analyzed, a classification (in terms of positivity or negativity) must be provided based on the diagnostic criteria. All these steps were performed using R language[10].

Threshold determination

ARPA extracts the fluorescence levels per cycle per well from the raw files (.eds extension file) generated by the RT-PCR machine. Then, ARPA determines the plate threshold by looking at the signal of each analyzed well between the 3rd and 10th cycles; the threshold was then set at 10 times the mean value of these signals. This heuristic technique is the same as that used by commercial software[11].

Amplification detection and quantification

To assess whether a given well exhibits amplification, ARPA performs several fittings of the observed signal curve. The described procedure is useful for identifying noisy amplification in which the fluorescence signal goes sporadically above the threshold value instead of monotonically increasing during the exponential phase of amplification. This assessment also allows for the identification of samples in which there is a late amplification (above the fixed CT threshold) but a correct sigmoidal behavior for a given probe.

The process to evaluate whether the curve exhibits logistic growth is as follows: the EDS file contains the raw curve data-normalized reporter (Rn) versus cycle. Using these points, it attempts to fit the curve to a logistic model (using the nonlinear least-squares method from the stats package)[10]. If this model is properly fitted ($R^2 > 0.9$) and exhibits logistic growth, then the sample is considered to exhibit amplification. If the logistic fitting fails ($R^2 < 0.9$), a second attempt

to fit the data to a logistic growth model is performed using the {growthrates} package[12]. If no logistic growth model could be fit ($R^2 < 0.9$), then this well is considered to exhibit no amplification.

In a manual RT-PCR analysis, the analyst will evaluate whether the curve shows the characteristic sigmoid shape as an indication that amplification occurred; therefore, the role of this step was to discern those wells in which amplification occurred versus plates in which no amplification occurred.

For wells in which amplification was detected, the next step involved identifying the intersection of the adjusted curve with the threshold value. By doing so, we were able to report a Ct value for a given well.

Diagnostic classification

Finally, ARPA classifies the samples based on the diagnostic criteria established in the analysis protocol. In the current implementation, a high fixed Ct value (equal to 40) was established to ensure that most amplifications were detected. Finally, the proposed diagnostic classification was returned for each sample. Probe E was designed to amplify the SARS-CoV-2 gene, so it must be present to determine whether a sample is positive for SARS-CoV-2. The probe RP amplifies a constitutive human gene, so it must be present to ensure that the amplification is successful. The absence of amplification for the probe RP indicates a poor QC analysis per plate. However, no final QC label is generated per plate, as we are aware that some laboratories could use different reaction settings as controls.

RESULTS

Test performance

We evaluated the performance of ARPA in human samples tested for SARS-CoV-2 using RT-PCR. A group of experts manually assigned diagnostic labels to 140 samples; 36 samples were labeled as positive and 104 as negative and no samples were labeled as invalid. We compared manually assigned labels with automatically assigned labels generated by ARPA. We assessed the performance of ARPA in all samples that were considered valid by both approaches. ARPA was classified as invalid for two of the samples; these samples were not considered in the performance metrics calculation.

Table 1. Confusion matrix for manual and ARPA-derived classification for samples classified as valid by both methods

Method	Manual	
ARPA	**Positive**	**Negative**
Positive	36 (26.08%)	2 (1.45%)
Negative	0	100 (72.47%)

ARPA: automated RT-PCR analysis; RT-PCR: reverse transcription polymerase chain reaction.

In this study, no independently validated ground truth is available. Therefore, we considered the labels assigned by human inspection as accurate. After ARPA classification, any discrepancy was considered a false assignment, and any agreement was considered a true assignment. Positive agreements were called true positives (TP), and negative agreements were called true negatives (TN). A real positive sample classified as negative by ARPA would be considered as a false negative (FN), and a real negative sample classified as positive would be a false positive (FP).

ARPA successfully recovered all the TPs (sensitivity = TP Rate = TP/TP + FN = 1), and correctly classified 98% of the TNs (specificity = TN rate = TN/FP + TN = 0.98). In summary, 97.3% of the samples (classified as valid by both methods) were assigned to any of the agreement categories: either TP or TN (Table 1). The amplification curves for one positive and one negative sample are shown in figure 1. Only two samples (1.45%) were incorrectly labeled as positive by ARPA, and two samples were classified as invalid by ARPA but manually labeled as negative. Importantly, no sample was incorrectly labeled as negative.

We also calculated the Cohen's kappa coefficient to provide a measure of reliability. This coefficient is used to quantitatively measure the agreement between the two raters or methods rating categorical states. It is more robust than the agreement rate, as

Figure 1. (**A**) Amplification curves for one sample labeled as positive by automated reverse transcription polymerase chain reaction analysis (ARPA). (**B**) Amplification curves for one sample labeled as negative by ARPA.

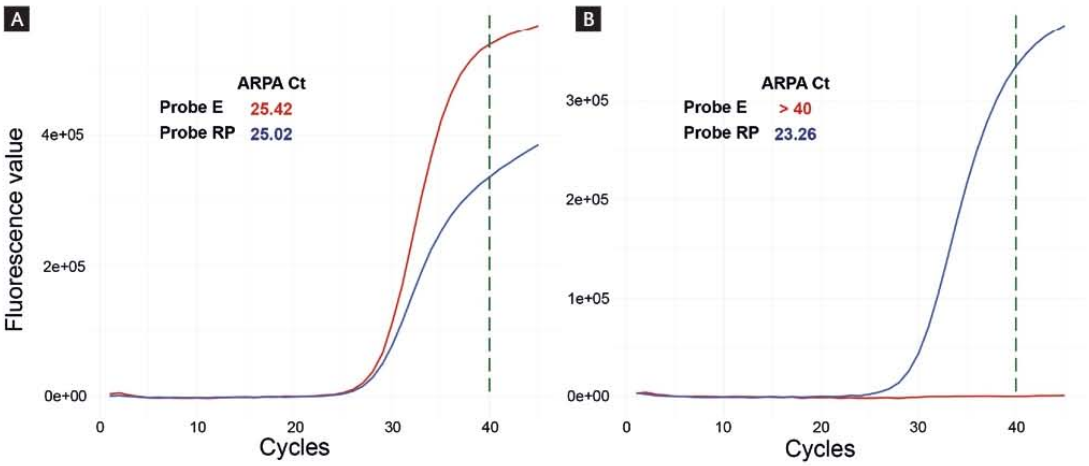

it takes into account the proportion of agreement expected by chance. The kappa coefficient between ARPA and manual assignment was 0.96 ($p < 0.01$), which has been suggested to be interpreted as almost perfect agreement[13].

ARPA implementation

We developed a user-friendly interface that can be installed on any Unix or MacOS platform to analyze the RT-PCR data. Raw files generated by the RT-PCR equipment are chosen by the user through this interface using a click and choose system that opens an explorer window and allows the user to navigate down to the folder where the raw files are stored. The same interface allows the user to select the directory to save the HTML reports (Fig. 2a). The user starts the analysis by clicking the button "Start analysis," and a progress bar appears at the bottom of the interface to show that the samples are being processed. In the background, the software reads the raw data, transforms it into amplification curves, calculates the fluorescence threshold and Ct values, assesses sigmoidal behavior, applies the classification logic, assigns a final classification per sample, and performs QC per plate. At the end of the analysis, a table with the analysis results is printed on the tab "Summary table." This table contains the name of each sample, the Ct values for each probe per sample, and the final classification per sample. All negative samples are colored with an aquamarine background; all positive samples are highlighted in red, and invalid samples have no background color. The QC table and one amplification curve per QC control are shown on the "QC Analysis" tab; the QC table contains a row per QC control and shows the Ct value per probe. Furthermore, the user can select any sample to visualize its amplification curve on the "Curves per sample" tab (Fig. 2b). Finally, all this information is saved in an HTML report. The report is generated by clicking the button "Generate reports" on the web interface. An HTML report is generated per sample, and a QC report is generated per plate.

ARPA takes approximately 1.5 s to analyze one sample, and an average of 48 s to analyze a whole run. The analyzed run had a minimum of 8 samples, a maximum of 40 samples, and a mean of 21.5 samples. Thus, ARPA could drastically reduce the time devoted to analysis and report-generation processes.

DISCUSSION

In this study, we developed a tool that automates the analysis of RT-PCR data for pathogen detection. This

Figure 2. Automated reverse transcription polymerase chain reaction analysis (ARPA) graphic user interface. (**A**) The EDS raw file and the directory to save the reports is selected by a click-and-choose system. The analysis is started by clicking the "Start Analysis" button and the reports are generated by clicking the "Generate reports" button. (**B**) ARPA presents the results per sample, and each sample's amplification curve as well as the QC results, on the online interface.

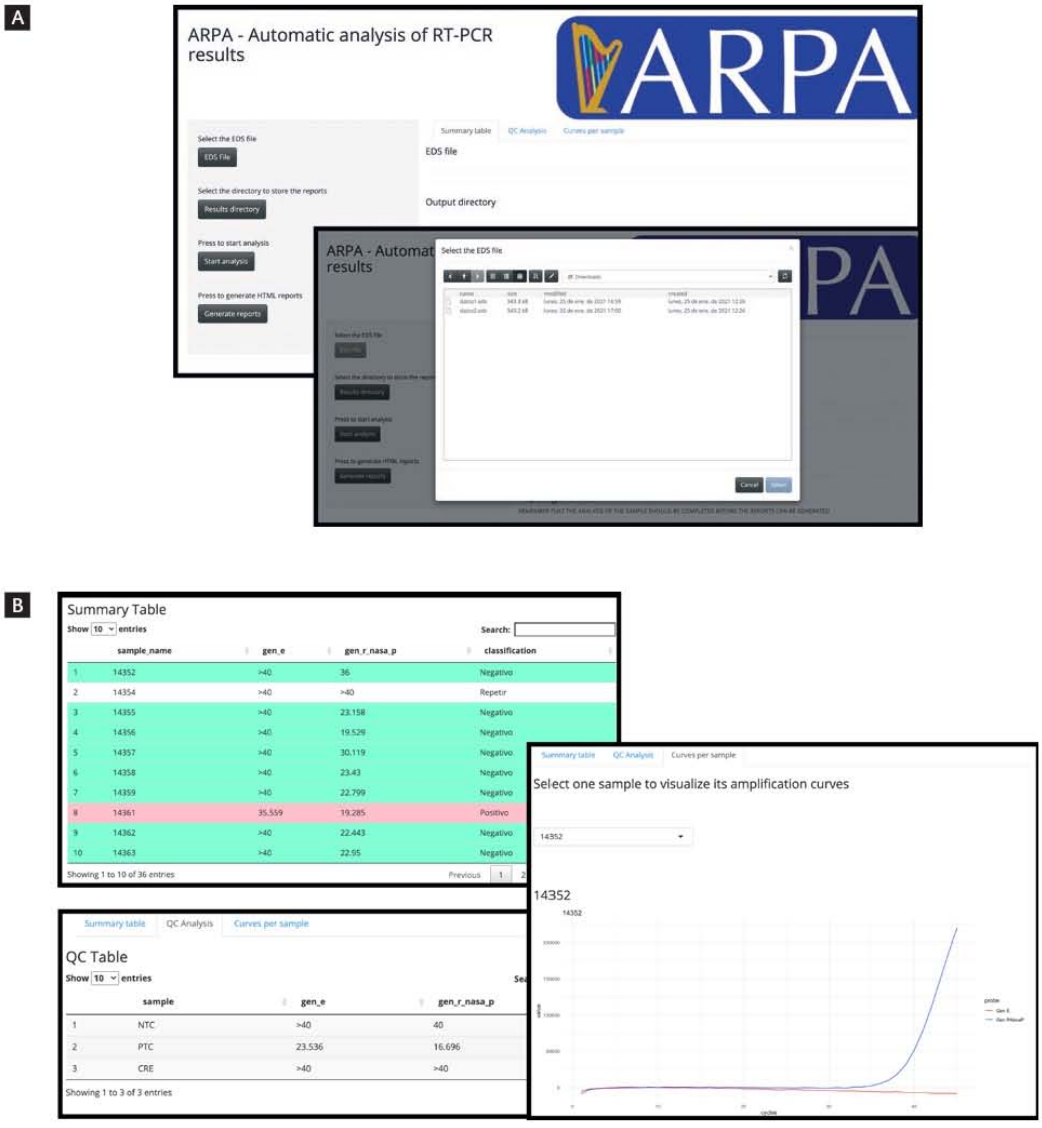

tool models the amplification curves as sigmoidal functions or logistic curves and restricts the amount of RNA that should be detected at the end cycle compared to the initial cycle. As in any statistical analysis, several thresholds were imposed along with the analysis, and each threshold was chosen to prefer type I errors over type II errors. Type I errors occur when a negative sample is incorrectly labeled as positive, and type II errors occur when a positive sample is incorrectly labeled as negative.

ARPA exhibited two type I and no type II errors. It labeled two samples positive that was evaluated as negative by manual method. In both cases, a strong amplification signal was observed for probe RP. In one sample, there was a small increase in the fluorescence signal detected in the probe E amplification (Fig. S1a), contrary to the other sample, which showed no evident increase (Fig. S1b). However, the probe E amplification curves in both samples behaved as sigmoidal; the fluorescence signal exceeded the fixed threshold before the established cycle (Ct < 40), and the fluorescence signal of the final cycle was above the threshold (at least 100 times higher than the signal at the initial cycle). In both cases, ARPA favors the detection of amplification even when the detected signal is too low to be considered positive by visual inspection.

In this study, samples were not selected based on their Ct values. All samples tested in the clinical laboratory were included in the performance analysis. We included samples with Ct values ranging from 22 to 34.8. Moreover, 12/36 positive samples showed a Ct value higher than 30 in the manual analysis. All of them were consistently labeled as positive by ARPA, suggesting that ARPA could handle difficult samples.

From a public health perspective, type II errors could increase pathogen propagation, as false-negative infected patients could disperse the pathogen. In contrast, type I errors would be the least harmful because false-positive non-infected patients would be asked to isolate for 15 days.

In conclusion, the type of error made by ARPA is the least harmful, as negative patients will be asked to isolate even when a manual inspection of the amplification curves would have suggested that they are not infected[14].

On the other hand, two samples were classified as invalid by ARPA but manually labeled as negative. In both cases, we observed a very late amplification of the probe RP, which manifests as a signal that starts to increase very close to cycle 40. This results in a fluorescence signal crossing the established fluorescence threshold after cycle 40 (Ct > 40) (Figs. 1c and 1d). Any sample with a Ct higher than 40 for probe RP amplification was automatically labeled as invalid by ARPA. Very late amplification could indicate either low-concentration or low-quality genetic material. In a real-case application, this small percentage of samples could be manually inspected to determine whether the experiment should be repeated.

To the best of our knowledge, few other tools have been developed to aid in the analysis of RT-PCR data. PCR.ai is a proprietary software developed by Diagnostics.ai, designed to automatically and rapidly interpret RT-PCR curves. PCR.ai runs directly on the RT-PCR platform and interfaces with the Abbott Laboratory Information Management System to make the results downloadable and accessible. The technical details of the implementation are not publicly available. In this study, the authors measured the time taken by either automatic or manual analysis, and concluded that there is a time saving that varies from 5 min to 40 min per run, which could translate into 160 h per year based on a run per day over a 5-day week[15]. As an automatic system, ARPA's implementation could reduce the time required for the diagnostic pipeline and reduce the workload of trained personnel to work on other critical tasks.

It has been shown that automating diagnostic procedures not only improves efficiency in terms of number of processed samples and higher reproducibility but it also reduces the likelihood of human errors such as mislabeling[16,17]. Therefore, ARPA could contribute to the streamlining of diagnostic procedures when high volumes of samples must be processed.

ARPA proved to be a sensitive and specific software that facilitates RT-PCR data analysis. It could be applied when a high volume of samples needs to be analyzed, freeing-up the time of trained personnel, reducing human errors, and increasing reproducibility.

SUPPLEMENTARY DATA

Supplementary data are available at Revista de Investigación Clínica online (www.clinicalandtranslationalinvestigation.com). These data are provided by the corresponding author and published online for

the benefit of the reader. The contents of supplementary data are the sole responsibility of the authors.

REFERENCES

1. World Health Organization. Global Surveillance for COVID-19 Caused by Human Infection with COVID-19 Virus: interim Guidance. Geneva: World Health Organization; 2020. p. 4.
2. Smithgall MC, Dowlatshahi M, Spitalnik SL, Hod EA, Rai AJ. Types of assays for SARS-CoV-2 testing: a review. Lab Med. 2020;51:e59-65.
3. Corman VM, Landt O, Kaiser M, Molenkamp R, Meijer A, Chu DK, et al. Detection of 2019 novel coronavirus (2019-nCoV) by real-time RT-PCR. Eurosurveillance. 2020;25:2000045.
4. Schefe JH, Lehmann KE, Buschmann IR, Unger T, Funke-Kaiser H. Quantitative real-time RT-PCR data analysis: current concepts and the novel "gene expression's CT difference" formula. J Mol Med. 2006;84:901-10.
5. Fleige S, Walf V, Huch S, Prgomet C, Sehm J, Pfaffl MW. Comparison of relative mRNA quantification models and the impact of RNA integrity in quantitative real-time RT-PCR. Biotechnol Lett. 2006;28:1601-13.
6. WHO Ebola Response Team. After Ebola in West Africa--unpredictable risks, preventable epidemics. New Engl J Med. 2016; 375:587-96.
7. Moreno-Contreras J, Espinoza MA, Sandoval-Jaime C, Cantú-Cuevas MA, Barón-Olivares H, Ortiz-Orozco OD, et al. Saliva sampling and its direct lysis, an excellent option to increase the number of SARS-CoV-2 diagnostic tests in settings with supply shortages. J Clin Microbiol. 2020;58:e01659-20.
8. Álvarez-Díaz DA, Franco-Muñoz C, Laiton-Donato K, Usme-Ciro JA, Franco-Sierra ND, Flórez-Sánchez AC, et al. Molecular analysis of several in-house rRT-PCR protocols for SARS- CoV-2 detection in the context of genetic variability of the virus in Colombia. Infect Genetics Evol. 2020;84:104390.
9. Peñarrubia L, Ruiz M, Porco R, Rao SN, Juanola-Falgarona M, Manissero D, et al. Multiple assays in a real-time RT-PCR SARS-CoV-2 panel can mitigate the risk of loss of sensitivity by new genomic variants during the COVID-19 outbreak. Int J Infect Dis. 2020;97:225-9.
10. R Core Team. R: a Language and Environment for Statistical Computing. Vienna, Austria; R Core Team; 2020. Available from: http://www.R-project.org.
11. Applied Biosystems. Data Analysis on the ABI PRISM® 7700 Sequence Detection System: setting Baselines and Thresholds. Available from: http://www.surf.ed.ac.uk/wp-content/uploads/2014/02/Setting-baselines-and-thresholds-.pdf.Published2002. [Last accessed on 2021 Jun 14].
12. Petzoldt T. Growthrates: estimate Growth Rates from Experimental Data; 2020. Available from: https://www.CRAN.R-project.org/package=growthrates.
13. Cohen J. A coefficient of agreement for nominal scales. Educ Psychol Meas. 1960;20:37-46.
14. Arevalo-Rodriguez I, Buitrago-Garcia D, Simancas-Racines D, Zambrano-Achig P, Campo RD, Ciapponi A, et al. False-negative results of initial RT-PCR assays for COVID-19: a systematic review. PLoS One. 2020;15:e0242958.
15. MacLean AR, Gunson R. Automation and standardisation of clinical molecular testing using PCR. Ai-a comparative performance study. J Clin Virol. 2019;120:51-6.
16. Greub G, Sahli R, Brouillet R, Jaton K. Ten years of R&D and full automation in molecular diagnosis. Future Microbiol. 2016; 11:403-25.
17. Byrne MD, Jordan TR, Welle T. Comparison of manual versus automated data collection method for an evidence-based nursing practice study. Appl Clin Inform. 2013;4:61-74.